

Radioactive Waste in Geologic Storage

Sherman Fried, EDITOR

Argonne National Laboratory


Based on a symposium
sponsored by the Division of
Nuclear Chemistry and Technology
at the 176th Meeting of the
American Chemical Society,
Miami Beach, Florida,
September 11–15, 1978.

A C S S Y M P O S I U M S E R I E S **100**

AMERICAN CHEMICAL SOCIETY

WASHINGTON, D. C. 1979



Library of Congress  Data

Radioactive waste in geologic storage.
(ACS symposium series; 100 ISSN 0097-6156)

Includes bibliographies and index.

1. Radioactive waste disposal in the ground—Congresses.

I. Fried, Sherman Meyer, 1917- . II. American Chemical Society. Division of Nuclear Chemistry and Technology. III. Series: American Chemical Society. ACS symposium series; 100.

TD898.R333 621.48'38 79-9754
ISBN 0-8412-0498-5 ACSMC8 100 1-344 1979

Copyright © 1979

American Chemical Society

All Rights Reserved. The appearance of the code at the bottom of the first page of each article in this volume indicates the copyright owner's consent that reprographic copies of the article may be made for personal or internal use or for the personal or internal use of specific clients. This consent is given on the condition, however, that the copier pay the stated per copy fee through the Copyright Clearance Center, Inc. for copying beyond that permitted by Sections 107 or 108 of the U.S. Copyright Law. This consent does not extend to copying or transmission by any means—graphic or electronic—for any other purpose, such as for general distribution, for advertising or promotional purposes, for creating new collective works, for resale, or for information storage and retrieval systems.

The citation of trade names and/or names of manufacturers in this publication is not to be construed as an endorsement or as approval by ACS of the commercial products or services referenced herein; nor should the mere reference herein to any drawing, specification, chemical process, or other data be regarded as a license or as a conveyance of any right or permission, to the holder, reader, or any other person or corporation, to manufacture, reproduce, use, or sell any patented invention or copyrighted work that may in any way be related thereto.

PRINTED IN THE UNITED STATES OF AMERICA

**American Chemical Society
Library**

1155 16th St., N.W.
Washington, D.C. 20036

In Radioactive Waste in Geologic Storage, Fried, S.;
ACS Symposium Series; American Chemical Society, Washington, DC, 1979.

ACS Symposium Series

Robert F. Gould, *Editor*

Advisory Board

Kenneth B. Bischoff

Donald G. Crosby

Robert E. Feeney

Jeremiah P. Freeman

E. Desmond Goddard

Jack Halpern

Robert A. Hofstader

James D. Idol, Jr.

James P. Lodge

John L. Margrave

Leon Petrakis

F. Sherwood Rowland

Alan C. Sartorelli

Raymond B. Seymour

Aaron Wold

Gunter Zweig

FOREWORD

The ACS SYMPOSIUM SERIES was founded in 1974 to provide a medium for publishing symposia quickly in book form. The format of the Series parallels that of the continuing ADVANCES IN CHEMISTRY SERIES except that in order to save time the papers are not typeset but are reproduced as they are submitted by the authors in camera-ready form. Papers are reviewed under the supervision of the Editors with the assistance of the Series Advisory Board and are selected to maintain the integrity of the symposia; however, verbatim reproductions of previously published papers are not accepted. Both reviews and reports of research are acceptable since symposia may embrace both types of presentation.

PREFACE

It is almost three years since the first American Chemical Society symposium on radioactive waste isolation and management was held in New York. The second symposium in Miami Beach marked an effort to draw attention to the rapidly growing accumulation of information in this field.

Interest in the safe disposal of radioactive waste has deepened and strenuous efforts are being made to understand the processes by which radionuclides may migrate (into the biosphere) from a deep geologic repository. This understanding will ultimately make possible a credible safety assessment of any deep geologic storage proposal. Therefore, this symposium focused on the conceptual, chemical, and geological aspects of the radioactive waste isolation program.

The work reported in this symposium on "Radioactive Waste in Geological Storage" covers the most recent radioactive waste disposal concepts and proposals as well as the experiments carried out to determine the most important parameters. The first four papers cover the general geologic and hydrologic considerations involved in a deep repository. The following four papers examine the leaching characteristics of the source terms. The remainder of the volume consists of papers on the sorption behavior of various nuclides on minerals, rocks, and clays as it relates to migration and the possible entrance into the biosphere.

The work presented here enables us to get a clearer picture of the problems involved in permanent isolation of radioactive wastes from the environment.

Chemistry Division
Argonne National Laboratory
Argonne, IL 60439
January 16, 1978

SHERMAN FRIED

The Department of Energy Program for Long-Term Isolation of Radioactive Waste

COLIN A. HEATH

Division of Waste Isolation, B-107, U.S. Department of Energy, Washington, DC 20545

I wish to thank the American Chemical Society and its members for the opportunity to discuss with you today the Department of Energy (DOE) program in radioactive waste management. This program, which is of vital concern to our country's energy and defense programs, has recently become the topic of newspaper articles, TV shows and much public discussion. I welcome this chance to describe to you some of the activities underway to move the program forward and perhaps answer questions that may have been raised during all this public discussion.

The Department of Energy is charged by the Congress with the responsibility for accepting high-level radioactive waste from commercial uses of nuclear power and providing for their management leading to final disposal. This final disposal must provide isolation of these wastes from the human environment for as long as they remain hazardous.

At the present time, there is some uncertainty as to what form the radioactive wastes from the commercial nuclear fuel cycle will take. Early development of the fuel cycle and the power reactors now providing electricity in several regions of the country was undertaken with the assumption that fuel elements would be periodically removed from operating reactors and subjected to reprocessing and recycle whereby unburned uranium and generated plutonium would be recovered from the fuel elements for refabrication and recycled back into operating reactors. The effluent by-products stream from this chemical processing was then to become a high-level waste which must be processed for permanent disposal.

Within the last two years, major concerns over the proliferation problems associated with the recycle of uranium and plutonium have lead the President of the United States to call for an indefinite delay in future plans for reprocessing pending an evaluation

Paper presented at the American Chemical Society Meeting in Miami Beach, Florida on September 13, 1978.

This chapter not subject to U.S. copyright.
Published 1979 American Chemical Society

of alternatives to provide proliferation resistant fuel cycles. The waste management program is therefore faced with the potential that the radioactive waste from the commercial fuel cycle could be in the form of spent fuel elements which have been declared to be waste or in the form of solidified high-level waste produced from the byproducts stream of the reprocessing plant.

The issues surrounding the use or nonuse of recycled reactor fuel and plutonium are exceedingly complex and will require a considerable amount of time before our society and the international community can reach a decision as to whether or not the risks of proliferation are appropriate to the benefits that might be received from the recycle of these materials. In the meantime, the Department of Energy's waste management program needs to get on with the long-neglected job of identifying the technology, systems, and facilities for providing for the permanent isolation of these wastes from the human environment. In order not to get bogged down in the dispute over proliferation, therefore, the program is proceeding on the basis that the waste could take either form. Preliminary evaluation indicates that, even though disposal of spent fuel will result in larger quantities of plutonium being placed in permanent isolation, there is no overriding safety reason which suggests that disposal of spent fuel will not be able to be accomplished with any more difficulty than disposal of solidified radioactive waste in which the plutonium content has been reduced by reprocessing.

Over the last twenty years, significant research and development has been performed concerning the ultimate disposal mechanism for radioactive waste. In 1957, the National Academy of Sciences recommended that deep beds of bedded salt be considered as potential locations for the disposal of radioactive waste materials. Following this recommendation a program of research and development was undertaken by the Atomic Energy Commission (AEC) to explore this approach. The high point of this program was the operation of Project Salt Vault in an abandoned salt mine in Lyons, Kansas.

This project placed encapsulated spent fuel elements from an experimental AEC reactor into storage holes drilled into the floor of the mine located in a salt bed. Valuable experimental information was obtained about the interaction between the waste form and the salt in which the waste was emplaced. It was in fact this experiment, conducted in 1968, which revealed that inclusions of moisture, or brine, in the salt beds have a tendency to migrate up a thermal gradient towards a heat source placed in the salt. Quantities of brine were measured as migrating to the deposited waste canisters and the interaction of this brine with the canistered material was observed.

The initial experiments conducted in Project Salt Vault were not extended to provide more detailed work. If it had been possible for this experiment to have continued to operate since 1970, we would definitely have a considerably greater amount of informa-

tion concerning the actual interactions between waste and the bedded salt than we presently have today. Unfortunately, a dispute between the AEC and the State of Kansas over potential use of this site as a permanent repository led the AEC to withdraw from further operations in Kansas. In retrospect, one can only regret that an arrangement was not made whereby the experimental facility would have been permitted to remain in operation with a clear understanding that the Federal Government would make no further attempt to qualify the site as a permanent repository.

Following the abandonment of Project Salt Vault, attention of the AEC turned towards the possibility of using a retrievable surface storage concept for temporary storage of radioactive waste until such time as a permanent isolation facility could be developed. At the time, this seemed to provide a reasonable and perfectly adequate plan to handle the waste from the commercial industry particularly since the large-scale reprocessing of commercial nuclear fuel hadn't started either. Since ten years was envisioned between separation of waste in a reprocessing plant and delivery for ultimate disposal to the Federal Government, there appeared to be plenty of time.

The rejection by the Council of Environmental Quality and the Environmental Protection Agency of the impact statement concerning the proposed Retrievable Surface Storage Facility (RSSF) made everybody realize that asserting the technical feasibility of ultimate geologic disposal was insufficient. These agencies took the position that the RSSF merely put off providing facilities for permanent disposal and diverted the effort to another interim measure. Dr. Seamans in one of his first acts as the new administrator of the Energy Research and Development Administration (ERDA) decided to withdraw the Environmental Impact Statement (EIS) associated with the RSSF and that establishment of a permanent waste repository should be given much greater budget priority.

A new large-scale program was initiated by ERDA in 1976 with an announcement that each of 36 states contained geologic formations which might be suitable for establishment of permanent waste repositories. ERDA established an Office of Waste Isolation managed by Union Carbide Corporation in Oak Ridge, Tennessee, to direct the program to establish the suitability of locations for repository sites and to develop the necessary technology to design, build and obtain licensing approval of these permanent geologic facilities. Two years after the initiation of this full-scale program, a number of changes have taken place both in the site selection and technical areas, and at this point approximately two years later, it is appropriate to provide a status report of where things stand today.

Organization of DOE's Waste Management Program

In May 1978 Secretary Schlesinger approved a reorganization within the Department of Energy which established an Office of

Nuclear Waste Management reporting directly to the Assistant Secretary for Energy Technology. Within the waste isolation program, the major technical activities are carried on at three field office locations. These locations and the supporting contractors are summarized in Table I.

Actual direction of the technical activities within the program is the responsibility of field offices. The primary field office in the waste isolation program is located in Columbus, Ohio as a satellite to the Richland Operations Office. Co-located with this office is the Office of Nuclear Waste Isolation (ONWI) recently established by Battelle Memorial Institute. This office directs geologic exploration outside those areas occupied by existing Department of Energy reservations. Current ONWI investigations are concentrating on various salt formations around the country. ONWI will also develop the supporting data base and technology and coordinate the development of waste isolation technology as it applies to a number of potentially possible geologic media.

The other three major activities within the waste isolation program are specific to particular sites. We are currently evaluating the potential of deep basalt flows below the Hanford reservation in the State of Washington. This work is managed by the Richland Operations Office and is being conducted by the Rockwell Hanford Company. An evaluation of a potential site is underway in southeast New Mexico for the location of the Waste Isolation Pilot Plant (WIPP) which is primarily a facility for the placement of transuranium contaminated wastes (TRU) from the defense program.

Finally, a study is underway to determine the suitability of the Nevada Test Site in southern Nevada which has been used in the past for both surface and underground testing of nuclear weapons, to see if it may possibly be suitable as a potential permanent radioactive waste repository site.

Technical Issues and the DOE Technical Program

Technical issues concerning the placement and disposal of radioactive waste can be broken into two categories. The first issue is whether or not we have available to us the technology to provide for the safe encapsulation, transportation, handling and placement of radioactive materials in an operating geologic facility. The second issue is, when the facility has been filled with these materials and subsequently decommissioned, will the placement of these materials in geologic formations provide the permanent isolation from the human environment that is sought.

There has been a past perception, particularly in the nuclear community, that the issues of waste isolation lie primarily in the political and socio-economic arena and that no real technical problems remain. I believe that this is correct with respect to the first category of issues, namely, there is no question that we understand how to encapsulate, transport and safely handle radio-

active materials and the placement of those in an operating mine is a technology available today. However, I must disagree somewhat with this view of the status of technology when it comes to the second category, namely, to prove that we can provide for permanent isolation of these materials from the human environment to the satisfaction of an independent licensing authority, and the general public. We must understand all of the processes involved to be able to guarantee to a reasonable degree that these wastes will indeed be permanently isolated.

Over the last year or so, several papers have been published which have been concerned with the adequacy of the technology for providing for permanent isolation of radioactive wastes. In all cases the concerns that have been raised have focused on the second set of issues, rather than the first, so that the apparent dispute between those who say that there are no technical problems and those who say that there are still some to be solved is perhaps more a dispute as to what particular set of problems are being described.

These papers have provided a valuable mechanism for independent peer review from technical experts not necessarily associated with the waste management program.

These review papers have included the circular by the U.S. Geological Survey, Circular 779, "Geologic Disposal of High-Level Radioactive Wastes - Earth-Science Perspectives"; the review by the Ad-Hoc Committee of Earth Scientists for the EPA; reviews by the Office of Science and Technology Policy and finally a review prepared by an Interagency Committee chaired by the Office of Science and Technology Policy whose paper was released for public comment on July 3, 1978.

Without going into great detail about the issues described in these papers, I would like to make the point that the response of the waste isolation program to these papers will be to use them to help us to design a technical program plan to ensure that these issues are adequately addressed, as indeed they must be, before we can commit radioactive waste to irretrievable permanent disposal. I would like, however, to spend a few minutes briefly summarizing the questions that have been raised and describe the various parts of the DOE program which are addressing them.

In the construction of a facility containing hazardous materials, multiple barriers are provided between the material and the human environment. Figure 1 illustrates schematically what these barriers might be. This figure illustrates that by supplying a number of multiple and redundant barriers, one gains additional assurance that true isolation can be maintained for very long periods of time. Although it is impossible to guarantee absolutely future events, one does not need absolute certainty that any single barrier will provide required isolation. The redundancy of barriers provides greater assurance that the required permanent isolation can be achieved.

The final design of a geologic repository will employ multi-

Table I
ELEMENTS OF DOE'S WASTE ISOLATION PROGRAM

<u>Field Office</u>	<u>Corresponding Projects</u>	<u>Lead Contractor</u>
Richland	Basalt Program	Rockwell Hanford
Richland-Columbus	ONWI	Battelle Mem. Inst. ONWI
Albuquerque	WIPP	Sandia/Westinghouse
Nevada	NTS Investigations	Sandia/LASL/LLL/USGS

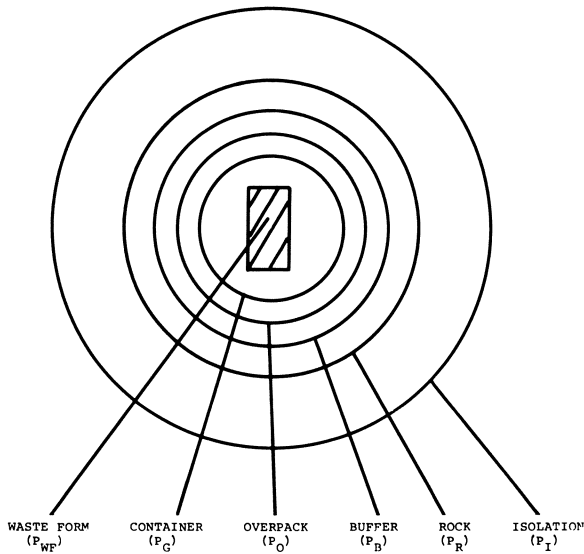


Figure 1. Barriers between waste and biosphere. Protection of biosphere = $P_{WF} + P_C + P_O + P_B + P_R + P_I$.

ple barriers but the exact form that each might take will depend on the specific conditions in the geological system that is finally chosen for the site.

Let me now turn to some of the specific areas of concern identified in the various reviews referred to and try to indicate exactly how we are addressing these issues.

Waste Form and Interactions. Several reviewers have expressed concern over the waste form and the potential for interactions between waste and surrounding minerals. Chemical and radiological interactions between the host rock with its contained water and either the waste form or the container might lead to disintegration of the packaging and partial dissolution of the waste. Early experiments with some of the proposed waste forms have indicated a high resistance to leaching by groundwaters, however, the environment to which these waste forms will be exposed will include a number of factors. First of all, the pressure which exists at the depths at which we are considering placing this material will change the physical behavior of liquids which may exist at those depths. Secondly, concern with the phenomena of brine migration has resulted in research which indicates that the solutions which might be formed in the presence of multiple ions may lead to a much higher degree of corrosion than had previously been considered.

Theoretical investigations of these phenomena are continuing in addition to which a number of specific in situ experiments are planned. We have over the last several years been planning and conducting electrically heated tests in both near-surface and deep facilities in order to simulate the radioactive heating that will come from deposited waste forms and to learn more about the effects of this heat upon the geologic media. As more information is being obtained about the potential geochemical interactions between the brines and these complex solutions, efforts will be made to duplicate solutions in situ to see if the mechanisms that are being postulated for possible dissolution and failure of containers will indeed occur.

At the present time we are conducting tests with electrical heaters in a sale mine in Louisiana, in a granite formation in Sweden, in a granite formation in Nevada and in shale formations both in Tennessee and Nevada. Early information developing from these heater tests will be used in the design of further, more sophisticated tests in which some of these geochemical interactions will be simulated.

We are presently constructing a near-surface test facility at the Hanford reservation which will be located in a basaltic flow in the side of a mountain there. This facility will have electrical heaters emplaced in it in 1979 and by 1980 we expect to emplace encapsulated cylinders containing spent fuel elements there. A second project under development will provide placement of spent fuel in similar containers in a deep granite facility at the

Nevada Test Site, hopefully as early as 1979. Both of these experiments are strictly to establish a better understanding of the interactions between the waste form and the media. In neither case is the experimental location considered as a permanent disposal location.

Properties of the Host Rock and Rock Mechanics. Considerable information will be needed about the properties of the host rock into which material will be placed. The host rock provides the first natural barrier to waste migration and strongly influences the detailed design of the engineered repository. Some media that exhibit creep or plastic flow might be capable of sealing repository workings by flow without fracture propagation or might self heal in the event of fault-induced fracturing. Creep is observed in rock salt and to a lesser extent in some shales. The creep properties of these materials can be measured in the laboratory but generally these observations are not completely accurate because of the lack of the restraining lithostatic pressure.

The recent report by the National Research Council of the National Academy of Sciences entitled "Limitations of Rock Mechanics in Energy Resource Recovery and Development", highlighted some of the problems which must be addressed. The rock strength and other mechanical properties of the media must be understood both under the impact of the thermal pulse represented by the release of heat from decaying radioactive waste materials and the perturbation represented by construction of the mine. The resulting thermal stresses must be understood in developing the layout and the allowable rate of heat generation from the individual canisters.

Calculational models are being developed to better understand the properties and behavior of rock in response to these stimuli. Measurement of properties at depth will probably be required in order to get a better understanding of the behavior of these rocks. These issues are important because rock motion or fracturing could result in changes to the overlying strata which might affect the flow of ground water in aquifers overlying the repository. In order to understand this properly, therefore, an extensive program of rock mechanics will be conducted.

Hydrogeologic Transport. After a repository is fully loaded and sealed, the most likely mechanism for the release of radionuclides to the biosphere would be by their dissolution and transport in ground water. Repositories located below the water table are expected to fill with ground water at some time after their sealing. The rate of ground water inflow will depend on the host rock permeability, the depth of the repository beneath the water table, the design of the shafts and bore holes, and the effectiveness of techniques for sealing the shaft and bore holes. After the repository has been sealed and later has become saturated, ground water flow through the repository will be influenced by the

mechanical response of the host rock to the repository construction and to the thermal pulse and by natural hydraulic gradients. The characterization of the hydrology of potential sites is as the present time a major item in our program. In most areas the capability of the United States Geological Survey is being employed to assess the existing hydraulic gradients in the areas being considered.

The ability of the ground water to dissolve wastes and transport them from the repository depends on the solubility of the waste forms at the temperatures that the repository will reach and the ion-exchange properties of the host rock and of all media between the repository and the potential release point to the biosphere. Consequently, measurements are presently being made on absorption coefficients of various radioisotopes with the minerals that are expected to be encountered in the geological environment. Measurements are being taken not only for single species but also for combinations of species with the range of pH values of the ground water that may be expected to be found. A number of models have been developed to estimate the potential transport of radionuclides by ground water. By varying boundary conditions and generic input data such as permeability, porosity and absorption capacity of geologic media these models yield the measure of relative importance of the flow path life, the flow velocity and aquifer absorption characteristics as barriers to radionuclide transport. Results from calculations with the model suggest that if a repository is sited with a flow path sufficiently long, such as may be found in regional aquifer systems, the retention of radionuclides in the geology for periods of thousands of years will be achieved.

A major issue that needs more work in the area of hydrogeologic transfer has to do with flow of ground water through fractured rock systems. There are a number of models that have been developed to date to try to obtain a better understanding of ground water flow through geologic media. But most of these assume the properties of porous or semi-porous media. Should the ground water flow be primarily through fractures, which of course is very site specific, models are not yet available to represent this flow accurately. It may very well be that site specific experiments will be required in order to characterize the flow through fractured media. Additional work in this area will be required before we will be in a position to identify the characteristics of flow paths where considerable quantities of fractured rock exist.

Risk Assessment. The overall compilation and assessment of the factors that must be considered in designing and siting geologic repositories is pulled together in a general discipline of risk assessment. Risk assessment calculations develop both generic and site specific models and calculate the potential transport times as a result of various phenomena. Calculations are being

performed for those situations in which the repository environment remains essentially unchanged and also for those conditions where significant unplanned events such as earthquakes, climate change or other phenomena take place. As each of these situations are analyzed, an understanding is gained of the importance of the various factors and the multiple barriers which might be provided between the radioactive materials and the environment.

An important element of risk analysis is assessing the importance of the uncertainties in the data now being used to evaluate various scenarios. By varying the value of the parameters that are used in the analysis, one can understand the importance of present uncertainties in significant variables by their impact on the calculated risk from the repository. These results will be used to direct the research program toward those elements which are most significant.

The overall design of the program by evaluating factors which could lead to risk of release to the environment involves the type of analysis that will be required during a licensing process. A detailed licensing plan is being prepared and will be published when available to describe those areas which will be of concern to the licensing authorities, the methods available to us to analyze those areas and the data that will be used in performing the analyses. The sensitivity analysis just described will indicate where additional data are required in order to gain more assurance in predicting potential risks that might occur from the placement of the repositories.

Conclusion

I have tried to present to you some of the considerations that go into designing the research and development programs which are and will be undertaken under the sponsorship of the Department of Energy. The new Office of Nuclear Waste Isolation has been charged with the task of compiling all of these various thoughts and considerations into a single program plan document. This document will incorporate the input of the licensing plan, the risk assessment and sensitivity analyses which have been performed and also the independent review that has been supplied by such groups as the USGS, the National Academy of Sciences, EPA and others.

This program plan will be published within the next few months and will be circulated for public review and comment. We hope that both the American Chemical Society and its individual members will provide us feedback on this plan. Hopefully, in this way a greater understanding of the technical components of the program will be achieved and we will be able to demonstrate that we are addressing the concerns that have been raised in a responsible manner.

If I can supply an overall assessment of where we stand in the program today, I believe that there is a consensus in the

scientific community that appropriate isolation of radioactive wastes can be obtained by placing them in geologic formations. There are several factors that have to be considered before specific sites can be identified and many of the gaps in our knowledge are indeed very specific to the sites in question. Primarily because of this site specific characteristic I believe one can say that the concept of radioactive waste isolation will not be proven until we are in a position of being able to identify a specific site with all of these multiple characteristics adequately characterized so that we can obtain a clearer understanding and approval by both the regulatory authorities and the general public.

The proposed facility in southeast New Mexico is the closest to being completely categorized in this way. It is in this context that the Department of Energy has proposed that this project be subjected to the licensing process by NRC even if the material to be placed there is only defense radioactive waste. Unfortunately, the sponsoring committees of the Congress who are concerned primarily with the issues of defense have taken the position that facilities related to the defense program should remain completely exempt from the licensing process.

Opposition to work leading to identification of specific sites is the greatest problem facing the program today. It is agreed in the scientific community that one cannot reach a final conclusion of the suitability of geologic isolation without looking at specific sites in detail. This of course is the one area to which there has been significant opposition. Members of the public and state and local leaders have stated that more specific information is needed as to the safety and potential suitability of radioactive waste disposal before one can allow even the examination or discussion of specific sites. On the other hand, scientific consensus is that until one does evaluate specific sites one is not going to be able to obtain the required information. In order to resolve this dilemma, we are seeking to construct a joint consultation process with state and local authorities to allow the examination of specific sites in order that we can answer the scientific questions that we must. The ongoing activities of the Interagency Review Group on Waste Management and its interaction with state and local officials and the public is the first step in obtaining the necessary consensus before proceeding.

We have reached a critical turning point in the DOE's waste management program. The program is now adequately funded, and with the assistance of many qualified and experienced scientists and engineers a comprehensive technical program is underway. A resolution must now be reached to allow us to extend our investigations into specific site locations. With input and feedback from groups such as this, and with cooperation at all levels of government, I am confident that we can proceed to resolve this very important national problem.

RECEIVED January 16, 1979.

WIPP: A Bedded Salt Repository for Defense Radioactive Waste in Southeastern New Mexico

W. D. WEART

Sandia Laboratories, Albuquerque, NM 87185

For twenty years the Department of Energy (DOE) and its predecessor organizations, the Atomic Energy Commission and the Energy Research and Development Administration, have pursued a research effort investigating the phenomena accompanying the emplacement of radioactive waste in rock salt. This program, which has not revealed any effects which would preclude the use of salt beds for geologic disposal of radioactive wastes, has led to the implementation of the Waste Isolation Pilot Plant (WIPP) project.

The WIPP, as presently conceived (Figure 1) will utilize the deep salt beds in southeast New Mexico to provide geologic isolation for transuranic (TRU) contaminated waste generated by this nation's defense programs. In addition, the WIPP will provide an underground "laboratory" where realistic and large-scale tests can be conducted using high-level waste (HLW). While variations and additions to this WIPP mission have been proposed from time to time, (the charter for this facility is presently under discussion within the DOE) these two central features have remained a fundamental part of the WIPP.

Sandia Laboratories began site evaluation studies in April, 1975 at a location previously recommended by the United States Geological Survey (USGS) and Oak Ridge National Laboratory (ORNL). Subsequent evaluation revealed this specific site to be geologically unacceptable and renewed site selection investigations resulted in the choice of the "Los Medanos" area which is now being thoroughly examined. The site selection phase is now virtually complete and the area is believed to be acceptable, in all technical respects, for continued development of the WIPP. Non-technical aspects of the site which have been quantified for consideration in the Environmental Impact Statement (EIS) are the demographic and socio-economic facets, the ecologic and archaeological features of the region and the potential for natural resources such as hydrocarbons and potash.

0-8412-0498-5/79/47-100-013\$06.00/0

© 1979 American Chemical Society

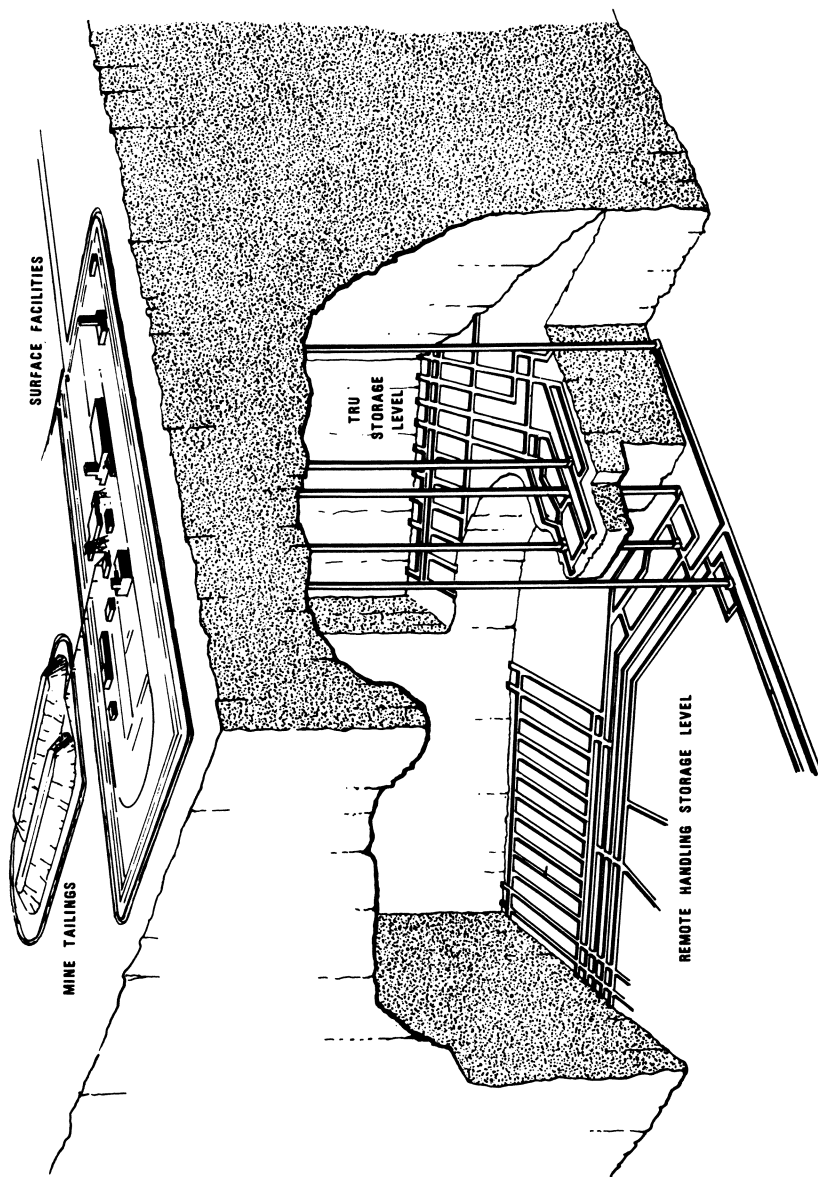


Figure 1. Artist's concept of WIPP. The WIPP will be constructed at two different levels. HLW experiments and high gamma TRU will be placed in the lower horizon. The bulk of the TRU waste will be on the upper level. New waste disposal corridors will be mined as existing rooms are filled.

Conceptual design studies for WIPP have been completed and architect engineering definition is now underway. A DOE Preliminary Environmental Impact Statement will be released by January, 1979. Present schedules call for construction to start in 1981 and for completion in 1985. First radioactive waste shipments could be accommodated in the spring of 1986.

WIPP Conceptual Design

Two distinct design concepts have been developed for the WIPP which address the two major missions which have been proposed for this facility. Both concepts assume that the facility should be capable of disposing of all defense TRU waste deriving from current production and in retrievable storage. The concepts both provide a facility for experiments with high-level waste. The early concept for WIPP (WIPP I) assumed an option for disposal of defense HLW. The more recent concept (WIPP II) deletes the defense HLW option and replaces it with a demonstration utilizing up to 1,000 canisters of spent fuel. In both concepts it was assumed the facility would be licensed by the Nuclear Regulatory Commission. At this time it is not known which design will be pursued.

Contact-handled TRU waste disposal will occupy a horizon about 2,100 feet deep while experiments with HLW and all heat producing TRU will be emplaced in a purer salt horizon 2,600 feet below the surface. WIPP II would require a smaller surface and underground facility since the large volume of existing defense HLW need not be accommodated. The experimental area and spent fuel demonstration would each utilize only 20 acres. The required capacity in the TRU horizon will not be reduced and the entire three square mile area would ultimately be required if the pilot operation is expanded to full-scale TRU disposal. A possible underground layout for WIPP II is shown in Figure 2 and Figure 3 schematically illustrates the emplacement operations. All wastes emplaced during the pilot phase will be retrievable. This period of time is considered to be 5 to 10 years for TRU waste and 15 to 20 years for HLW.

The volumes of defense TRU waste which may become candidates for disposal in WIPP are summarized in Table I. Presently, only the retrievable and yearly production portions are planned for WIPP disposal. The WIPP will have a TRU through-put capacity of 1.2×10^6 ft³ per year on a three shift per day basis. During the pilot phase, it is anticipated that waste volume would initially be restricted, perhaps to 500,000 ft³ per year. This volume would require about 930 truck shipments and 1,040 railcar shipments. This assumes three-fourths of the waste comes by rail.

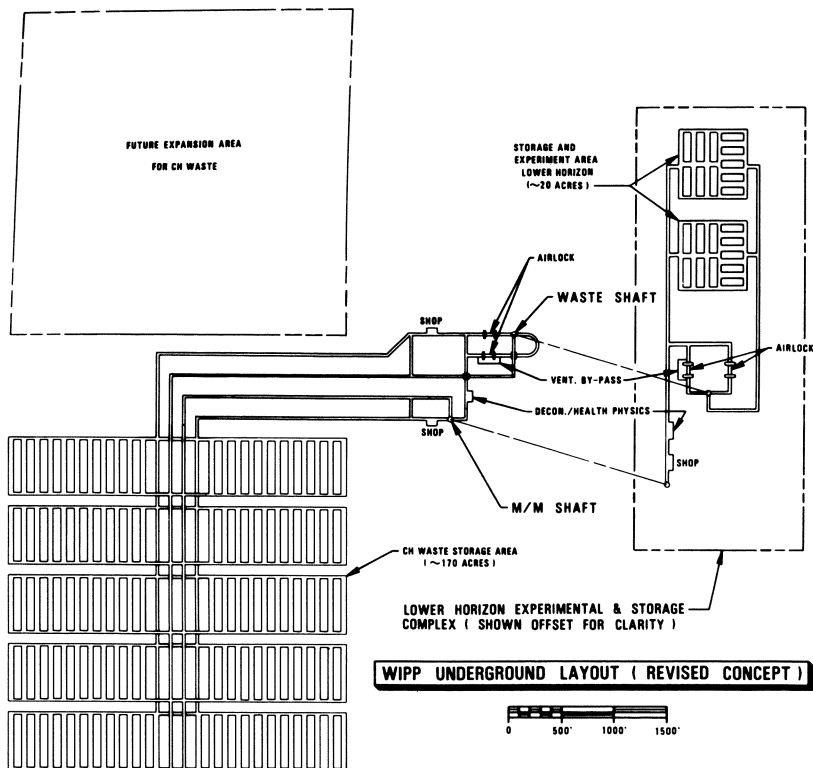


Figure 2. Underground layout proposed for WIPP II concept.

All waste would enter the repository through a single shaft. Personnel, mined salt, and ventilation air would all travel the man and materials shaft. TRU waste rooms are about 400 ft long, 45 ft wide, and 16 ft high. Extraction ratio is about 30%.

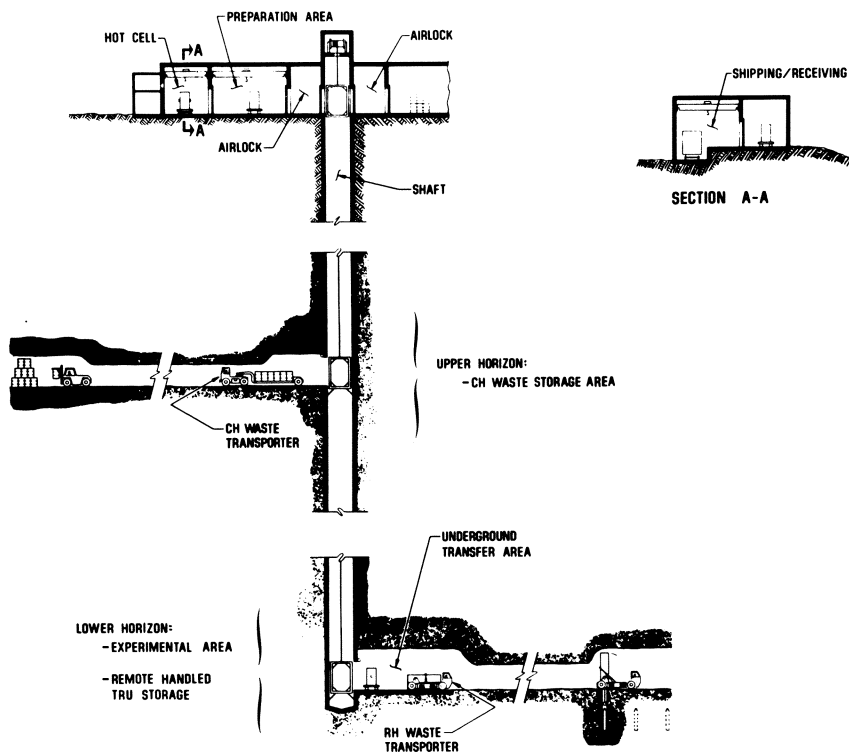


Figure 3. Emplacement operations.

Contact-handled TRU waste will be handled using conventional systems. Remote-handled waste, including HLW experimental canisters, will be placed in a transfer cask for lowering down the shaft and transferred to a specially designed transporter for movement to the storage rooms where it will be emplaced in prepared drill holes.

TABLE I
DEFENSE WASTES (1985)

Contact Handled

Retrievably Stored TRU	$3.7 \times 10^6 \text{ Ft}^3$
Buried TRU	$13 \times 10^6 \text{ Ft}^3$
Yearly Production TRU	$0.25 \times 10^6 \text{ Ft}^3$
Decontamination/Decommissioning (D&D)	5 to $95 \times 10^6 \text{ Ft}^3$

Remote Handled

Retrievable TRU	$90 \times 10^3 \text{ Ft}^3$
Buried TRU	$300 \times 10^3 \text{ Ft}^3$
Yearly Production	$7 \times 10^3 \text{ Ft}^3$
D&D	0.1 to $2.3 \times 10^3 \text{ Ft}^3$

Site Evaluation for the WIPP

The area identified for detailed site studies is located approximately 26 miles east of Carlsbad, New Mexico (Figure 4). Geologically this site is situated in the northern part of the Delaware Basin, a sub-element of the Permian Basin, which contains extensive, thick evaporite deposits of salt and anhydrite of Permian (200 million years) age (Figure 5). Extensive geophysical surveys, geologic and hydrologic studies and numerous boreholes have been utilized to evaluate the region with respect to the site selection criteria. Some of the factors considered in this evaluation are shown in Table II. Studies by Anderson (1) and earlier investigators have been useful in indicating the possible geologic features in the Delaware Basin that could pose threats to long-term repository integrity. Site selection was structured to search for and avoid these features. Those factors with greatest potential impact on WIPP site selection will be briefly discussed.

Since the most plausible natural mechanism for breaching the repository is through dissolution of the salt barrier by groundwater, this aspect was given extensive study. Regional geologic studies (1, 2) in the Delaware Basin have revealed areas of past and present dissolution activity. Knowledge of these regional dissolution fronts and of local collapse

Publication Date: April 6, 1979 | doi: 10.1021/bk-1979-0100.ch002

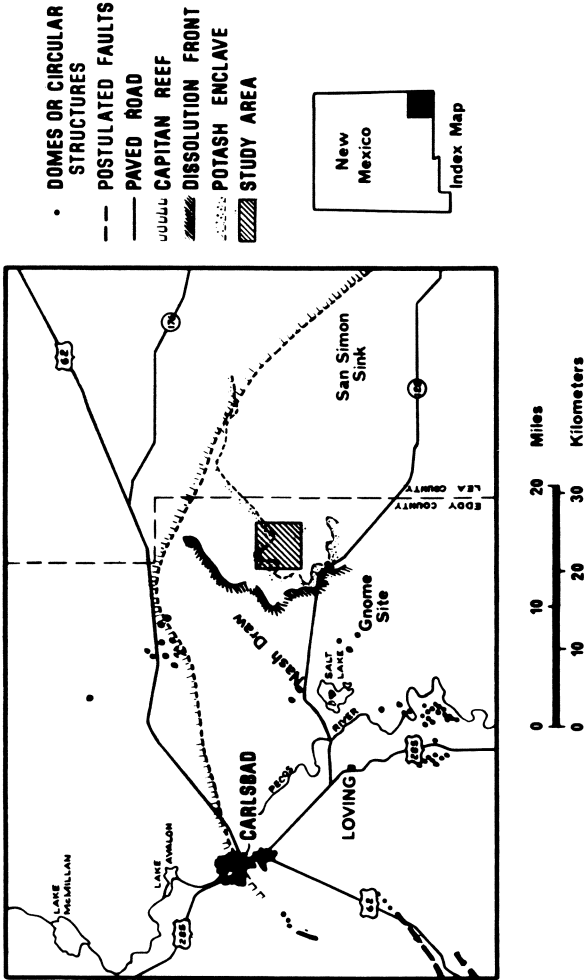


Figure 4. Location map for proposed WIPP site. WIPP is located 26 mi east of Carlsbad, New Mexico. Other features of interest to site selection shown on this map are the salt dissolution front and the 1976 location on the potash leasing area.

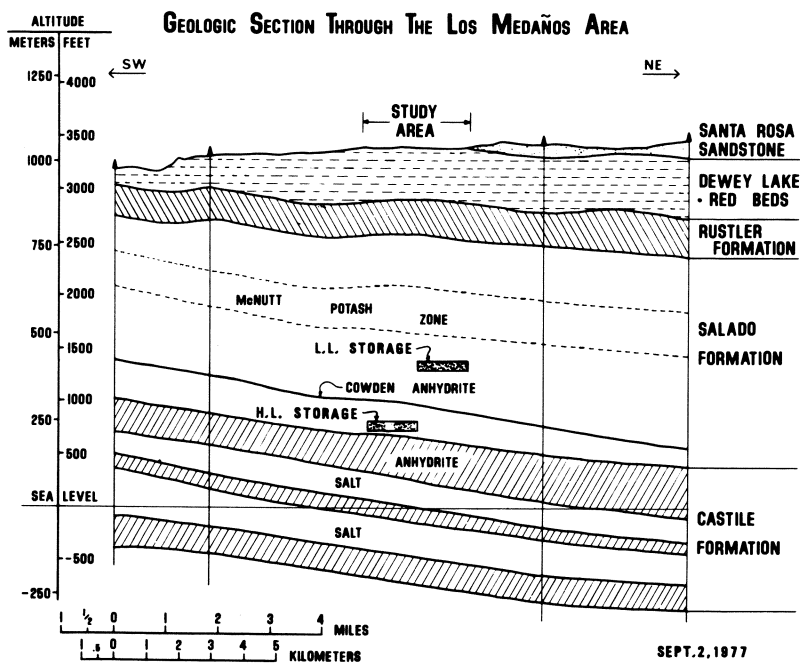


Figure 5. Geologic cross section at the WIPP site.

ERDA #9 is a corehole in the center of the proposed site. Depths to the Salado horizons proposed for the repository are about 2100 and 2600 ft. Any potash mineralization, if it exists, is within the McNutt Unit, several hundred feet above the repository horizons.

TABLE II
SITE SELECTION FACTORS CONSIDERED FOR WIPP

Depth	Hydrology	Natural Resource Potential
Thickness	Dissolutioning	Demography
Purity	Deep Drill Holes	Topography
Lateral Extent	Mining Activity	Land Ownership
Tectonics	Oil Field Activity	Land Use
Geologic Structure		

features due to salt dissolution has allowed implementation of geophysical investigations to assure that such features do not exist in, or near enough to, the site to present a hazard to long-term repository integrity. Geologic studies (3, 4) indicate the regional dissolution front west of the site area (Figure 4) is progressing eastward at a rate of less than 6 to 8 miles per million years and is moving downward at a rate of about 500 feet per million years. These values assure the repository beds will not be breached by regional dissolutioning for many million years. Since these are average rates covering the past few million years, the effect of previous pluvial cycles is included and, consequently, the forecast also incorporates the effect of similar future pluvial cycles.

Application of Rb-Sr isotope geochronology methods to the bedded salt deposits of the WIPP area have revealed that no significant recrystallization or formation of brine have occurred within the Salado salt since early in its diagenesis over 200 million years ago. Examination of petrographic structures and mineral relationships support these observations. It is evident, however, that some beds such as those containing sylvite or polyhalite, did experience mineral replacement and recrystallization during diagenesis. The natural long-term stability of the selected site and avoidance of those local dissolution features which have the potential for jeopardizing the long-term integrity of the repository, provide a high confidence in the ability of the site to isolate wastes from the biosphere for very long times indeed.

Local dissolution features are recognized in the Delaware Basin. These may be of either shallow or deep origin, and it is the latter which may pose the greater potential hazard to the repository. These features, often called collapse chimneys or breccia pipes, form when localized dissolution occurs deep in the evaporite section, possibly at the base of the salt beds, resulting in a cavern into which overlying beds

collapse. These collapse chimneys are known to exist in portions of the basin which have seen extensive dissolution activity. Seismic and resistivity surveys reveal these features and application of these techniques to the site area indicates the site area is free of them. Studies are in progress to better understand the genesis of collapse chimneys and to evaluate the age, chronology, permeability and the dissolution consequences to adjacent salt beds for a known chimney.

Dissolution may also occur through man-made boreholes if these holes penetrate through the salt and establish water circulation by connecting water-bearing rocks above and below the salt beds. To mitigate against this concern, a conservative buffer of one mile between the repository and any such holes has been required. When an adequate borehole plug has been demonstrated, it may be possible to relax this restriction.

Geologic features such as anticlines and faults must be considered in site selection. Salt flow structures, which are known to be present in portions of the Delaware Basin, may distort the rock units sufficiently to make mining operations difficult and may also lead to fracture of the more brittle anhydrite beds occurring within the salt. This fracture porosity may allow brine to accumulate and, in some instances, form brine reservoirs of significant volume. These features may be detected and examined by seismic surveys and by drilling exploratory holes when indicated. The WIPP site is believed to be free of unacceptable salt flow structures. Likewise, major recent faulting near the repository could be a concern for long-term repository integrity if it should lead to increased rates of dissolution. Open faults or fractures within the salt are not observed or anticipated due to its plasticity but overlying aquifers and aquitards could be affected by faulting. Techniques used to search for faults at the WIPP site are field geologic mapping, aerial and satellite imagery, and the geophysical investigatory techniques of seismic reflection, resistivity, aeromagnetism and gravity. No significant faults have been detected within the WIPP site. The region is relatively aseismic and tectonically stable.

Natural resources within any major salt basin are an ever-present potential. In preliminary siting of WIPP, known hydrocarbon trends and potash deposits were avoided by the three-square mile repository area. Some potash and potentially some hydrocarbons exist within the buffer zones established for WIPP. The estimated amount of these resources, which may be denied by WIPP, are 13.1 million tons of potash product (K_2O); 23.5 billion cubic feet of gas and 42.5 thousand barrels of oil. Many of these resources may not be economically recoverable depending on many economic and mineralogic factors. For example, the United States Bureau of

Mines studies indicate as much as 5.5 million tons of potash product may be presently "economic" out of the total 13.1 million tons. These resource values are small compared to the total United States reserves but must be considered as a potential target or inducement for future generations. Studies now underway may show that these resources can be developed without jeopardy to the repository. The issue of future penetrations by man is one that cannot, however, be ruled out. This is true for any geologic repository but the probability of such penetration may be somewhat greater for sedimentary and/or salt basins. This eventuality is considered in the repository safety analyses by determining the consequences of such penetrations if they should occur.

Future penetration of the repository by man is one of the several potential failure scenarios which has been calculated. One particular scenario which will be described assumes an open, unplugged borehole penetrates through the repository and connects aquifers above and below the salt. This case is of much greater concern than for a hole which terminates within the salt. In this latter instance, there is no mechanism to continue dissolution of salt and the hole will gradually be squeezed closed. Using the hydrologic parameters experimentally established for the WIPP site, the dissolution of salt by flow in the borehole and transport of the various radioisotopes through the aquifers has been calculated and concentrations and/or possible body burdens of radioactivity determined. Figure 6 illustrates results of calculations for the case where the penetration occurs 1,000 years after sealing a repository which has been filled with both TRU and high-level defense waste. Conservative (worst case) assumptions have been used for this particular calculation. For example, it is assumed that the waste dissolves as rapidly as the salt and that the maximum permeability of the measured range of values exists throughout the site area. Transport of transuranic isotopes through the Rustler aquifers to the exit point at Malaga Bend on the Pecos River, about 14 miles away, is such that it requires about 100,000 years for uranium isotopes to reach their maximum concentration. At this time, a hypothetical man who daily ingested the amount of radioactivity contained in 20 liters of Pecos River water would, over a 50-year lifespan, accumulate a whole body dose less than the annual whole body dose acquired in one year due to natural causes. There is negligible contribution to the radioactive burden from plutonium isotopes due to their high sorption and retardation in the aquifer system. During the 100,000 years following the postulated repository breach, plutonium concentrations in the Pecos River, as indicated by the calculations, would not exceed 10^{-20} $\mu\text{Ci/liter}$. Thorium isotopes also have a high adsorption coefficient but show greater discharge concentrations than plutonium because they

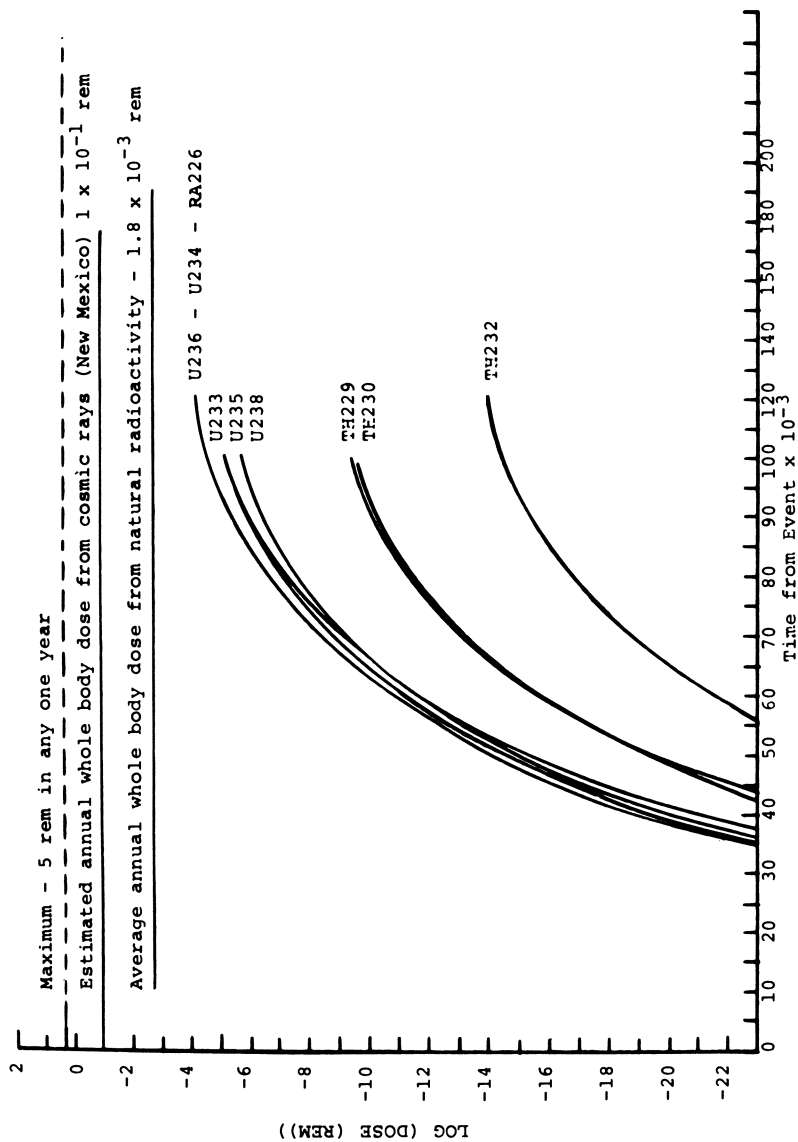


Figure 6. Transuranic isotope concentrations—Scenario 1.
 Integrated total body dose for a 50-yr "Malaga man"—HLW + LLW. Maximum measured permeability used in the transport calculation. Event initiation at 1,000 yr after sealing.

represent daughter products of the more rapidly transported uranium isotopes.

One may also examine the concentration in the aquifers at points closer to the repository. Figure 7 illustrates the concentration profiles at a distances of 1.0 or 0.83 miles from the repository breach for the three isotopes which attain the highest concentration relative to present maximum permissible concentrations (MPC) in water. None of these three isotopes, I-129, Ra-226 and U-236, reach their current MPC. The fluctuations in the I-129 curve represent the engulfment of successive HLW rooms by the solution front.

Similar calculations have been performed for a more severe but much less plausible scenario (Scenario II) which assumes the repository failure occurs at 100 years after decommissioning by massive (3×10^6 liters/year) flow of water down into the repository at one edge and back out to the same aquifer at another point in the repository, dissolving only the salt in the repository horizons. The isotopes of significance for this time frame which were not important in the 1,000 year breach are strontium 90 and cesium 137. The time for transport to the biosphere at Malaga Bend on the Pecos River is long enough that neither isotope represents a significant hazard. The transuranic concentrations shown in Figure 8 for this scenario are higher due to the solutioning mode, not the earlier time frame at which the repository breach was postulated. Intercepting the aquifer with a drill hole at a distance of two miles would find concentrations, 200 years after the breach, above current MPC's for Sr⁹⁰ and Cs¹³⁷ as shown in Figure 9. These calculations also assumed the upper values of measured permeability and that the waste leaches as rapidly as the salt dissolves. More realistic leach rates for the 100 year time frame are being determined and will be applied to this calculation. Significant reduction in the near-field aquifer concentrations are expected from this refinement and the near-field concentrations are not expected to exceed MPC's.

These types of calculations indicate that, even when adopting very conservative assumptions, the risk to the general population by human penetration of the repository in the distant future is very small.

WIPP Experimental Program

A broad based experimental program to investigate the phenomena which accompany the introduction of radioactive waste into salt is an integral part of the WIPP project. The purpose of the experimental program is two-fold: (1) to provide the necessary information to allow confident conversion from retrievable "pilot" operations to full-scale repository disposal operations and; (2) to establish the technical base

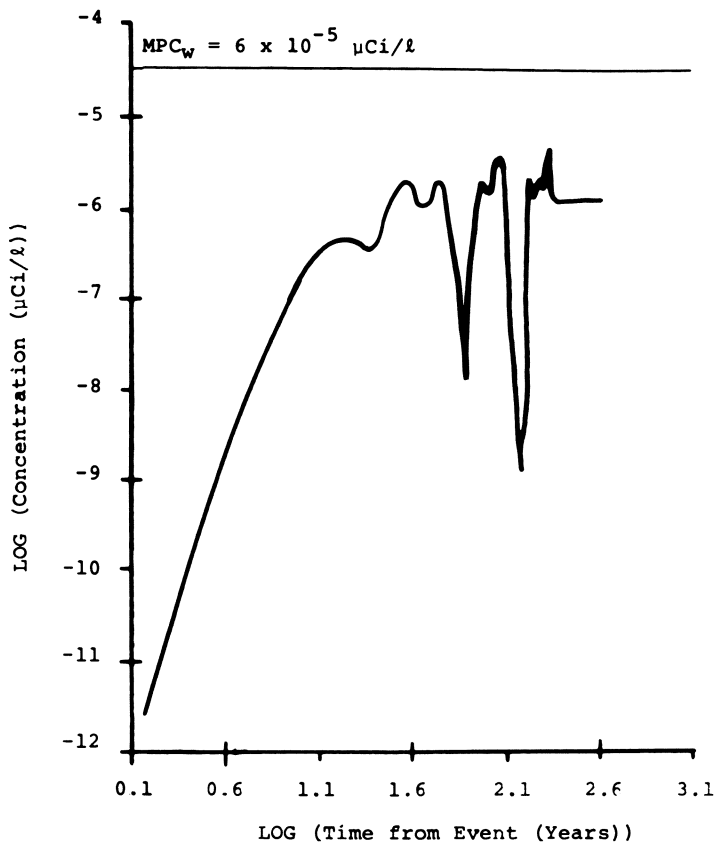


Figure 7a. I129 concentration profile at 1 mi—HLW. Scenario 1. Maximum measured permeability used in the transport calculation. Event initiation at 1,000 yr after sealing.

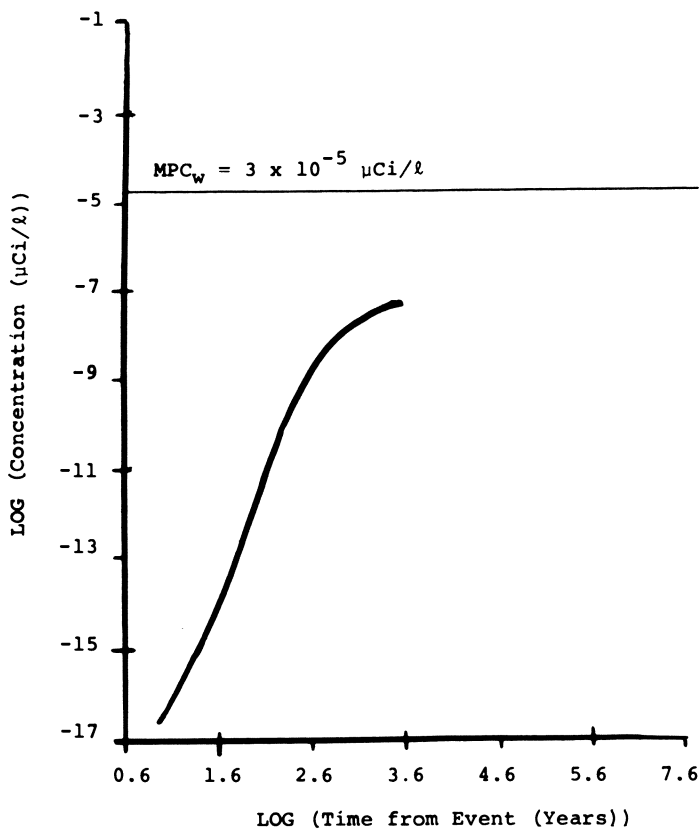


Figure 7b. RA226 concentration profile at 0.83 mi—LLW. Scenario 1. Maximum measured permeability used in the transport calculation. Event initiation at 1,000 yr after sealing.

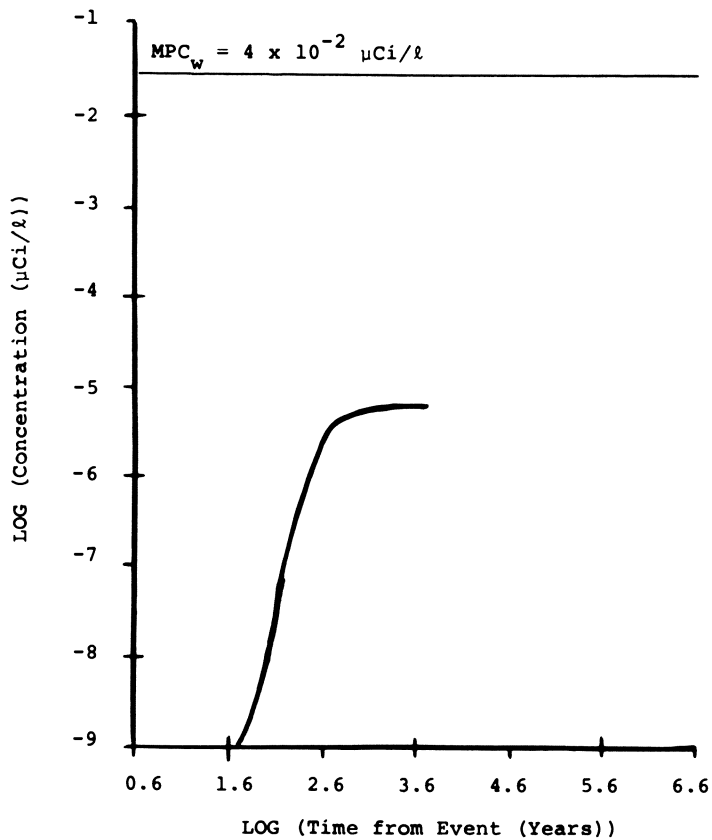


Figure 7c. U236 concentration profile at 0.83 mi—LLW. Scenario 1. Maximum measured permeability used in the transport calculation. Event initiation at 1,000 yr after sealing.

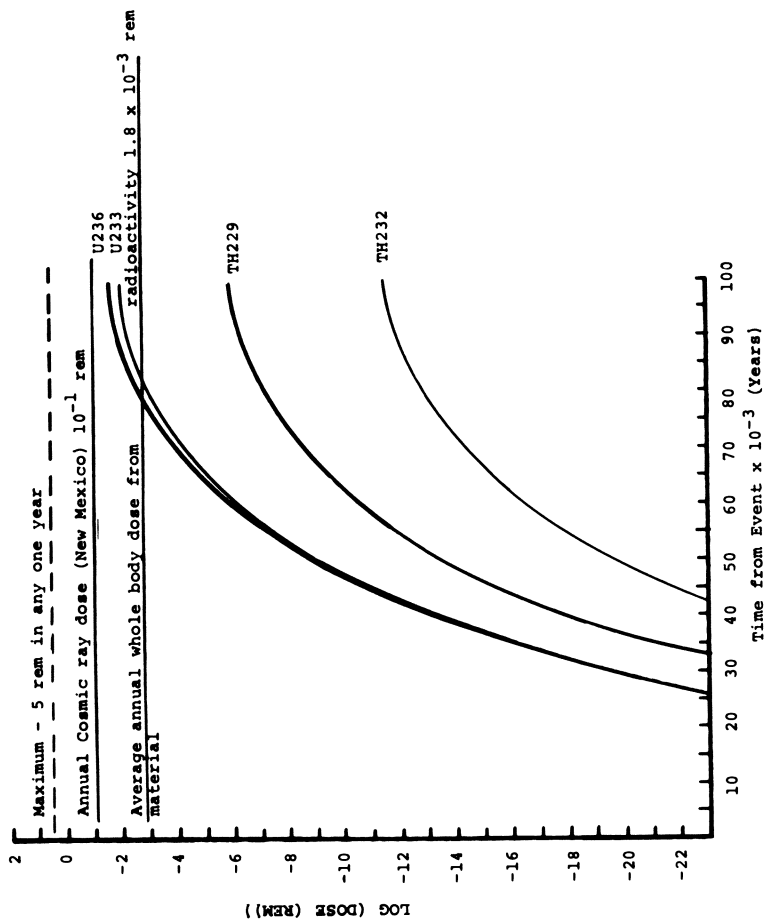


Figure 8. TRU concentrations, Scenario 2. Integrated total body dose for 50-yr "Malaga man"—HLW + LLW. Maximum measured permeability used in the transport calculation. Event initiation at 1,000 yr from sealing.

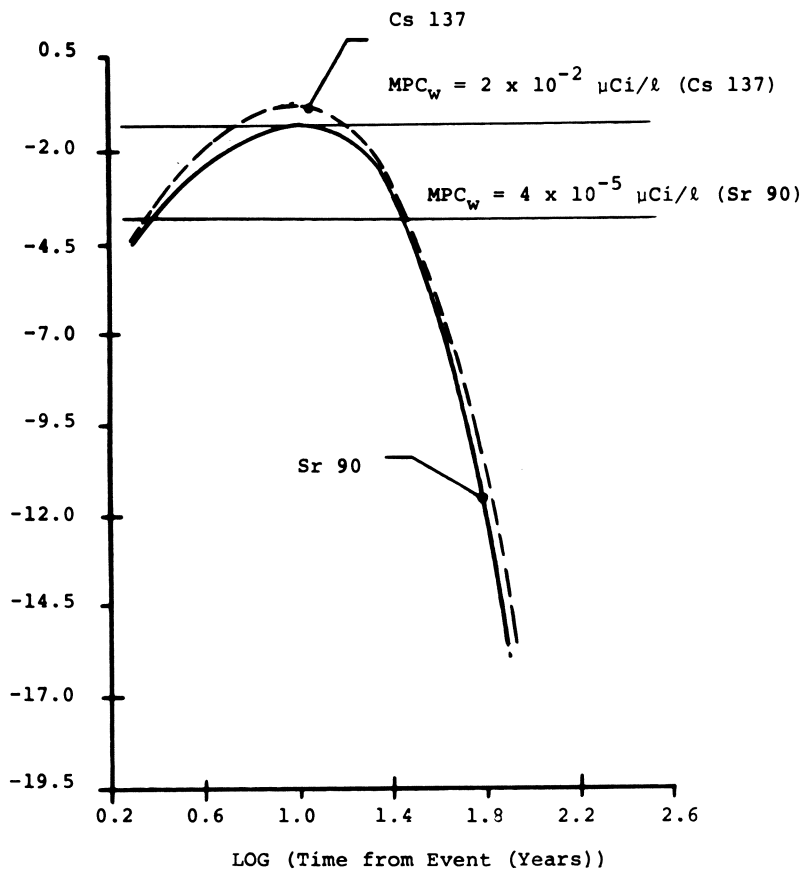


Figure 9. ^{90}Sr , ^{137}Cs concentration, Scenario 2.

^{90}Sr and ^{137}Cs concentrations at 2 mi in the Ruster aquifer following a Scenario 2 breach initiated 100 yr after sealing. Maximum measured permeability used in the transport calculation.

necessary to permit NRC licensing of HLW repositories in salt. These experiments will utilize all categories of waste as well as simulations using electric heaters. Prior to the construction of the WIPP facility, radioactive experiments will be limited to laboratory and bench-scale studies. Existing mines in salt beds are being used to conduct experiments not requiring radioactive material.

During the course of the experimental program, many phenomena will be investigated in detail. Most of these studies will address details of waste/salt interaction, radionuclide migration and salt stability. Results may affect the mode of long-term operation and design of the repository. A few of the technical issues, however, are considered by some to be very fundamental to the concept of geologic disposal in salt. Although the effects arising from these phenomena have been bounded by conservative calculations with acceptable results, it is obvious that a more quantitative understanding is desirable at the earliest possible date. Some of these issues will be discussed in the following section.

Stability of Salt Repositories Under Thermal Load

There are three issues often raised with regard to the mechanical behavior of the canister-salt-repository system when HLW is the emplaced waste form.

1. Motions of the canister relative to the salt
2. Closure rates of repository drifts relative to retrieval requirements to keep drifts open
3. Gross buoyant motion of the repository due to heating of large areas and volumes of salt

High-level waste canister motions in salt have been calculated for the various conditions which could be encountered in salt (5). Using the mechanical properties of salt measured as a function of temperature and assuming ten-year old waste with an initial thermal output of 3.5 kilowatts per canister, the calculated total motion of the canister is less than one meter relative to the surrounding salt.

The potential for altering the mechanical strength of the salt near the canister due to brine migration up the thermal gradient has not been incorporated in such calculations. Experiments on one-meter cylinders of salt are now in progress and in-situ tests will be conducted in salt beds of differing brine content to quantify this potential effect. The salt bed proposed for WIPP high-level waste experiments has an average brine content on the order of 0.5% or less - believed too low to allow the postulated mechanism to occur. However, should the canister motion be accentuated by local weakening of the salt, thin anhydrite layers present at the WIPP site would restrict total canister motion to less than 10 meters.

Thermally accelerated closure of HLW drifts will occur in the salt beds. This is a desired phenomena but it must be limited to an acceptable rate to allow normal operations while the rooms are being filled to capacity. Additionally, during large-scale demonstrations or "pilot" operations where retrievability must be assured, the closure rate must be further limited by reduced thermal loading and/or lower excavation ratios. Other approaches which could be adopted are construction of "oversize" rooms or occasional enlarging of the converging rooms. A typical 15-foot high HLW room in WIPP salt with a 20% extraction ratio and a thermal loading of 30 kW/acre could show about a three foot decrease in height over 5 years unless the above measures are adopted.

The large-scale bouyancy effects of an idealized heated repository have also been calculated (6). Expansion of the heated salt will result in a density differential with respect to the surrounding salt. This plus the reduced viscosity of the hot salt tends to form slow convective cells in the salt. Calculations of a repository in homogeneous salt loaded with 10-year old HLW at 100 kilowatts per acre show a peak upward velocity (approximately 1.5 cm/year) of the repository horizon would occur between 200 and 300 years and then slowly decrease. Displacement would be about 6.5 meters at 400 years. Incorporating a more viscous layer above the repository level to more closely simulate the actual WIPP site geology leads to maximum velocities about one-third those obtained in homogeneous salt. After 400 years the upward displacement for this latter case would be about 2.1 meters. More representative modeling of the geologic stratification in calculations now underway will reduce these values still more. Surface uplift due to thermal effects in either of the cases mentioned is about 0.5 meter at 400 years. This would be imposed on an earlier but equivalent subsidence which occurs due to collapse of the drifts and compaction of the backfill salt.

Validation of these calculations will require several years of precision measurement on an experimental area. Higher thermal loading densities may be employed to accelerate bouyant effects and allow more rapid validation of the code calculations.

Waste/Rock Interactions and Brine Migration

The issue of brine migration in a thermal gradient was previously mentioned in the discussion of thermal effects and canister motions. This phenomenon is not an issue for TRU waste disposal but must be considered for HLW repositories in salt. Since its main effects could be to enhance high-level waste canister motion through "weakened" salt, to corrode the waste canister and to provide a leachant for the waste, the

impacts in WIPP relate mostly to the ease with which retrieval operations may be conducted. For a HLW repository, a less leachable waste form would reduce the consequences of penetration by man. HLW canister integrity has never been considered necessary for adequate long-term isolation in salt repositories but is important if several years of "retrievable storage" are envisioned. These concerns have been recognized and addressed to assure retrieval of the WIPP HLW experiments. Laboratory experiments to quantify corrosion resistance and determine lifetimes of candidate canister materials are underway using anticipated conditions of temperature, pressure, chemistry and radiolysis. In any event, overcoring the waste has always been the retrieval method preferred for WIPP experiments where the number of test specimens involved is relatively small. Thus, impacts of brine migration do not seem to present an obstacle to the concept of disposal in WIPP salt beds. Brine migration and its effects are, however, an area of uncertainty which will be quantified by heater experiments in mines long before any waste is emplaced. In-situ measurements will determine the extent to which brine will migrate to a heat source and the subsequent chemical and physical behavior that could occur if that migration surrounds the canister with brine. The extent to which the salt's mechanical strength is affected will be established. Many of the anticipated chemical and geochemical reactions are now being examined in laboratory experiments. In the event these effects were found to be more serious for retrieval operations and to the repository than anticipated, mitigating measures, now being experimentally tested, could be applied.

Waste Leaching

For purposes of the WIPP program, it is desirable to quantify the leach rate of radioisotopes from potential waste forms to allow realistic source terms to be used in calculations of repository failure scenarios. Lack of quantitative data on long-term stability of the waste form and the potential leaching have resulted in the use of very conservative assumptions in present calculations. Consequence calculations of postulated WIPP repository failures have, to date, assumed the waste form and associated radioisotopes are dissolved as readily as the salt. Even so, the results of the safety analyses show that consequences are not unduly severe. Ability to rely on waste form would reduce the calculated consequences of the direct drill hole penetration scenario to more desirable levels. Leaching studies, under realistic conditions of temperature (up to 300°C) and pressure (up to 3000 psi) with saturated brine leachant, are now in progress at Sandia and other laboratories to develop quantitative data for the possible WIPP waste forms.

Isotope Sorption and Retardation

If the salt beds surrounding the repository were to be breached by any mechanism, then the transport of radioactivity through the resultant hydrologic system becomes an important part of the multiple barrier system. The major portion of any potential radionuclide transport path through the geosphere will be via the aquifers above or below the salt. Considerable laboratory work has been done to establish distribution coefficients (the distribution coefficient, K_d , may be defined as the ratio of the quantity of nuclide sorbed on the media to the quantity of nuclide remaining in solution) for various isotopes being transported through these media by brine solutions (7). Of particular importance to WIPP, plutonium has a large sorption under these conditions with a distribution coefficient K_d of about 2,500 or greater. Consequently, the rate of migration of the plutonium in WIPP aquifers is orders of magnitude slower than that of the transporting brine. It has often been stated that salt itself has no significant ability to retard isotope transport. Sandia studies (7) indicate that on the contrary, the impurities in salt (the residue that would form the transport channel in the event of any salt dissolution) will provide significant retardation with K_d on the order of 20 to 60 for plutonium when based on total weight of halite samples and greater than 10^4 when based on the residue weight. Another concern, related to the organic component of the TRU waste, is the potential formation of chemical chelates which could enhance the migration of radionuclides. This aspect is the subject of laboratory investigation. Further work is being performed in this general area of radionuclide transport and sorption to establish the effective K_d 's and reduce the range of uncertainty under conditions of fracture permeability and with anticipated solutions and aquifer media. Laboratory work is also in progress to develop an additional geochemical barrier (a radionuclide "getter") which could be incorporated into the backfill material or placed around the waste canister. Such getters may be able to effectively retard the migration of nuclides from the immediate vicinity by means of ion exchange, chemical reaction or physical sorption processes.

Gas Generation in the Repository

Thermal, chemical, radiolytic and bacterial decomposition of organics in existing TRU waste with resultant generation of gases is a potential concern for WIPP. Principal gases that one can anticipate are H_2 , CO_2 , CO and CH_4 . During operations, these gases may be safely removed by ventilation. After sealing the repository or individual rooms, the pressure such gases might exert against the seals over long periods of

time must be considered. Present measurements of salt permeability indicate the gases will not diffuse through the salt rapidly enough to avoid this concern. The rate at which salt backfill will recompact and recrystallize and what its permeability will be are not yet well quantified. Studies are being supported at various laboratories to quantify the gas generation rates and quantities possible from the various processes acting on the organics in existing TRU defense waste. These data will be used to determine whether there is a technical repository requirement for incinerating the TRU waste to remove the organic components.

Gases may also be produced from chemical and radiolytic interactions of high-level waste and the anticipated brine which may migrate to the waste canisters. Canister corrosion is expected to occur and can result in H_2 and HCl generation. These reactions must be examined and quantified under the anticipated conditions of pressure, temperature and leachant chemistry to determine whether they can be accommodated or should be prevented in a full-scale HLW repository.

Summary

In summary, a site has been identified for the WIPP which, to date, meets the technical requirements for a geologic repository in bedded salt. This information will be presented to the Department of Energy to allow that agency to determine whether it wishes to pursue this site for development of a waste repository. Several technical issues have not yet been resolved in all their detail but may be adequately bounded to allow the WIPP to proceed without undue concern for its short- and long-term safety. A major function of the WIPP will be to provide an in-situ facility where the detailed phenomenology may be further investigated and become thoroughly understood. Many of the unresolved issues described will be settled through laboratory research and non-radioactive experiments in other mines before WIPP construction starts in 1981.

ABSTRACT

The Department of Energy is proposing to demonstrate the acceptability of geologic disposal of radioactive waste by locating a Waste Isolation Pilot Plant (WIPP) in the salt beds 26 miles east of Carlsbad, New Mexico. The WIPP will serve as a permanent repository for defense generated transuranic contaminated waste and will also be used as a facility in which experiments and demonstrations with all radioactive waste types can be conducted. A conceptual design has been completed and an environmental report on actual and possible impacts will soon be released. There are many technical issues which must be pursued in connection with WIPP. Many of these involve natural geologic and hydrologic phenomena. The introduction of

radioactive wastes into this environment raises more issues which are being investigated in the laboratory and which, in many instances, must also be studied in situ. WIPP will be an underground laboratory where large-scale experiments on thermal effects and waste/rock interactions will be examined. Some of these physical and chemical problems will be summarized in this paper.

Literature Cited

1. Anderson, Roger Y., Deep Dissolution of Salt - Northern Delaware Basin, New Mexico, to be published, 1978
2. Bachman, George O., Geologic Processes and Cenezoic History Related to Salt Dissolution in Southeastern New Mexico, USGS Open File Report 74-194, 1974
3. Bachman, George O. and Johnson, R. B., Stability of Salt in the Permian Salt Basin of Kansas, Oklahoma, Texas and New Mexico, USGS Open File Report, USGS-4339-4, 1973
4. Piper, Arthur M., Subrosion in and about the Four-Township Study Area Near Carlsbad, New Mexico, Report to Oak Ridge National Laboratory, Contract 3745, 1973
5. Dawson, P. R. and Tillerson, J. R., Nuclear Waste Canister Thermally Induced Motion, Sandia Laboratories, SAND78-0556, 1978
6. Dawson, P. R. and Tillerson, J. R., Salt Motion Following Nuclear Waste Disposal, Proceedings of the International Conference on Evaluation and Prediction of Subsidence, to be published, 1978
7. Dosch, R. G. and Lynch, A. W., Interaction of Radionuclide with Geomedia Associated with the Waste Isolation Pilot Plant (WIPP) Site in New Mexico, Sandia Laboratories, SAND78-0297, 1978

RECEIVED January 16, 1979.

Hydrologic Considerations Related to Management of Radioactive Waste

GEORGE D. DEBUCHANANNE and WARREN W. WOOD¹

U.S. Geological Survey, Reston, VA 22092

The objective of geologic isolation of radioactive wastes is to preclude their reaching the biosphere until after they have decayed to the extent that they no longer constitute a health hazard. Concern over radioactive wastes from military, industrial and research uses has elicited many lines of commentary and deep concern from many individuals. In California, the concern about waste disposal was the focal point in establishing a moratorium on the construction of new reactors until a satisfactory waste disposal technology could be demonstrated.

There are several pathways by which buried wastes can enter the biosphere; these include emission of gases from decaying organic material buried with the waste, erosion of overlying material resulting in waste exposure, waste movement to the land surface through tectonic activity, intrusion by man, and leaching and seepage into ground-water systems. It is generally agreed that the long-range problem of intrusion by man is the most likely mechanism for contact with the biosphere, as institutional control, even on the most restrictive burial sites, is likely to be less than 100 years. The earth science community generally perceives that transport by ground water is the most important natural mechanism for bringing buried wastes to the biosphere. The hydrologic evaluation associated with the transport of radionuclides from a repository can be centered on three areas of uncertainty: (1) characterizing the existing hydrologic system at a given site, (2) predicting events that will alter the hydrologic properties with time, and (3) evaluating the interaction of the wastes with the burial environment.

Most ground-water hydrologists would prefer to speak in terms of waste isolation, emplacing waste in a repository, or waste dispersion, rather than disposal. Disposal, of course, not only implies that no attempt will be made to retrieve the material but it also implies future neglect. Isolation as, for example,

¹Current address: Department of Geosciences, Texas Tech University, Lubbock, Texas 79409.

This chapter not subject to U.S. copyright.
Published 1979 American Chemical Society

in a repository, or planned dispersion, on the other hand, carry with it the implication that the wastes at a site would be monitored and managed. All sedimentary rock sequences permit some movement of water through them, and, of course, moving water will leach the buried waste resulting in transport with the moving water. Realistic answers to problems of waste isolation must consider a philosophy of controlled dispersion over very long time periods.

Volume of Waste

The DOE (Department of Energy) which is the lead agency in matters of nuclear energy, has specified three categories of waste: (1) high-level, (2) transuranium contaminated, and (3) other than high-level waste, generally called low-level. High-level waste results from reprocessing of spent nuclear reactor fuel. The transuranic-contaminated waste (TRU) contains concentrations greater than 10 nanocuries per gram (nCi/g) of the man-made elements with atomic numbers greater than 92. The remainder of the waste, with the exception of mine and mill tailings and spent fuel rods is considered low level. Fuel rods have only recently been considered a waste form as a result of the Administration's decision to eliminate reprocessing of spent nuclear fuel and are classified as high-level waste.

Low-Level Waste. Low-level wastes are further divided into categories of special nuclear material, source material, and by-product material, depending on the isotopes contained. Special nuclear material refers to uranium 233, plutonium 239, and uranium containing more than the natural abundance of uranium 235. Source material refers to materials containing 0.05 percent or more of thorium or uranium in any physical or chemical form except that covered under special nuclear material. By-product materials consist of all other radioactive materials including fission and activation products.

Burial of transuranium and low-level waste in shallow pits and trenches has occurred since the early days of the Manhattan Project. In the United States, 14 burial sites have been operated by the Department of Energy, 12 of which are presently active; and six state-owned sites have been operated by licensed commercial firms. Three of the commercial sites are presently active (figure 1).

Through 1977, approximately 1,306,000 cubic meters (1) of military waste material had been buried in approximately 280 hectares at the DOE sites. The rate of accumulation at these sites has remained relatively constant and is now approximately 33,000 cubic meters per year. Through 1977, approximately 500,000 cubic meters of waste had been buried in 300 hectares at the six commercial sites (2). The present annual rate of burial is approximately 60,000 cubic meters (3) and is increasing rapidly

Publication Date: April 6, 1979 | doi: 10.1021/bk-1979-0100.ch003

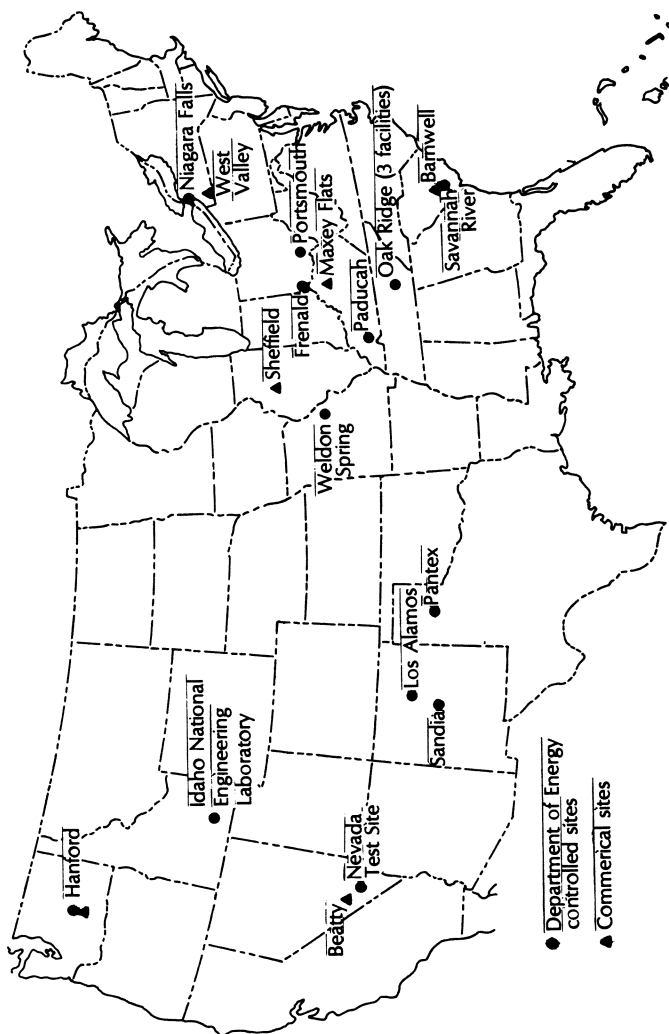


Figure 1. Locations of burial grounds of solid low-level radioactive waste

(figure 2).

Between 1946-1970, approximately 28,000 fifty five-gallon drums of military and commercial low-level waste were disposed of in the Atlantic Ocean and approximately 47,000 in the Pacific (4). This practice was discontinued in 1970 and since then all low-level waste has been buried in shallow trenches.

Holcomb (2) reports that through 1976, commercial burial grounds had disposed of 951,468 kilograms (kg) of source material, approximately 4 million curies of by-product material, and 1,667 kg of special nuclear material as well as 113 kg of TRU waste (3). The DOE sites, according to Duguid (1), contain 7,292,124 kg of source material and 11 million curies of by-product as well as more than 700 kg of TRU waste. An additional 6 million liters of a waste-cement grout slurry has been injected into hydrofractured shale at the Oak Ridge disposal site in Tennessee.

High-Level Waste. There are approximately 285 million liters containing approximately 590×10^6 curies (5) of military and 2.3 million liters of commercial high-level liquid waste (6) presently stored in tanks. Although the volume of high-level military waste is much greater, the curie content of strontium 90 of both sources is approximately the same if stored spent fuel rods from commercial reactors are included in the inventory. The total curie content will be the same for both sources by 1985 at the present rate of use (5). To date, there has been no disposal of any high-level waste.

Waste Disposal Problem

Radioactive waste isolation in a geologic medium is an example of a problem that will extend beyond the foreseeable duration of existing human institutions. The potential effects are extremely important and present a significant challenge to institutions designed for dealing with problems of lesser complexity and shorter duration. In this case, not only are the human institutions strained, but the science of hydrology presently lacks techniques and methodology to define adequately the flow in several common types of hydrologic systems.

There are three areas of hydrologic uncertainty involved in the geologic isolation of radioactive waste. The first concerns the characterization of existing hydrologic systems; that is, our inability to quantitatively define the existing conditions controlling the movement of radionuclides. The second is the uncertainty of predicting disruptive events such as earthquakes and climatic changes which alter the properties and hydrologic conditions of the system. The third area of uncertainty is how the waste itself and the method of emplacement affect the hydrology of a system.

Disruptive events are generally not considered important in

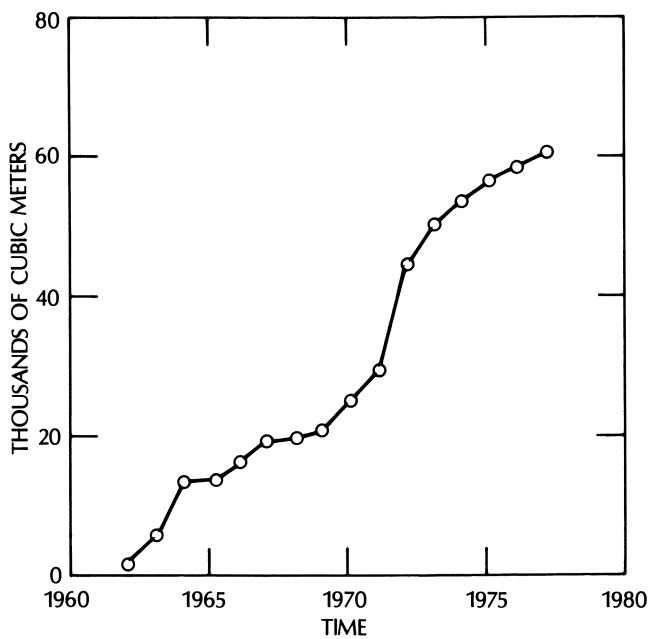


Figure 2. Yearly total volume of commercial low-level waste buried within the conterminous United States

the evaluation of low-level disposal sites because of the small amount of long-lived radionuclides present. However, the other areas of uncertainty would affect modes of geologic isolation of high-level waste. The effect of waste emplacement on the hydrologic properties of the site have generally been given only cursory evaluation in past studies of low-level waste sites. This has proved to be shortsighted, and selection criteria for new sites will almost certainly contain specific guidelines on such things as cap or cover design and type of waste form permitted to be buried.

These three broad areas of uncertainty form the basis of present and proposed research on radioactive waste and are the subject of this paper. Consider first the problem in defining existing systems in terms of the hydrogeologic properties in relation to transport by ground water. Traditionally, ground-water hydrologists have been involved with finding and evaluating supply systems for irrigation, industrial, municipal, and domestic users. Waste isolation studies have been jokingly referred to as "anthydrology" because hydrologists are being forced to study flow systems exhibiting very low, rather than high, ground-water fluxes. This change in philosophy has presented a major challenge to the study of ground-water hydrology, involving focusing more attention on the fundamentals of flow and geochemical reactions in materials of low permeability. These low permeability sites require new methodology and techniques to evaluate the systems.

One of the approaches in evaluating the permeability of an aquifer system is to perform an aquifer test by pumping a well and observing the water-level decline with time in nearby observation wells. In systems of low permeability, sufficient water for a pumping test is generally prima facie evidence that it is unacceptable as a disposal site. Consequently, a new set of "parlor tricks" is needed to define the permeability of those types of media.

Suitable techniques are not available to evaluate material of low permeability in an area the size of either a high or low-level repository. Only a very small area of a few tens of centimeters, such as the area in a core hole or that immediately adjacent to the observation well, presently can be evaluated. Drilling many holes and applying techniques suitable for characterizing small areas would create numerous potential waste-migration pathways. That is, testing a site adequately by these limited methods would destroy any integrity that the site possessed. Additionally, a new technique is needed to identify small zones of high permeability within a large volume of rocks with low permeability. These highly permeable zones may be fractures or changes in facies of the media, solution openings, or they may result from any other factor that can locally alter the permeability of a hydrologic system.

Another area of uncertainty in describing existing systems

pertains to flow and transport through fractures. Both stochastic and deterministic approaches are presently being pursued in attempting to model flow in fractured media. Opinion within the ground-water profession is divided on which will yield the best information as neither one has been successfully applied in the field. With the current state of ability to define a given hydrologic system, it would appear that the stochastic approach may give the most useful results. However, if new geophysical or other techniques become available to permit definition of a fracture system, the deterministic modeling approach might be more useful.

For years, hydrologists concerned with water supply have used models developed for flow in granular media to predict flow in highly fractured media. However, any apparent success in this approach was fortuitous because (a) the pumping well integrated a large area and was able to "see" many fractures as if they were pores in a granular media, and (b) because the permeability contrast between the two types of flow was relatively small in the system. Neither of these situations prevails in rocks of low permeability. Although there has been some success in predicting water-level changes in fractured media of relatively high permeability, there has been little or no success in predicting the movement of dissolved materials in these media. The oil industry has developed and used a double porosity model to describe flow in certain fracture systems (7). Little data on application to actual field problems are available in the literature suggesting that this model has had only limited success and has been used only after the fact, not in a predictive mode.

Defining the movement of water in rocks of low permeability by chemical methods, such as the use of tracers, age dating of water, and isotope ratios, has met with limited success for the same reasons as have the physical methods. That is, they are incapable of describing the permeability distribution in an adequately large area.

The unsaturated zone, where most of the low-level waste is buried, could probably be used for high-level waste after cooling but it does not lend itself to the regional approach to defining permeability. Additionally, the laboratory methods of evaluating permeability of unsaturated material are extremely difficult to perform consistently. However, an air permeability technique that may prove useful in evaluating the zone between the surface and the water table was developed by Weeks (8). The technique uses normal barometric fluctuations measured at different depths in the formation to determine permeability to air which can be used to determine permeability to water.

Consider now the effects of the waste and emplacement of the waste on the hydrology of the system. Present thinking suggests that a mined underground cavity in bedded salt will be the first choice for a repository for high-level waste. The rationale for

this choice of medium is that the presence of a thickly bedded salt which has been present for millions of years without dissolution must preclude the existence of any significant regional ground-water flow through the salt. Arguments against this thinking are weak if breccia pipes, solution cavities, brine pockets or other evidence of solution are absent from the formation. However, other areas of concern to the hydrologist are: (1) the hydrologic effects of excavation of the shaft and cavity on hydrology; for instance, will fractures develop and permit a breach of the confining beds that have protected the salt for geologic periods of time and consequently permit flow of ground water? (2) Will the backfill of the mined cavity after emplacement of the waste be sufficiently dense to prevent excessive subsidence and cracking of overlying beds and therefore permit access of ground water? (3) Will the heat caused by the radioactive decay of the waste cause thermal expansion and subsequent contraction, resulting in collapse of the overlying formation and access of ground water to the repository through fractures? (4) Will the heat of the waste cause interstitial or grain-boundary water to migrate toward the waste and thereby significantly alter the structural properties of the salt in the immediate area of the waste? (5) How will the radionuclides behave chemically in a brine under reducing conditions at relatively high temperatures? That is, will their sorptive characteristics be significantly altered, and if so, what type of predictive capabilities do we possess for these conditions?

Better cap designs (trench covers) are needed for low-level waste sites so that the materials are less permeable. Present practice results in as much as 50-percent void space in the trench, in part from the decay of organic material and in part from the procedures for waste emplacement. This results in compaction of the buried waste and subsidence of the cap. The chemical characterization of low-level waste is more difficult than that of high-level waste because of the heterogeneous nature of the waste and associated materials. Thousands of organic chemicals including chelating agents may form complexes with nuclides rendering them nonsorbable. Also, a viable microbiological population continually alters the composition and nature of the waste.

The chemical behavior of waste in the unsaturated zone is a large unknown. For example, definition of the number of sorption sites available to a solute is difficult or impossible because unknown and variable amounts are occupied by interstitial gas rather than water. Are the kinetics of reaction affected by less-than-complete saturation? These are not trivial questions, as most of the low-level disposal sites are constructed in the unsaturated zone. Winograd (9) suggested that certain areas underlain by thick unsaturated zones might make feasible repositories for high-level wastes.

Two areas of uncertainty, that concerning the characteriza-

tion of existing hydrologic systems and that associated with the hydrologic effects of waste emplacement and waste-rock interactions, lend themselves to the scientific approach of testing a hypothesis by a suitably designed experiment. The final general category of uncertainty to be discussed, that of disruptive events, is more difficult to overcome because of the geologic time involved and the lack of basic knowledge about the fundamental processes involved. That is to say, geology is still basically a science of description rather than prediction.

For example, we don't know the basic mechanism controlling the development of continental glaciation and its recurrence interval. Again, this is not a trivial question because the hydrology of almost every area selected for a repository would change significantly if the type of glaciation that ended 10,000 years ago were to recur. The distribution of hydraulic head would be altered significantly as would the total flux of ground water moving through a given system. The length of ground-water flow paths would become shorter and the rate of erosion of surficial material might be significantly increased.

There is need to avoid locating a repository in an area where igneous intrusions would be likely to occur. This should not be difficult as we have millions of years of geologic records and an observed systematic pattern of intrusion. However, when we consider seismic events, our history is limited to about 200 years. That is, it would be extremely difficult to say that a given area will not have an earthquake of, say, magnitude 8 or greater (Richter scale) in the next 250,000 years. Our concern with earthquakes is not so much that the waste would be brought directly to the surface, but that fractures in the formation chosen for the repository would permit ground-water movement which could ultimately transport the waste to the human environment.

To quote a recent publication of the U.S. Geological Survey, "Past geologic events such as faulting, seismic disturbances, or climatic changes have not been random, but a deterministic explanation for their frequency, place of occurrence, magnitude and rate of change are difficult to establish. Regardless of whether deterministic or probabilistic models are favored to explain particular past geologic events, the use of the geologic record to predict future events is a formidable task." (10)

This is not to say that all is doom and gloom. Although many of these tasks are formidable, the earth-science community believes them to be tractable and that a successful geologic repository for radioactive waste can be constructed. We only plead that our ignorance of earth's processes be considered in the development of a repository and that any repository constructed prior to the acquisition of the needed fundamental knowledge contain many independent natural and manmade barriers to radionuclide transport to compensate for our lack of knowledge.

Literature Cited

1. Duguid, J.O., "Assessment of DOE low-level radioactive waste solid disposal storage activity", Battelle Columbus Laboratory, BMI-1984, 1977.
2. Holcomb, W.F., Nuclear Safety, 1978, 19, (1), 50-59, "A summary of shallow land burial of radioactive waste at commercial sites between 1962 and 1976, with projections".
3. National Academy of Sciences, "The shallow land burial of low-level radioactively contaminated solid waste", 2101 Constitution Ave., N.W., Washington, D.C. 20418, 150, 1976.
4. Dyer, R.S., "Environmental surveys of two deep sea radioactive waste disposal sites using submersibles" in Symposium, Management of Radioactive Waste from the Nuclear Fuel Cycle, IAEA, 317-338, 1976.
5. Krugmann, H., and von Hippel, F., Science, 1977, 197, 883-885, "Radioactive waste: a comparison of U.S. military and civilian inventories".
6. GAO Report to Congress, "Nuclear energy dilemma: disposing of hazardous radioactive waste safely", 73, 1977.
7. Rossen, R.H., Soc. Petr. Eng. Jour., June 1977, "Simulation of naturally fractured reservoirs with semi-implicit source terms".
8. Weeks, E.P., "Field determination of vertical permeability to air in the unsaturated zone", U.S. Geol. Survey Prof. Paper 1051, 41, 1978.
9. Winograd, Isaac J., EOS, 1974, 55, (10), 884-894, "Radioactive waste storage in the arid zone".
10. Bredehoeft, J.D., England, A.W., Stewart, D.B., Trask, N.J. and Winograd, I.J., "Geological disposal of high-level radioactive wastes--earth-science perspectives", U.S. Geol. Survey Circ. 779, 1978.

RECEIVED January 16, 1979.

Disposal of Radioactive Waste in Granitic Bedrock

B. ALLARD¹, J. RYDBERG, H. KIPATSI, and B. TORSTENFELT

Department of Nuclear Chemistry, Chalmers University of Technology,
Fack, S-402 20 Göteborg 5, Sweden

A requirement, as stated in a recent Swedish law, for a continuation of the extensive nuclear power program in Sweden (6 operating power reactors at present and 7 more in operation in 1985) is that the engineering problems and safety aspects connected with the disposal of the high-level waste (HLW) or the unprocessed spent uranium fuel (SUF) are thoroughly investigated. A completely safe disposal of either HLW or SUF must be guaranteed and technically proven by the nuclear power industry.

The Nuclear Fuel Safety Project (Kärnbränslesäkerhet, KBS) was started in December 1976 with the purpose of studying all important aspects of waste disposal in Sweden. Two different alternatives for final storage of HLW and SUF, respectively, have so far been suggested and studied in detail by KBS (1). Some data for these two concepts are given in Table I and in Figure 1.

For both alternatives a storage in granitic bedrock at a depth of 500 m is considered. This is well below the groundwater table. The waste canisters will be placed in vertical holes in horizontal tunnels and both holes and tunnels will be filled with a backfill material (c.f. Figure 1).

In this paper some of the chemical aspects of such a waste storage in granitic bedrock are discussed (2-7).

The Multi-Barrier Principle

For a repository in the ground there are several independent barriers between the waste and the biosphere, such as

- long-term geological stability and very limited groundwater flow at the selected site
- resistant canister material
- waste form with low solubility
- backfill material with nuclide retaining properties
- chemical retention in the ground.

¹ Current address: Transuranium Research Laboratory, Oak Ridge National Laboratory, P. O. Box X, Oak Ridge, Tenn. 37830, USA.

American Chemical Society
0-8412-0498-5/79/47-100-047\$07.00/0
© 1979 American Chemical Society
1155 16th St. N.W.
Washington, D.C. 20036

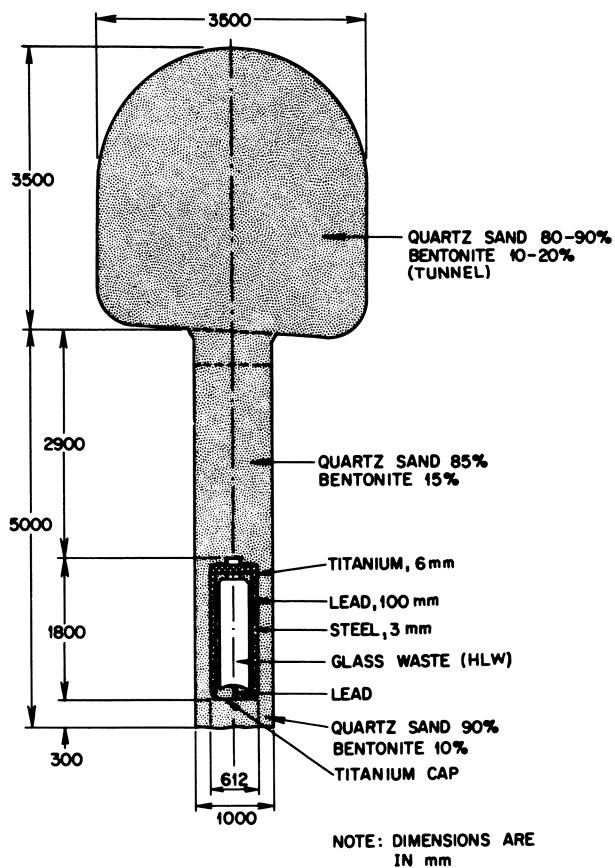


Figure 1a. Storage of HLW in the ground (KBS) (1)

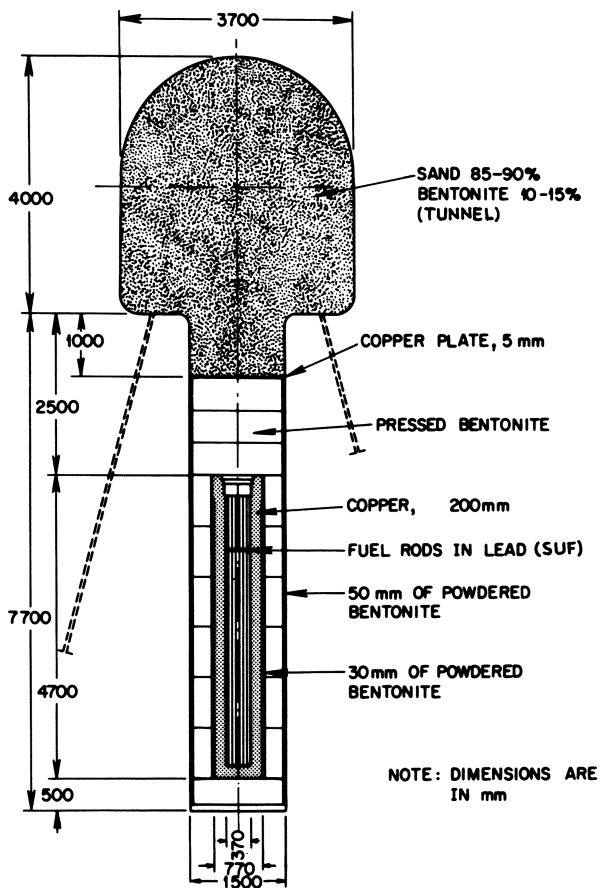


Figure 1b. Storage of SUF in the ground (KBS)(1)

Table I
Some data for the two concepts for storage of HLW and SUF
as suggested by KBS (1)

Canister property	Reprocessed vitrified HLW	Unreprocessed SUF
Equivalent waste amount ^a	From 1 ton SUF ^b	1.3 ton SUF
Central part composition	420 kg borosilicate glass with 9% FP ^c	550 fuel pins + lead in voids
Central part weight	450 kg, incl. 3 mm stainl. steel cladding	2 ton fuel + 2.5 ton lead
Outer canning	100 mm lead + 6 mm titanium	200 mm copper
Total canister:		
Dimensions	0.6·1.8 m	0.8·4.7 m
Weight	3.9 ton	20 ton
Canister surface temp:		
Max ^d	65°C	77°C
After 1000 y	35°C	50°C
Bentonite backfill (outer barrier)	0.2 m	0.4 m
Rock hole dimensions	1.0·5.0 m	1.5·7.7 m

^aAt 33,000 MWd/ton U burn-up

^b38 kg fissions products (FP), <3 kg U, <0.05 kg Pu, <1 kg other transuranium elements

^cGlass of this composition will be returned to Sweden after reprocessing at the French site at La Hague

^dMaximum temperature reached about 15 years after fuel discharge from the reactor

Geological Stability. A long-term geological stability is a necessary requirement for a waste repository in the ground. Otherwise the whole concept of geological storage fails. The granitic bedrock of eastern Scandinavia belongs to the Fennoscandian shield which is one of the most stable parts of the earth's crust. This region has been largely unaffected by tectonic activities in other parts of Europe during the past 900 million years. Existing faults and fractured zones are of early origin, and any future local tectonic movements would most likely be located along already existing faults. Ten to twenty glacial periods during the quarternary period have not significantly changed the fracture pattern or the

water permeability of the rock, and isostatic movements due to future glaciations will not affect a 500 m deep depository.

Five different areas within the Fennoscandian shield have been examined in the KBS-project (Forsmark, Karlshamn, Oskarshamn, Stripa and Studsvik). The permeability in these areas is 10^{-9} m/s as an average but usually below $4 \cdot 10^{-10}$ m/s in dense rock. In some locations values below $2 \cdot 10^{-12}$ m/s were recorded (the detection limit)(8). The time for the groundwater to migrate from a depth of 500 m to the surface is 3000 years or more in these places (9). In the dense parts of the rock the migration of only a few meters would require thousands of years. The groundwater flow at a depth of 500 m is 0.1 - 0.2 l/m²·y or less (10).

For a waste storage site a fault-free block surrounded by faults at some distance (a few km away) would be required. Such areas can be found at many locations within the Fennoscandian shield.

Canister Material. Considering the low groundwater flow and the composition of the groundwater it will take many thousands of years to dissolve the outer titanium cladding of the HLW-canister (11), and millions of years would be required to transfer all lead around the glass container into water soluble complexes (12). However, stress or pinhole corrosion leading to local penetrations already after 500 years can not be excluded. The formation of voluminous lead hydroxide would probably prevent free groundwater flow around the exposed glass even after penetration of the canning.

Under the conditions to be expected in deep granitic groundwater copper is thermodynamically stable. Considering possible oxidation mechanisms and the concentrations of potential oxidants in the ground the lifetime of the copper canister around the SUF would be at least several hundred thousand years before penetration occurs, probably more than a million years (13).

Waste Form. The leach rates of radionuclides by groundwater are slow both for vitrified HLW and for SUF. A glass lifetime of at least 3000 years is expected, assuming unlimited supply of water (14). If the limited solubility of glass in groundwater is considered as well as the low water flow the lifetime would be several orders of magnitude larger.

The dissolution time for the unprocessed fuel would be at least 1 million years due to the limited water supply, even if a rapid oxidation of uranium to the hexavalent state and a subsequent formation of water soluble carbonate complexes are assumed (15). Since the conditions are reducing in the groundwater (see below) the dissolution time would probably be several orders of magnitude larger. The insignificant dissolution of uranium and fission products observed in the Oklo-deposit (16) is an example of a similar extremely slow leaching process in the natural environment.

Backfill Material. The canisters are surrounded by a backfill material. This barrier will serve several different purposes, such as to

- keep the canisters in a fixed position
- transfer heat from the canisters to the surrounding rock
- release stresses from the canisters
- fill up the hole around the canisters as well as penetrate into major cracks and fissures
- act as a chemical barrier
- be non-transmissive for water (prevent free water flow).

Thus, a proper backfill material may act as a very effective chemical and mechanical barrier, preventing free migration of radionuclides released from the waste containers.

Chemical Retention in the Ground. Due to chemical interactions with the rock and with species in the groundwater the radionuclides will be retarded. This would be the final barrier preventing a release into the biosphere.

The biological hazards from HLW and SUF are dominated by ^{90}Sr and ^{137}Cs during the first centuries after discharge from the reactor and by the actinides with daughter products plus some long-lived fission products (^{99}Tc , ^{129}I and others) in the long-term perspective. Within the KBS-project the sorption of 14 different elements (Cs, Sr, Ra, Zr, Tc, I, Ce, Nd, Eu, Th, U, Np, Pu and Am) has been studied for different ground material and under environmental conditions (2,3). These studies were required for the evaluation of the effectiveness of the ground as a chemical barrier and will be discussed below. The mechanism of the radionuclide release from the canisters into the groundwater as well as the effectiveness of the other barriers mentioned above will not be discussed any further.

Geochemistry of the Repository

The Hostrock and Backfill Material. Most crystalline igneous rocks, including granite and gneiss, are composed of a comparatively small number of rock forming silicate minerals like quartz, feldspars (albite, microcline, anorthite etc.) micas (biotite, muscovite) and sometimes pyroxenes, amphiboles, olivine and others. Besides, there is a rather limited number of common accessory minerals like magnetite, hematite, pyrite, fluorite, apatite, calcite and others. Moreover, the weathering and alteration products (clay minerals etc.) from these major constituents of the rock would be present, especially on water exposed surfaces in cracks and fissures.

In the Swedish KBS-project a mixture of bentonite and quartz (10:90) or compacted bentonite were proposed at an early stage as possible backfill materials. Bentonite is a rather common montmorillonitic clay with good mechanical properties and chemical

stability under the conditions expected in a repository and moreover with a high ion exchange capacity (17).

The Groundwater Composition. The composition of the groundwater can be related to (18,19)

- equilibria and exchange reactions with the minerals of the rock
- exchange reactions with the atmosphere and the biosphere
- intrusions of e.g. saline water not in equilibrium with the other components of the rock/groundwater system.

The most important species in the groundwater are HCO_3^- - CO_3^{2-} , which largely origin from the atmospheric CO_2 and are usually not in true equilibrium with the rock itself. Even in groundwater from rocks with only traces of carbonate minerals, the HCO_3^- -concentration would usually be 1 mM or higher. The pH-value is determined by the HCO_3^- -concentration (roughly inverse proportionality).

Deep groundwaters from igneous rocks are usually saturated with respect to CaCO_3 , which limits the maximum Ca^{2+} -concentration and thereby also indirectly determines the F^- and H_2PO_4^- -concentrations due to the limited solubility of CaF_2 and Ca-phosphates. Both F^- and H_2PO_4^- are usually found in the groundwater due to the presence of accessory minerals like fluorite and apatite in the rock.

Because of exchange reactions with the clay minerals the concentrations of Ca^{2+} , Mg^{2+} and Na^+ are interrelated unless relict saline water is present, giving too high Na^+ -concentrations.

Both SO_4^{2-} (originally coming from surface water) and K^+ tend to be present at relatively constant concentrations independent of other species in the water. The Cl^- -concentration is usually low unless saline water is present.

Thus, the composition of the groundwater from a large variety of igneous rocks can be predicted within rather narrow concentration ranges for the major constituents. In Table II the expected concentration ranges are given, considering geochemical equilibria and analysis data from deep groundwater (18,19). The composition of the two artificial groundwaters used for the laboratory measurements are also given (2,3). The standard water Aq₂₉₃ would represent an average groundwater. In Aq₁₁₀₅ the concentrations of Na^+ and Cl^- have been increased by a factor of about five and all the other species by a factor of two, in order to simulate the effect of salt water intrusion.

Beside the inorganic components given in Table II organic acids, mainly fulvic acids, would be present in the groundwater. The concentrations of these organics in deep groundwater from igneous rocks are usually in the order of tenths of mg/l (19), and rarely much higher.

The Redox Potential. The groundwaters at great depths in igneous rocks are essentially free from dissolved oxygen (20). The redox potential is determined and buffered by the presence of redox couples, mainly Fe(III)/Fe(II) . For the reaction

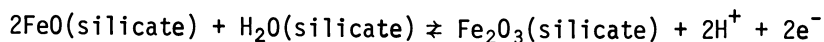
Table II
Groundwater composition in granitic bedrock at great depth
and the artificial standard waters used
(original concentrations are given)

Specie	Probable conc. range		Artificial standard waters			
	Min mg/l	Max mg/l	Aq ₂₉₃ mg/l	mM	Aq ₁₁₀₅ mg/l	mM
pH	7.2-8.5		8.2		8.2	
NH ₄ ⁺	0.1	0.4				
Na ⁺ ^a	10	100	42	1.83	288	12.53
K ⁺	1	5	4	0.13	10	0.26
Mg ²⁺	5	20	7.5	0.31	15	0.62
Ca ²⁺	25	50	37.5	0.94	75	1.87
Mn ²⁺	0.1	0.5				
Fe ²⁺ ^b	0.5	20				
F ⁻	0.5	2	0.7	0.04	1.5	0.08
Cl ⁻ ^a	5	100	93	2.62	500	14.10
HCO ₃ ⁻	60	400	100	1.64	200	3.28
SO ₄ ²⁻	1	15	7.5	0.08	15	0.16
SiO ₂	5	30				
NO ₂ ⁻	0	0.1				
NO ₃ ⁻	0.1	0.5				
PO ₄ ³⁻	0.01	0.1				
HS ⁻	0	1				
Σ			293	8.6 ^c	1105	31.8 ^c

^aConsiderably higher when contaminated with salt water

^bRelated to the redox potential; 0 in aerated groundwater

^cIonic strength at equilibrium



illustrating the redox equilibrium between iron containing layer silicates, the following Eh-pH-relationship can be deduced (21):

$$\text{Eh} \approx 0.21 \pm 0.1 - 0.06\text{pH} \quad (\text{V}) \quad (1)$$

assuming extreme combinations of Fe(III)- and Fe(II)-concentrations (between 0.1 and 40% by weight as the oxides). These extreme Eh-pH-relationships are likely to cover the expected redox potential range in the rock/groundwater system of almost any igneous rocks.

Among the long-lived radionuclides, the sorption behaviour of Tc, U, Np and Pu would be highly dependent on the oxidation state which would be determined by the redox potential and pH of the water. In Figure 2 the $\text{Fe}_2\text{O}_3/\text{FeO}$ -equilibrium curves according to eqn (1) are given together with calculated equilibrium curves for $\text{TcO}_4^-/\text{TcO}_2(\text{s})$, $\text{U(VI)}/\text{U(IV)}(\text{aq})$, $\text{Np(V)}/\text{Np(IV)}(\text{aq})$ and $\text{Pu(IV)}/\text{Pu(III)}(\text{aq})$ (22,23). These equilibrium curves were calculated considering the hydrolysis that would be expected in groundwater with a pH around 8. Some *in situ* measurements from deep granitic groundwaters are included (Stripa and Finnsjön, Sweden)(24), and from a uranium mine (Svornost, Czechoslovakia)(25) with corresponding uranium concentrations. From these data the redox sensitive elements would be expected to exist predominantly as Tc(IV), U(IV), Np(IV) and Pu(III), respectively, in reducing groundwater. The scarce *in situ* data for uranium do not contradict the proposed preference to the tetravalent state.

Sorption Measurements

The transport process from the repository is schematically illustrated in Figure 3. Radionuclides and corrosion products would diffuse from the canister into the groundwater, and the migration will then be retarded first in the backfill barrier and after that in the bedrock.

With the suggested encapsulation (lead or copper) the formation of radiolysis products or changes of the properties of the backfill material due to irradiation can be neglected.

The Distribution Coefficient. As a measure of the sorption and retarding capacity of the rock and clay the mass related distribution coefficient K_d [m^3/kg] was used, defined as

$$K_d = q_A/C_A \quad (2)$$

where q_A = nuclide concentration in the solid phase [moles/kg]
 C_A = nuclide concentration in the water [moles/m^3]

Physico-Chemical Conditions. The chemical interactions between radionuclides and the surrounding ground material would be due to several different mechanisms, such as

- ion exchange
- adsorption reactions of ions or complexes
- reversible formation of non-soluble complexes
- irreversible formation of non-soluble complexes; mineralization
- formation of colloid particles.

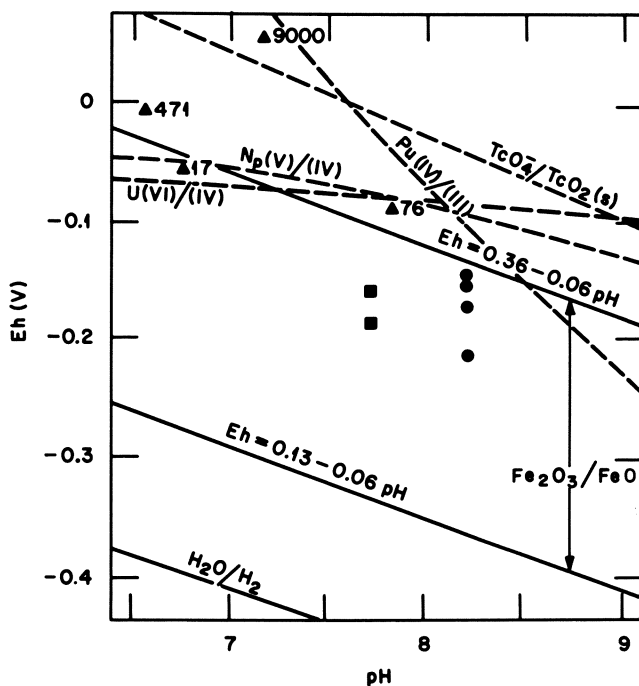


Figure 2. Potential (Eh)-pH-diagram with $TcO_4^-/TcO_2(s)$ - $U(VI)/U(IV)$ -, $Np(V)/Np(IV)$ -, $Pu(IV)/Pu(III)$ -, and $Fe(III)/Fe(II)$ -equilibrium curves as well as some in situ measurements of Eh-pH and Eh-pH-[U] ($\mu g/l$) in groundwater from igneous bedrock. (●), Stripa; (■), Finnsjön; (▲), Svornost.

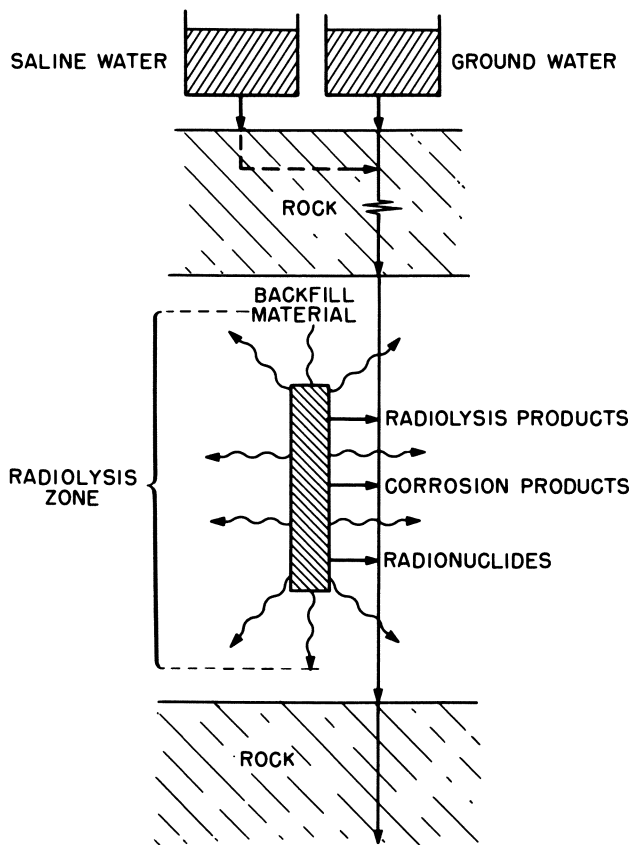


Figure 3. *The groundwater/rock system around a waste depository*

Among the properties of the two-phase system rock/groundwater that would be of importance for the sorption of an individual radionuclide are

- composition of the solid material
- composition of the groundwater
- nuclide concentration
- temperature
- particle size, surface to volume ratio
- flow rate, contact time.

Since granite and bentonite/quartz were decided to be the host rock and backfill material, respectively, at an early stage of the project, these two materials were studied for all of the 14 radionuclides selected and for both of the two artificial groundwaters given in Table II. The radionuclides used in the laboratory experiments are given in Table III.

In order to study the potential reducing capacity of some of the common accessory iron containing minerals measurements were performed with pyrite, magnetite, hornblende, biotite and chlorite in deaerated groundwater for Tc and U. Moreover, the effect of addition of a reducing agent (Fe^{2+}) was investigated.

Two nuclide concentrations ($<10^{-8}$ M and $\approx 10^{-5}$ M) were used, representing slow and fast dissolution of the waste.

Measurements were performed at two temperatures, 65°C and 25°C, representing roughly the maximum temperature in the rock and the temperature of undisturbed rock.

Due to the low water flow rate expected in the ground around the depository the contact times would be long between the water and the rock and waste. Beside measurements at short contact times (less than one week) some long-time studies were performed (contact times of 6 months).

Measurements were also performed (with Cs, Sr and Am) on granite particles of various surface to volume ratios which would give some qualitative information on the sorption mechanisms involved.

The experimental conditions are summarized in Table IV.

Experimental Technique. The solid material (1-3 g) with known particle size and standard water (30-50 ml) containing the radionuclide of interest were shaken in glass bottles for 8-12 hours at constant temperature (25°C or 65°C). The phases were separated by centrifugation (50 min, 7000 rpm) and the distribution coefficient of the radionuclide was determined from measurements of the remaining activity of the water. Filtration of the samples through 0.2 μm membrane filter did not change the values.

The distribution coefficients were remeasured after a contact time of 7 days and also after 6 months (only at 25°C).

Measured Distribution Coefficients

Measured mass related distribution coefficients for granite

Table III
Radionuclides used in laboratory measurements of
distribution coefficients

Nuclide	Half-life
^{89}Sr	51 d
^{95}Zr	64 d
$^{99\text{m}}\text{Tc}$	6.0 h ^a
^{132}I	2.4 h ^b
^{134}Cs	2.1 y
^{144}Ce	285 d
^{147}Nd	11 d
^{152}Eu	12 y
^{226}Ra	1620 y
^{230}Th	$7.7 \cdot 10^4$ y
^{233}U	$1.6 \cdot 10^5$ y
^{237}Np	$2.1 \cdot 10^6$ y
^{239}Pu	$2.4 \cdot 10^4$ y
^{241}Am	430 y

^aDaughter product of ^{99}Mo , half-life 66 h

^bDaughter product of ^{132}Te , half-life 78 h

and bentonite/quartz (10:90) are given in Table V and VI. The results are summarized in Figure 4 and 5 (for long contact time, 25°C).

Generally, the sorption on the crushed granite is equal to or greater than the sorption on the clay mixture, which may seem surprising since the ion exchange capacity of granite would be low. The sorption is, however, not merely an ion exchange reaction. Moreover, only 10% of the clay mixture would be expected to have any ion exchange properties.

The sorption of the anionic Tc (as TcO_4^- in an aerated system) and I (as I^-) is low, both on granite and bentonite, which is expected since the active surfaces and sites of the sorbents would be negatively charged.

The sorption of the monovalent Cs is surprisingly low on bentonite, which would act as a cation exchanger, while the sorption on granite is unexpectedly high. The sorption of Np, which would be pentavalent (species of NpO_2^+ in an aerated system) is similar

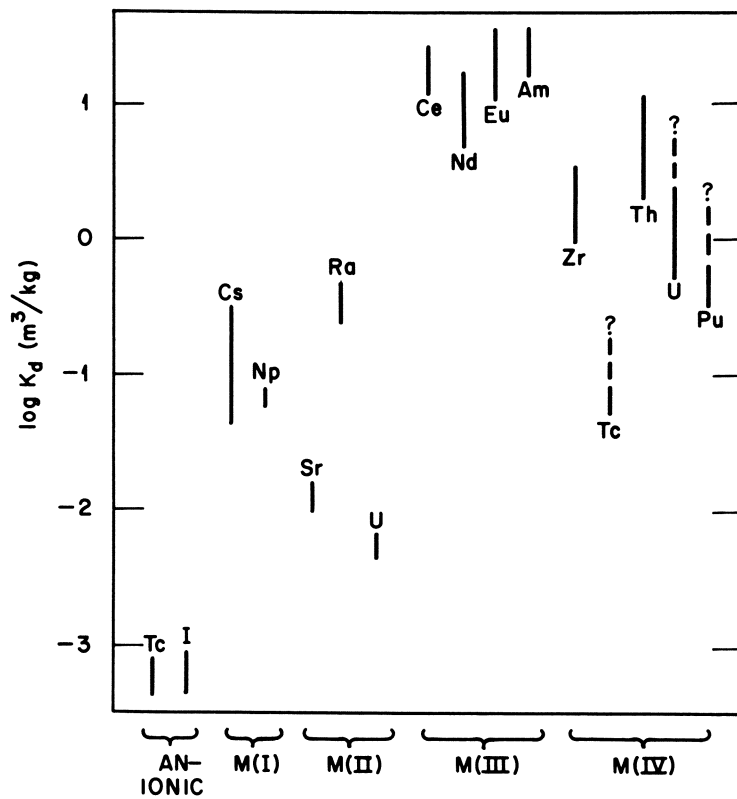


Figure 4. Range of distribution coefficients for granite at 25°C (cf. Table V)

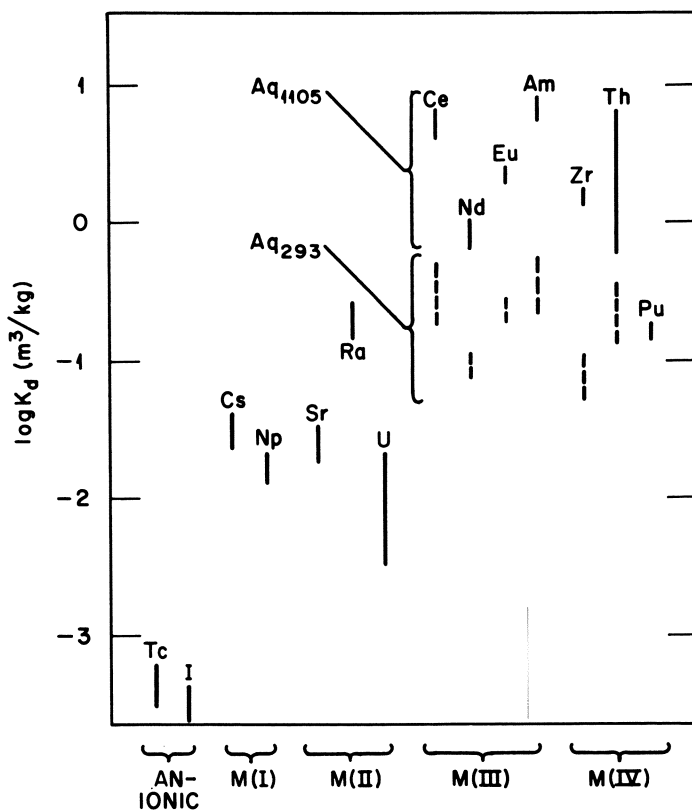


Figure 5. Range of distribution coefficients for bentonite/quartz mixture (10:90) at 25°C (cf. Table VI)

Table IV
Experimental conditions for the distribution studies

Solid phase	Granite	Bentonite ^a	Ferrous minerals ^b	Granite
Water composition	Aq ₂₉₃ Aq ₁₁₀₅	Aq ₂₉₃ Aq ₁₁₀₅	Aq ₁₁₀₅ (deaerated)	Aq ₁₁₀₅
Radionuclides	c	c	Tc, U	Cs, Sr, Am
Nuclide conc.	≈10 ⁻⁵ M <10 ⁻⁸ M	≈10 ⁻⁵ M <10 ⁻⁸ M	<10 ⁻⁸ M	<10 ⁻⁸ M
Temperature	25°C 65°C	25°C 65°C	25°C	25°C
Particle size	0.063- 0.105 mm		0.063- 0.105 mm	4 fractions (<0.15 mm)
Contact time	8-12 h 7 d 6 months	8-12 h 7 d 6 months	1 d 14 d	6 h 7 d

^aBentonite/quartz (10:90)

^bPyrite, magnetite, hornblende, biotite, chlorite, granite + 10-20 mg/l Fe²⁺

^c14 nuclides according to Table III

to the sorption of Cs.

For the divalent elements the distribution coefficient for Ra is significantly higher than for Sr. The only species in the groundwater that can explain this behaviour is SO₄²⁻, since the solubility product of RaSO₄ (log K_s = -10.37) is considerably lower than that of SrSO₄ (log K_s = -6.50) (26).

For U, which would exist in the hexavalent state (species of UO₂²⁺ in an aerated system) the distribution coefficients are low. This is expected in a groundwater containing CO₃²⁻, leading to the formation of soluble anionic complexes.

Both the trivalent and tetravalent elements (Ce, Nd, Eu, Am and Zr, Th, Pu, respectively) have high distribution coefficients, although the values for Pu are lower than expected.

Effect of the Water Composition. For Cs, Sr, U and Np somewhat higher distribution coefficients are obtained for Aq₂₉₃ than for Aq₁₁₀₅ (an increase by a factor of three or less). This effect is expected, since an increased salt concentration would give a larger number of charged particles in the water which may compete for the available sites on the solid sorbent.

For the tri- and tetravalent elements Ce, Nd, Eu, Am and Zr, Th, Pu, a similar trend is observed in the granite system but not

Table V
 Mass related distribution coefficients for granite.
 (Particle size: 0.063-0.105 mm, contact time:
 7 days or 6 months (within parenthesis);
 aerated systems)

Element	Nuclide conc. ^a	log K _d , m ³ /kg					
		Aq ₂₉₃		Aq ₁₁₀₅			
		25°C	()	65°C	25°C	()	65°C
Cs	I	-0.9 ^b	(-0.5)	-1.2	-1.2 ^c	(-0.6)	-1.4
	II	-1.5	(-1.2)	-1.5	-1.7	(-1.4)	-1.1
Sr	I	-2.1	(-1.8)	-2.0	-2.2 ^c	(-2.0)	-2.0
	II	-2.0	(-1.8)	-1.8	-2.2	(-2.0)	-2.0
Ra	I	-1.0	(-0.3)	-1.2	-1.0	(-0.6)	-1.1
Zr	I	0.1	(0.5)	0.8	0.1	(0.0)	0.5
	II	0.3	(0.4)	0.5	0.5	(0.5)	0.8
Tc	I	-3.3		<-3	-3.1		<-3
I	I	-3.1		<-3	-3.2		<-3
	II	-3.2		<-3	-3.2		<-3
Ce	I	1.1	(1.4)	1.3	0.8	(1.4)	0.7
	II	0.8	(1.1)	0.9	0.7	(1.3)	1.0
Nd	I	0.6	(1.1)	0.6	0.3	(0.9)	0.3
	II	0.5	(1.3)	0.9	0.2	(0.7)	0.0
Eu	I	0.9	(1.2)	1.3	1.0	(>1.5)	1.4
	II	1.0	(1.3)	1.2	1.1	(1.0)	1.4
Th	I	-0.1	(0.6)	0.1	-0.2	(>1.0)	-0.1
	II	0.1	(0.7)	0.0	-0.3	(0.3)	-0.1
U	I	-2.2	(-2.2)	-1.9	-2.2	(-2.2)	-2.2
	II	-2.3	(-2.3)	-2.2	-2.4	(-2.3)	-2.4
Np	I	-1.4	(-1.2)	-1.3	-1.6	(-1.1)	-1.4
Pu	I	-0.8	(>-0.5)	-1.0	-1.2	(>-0.5)	-1.0
Am	I	1.1	(1.5)	1.1	0.7 ^c	(1.2)	0.8

^aI: <10⁻⁸ M, II: ≈10⁻⁵ M

^bMeasurements on granite from other locations have given higher values (up to -0.2)

^cMeasurements on granodiorite gave the values -0.6 for Cs, -2.5 for Sr and 0.5 for Am

Table VI
 Mass related distribution coefficients for bentonite/quartz
 mixture (10:90). (Particle size for the quartz: 0.02-0.06 mm;
 contact time: 7 days or 6 months (within parenthesis);
 aerated systems)

Element	Nuclide conc. ^a	log K _d , m ³ /kg					
		Aq ₂₉₃		Aq ₁₁₀₅			
		25°C		65°C	25°C		65°C
Cs	I	-1.5	(-1.4)	-1.8	-1.6 ^b	(-1.5)	-2.1
	II	-1.6	(-1.5)	-1.8	-1.7	(-1.6)	-2.2
Sr	I	-1.5	(-1.5)	-1.3	-1.5 ^b	(-1.5)	-1.5
	II	-1.3	(-1.7)	-1.2	-1.5		-1.4
Ra	I	-1.3	(-0.8)	-1.1	-1.4	(-0.6)	-1.2
Zr	I	-1.1	(0.2)	-0.7	-0.2	(0.2)	0.0
	II	-1.3		-1.0	-0.2	(0.2)	0.0
Tc	I	-3.5		<-3	-3.2		<-3
I	I	-3.5		<-3	-3.6		<-3
	II	-3.5		<-3	-3.4		<-3
Ce	I	-0.7	(-0.7)	-1.0	0.2	(0.8)	0.0
	II	-0.6	(-0.3)	-1.1	0.1	(0.6)	0.2
Nd	I	-1.1	(-1.1)	-0.9	-0.1	(0.0)	-0.1
	II	-1.0	(-1.0)	-1.0	0.0	(-0.2)	-0.2
Eu	I	-0.7		-0.4	0.1	(0.4)	1.0
	II	-0.6		-0.3	0.3	(0.3)	0.9
Th	I	-1.3	(-0.5)	-1.2	-0.6	(0.8)	-0.5
	II	-1.4	(-0.9)	-1.2	-0.5	(-0.2)	-0.5
U	I	-2.0	(-1.8)	-1.7	-2.5	(-2.4)	-2.4
	II	-2.1	(-1.7)	-1.9	-2.6	(-2.5)	-2.6
Np	I	-2.0	(-1.9)	-1.8	-2.0	(-1.7)	-1.8
Pu	I	-1.1		-0.8	-1.2	(-0.8)	-0.8
Am	I	-0.7	(-0.3)	-0.6	0.6 ^b	(0.9)	0.2

^aI: <10⁻⁸ M, II: ≈10⁻⁵ M

^bMeasurements on silt taken from a natural crack in granite gave the values -0.7 for Cs, -1.7 for Sr and 1.2 for Am

in the bentonite system, where the distribution coefficients are lower in Aq_{293} (by a factor of 5-10). This effect seems to be related to some property of the solid and not caused by the differences in the water composition. Probably a small fraction of the clay exists in a colloidal state in Aq_{293} (with low salt concentration), and these colloid particles, which pass through a 0.2 μm filter, act as carriers of the radionuclides, giving low apparent distribution coefficients. In Aq_{1105} (with high salt concentration) these particles are dispersed, giving higher distribution coefficients. In subsequent experiments (27) the clay was washed twice before the radionuclide was added. By this washing procedure the smallest colloidal particles were removed along with the washing solution and no similar salt effect was observed.

Nuclide Concentrations. The two nuclide concentrations chosen for the experiments, $<10^{-8}$ M and $\approx 10^{-5}$ M, are so low that the ionic strength of the water is not significantly affected. Nor is it likely that the solid sorbent would be saturated with respect to the sorption capacity of any individual radionuclide species.

Differences between the observed distribution coefficients of a certain element at different concentrations are small. The only significant exception is Cs which has a higher distribution coefficient at low concentration than at high in the granite system (by a factor of less than two). This may in fact reflect the poor ion exchange capacity of the granite.

Temperature Effects. The effect of a temperature increase from 25°C to 65°C is usually a small increase of the distribution coefficient (less than a factor of three). For the sorption of Cs on bentonite, which would correspond to an ion exchange process, the effect of increased temperature is the opposite.

Redox Reactions and Valence States. The proposed reduction of Tc and U to the tetravalent state is indirectly indicated from the distribution measurements in non-oxidizing systems (c.f. Figure 2 and Table VII). By the addition of 10-20 mg/l of Fe^{2+} (c.f. Table II) a drastic increase of the distribution coefficient was observed both for Tc and U. Minerals like magnetite and chlorite also seem to have some reducing effect even after a short contact time.

Since the redox potentials for $\text{Np(V)}/\text{Np(IV)}$ and $\text{Pu(IV)}/\text{Pu(III)}$ are above the potential for $\text{U(VI)}/\text{U(IV)}$ the expected oxidation states would be Np(IV) and Pu(III) (or possible Pu(IV)) for these elements, as already stated above.

Work is in progress to study the reducing effect on U(VI) of granite and common ferrous accessory minerals.

Sorption Kinetics and Mechanisms. Measurements of distribution coefficients vs contact time and particle size (expressed as the surface to mass ratio, $6/\rho \cdot d$, where ρ is the density of the

Table VII
Mass related distribution coefficients for Tc and U
under non-oxidizing conditions (25°C, Aq₁₁₀₅)

System	Contact time	log K _d , m ³ /kg Tc U
Granite, aerated	6 months	<-3 -2.4- -2.2
Granite, deaerated	1 d	<-3 -2.4- -2.2
Granite, deaerated + 10-20 mg/l Fe ²⁺	1 d	-1.3 -1.9
	5 d	-0.3- 0.3
Magnetite	1 d	-2.6
	14 d	-2.3- -2.0
Chlorite	1 d	<-3
	14 d	-1.8- -1.5
Biotite, pyrite hornblende	1 d	<-3
	14 d	-2.3- -2.2

solid material, [kg/m³], and d is the particle diameter, [m]) are given in Figure 6 for Cs, Sr and Am on granite.

For Cs the sorption is largely independent of the particle size. A volume dependent ion exchange process involving diffusion into the particles seems possible.

For Sr a significant increase of the distribution coefficient with increased surface to mass ratio is observed. Equilibrium is obtained within 6 hours. Evidently Sr is largely adsorbed by a surface reaction. A similar behaviour would be expected for Ra, although the formation of non-soluble RaSO₄ would give a higher distribution coefficient (c.f. above).

For Am there is no evident particle size dependence. The kinetics are considerably slower than for Cs (and Sr). Possibly the sorption process is a volume dependent adsorption with contributions from ion exchange. The sorption and also the diffusion into the particles should be governed by the complicated hydrolysis reactions to be expected at environmental pH. Other tri- and tetravalent elements would be expected to show a similar slow non-surface related sorption behaviour.

Generally, a significantly increased distribution coefficient is obtained after a contact time of 6 months in comparison with 1 week (by a factor of less than five), especially for the tri- and tetravalent elements (and Ra) on granite. Evidently the diffusion of hydrolyzed products into the grains is a slow process.

Radionuclide Species in Groundwater

From stability constants available in the literature (26) it is

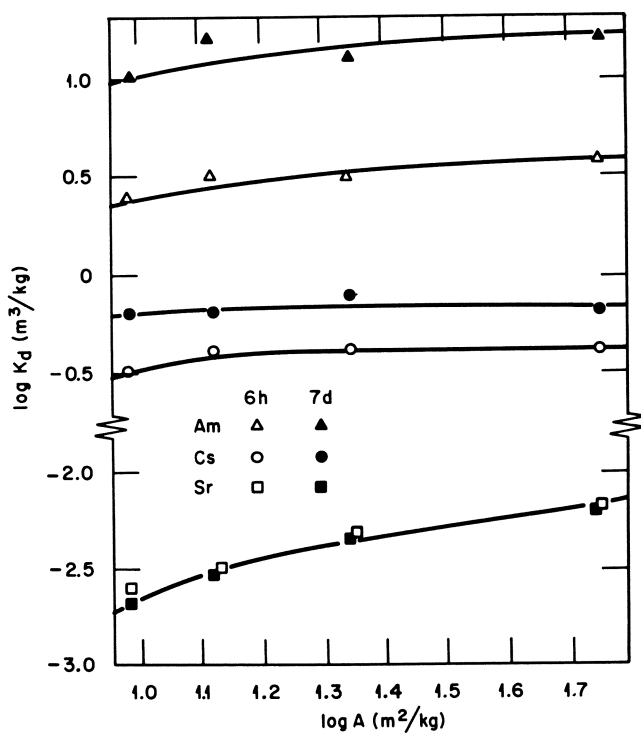


Figure 6. Distribution coefficients as functions of contact time and surface to mass ratios for Cs, Sr, and Am on granite (25°C, Aq₁₁₀₅)

evident that the most important anionic species in the groundwater would be OH^- , HCO_3^- - CO_3^{2-} , SO_4^{2-} , H_2PO_4^- - PO_4^{3-} and F^- .

Monovalent elements like Cs would not form any complexes in the groundwater.

The maximum concentration of the divalent elements Sr and Ra would be limited by the precipitation of non-soluble sulfate (for Ra) or carbonate (for Sr). Species in solution would be M^{2+} and a small fraction of MSO_4 and possibly also MHCO_3^+ .

The maximum concentration of trivalent elements like the lanthanides and Am would be determined by the solubility product of either the phosphate, the hydroxide or the carbonate (depending on the concentration of the corresponding anion and pH of the groundwater). Species in solution would largely be hydrolysis products, MCO_3^+ and possibly a small fraction of MF^{2+} and MSO_4^+ . A considerable part of the soluble fraction would be non-charged or anionic (28).

For the tetravalent elements the maximum concentration in solution will be limited solely by the precipitation of hydroxides which might be transferred into dioxides, possibly irreversibly. Species in solution would be hydrolysis products. A large part of the soluble fraction would be non-charged or anionic (28).

Penta- and hexavalent species (of Np and U, respectively) would not be expected to form in undisturbed deep groundwater, as discussed above. In oxidizing environment, however, these valence states would exist and the solubility would be high due to the formation of anionic mixed hydroxy-carbonate complexes.

Proposed species in granitic groundwater are given in Table VIII. Since many of the relevant stability constants are not known, especially for actinide complexes with OH^- , CO_3^{2-} and PO_4^{3-} , any final conclusive predictions of speciation in groundwater are impossible.

Migration in the Ground

The Retention Factor. The water velocity v_{aq} [m/s] in fractured rock can be calculated from the basic flow equation

$$v_{\text{aq}} = K_p \cdot i / \phi \quad (3)$$

where K_p = permeability [m/s]

i^p = hydraulic gradient [m/m]

ϕ = rock porosity (void fraction) [m^3/m^3]

The effects of chemical interactions on the migration of radionuclides in the backfill material and in the ground can be described by the retention factor K_i , defined as (29)

$$K_i = v_{\text{aq}}/v_A = 1 + K_d \cdot \rho_s \cdot \frac{1-\phi}{\phi} \quad (4)$$

where v_A = velocity of the nuclide [m/s]

ρ_s = density of the solid [kg/m^3]

Table VIII
Proposed radionuclide species in non-oxidizing
granitic groundwater

Element	Precipitating species limiting the solubility	Predominating species in solution
M(I): Cs		Cs ⁺
M(II): Sr	SrCO ₃ , (SrSO ₄)	Sr ²⁺ , (SrSO ₄)
Ra	RaSO ₄	Ra ²⁺ , (RaSO ₄ , RaHCO ₃ ⁺)
M(III): Ln ^a	M(OH) ₃ , M ₂ (CO ₃) ₃ (?)	M(OH) _x ^{3-x} , x = 2,3,(4?)
An ^a	MPO ₄ (?)	MCO ₃ ⁺ (?), (MF ²⁺ , MSO ₄ ⁺)
M(IV): An ^a	An(OH) ₄ → AnO ₂	An(OH) _x ^{4-x} , x = 3,4,(5?) ^b
Tc	Tc(OH) ₄ → TcO ₂	

^aLn = lanthanide, An = actinide

^bFormally An(OH)₅⁻ would be expected to form. A transfer to a non-stoichiometric hydroxy compound at high pH, possibly negatively charged, would be more likely

As a first approximation it can be assumed that the water and nuclide transport would take place only in major fractures of the rock and also that the nuclide retention is merely a surface reaction limited by the exposed fracture surface area.

Laminar flow between parallel plates can be described by (30)

$$v_{aq} = \frac{g}{12\nu} \cdot (2b)^2 \cdot i \quad (5)$$

where g = gravity acceleration [m/s²]

ν = viscosity of the water [m²/s]

$2b$ = fracture aperture [m]

The fracture aperture $2b$ can be estimated from (4)

$$2b = 0.01 \cdot (K_p \cdot S)^{1/3} \quad (6)$$

where S = fracture distance [m]

A transformation is required of the mass related distribution coefficient K_d into a surface related distribution coefficient K_a [m³/m²], defined as

$$K_a = s_A / C_A \quad (7)$$

where s_A = nuclide concentration on the solid [moles/m²]

By direct measurements of the radionuclide sorption on exposed rocks, surface related distribution coefficients K_a can be determined and conversion factors calculated according to (3)

$$A = K_d/K_a \quad (8)$$

where A = apparent surface to mass ratio [m^2/kg]

Thus, from eqn (3), (4) and (8) the nuclide velocity v_A can be estimated for rock with low porosity as

$$v_A = \frac{K_p \cdot i}{K_a \cdot A \cdot \rho_s} \quad (9)$$

which allows a calculation of the retention factor for the fractured rock (4,6). Here $A \cdot \rho_s$ defines the fracture surface per rock volume.

Retention in the Backfill Material. The radionuclide hold-up time in the backfill barrier for the KBS-concepts is in the order of thousands of years or less (15). Thus, only a few of the long-lived radionuclides in HLW and SUF (^{90}Sr , ^{137}Cs and ^{241}Am) will be able to decay within the clay barrier and the more long-lived nuclides will just be delayed in their migration out into the bedrock. In the long-term time span the backfill material is of minor importance, as far as the retaining effect is concerned.

Retention in the Hostrock. For granite, apparent surface to mass ratios of about $3 m^2/kg$ for Cs, $2 m^2/kg$ for divalent elements and $<10 m^2/kg$ for tri- and tetravalent elements have been estimated, based on K_d/K_a -measurements on Cs, Sr and Am on granitic macro surfaces (3,31). Retention factors are given in Table IX, as generated from measured K_d -values (from Table V), assuming long contact time, non-oxidizing conditions and representative fracture and permeability data for the rock (1).

If the nuclides would diffuse into micro fissures of the rock, which seem to be the case for Cs and Am (see above), and not solely be adsorbed on the exposed fracture surfaces, the retention factors would be several orders of magnitude larger.

In the KBS-report (1) retention factors have been generated for different input parameters and the migration to the biosphere has been calculated by use of a modified version of the computer program GETOUT (15,32,33) and by the program BIOPATH (34). In the most probable alternative, using data for the storage of SUF (1), the first activity to be detectable in any recipient on the surface would come from ^{129}I after about 100000 years. The activity from the long-lived actinides would appear after about 70 million years. If the long dissolution time of the uranium oxide matrix is disregarded the main peak could appear already after 1 million years. Maximum radiation dose to any critical group would be about 10 mrem/year (after 70 million years) in the most probable case.

Table IX
Proposed retention factors (K_i) in granite
(25°C, long contact time, non-oxidizing conditions)

Element	K_i^a
Cs	18000
Sr	1300
Ra	41000
Zr	52000
Tc	800
I	1
Ce	410000
Nd	330000
Eu	330000
Th	82000
U	30000
Np ^b	30000
Pu	5000
Am	490000

^aCalculated for $K_p = 10^{-9}$ m/s, $2b = 10^{-5}$ m and $S = 1$ m

^bA K_d -value similar to the value for U is assumed

Conclusions

It is essential that the ground, which is the final barrier and the only barrier not man-made, by itself can prevent the migrating radionuclides from an underground waste depository from giving unacceptable doses to any critical group in the future. Although the sorption processes in the ground are not clearly understood, the results obtained so far seem to be adequate to prove the feasibility of an "absolutely safe" disposal, as required by the Swedish law. The majority of the international experts and organizations that have been consulted for critical reviewing of the KBS-reports also seems to accept the validity of the conclusions drawn regarding the safety of the disposal method (35).

Literature Cited

1. The Nuclear Fuel Safety Project (Kärnbränslesäkerhet, KBS), Fack, S-102 40 Stockholm, Sweden, has so far presented the studies on waste storage in two main reports: "Handling of Spent Nuclear Fuel and Final Storage of Vitrified High-level Reprocessing Waste", Part I-V, Dec. 7, 1977, and "Handling of Spent Nuclear Fuel and Final Storage of Unreprocessed Spent Fuel", Part I-II, June 28, 1978.

These reports are based on 120 technical reports (here denoted by KBS TR) on different technical aspects of waste treatment and ground disposal. More than 70 university departments and consulting companies in Sweden and abroad have been engaged in the preparation of these reports. The research on storage of radioactive waste in the ground is still in progress, both within the Nuclear Fuel Safety Project but also within a Swedish-American joint project between Swedish Nuclear Fuel Supply Co (Svensk Kärnbränsleförsörjning AB, SKBF), Fack, S-102 40 Stockholm, Sweden, and Lawrence Berkeley Laboratory, Earth Science Division, University of California, Berkeley. Unless specific references are quoted, the data presented in this paper are taken from the two main KBS-reports or from technical reports cited therein.

2. Allard, B., Kipatsi, H. and Rydberg, J., "Sorption of Long-Lived Radionuclides on Clay and Rock". Part I, KBS TR 55, 1977
3. Allard, B., Kipatsi, H. and Torstenfelt, B., "Sorption of Long-Lived Radionuclides on Clay and Rock", Part II, KBS TR 98, 1978
4. Neretnieks, I., "Retardation of Escaping Nuclides from a Final Depository", KBS TR 30, 1977
5. Grundfelt, B., "Transport of Radioactive Effluents with Groundwater from a Repository", KBS TR 43, 1977
6. Grundfelt, B., "Nuclide Migration from a Repository for Spent Fuel", KBS TR 77, 1978
7. Landström, O., Klockars, C.-E., Holmberg, K.-E. and Westerberg, S., "In Situ Experiments on Nuclide Migration in Fractured Crystalline Rocks", KBS TR 110, 1978
8. Hult, A., Gidlund, G. and Thoregren, U., "Permeability Determinations", KBS TR 61, 1978
9. Gidlund, G., "Analyses and Age Determinations of Groundwater from Great Depth", KBS TR 62, 1978
10. Stokes, J. and Thunvik, R., "Investigations of Groundwater Flow in Rock Around a Repository for Nuclear Fuel Waste", KBS TR 47, 1978
11. "The Corrosion Resistance of Potential Canning Materials for Nuclear Fuel Waste", KBS TR 31, 1977
12. Gelin, R., "Dissolution and Transport of Lead from Waste Canisters by Groundwater", AE-TPM-SM-75, AB Atomenergi, Studsvik 1977
13. "Copper as Encapsulation Material for Unreprocessed Nuclear Fuel Waste", KBS TR 90, 1978
14. Blomqvist, G., "Leaching of French, British and Canadian Glass Containing High-level Radioactive Waste", KBS TR 08, 1977
15. Neretnieks, I., "Transport of Oxidants and Radionuclides Through a Clay Barrier", KBS TR 79, 1978
16. Cowan, G. A., "Migration Paths for Oklo Reactor Products and Application to the Problem of Geological Storage of Nuclear Wastes", IAEA Symp., Paris, Dec. 19-21, 1977

17. Pusch, R. and Jacobsson, A., "Properties of Bentonite Buffer Materials", KBS TR 32, 1978
18. Allard, B., "The Composition of Groundwater from Plutonic Bedrock", ORNL-report, Oak Ridge National Laboratory, in prep.
19. Jacks, G., "Groundwater Chemistry at Depth in Granites and Gneisses", KBS TR 88, 1978
20. Rennerfelt, J., "Composition of Groundwater at Great Depth in Granitic Bedrock", KBS TR 36, 1977
21. Tardy, Y. and Garrels, R. M., Geochim. Cosmochim. Acta (1974), 38, 1101
22. Allard, B., Kipatsi, H. and Torstenfelt, B., "Technetium: Reduction and Sorption in Granitic Bedrock", subm. to Radiochem. Radioanal. Lett.
23. Allard, B., Kipatsi, H. and Liljenzin, J. O., "Calculated Species of Uranium, Neptunium and Plutonium in Neutral Aqueous Solution", subm. to Radiochem. Radioanal. Lett.
24. Grenthe, I., "Determinations of the Redox Potential in Groundwater from Stripa and Finnsjön", App, B5 in KBS TR 90, 1978 (ref. 13)
25. Pačes, T., Geochim. Cosmochim. Acta (1969), 33, 591
26. Smith, R. and Martell, A. E., "Critical Stability Constants. Vol. 4: Inorganic Complexes", Plenum Press, New York 1976
27. Allard, B. and Beall, G., work in progress
28. Allard, B. and Beall, G., "Predictions of Actinide Species in the Groundwater", Workshop on Environmental Chemistry of the Actinide Elements, Warrenton, Oct. 9-12, 1978
29. Apps, J. A., Cook, N.G. W. and Witherspoon, P. A., "An Appraisal of Underground Radioactive Waste Disposal in Argillaceous and Crystalline Rocks: Some Geochemical, Geomechanical and Hydrogeological Questions", LBL-7047, UC-70, Lawrence Berkeley Laboratory, Berkeley 1978
30. Bird, R. B., Steward, W. E. and Lightfoot, E. N., "Transport Phenomena", John Wiley and Sons, New York 1960
31. Allard, B., Kipatsi, H., Torstenfelt, B. and Rydberg, J., "Nuclide Transport by Groundwater in Swedish Bedrock", Symp. on Radioactive Waste Management, Boston, Nov. 28 - Dec. 1, 1978, in press
32. Burkholder, H. C., Cloninger, M. O. and Jansen, D., "Incentives for Partitioning High-level Waste", BNWL-1927, Battelle Pacific Northwest Laboratories, Richland 1977
33. Grundfelt, B., "Translation and Development of the BNWL-Geosphere Model", KBS TR 10, 1977
34. Bergman, R., Bergström, U. and Evans, S., "Ecological Transport and Doses from Radionuclides Carried by Groundwater", KBS TR 40, 1977
35. "Report on Review Through Foreign Expertise of the Report Handling of Spent Nuclear Fuel and Final Storage of Vitrified High-level Reprocessing Waste", Liber, Stockholm 1978

RECEIVED January 16, 1979.

Leaching of Fully Radioactive High-Level Waste Glass and Waste-Geologic Environment Interaction Studies

D. J. BRADLEY

Pacific Northwest Laboratory, operated by Battelle Memorial Institute for the U.S. Department of Energy, Richland, WA 99352

As part of continuing studies in waste management, the Pacific Northwest Laboratory (PNL), operated by Battelle Memorial Institute for the Department of Energy (DOE), has been conducting the High-Level Waste Immobilization Program. The purpose of this program is to develop and demonstrate technology for incorporating nuclear wastes into final waste forms.

Release rate data for radionuclides from fully radioactive waste forms are needed to evaluate the safety of nuclear waste glass. Presently, contact with water is considered the most important release path; therefore, the release properties of waste glass in water are of primary concern.

This report describes the preparation and leach testing of fully radioactive zinc borosilicate glass, prepared from power reactor waste. Leach tests were conducted on this fully radioactive waste glass to:

- determine the release rates of radioactive material from the glass
- compare leach rates to those of nonradioactive waste of the same composition
- study elements not included in simulated waste glasses
- recommend further studies needed in this area.

0-8412-0498-5/79/47-100-075\$05.00/0
© 1979 American Chemical Society

To evaluate the safety of geologic repositories, PNL is also conducting the Waste Isolation Safety Assessment Program (WISAP) for the DOE. Task #2 of the WISAP program is aimed at providing release rate data from potential waste forms to be used in geologic storage. Experiments simulating simple to complex waste form release in geologic media are outlined.

EXPERIMENTAL PROCEDURE

Nuclear waste glasses are complex mixtures of more than 30 elements, usually prepared by methods quite different than those used commercially to produce plate glass, for example. Canisters of glass (1-ft-dia x 6-ft-tall) have been prepared by direct furnace melting of a mixture of the waste oxides and an appropriate glass frit. The present experiment simulated this procedure on the laboratory scale.

In July 1975, 2.7 kg of spent irradiated power reactor fuel was dissolved using lab-scale equipment in the hot-cell facilities at PNL. This fuel had an average burnup of 55,000 MWD/MTU. After extraction of uranium and plutonium, the resulting liquid waste was boiled down and heated to 500°C to yield 380 g of fine granular oxide material called calcine. We then analyzed this calcine for radioisotopic content, which included activation products, fission products and actinides. A zinc borosilicate glass frit was blended with this waste calcine in a 3:1 weight ratio to make the waste glass. The composition of the product glass based upon frit composition, ORIGEN,⁽¹⁾ and the calcine analysis is shown in Table I. As you can see, the glass has a complex composition. We made the waste glass in 100-g batches by melting the frit and calcine in a stainless steel 304L cylinder which was placed inside a resistance-heated furnace. The dimensions of this cylinder were 3.8 cm dia x 12.7 cm height, with a wall thickness of 0.165 cm. The waste was brought up to the melting temperature of 1050°C in two hours, held there for three hours, and then allowed to furnace cool at an average rate of 220°C/hour.

After cooling we sectioned the stainless steel canister containing the waste glass by using a water-cooled diamond saw. Figure 1 depicts this operation and shows the four sections that we used for this leaching study. All sections appeared homogeneous without large cracks or voids. This same procedure on subsequent glass runs provided samples of fully radioactive glass for metallography and electron microscopy. Information on those analyses, along with glass-making volatilization data is reported in BNWL-2252⁽²⁾ and BNWL-2625.⁽³⁾ Further details on sample preparation, plus a complete list of the leaching data obtained, are available in PNL-2664.⁽⁴⁾

We began the leaching test on the four glass sections in February 1976, using the apparatus shown in Figure 2. Prior to

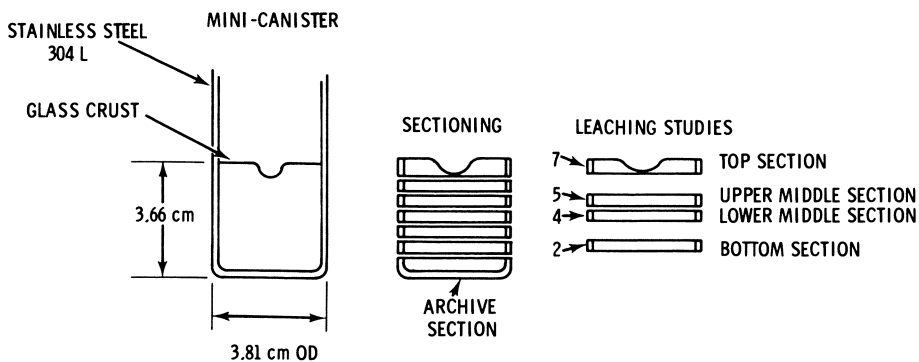


Figure 1. Sectioning of high-level waste glass canister

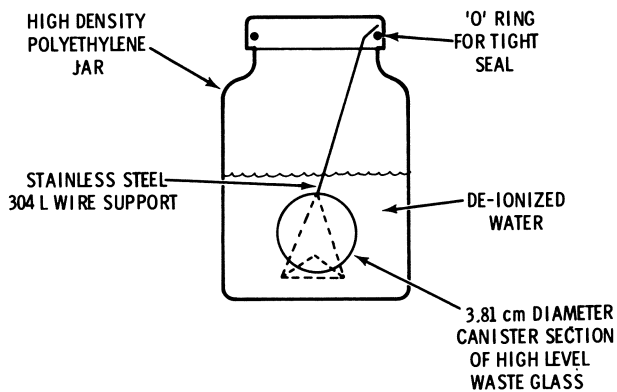


Figure 2. Long-term IAEA leaching apparatus

Publication Date: April 6, 1979 | doi: 10.1021/bk-1979-0100.ch005

TABLE I. Fully Radioactive Waste Glass Composition

<u>Component</u>	<u>Weight Percent</u>
SiO ₂	27.8
ZnO	21.7
B ₂ O ₃	11.3
UO ₂	10.3
Na ₂ O	4.1
K ₂ O	4.1
SrO	1.9
ZrO ₂	1.6
MoO ₃	1.6
MgO	1.5
CaO	1.5
BaO	1.5
Nd ₂ O ₃	1.5
CeO ₂	1.0
Cs ₂ O	0.8
BaO	0.5
La ₂ O ₃	0.45
Pr ₂ O ₃	0.44
PdO	0.43
Tc ₂ O ₇	0.39
Sm ₂ O ₃	0.29
NpO ₂	0.22
Y ₂ O ₃	0.19
PuO ₂	0.12
RuO ₂	0.09
Eu ₂ O ₃	0.06
AmO ₂	0.06
Gd ₂ O ₃	0.05
Cm ₂ O ₃	0.02
SbO	0.01
CoO	1.1 x 10 ⁻⁴
MnO	6.0 x 10 ⁻⁶
	<u>95.5 (a)</u>

(a) The remaining material is made up of chemicals used in the fuel dissolution and uranium/plutonium separation operations.

the start of the leach test, all sections were washed in acetone to remove surface particles, then the sections were dried in air. Deionized water was used as the leachate and the ratio of leachate volume (cm³) to sample surface area (cm²) was 26 cm.

The leachate was changed according to the International Atomic Energy Association (IAEA) procedure,⁽⁵⁾ which calls for sampling daily for four days, weekly for eight weeks, monthly for six months, and semi-annually from then on. On leachate-changing day, a 10 ml aliquot was removed from the container and acidified to a pH of 1 with concentrated nitric acid. This acid was added to prevent adherence of isotopes on the sample container walls. Analysis of the sample consisted of:

- gamma spectroscopy
- separation of cesium and strontium⁽⁶⁾
- recount by gamma spectroscopy
- beta counting of separated ⁹⁰Sr
- alpha energy analysis.

Bulk glass leach rates based on various isotopes were calculated by the equation:

$$R_i = \frac{a_o}{A_o S t}$$

- where: R_i • incremental leach rate, g/cm²-day
 a_o • activity of isotope in leachate, sec⁻¹
 A_o • specific activity of isotope in sample, sec⁻¹-gram (based on measured activity of the high-level waste calcine), assumed to be homogeneous. All activities a_o and A_o were decay corrected to the same time.
 S • geometric surface area of sample, cm²
 t • leaching time, days.

DISCUSSION

Figures 3a and 3b show logarithmic plots of the leach rate in g/cm²-day based on various isotopes as a function of time. You can see that the leach rates decrease rapidly at the beginning of the test and level off after about ten days. This behavior is consistent with previous studies on simulated waste glasses.^(2,3)

Plots of isotopic leach rates from the other waste glass sections show good agreement with those in Figure 3a and 3b. This can be seen clearly in Figures 4 and 5. Figure 4 shows ¹³⁷Cs and ⁵⁴Mn leach rates representing sections from the top to the bottom of the waste glass cylinder. Figure 5 plots the same rates for ¹⁵⁴Eu and ²³⁹⁺²⁴⁰Pu. You can see that the leach rates vary little from top to bottom of the waste canister. Although these four isotopes represent a wide range in mass and

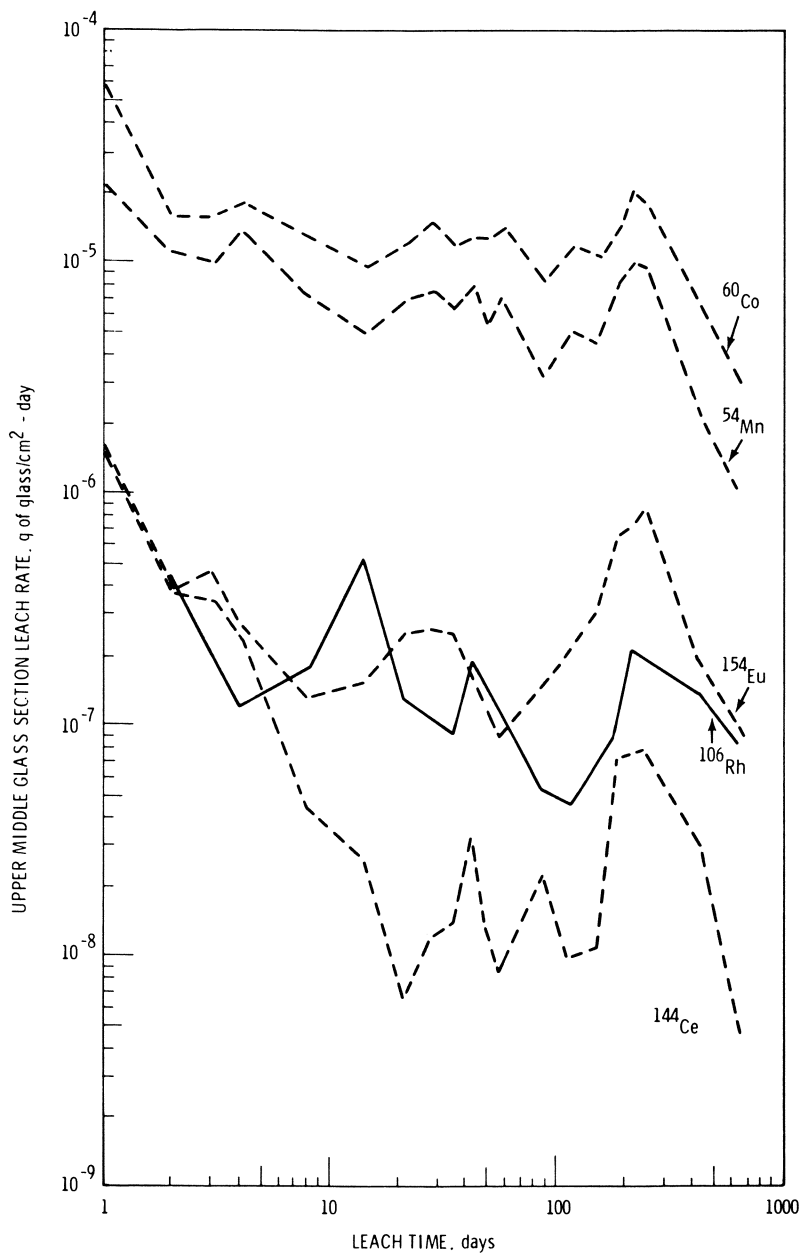


Figure 3a. Leach rate as a function of time—upper-middle glass section

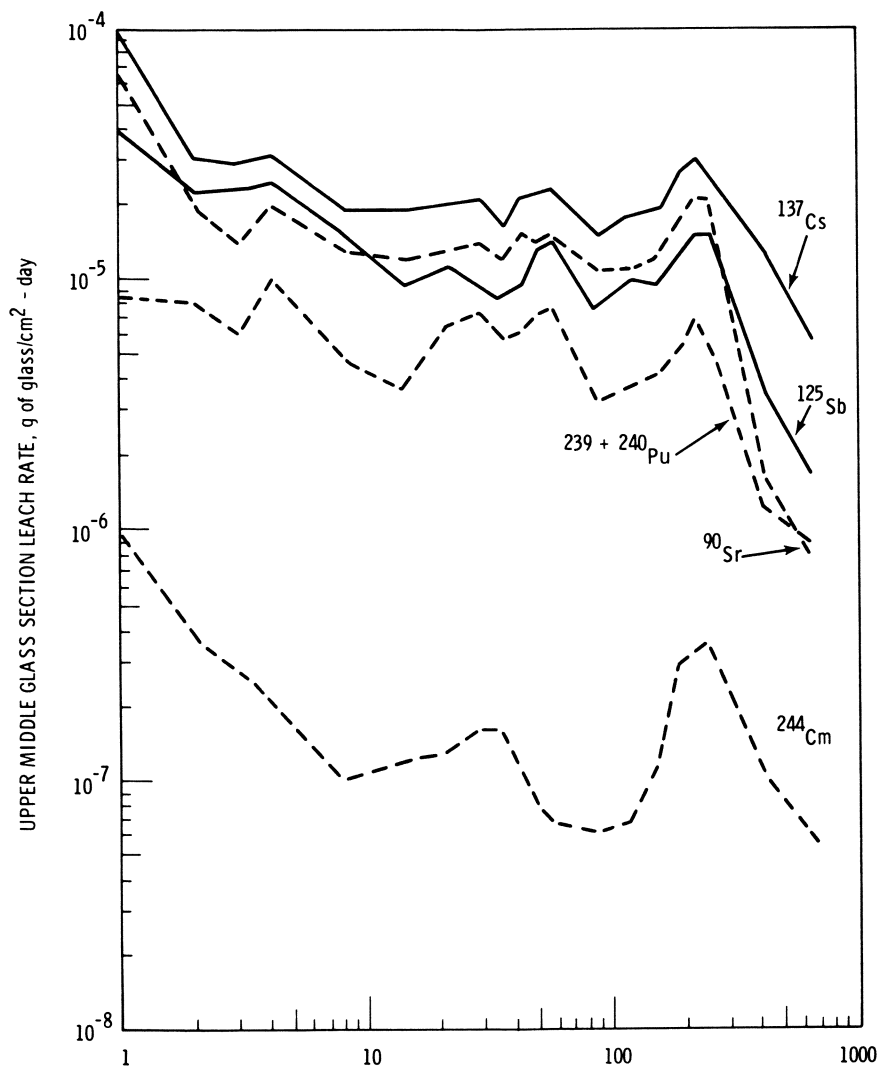


Figure 3b. Leach rate as a function of time—upper-middle glass section

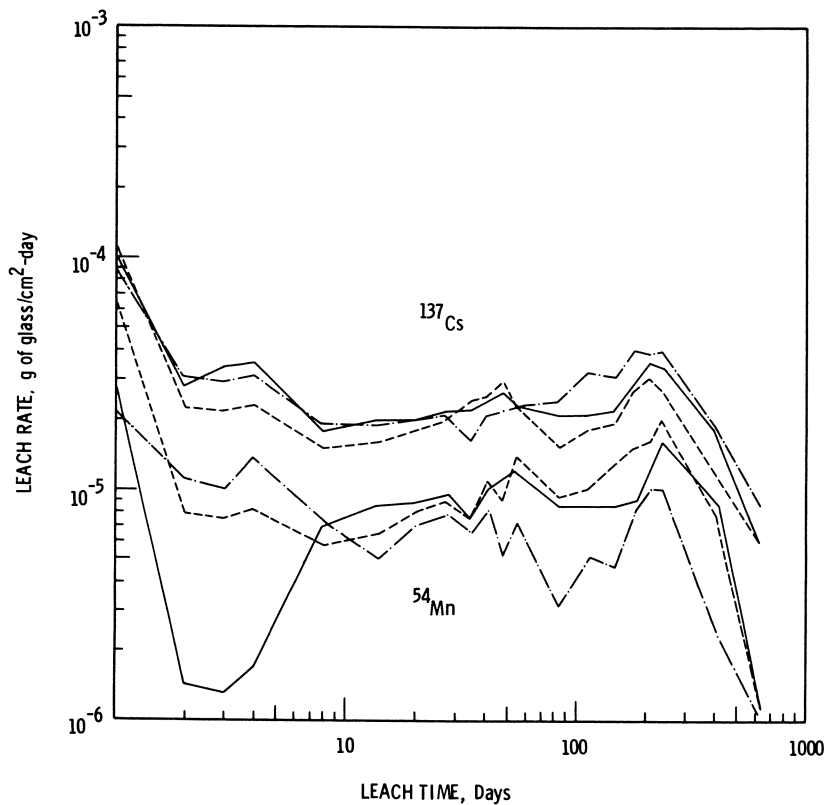


Figure 4. Leach rate as a function of time and glass section for ¹³⁷Cs and ⁵⁴Mn: (—), bottom section; (- · -), upper-middle section; (- - -), top section.

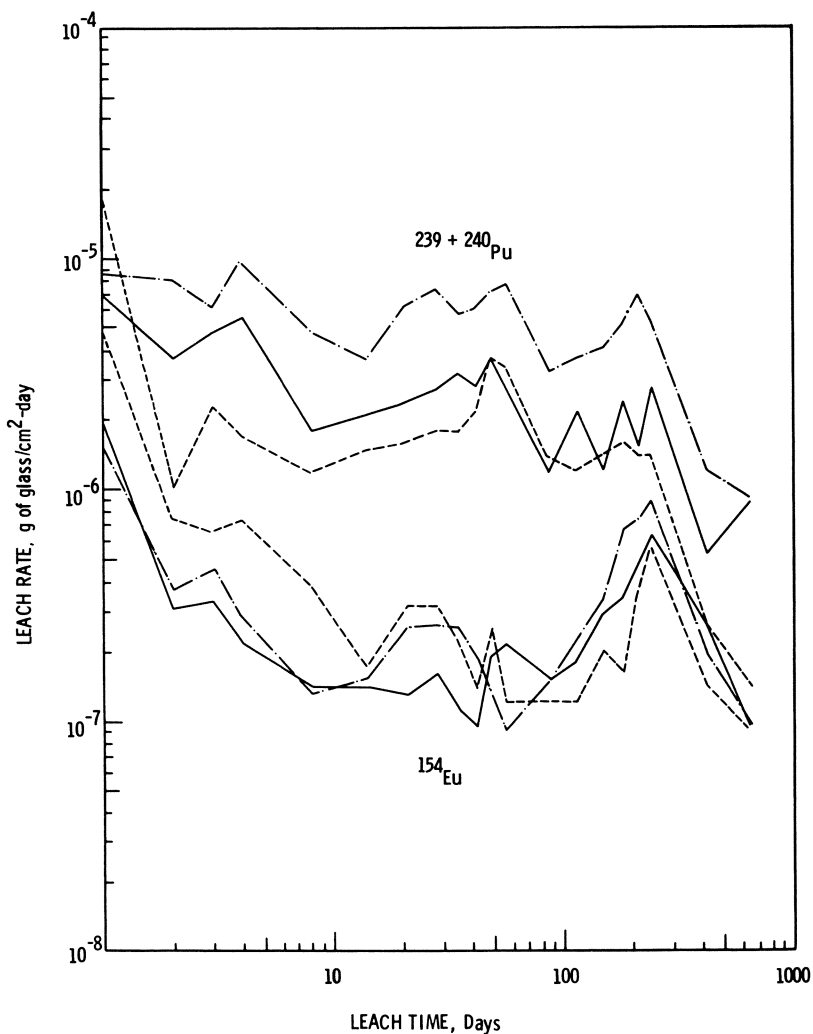


Figure 5. Leach rate as a function of time and glass section for ²³⁹⁺²⁴⁰Pu and ¹⁵⁴Eu: (—), bottom section; (- · -), upper-middle section; (- - -), top section.

expected volatility, they indicate that there are no significant inhomogeneities in the glass column. This conclusion is supported by recent gamma spectroscopy on the high-level waste glass sections.⁽³⁾

The leach rates seen here can be compared to those from a similar test on simulated waste glass of the same composition. The leach rates for cesium and strontium from the fully radioactive glass were the same as the leach rates of the simulated glass.⁽⁵⁾ Although both tests were done on bulk glass samples, they differed in configuration. The fully radioactive samples were disks [~ 0.3 cm (height) x 3.5 cm (diameter)], and the simulated glass sample was a cylinder [0.73 cm (height) x 0.98 cm (diameter)].

The size of the sample being leached has a large effect on the apparent leach rate. Differences up to a factor of 100 were noted between -42+60 mesh particles and bulk samples such as used in this test.⁽³⁾ In contrast, radiation is believed to have a very small effect on leach rates; this has been shown for the case of alpha radiation.⁽⁸⁾ Further studies on the effects of radiation on leach rate are in progress.

Curves showing the cumulative fraction leached were also calculated from the leaching data based on the equation:

$$\text{cumulative fraction} = \frac{\sum a_o}{A_o w}$$

where: a_o • activity of isotope in leachate, sec⁻¹
 A_o • specific activity of isotope in sample, sec⁻¹
 w • sample weight, grams.

Figure 6 shows these cumulative leach fractions from the top waste glass section. A ranking of the elements studied, based on the fraction released after 639 days of solution contact, is given in Table II. This order of leaching can also be seen in Figures 3a and 3b.

TABLE II. Element Release Fractions After 639 Days

Element	Fraction Released at 639 Days ^(a)	Source
Cs	2.8×10^{-2}	Fission product
Sr	2.0×10^{-2}	Fission product
Co	1.6×10^{-2}	Activation product
Sb	1.1×10^{-2}	Fission product
Mn	7.7×10^{-3}	Activation product
Pu	2.3×10^{-3}	Actinide
Eu	2.6×10^{-4}	Fission product
Cm	1.9×10^{-4}	Actinide
Ce	4.8×10^{-5}	Fission product

(a) Averaged over the four glass sections.

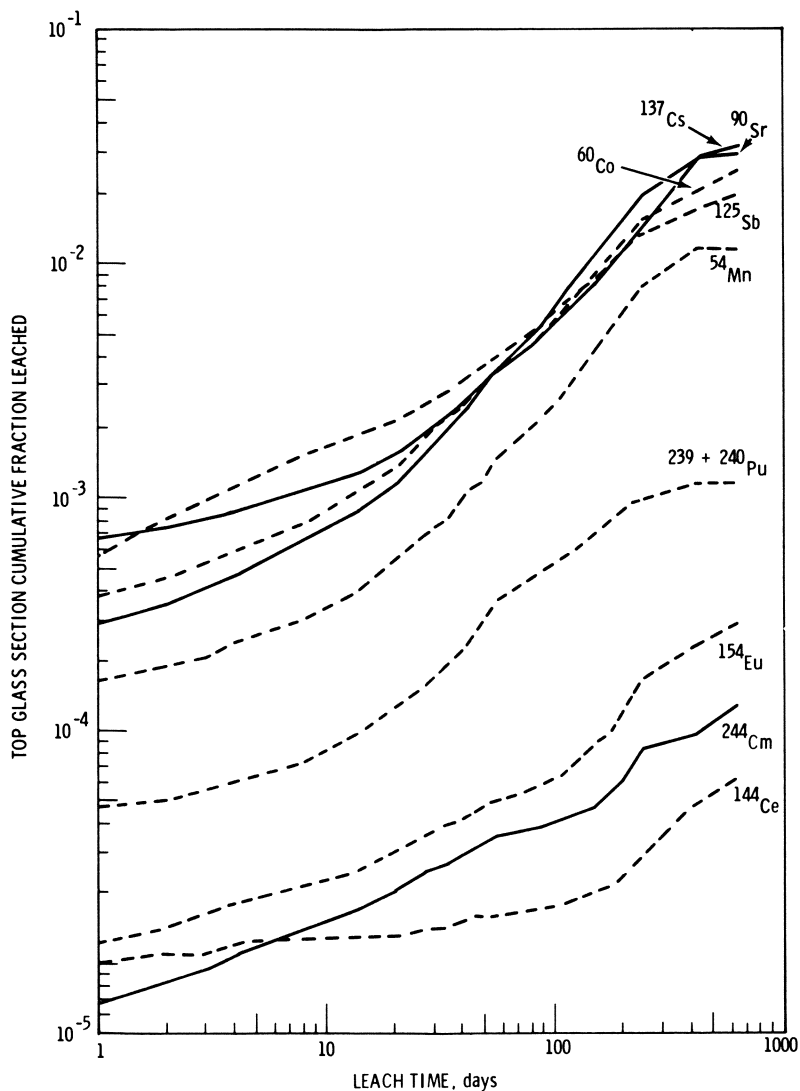


Figure 6. Cumulative fraction leached as a function of time—top glass section

In several respects, this ranking is not unexpected; low charge, high mobility ions like Ca^{1+} and Sr^{2+} should leach more easily than the rare earth and actinide elements. Although plutonium and cerium have similar properties as pure oxides, Plutonium was found to have a higher release rate than Cerium or Curium. Obviously, much more work is needed to understand these differences than was possible with this study.

Fractional release can be expressed using Fick's Law;⁽⁷⁾

$$F_r = bT^m$$

or

$$\log F_r = m \log T + \log b = m \log T + B$$

where

- F • Isotope fraction released
- T • Time
- B • Intercept
- m • Slope of the line.

The slope is indicative of the type of release mechanism. A slope of 0.5 indicates a diffusion-controlled release; a slope of 1.0 indicates that a corrosion-related mechanism is operable.^(7,9,10) The diffusion release mechanism is characterized by surface adsorption, ion exchange, and migration. Chemical corrosion, or alteration of the silicate lattice, is characterized by hydroxyl attack on silicon or by hydrogen attack on bridging oxygens.⁽¹¹⁾

The leachate sampling frequency had little effect on leach rate until the semi-annual frequency was reached. The change in leach rate, as reflected in Figures 3a, 3b, 4, 5, and 6, was dramatic in changing from monthly to semi-annual sampling. The apparent mechanism shifted from lattice alteration to diffusion release; this shift illustrates the important role of dissolved species in lowering the leach rate. These results are consistent with the work of El-Shamy⁽¹²⁾ and Paul.⁽¹³⁾

From the curves of cumulative fraction release, the general trend over the total testing time shows two different slopes for each element. All of the elements have a slope less than 0.50 at the beginning of the leach test, indicating a type of diffusion-controlled release. After a period of time, this slope gradually approaches a value of 1, indicating a combination of release mechanisms. This result is consistent with discussions of release mechanisms in the literature.^(7,11) Table III summarizes these results by element for the top section of high-level waste glass.

TABLE III. Slopes of Initial and Long-Term Release Mechanisms

<u>Elements</u>	<u>Initial Slope/ Time Period, Days</u>	<u>Long-Term Slope/ Time Period, Days</u>
Mn	0.31/1-8	0.84/8-639
Co	0.33/1-8	0.81/8-639
Sr	0.24/1-8	0.76/8-639
Sb	0.47/1-30	0.67/30-639
Cs	0.40/1-8	0.91/8-639
Ce	0.12/1-100	0.70/100-639
Eu	0.31/1-20	0.66/20-639
Pu	0.21/1-8	0.64/8-639
Cm	0.39/1-150	0.72/150-639

The scope of this work was not intended to include study and analysis of leaching mechanisms beyond this point, but the data do show that the mechanism is dependent on time, sampling frequency, and type of element. Also, over the long testing period, two different mechanisms account for the release of material. More work is needed to increase our understanding of these high-level waste glass-solution interactions.

Release rate data from actual radioactive waste forms is needed to evaluate the safety of emplacing nuclear wastes in geologic media. However, in addition to waste form development studies, such as the leach test just described, a comprehensive program was started to obtain release data from candidate waste forms for geologic disposal.

This work is the objective of Task #2 of the Waste Isolation Safety Assessment Program at PNL.⁽¹⁴⁾ We currently are evaluating the effect of leach solution composition on radioisotope release. Figure 7 shows the progression of experiments from simple waste form/solution interactions to those combining the waste form with the containment, solution, backfill, and rock media under hydrothermal conditions. Studies using site-specific conditions are also planned, along with possible large-scale hot-cell or in situ tests. The waste forms and experiments currently being studied and planned are depicted in Figure 8.

CONCLUSIONS

The release rate was determined for 10 radioisotopes from fully radioactive waste glasses in deionized water for a period of 1.75 years. For cesium and strontium, good agreement exists between the leach rates for simulated and fully radioactive glass of the same composition.

The release rate mechanism is dependent on time, sampling frequency, and type of element. For this study, only sampling intervals greater than one month had significant impact on the leach rate. Over the long testing period two different release

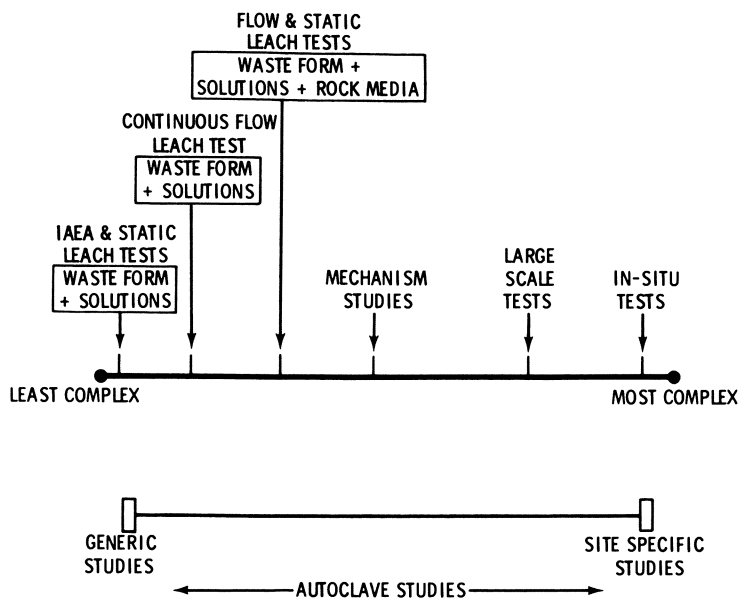


Figure 7. WISAP Task #2 leaching program

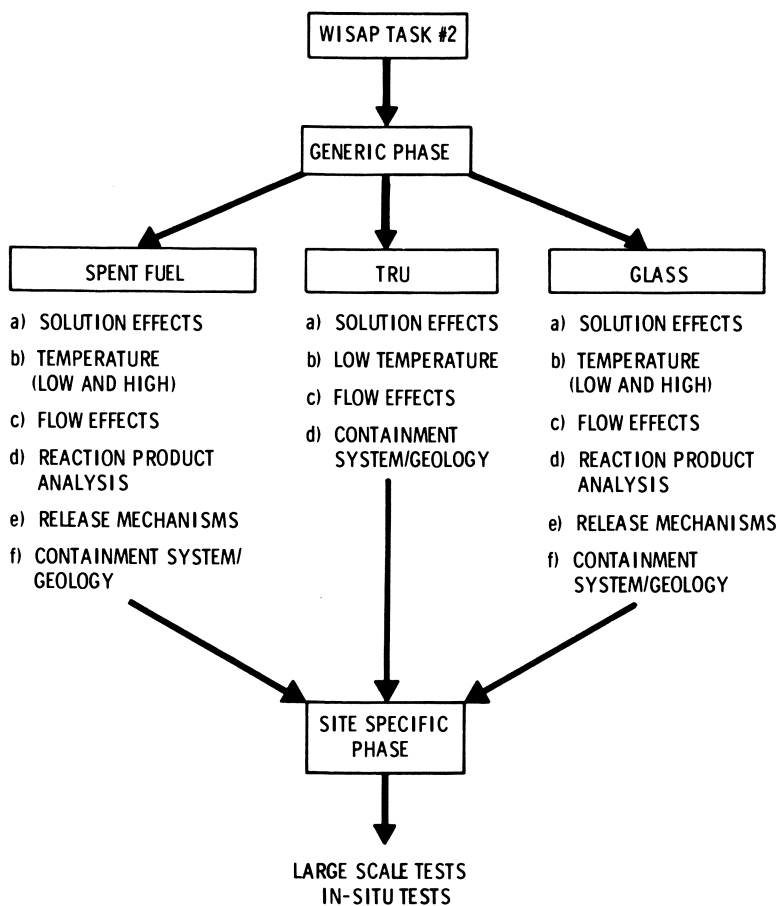


Figure 8. Waste form release experiment outline

mechanisms occurred. This is consistent with previously reported observations.

Special areas needing additional work are:

- the effect of surface area to leachate volume ratio on leaching
- the nature and importance of protective films formed during leaching
- solution saturation/chemical-back reactions
- actinide oxidation states/bonding
- radiation/radiolysis effects.

Release rates of radioisotopes should be determined from actual nuclear wastes. The release rates of these isotopes must be measured under conditions of geologic storage. To obtain this data, Task #2 of the WISAP will study release from waste forms under a variety of conditions to simulate geologic storage of nuclear waste materials.

ACKNOWLEDGMENTS

The author appreciates the help of Y. B. Katayama on the glass preparation; J. H. Westsik, J. E. Mendel, and R. P. Turcotte on the text; and J. C. Nelson, C. E. Bigelow, and J. R. Crockett for performing the hot-cell work.

LITERATURE CITED

1. M. J. Bell, ORIGEN - The ORNL Isotope Generation and Depletion Code, ORNL-4628, Oak Ridge National Laboratory, Oak Ridge, TN 37830, May 1973.
2. J. E. Mendel, W. A. Ross, F. P. Roberts, Y. B. Katayama, J. H. Westsik, Jr., R. P. Turcotte, J. W. Wald, and D. J. Bradley, Annual Report on the Characteristics of High-Level Waste Glasses, BNWL-2252, Battelle, Pacific Northwest Laboratories, Richland, WA 99352, June 1977.
3. W. A. Ross, D. J. Bradley, R. L. Bunnell, W. J. Gray, Y. B. Katayama, G. B. Mellinger, J. E. Mendel, F. P. Roberts, R. P. Turcotte, J. W. Wald, W. E. Weber, and J. H. Westsik, Jr., Annual Report on the Characteristics of High-Level Waste Glasses, BNWL-2625, Battelle, Pacific Northwest Laboratories, Richland, WA 99352, May 1978.
4. D. J. Bradley, Leaching of Fully Radioactive High-Level Waste Glass, PNL-2664, Battelle, Pacific Northwest Laboratories, Richland, WA 99352, May 1978.
5. E. D. Hespe, ed., "Leach Testing of Immobilized Radioactive Waste Solids, A Proposal for a Standard Method." Atomic Energy Review 9:1, 1971.

6. P. Arthur and O. M. Smith, "Semi-Micro Qualitative Analysis," International Chemistry Series, McGraw Hill, New York, NY, 1942.
7. Y. B. Katayama, Leaching of Irradiated LWR Fuel Pellets in Deionized and Typical Ground Water, BNWL-2057, Battelle, Pacific Northwest Laboratories, Richland, WA 99352, July 1976.
8. J. E. Mendel, W. A. Ross, F. P. Roberts, R. P. Turcotte, Y. B. Katayama and J. H. Westsik, Jr., "Thermal and Radiation Effects on Borosilicate Waste Glasses." In: IAEA Symposium on Management of Radioactive Waste from the Nuclear Fuel Cycle, IAEA-SM-207/100, 2:49, Vienna, 1976.
9. L. L. Hench, "Leaching of Glass," Workshop on Ceramic and Glass Radioactive Waste Forms, Germantown, MD, January 1977.
10. R. W. Douglas and T. M. M. El-Shamy, "Reactions of Glasses with Aqueous Solutions," Journal of American Ceramic Society, 50(1):1-8, January 21, 1967.
11. F. E. Diebold, Discussions of Glass - Water Interactions, ARH-2905, September 15, 1973.
12. T. M. M. El-Shamy, PhD. Thesis, University of Sheffield, Sheffield, UK, 1966.
13. A. Paul, Chemical Durability of Glasses, A Thermodynamic Approach, University of Sheffield, Sheffield, UK, 1977.
14. H. C. Burkholder, J. Greenborg, J. A. Stottlemeyer, D. J. Bradley, J. R. Raymond, and R. J. Serne, Waste Isolation Safety Assessment Program Summary of FY 1977 Progress, PNL-2451, Battelle, Pacific Northwest Laboratories, Richland, WA 99352, November 1977.

RECEIVED January 16, 1979.

Single-Pass Leaching of Nuclear Melt Glass by Groundwater

DAVID G. COLES, HOMER C. WEED, DONALD D. JACKSON,
and JAMES S. SCHWEIGER

Nuclear Chemistry Division, L-233, Lawrence Livermore Laboratory,
P.O. Box 808, Livermore, CA 94550

The work presented in this report was supported by the Department of Energy (DOE) through the Nevada Operations Office (NVOO) as part of the Radionuclide Migration Program at the Nevada Test Site (NTS). The purpose of this program is to investigate the potential for underground migration of radionuclides in groundwater from the sites of underground nuclear explosions. Borg et al. have comprehensively reviewed this subject and have included an annotated bibliography (1). Levy (2) discusses in detail the specific aspects of an underground nuclear explosion which are relevant to radionuclide contamination of the groundwater. The technology required to study the NTS groundwater problem is very similar to that required for studying the geologic disposal of high-level vitrified nuclear reactor wastes.

The energy crisis of the 1970's has emphasized the need for nuclear power and consequently there is considerable interest in developing an environmentally-acceptable means for disposing of the resultant nuclear wastes. deMarsily et al. (3) have discussed the feasibility for geologic disposal of nuclear wastes and have concluded that ion exchange with the rock surrounding the repository is the most important barrier between the waste and the biosphere. The Study Group on Nuclear Fuel Cycles and Waste Management of the American Physical Society (4) concluded that the management of nuclear waste was well within existing technology and that economic and political questions provided the greatest problems for nuclear energy use. They also state that hydrogeologic transport is the most likely route for contamination of the biosphere by a waste repository.

Information on the interaction of radionuclides with groundwater in deeply-buried, high-level, long-term "waste repositories" is available at only a few locations. One is the OKLO natural reactor in Gabon which has for over 1.7 billion years retained some of the radionuclides also present in nuclear wastes (5). Another is the Nevada Test Site, where radionuclides were first deposited underground on September 19, 1967 during the 1.7 kt

0-8412-0498-5/79/47-100-093\$05.50/0

© 1979 American Chemical Society

Rainier event. The first of 78 tests beneath the regional water table was the 200 kt Bilby event on September 13, 1963; others have been detonated up to May, 1976. OKLO and NTS are among the few areas available for study, where radionuclide compositions have interacted with groundwater for significant periods of time. The cavities from tests beneath the water table are analogous to 78 small flooded waste repositories. The analogy between a NTS nuclear cavity and a waste repository is particularly close since the activity has to be leached from the puddle glass or chimney debris before entering the groundwater system and leaching from the puddle glass is similar to leaching from high-level vitrified reactor waste. Nuclear explosion phenomenology has been reviewed by Borg et al. (1) and the distribution of radionuclides within the glass and the rubble chimney has been discussed by Borg (6) and by Dupuis (7). Generally, refractory elements remain in the melt glass and volatile elements condense out on the chimney rubble.

A field test at NTS was recently undertaken in order to determine the amount of various radionuclides which had been leached from the melt glass and chimney rubble produced during the Cambric event (8). Samples were obtained at different zones within the chimney and cavity, and analyzed to determine the radionuclide source term available for possible groundwater transport. However, little quantitative data on the rate of leaching from the melt glass resulted. Recent quantitative laboratory data on the static leaching of both melt glass and chimney rubble have been obtained by Wolfsberg (9). He has been able to do some limited comparisons between these laboratory measurements and the field measurements obtained on the Cambric cavity.

In the past, most leaching experiments have been done using a static or batch method in which samples of glass were immersed in water or water solutions for some specified period of time. The resultant aqueous phase was separated from the glass and analyzed for the element or radionuclide of interest. Paige (10) has described a leaching experiment in which the liquid is recirculated over the glass in an extraction-like apparatus, Mendel (11) has prepared a review of leaching test methodology, and the IAEA has suggested a static (batch) leaching procedure as a standard procedure (12). Others have studied glass durability (13,14) and performed a field test on vitrified reactor wastes (15). Some very limited leaching tests on nuclear explosion melt glass were reviewed by Borg et al. (1).

Our leaching concept differs significantly from those discussed previously because it uses a dynamic flow-through system in which the solid sample is continually exposed to fresh leaching solution. Such a dynamic system is designed to simulate actual underground conditions. It is a nonequilibrium system in which the displacement from equilibrium can be varied by changing the flow rate. The samples leached in our study are carefully selected nuclear explosion melt glasses, chosen to represent

typical NTS radionuclide transport sources. They are well characterized and are close analogues to vitrified high-level reactor wastes.

This interim report covers the results of the first 120 days of leaching out of a planned 420 days. A final report will be issued after the experiment is terminated January 3, 1979.

Experimental

Equipment design: The details of the equipment are described by Weed and Jackson (16). Specially-designed sample cells retain the glass by means of 0.1 μm pore size Nuclepore filters on the inlet and the outlet sides (see Figure 1). A schematic drawing of the system is shown in Figure 2. Water is metered through the cells with two peristaltic pumps located immediately upstream from the cells; each pump can drive up to 10 pumping cassettes simultaneously. Connecting lines consist of small-bore plastic tubing and Luer press-fit plastic connectors, and all the rest of the fluid handling system is made of plastic. The water is fed by gravity from an atmospherically-isolated supply carboy and is filtered twice before entering the pumps. The 20 sample cells are held at 25°C in a constant temperature bath. Tubes exiting from the tops of the cells enter directly into plastic bottles. Two cells (#7 and #17) are arranged so that the flow is downward.

Sample characterization: Gram quantities of NTS nuclear explosion melt glass were obtained from core samples of the cooled puddles in the bottom of the explosion cavity. Samples from three separate tests were obtained for leaching in this experiment. All three tests had been detonated from 1.5 to 0.5 years prior to the commencement of leaching and were chosen for their high fission to fusion ratio in order to provide the highest levels and greatest variety of radionuclides in the glass. For this interim report, only leaching data from the most recent (Melt Glass #3) test are presented here since this glass contains the highest activity concentration and hence gives optimum analytical sensitivity for radioactivity in the leachate.

Samples from individual cores were hand separated at NTS from drilling mud and rock chunks. Samples were selected for the experiment if their size exceeded 1 cm diameter and if they were hard, vitreous, and radioactive. Each core yielded from one to eight pieces of material that met these criteria. Samples were obtained from four cores from Test 1, ten cores from Test 2, and five cores from Test 3.

Upon receipt of the samples in the laboratory, they were cleaned with distilled water in an ultrasonic cleaner aided by a small brush, air dried, and photographed for later reference. It was assumed that the surface leaching of these chunks was small compared to the surface area available for leaching after the samples were ground. A representative sample from each core was

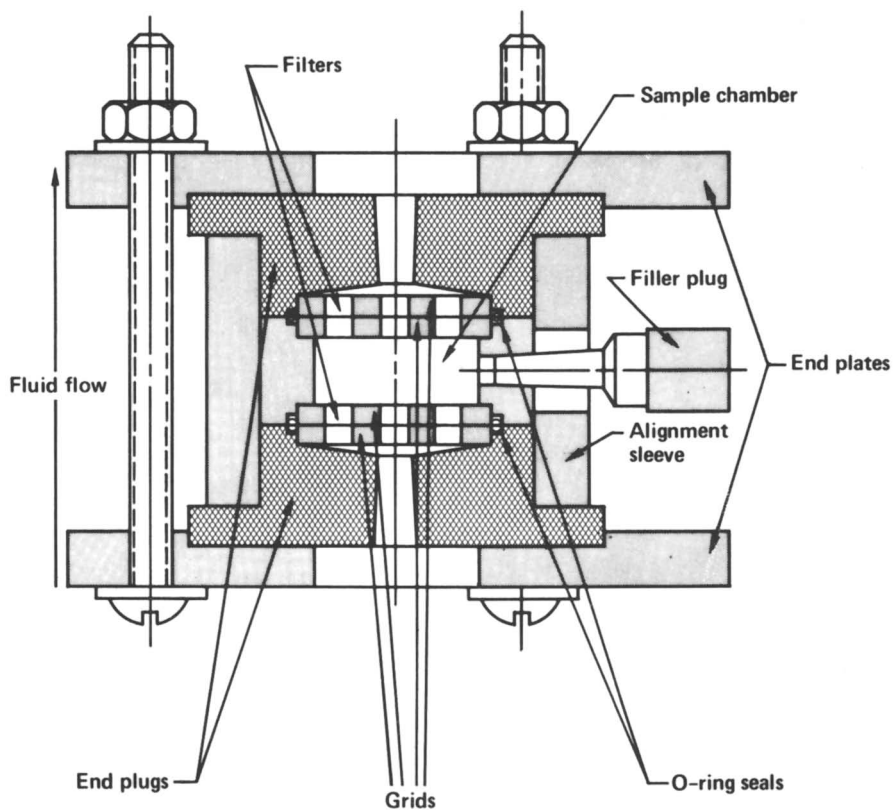


Figure 1. Sample holder assembly, one-pass leaching system

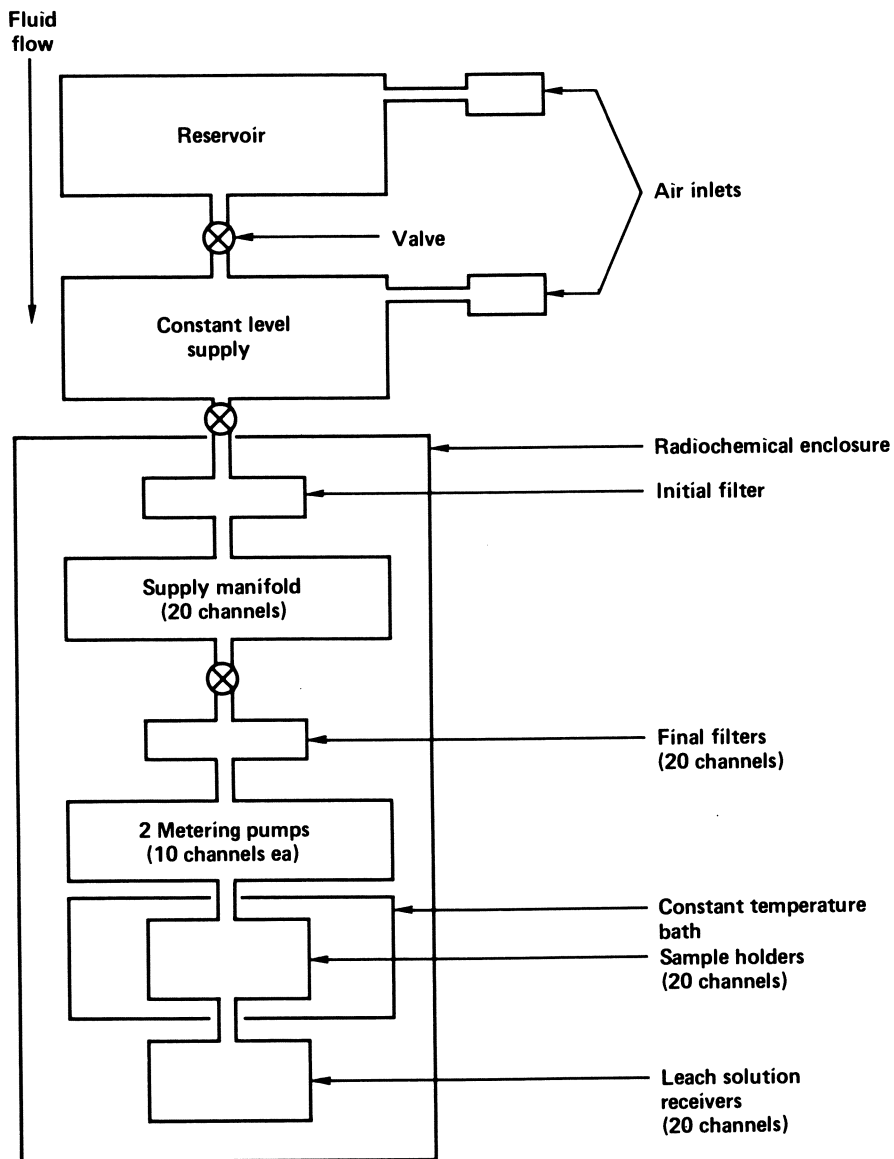


Figure 2. One-pass continuous leaching system—functional diagram

Publication Date: April 6, 1979 | doi: 10.1021/bk-1979-0100.ch006

then gamma-counted on a Ge(Li) gamma-ray spectrometer in order to see if any core was significantly different from the other cores. In particular, the ratio of a selected refractory element (e.g. ^{144}Ce) to a volatile element (or an element with a volatile precursor, e.g. ^{137}Cs) was carefully observed. In all cases it was determined that each core represented melt glass.

All samples were then ground to -100 mesh and the (-100 + 325) mesh fraction was used for the leaching experiment. Thus the sample representing each core contained particles from 43 to 147 μm diameter. That particular size range was chosen so that the smallest particles were much larger than the leaching cell filter pores (430 times larger in this case). Also, they could be handled without generating radioactive dust but were still small enough to release a detectable amount of radioactivity upon leaching.

After grinding, sieving, and mixing, a 0.5 g aliquot from each core composite (10-30 g total) was gamma-counted to document the activity of each core for later correlation with the physical nature of the original core chunks and with the x-ray diffraction data. Table I lists the x-ray data: the cores range from 65 to 100 percent glass content. From these data and the consistency of the correlation between gamma-counting data and x-ray data it was determined to mix all core samples from Test 1 to produce a Test 1 composite sample. The Test 2 composite sample and the Test 3 composite sample were prepared in a similar manner. After intensive mixing, triplicate 0.5 g samples from each composite sample were analyzed by gamma spectroscopy and the mean of these triplicate analyses was used as the preleach glass radionuclide content (Q_0) for each composite test sample. Radionuclides observed in the glass and the leachate are listed in Table II.

Triplicate aliquots were taken for particle size analysis and two of those aliquots were mixed for BET surface area analysis: results are in Table III. The nine samples were individually sieved for size distribution. A chi-squared test was performed on each triplicate set in order to check the apparent efficiency of composite mixing. For all three composite samples, there was a 90 percent probability that each of the three replicates from each composite sample came from the same population. The A and C samples were combined and evaluated for surface area by nitrogen adsorption (BET). The B samples were then subjected to scanning electron microscopy (SEM) analysis. Figures 3-5 are SEM photographs of each glass composite at 2000-fold magnification. These photographs show conchoidal fracturing indicative of glass, as well as some very fine particles attached to the larger particles.

Leaching experiment: The experimental scheme is shown in Figure 6. The variables in this experiment are the three glass compositions from three different tests and the two flow rates. The glass compositions have just been discussed. The linear flow rates are 36 and 6.7 cm/day, corresponding to volume flow rates

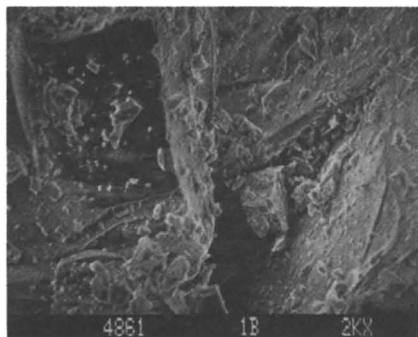


Figure 3. SEM photograph of Glass #1 (1280X)

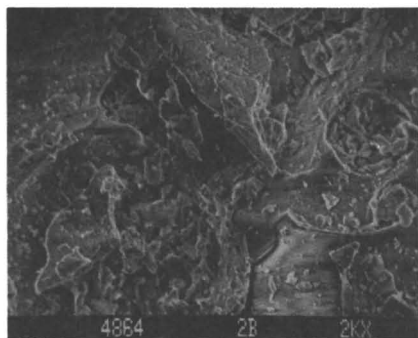


Figure 4. SEM photograph of Glass #2 (1280X)

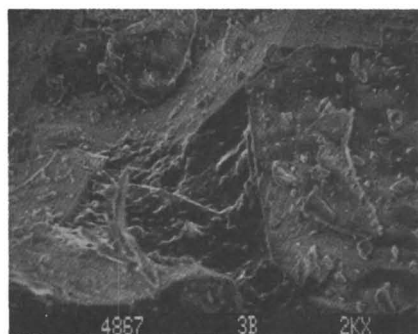


Figure 5. SEM photograph of Glass #3 (1280X)

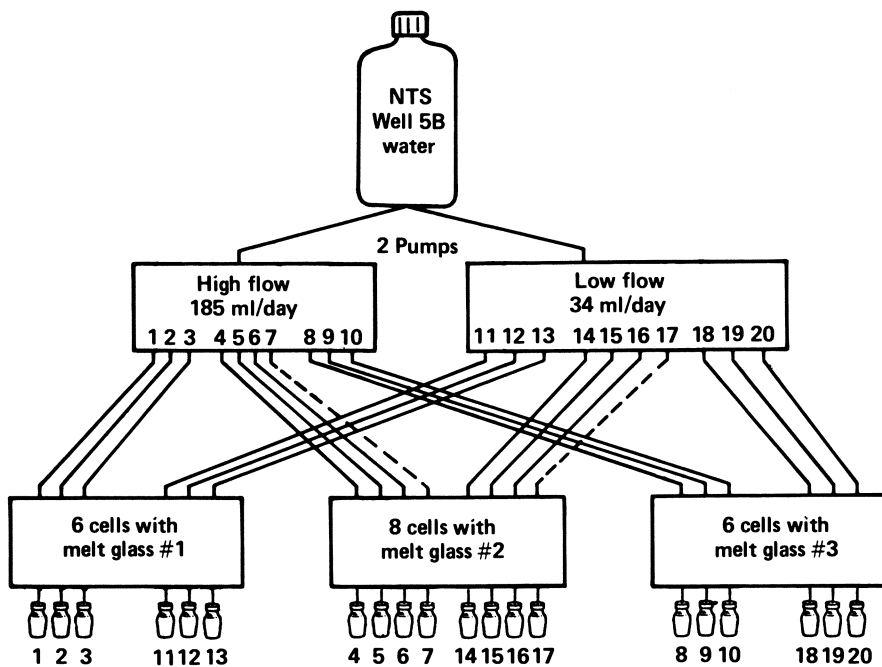


Figure 6. Experimental matrix—melt glass leaching experiment: (---), flow is downward through sample; (—), for all others flow is upward.

Table I. X-Ray Diffraction Analysis of NTS Melt Glass Samples

Melt Glass No. Core No.	Glass	Quartz	α Cristobalite	Feldspar
1-7	75%	5%	T*	10%
1-8	75	5	T	10
1-12	\approx 100	T	-	T
1-18	\approx 100	T	-	T
2-5	75	5	T	5
2-7	75	5	T	5
2-8	85	5	-	T
2-9	85	5	-	T
2-10	75	5	T	5
2-11	75	5	-	5
2-12	65	10	T	5
2-13	75	5	-	5
2-14	75	5	T	5
2-15	75	5	T	5
3-5	85	5	T	T
3-6	85	5	T	T
3-7	85	T	-	T
3-8	85	5	T	T
3-10	\approx 100	T	T	T

*T = trace

Table II. Radionuclides Observed in the Melt Glass and Leachate Samples

^{22}Na	^{124}Sb
^{54}Mn	^{125}Sb
$^{59}\text{Fe}^{\text{a}}$	$^{134}\text{Cs}^{\text{b}}$
^{57}Co	^{137}Cs
^{58}Co	$^{141}\text{Ce}^{\text{b}}$
^{60}Co	^{144}Ce
$^{65}\text{Zn}^{\text{a}}$	$^{155}\text{Eu}^{\text{b}}$
^{95}Zr	$^{168}\text{Tm}^{\text{b}}$
$^{103}\text{Ru}^{\text{b}}$	$^{182}\text{Ta}^{\text{b}}$
^{106}Ru	

^a not observed in any leachate samples^b observed only sporadically in leachate samples

of 185 and 34 ml/day. Temperature (25°C) and water composition were kept constant. Six samples of each glass were included in order to provide triplication at each flow rate. Also, two cells containing Melt Glass #2 (#7 and #17) were arranged with reverse flow (inlet at the top and outlet through the bottom). This was done to minimize stirring of the glass as might be expected with the upward flowing cells. In retrospect, we think these two cells should probably have been filled with ground obsidian and used for radiochemical blanks.

The water used for the leaching was from the NTS water well 5B, chosen because it represents a typical NTS groundwater. The composition of this water was determined by spectrochemical analysis and is shown in Table IV. A 208-liter polyethylene-lined drum was filled with this water approximately every two months and shipped to Livermore. Two-month renewal intervals were chosen since the leaching apparatus consumed water at about that rate. The pH of this water was determined at Livermore one week after collection and found to be 8.13 ± 0.01 .

Preweighed samples (about 0.5g) were loaded into each cell by plugging the inlet port, pulling a vacuum on the exit port, and pouring the ground glass through a funnel into the side access port. This procedure greatly reduced the chances for spillage of the powder or spreading of dust. The cell was then filled with well 5B water and put on-line by connecting it to a previously filled inlet line.

The sampling schedule was chosen in order to accumulate early data rapidly since we expected the largest changes in the leach rate at the beginning of the experiment. Also, when plotted on log paper, this sequence maintained approximately equal time separation between data points.

The procedure was to collect and composite all water accumulated from the start through Day 1, then through Day 2, and so on. Composite samples were collected on Days 1, 2, 3, 6, 11, 32, 38, 70, and 120. Thus the composite sample collected on Day 6 also included leachate from Days 4 and 5; that collected on Day 70 included leachate from Days 39 through 69; and so on. The sample for Day 230 has been collected but results from it are not included in this discussion. The last composite sample (Day 420) will be collected on 3 January 1979. Collection at Day 32 was planned for Day 20 but a scheduling error moved it back 12 days.

Samples were collected in polyethylene bottles and at the end of a sampling period or when the bottles were nearly full, they were transferred completely into a one-liter polyethylene bottle which had been lined with a 5 x 10 x 30 cm polyethylene bag. The sample in the bag was then evaporated at 85°C. If more than one filling was required (as was expected for long sampling intervals) the bag-lined bottle could be refilled several days after the evaporation was concluded. The final composite sample, after evaporation, consisted of a few grams of salts in the bottom of the polyethylene bag. The bag was rolled so that

Table III. Melt Glass Surface Area and Size Analysis

Sample	Surface Area (m ² /gm)	Diameter (μm)		
		10%	50%	90%
MG# 1A		50	87	136
1B		45	84	135
1C		45	85	136
1A + 1C	0.396			
MG# 2A		42	80	132
2B		45	79	133
2C		44	81	132
2A + 2C	0.465			
MG# 3A		41	79	133
3B		42	78	132
3C		42	78	132
3A + 3C	0.457			

Table IV. Composition of Well-5B Water, NTS¹

Element	(μg/ml)	Element	(μg/ml)	Element	(μg/ml)
Al	<0.004	K	12.	Pb	0.032
As	<0.05	Li	0.043	Si	28.
B	0.023	Mg	2.5	Sr	0.030
Ca	7.9	Mn	0.007	Ti	<0.0005
Cd	0.004	Mo	0.015	V	0.011
Co	0.004	Na	97.	Zn	<0.001
Cu	<0.001	Ni	<0.004	Zr	<0.0005
Fe	0.13	P	<0.07		

pH at Livermore = 8.13 ± .01

pH² - High flow rate = 8.40 ± .06

pH² - Low flow rate = 8.65 ± .03

¹As determined by spectrochemical analysis, LLL, all errors <10%.

²pH values are the mean of measurements taken for the first five sampling periods.

the salts were kept in the center, placed in a 31.75 mm (1.25 inch) diameter die, and then compressed for 10 minutes at 30.3 MPa (4400 psi) and 150°C. The resultant pellet containing the leached activity was gamma-counted on a low-background Ge(Li) gamma-ray spectrometer for 24 hours. An experiment on a ^{137}Cs -spiked groundwater sample indicated that the expected polyethylene-salt inhomogeneities in the pellet resulted in error of less than 5 percent.

Results and Discussion

Table V presents the leaching data for Melt Glass #3 only. Glasses #1 and #2 were omitted from this interim report since they were both older than #3 and provided lower sensitivity for radionuclide detection. The data in Table V were calculated using the following equation: (12)

$$R = (Q/Q_0)(1/\Delta t)(1/S) \quad (1)$$

where

Q = total activity leached during Δt

Q_0 = total activity in glass before leaching

Δt = interval of leaching, days

R = fraction leached per day per m^2 surface area

S = total sample-surface area, m^2

Figures 7-10 present R as a function of mean leaching time t at high and low flow rates for all radionuclides except Pu. Rates for Pu will be presented later when Pu analyses are completed. Usually R increases with increasing flow rate, but the increase is probably not significant for any nuclide except ^{144}Ce . Also, R usually decreases with time in agreement with the relation discussed by Diebold (17):

$$R = at^{-0.5} + b \quad (2)$$

where a involves diffusion through a surface film as a rate determining step and b involves glass dissolution at long times as a rate-determining step. Exceptions to this occur for ^{95}Zr and ^{137}Cs at long times and for ^{144}Ce at low flow rate. Rates for the following nuclides are in qualitative agreement with Equation (2): ^{22}Na , ^{54}Mn , ^{57}Co , ^{58}Co , ^{60}Co , ^{106}Ru , ^{124}Sb , ^{125}Sb . Since the experimental work is not complete, no attempt has been made at this stage to obtain numerical values for a and b.

Two possible causes for the increase in leach rates at long times for ^{95}Zr and ^{137}Cs are increased glass dissolution rates or cross-contamination of the leachate samples. At this point

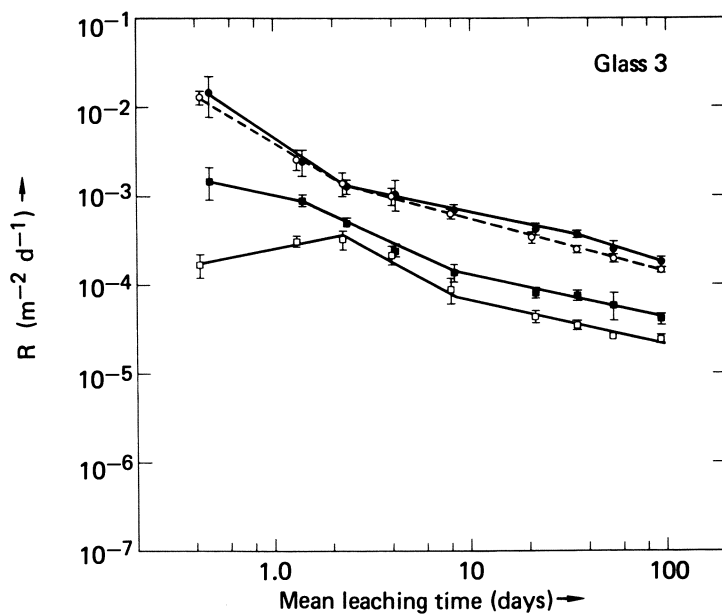


Figure 7. Leaching rates of ^{22}Na and ^{54}Mn at high and low flow rates vs. mean leaching time: (\bullet), ^{22}Na hi; (\circ), ^{22}Na low; (\blacksquare), ^{54}Mn hi; (\square), ^{54}Mn low.

TABLE V. LEACHING

Day	High/ Low	Volume flow rate ($\bar{X} \pm 1\sigma$)	Δt^a (days)	Median time ^b (days)	$R \times 10^4$			
					^{22}Na	^{54}Mn	^{57}Co	^{58}Co
01	High	194 \pm 3%	0.936	0.468	150 \pm 70	15 \pm 6	12 \pm 4	10 \pm 3
02	High	193 \pm 4	0.930	1.40	25 \pm 8	9 \pm 1	7.2 \pm 0.7	6.5 \pm 0.7
03	High	191 \pm 8	0.984	2.36	13 \pm 2	4.9 \pm 0.7	4.4 \pm 0.5	3.9 \pm 0.5
06	High	194 \pm 4	2.68	4.19	11 \pm 4	2.5 \pm 0.3	2.3 \pm 0.2	2.1 \pm 0.4
11	High	197 \pm 3	5.27	8.17	7.2 \pm 0.7	1.4 \pm 0.3	1.3 \pm 0.3	1.2 \pm 0.4
32	High	189 \pm 6	21.3	21.4	4.2 \pm 0.6	0.8 \pm 0.1	0.83 \pm 0.08	0.72 \pm 0.08
38	High	217 \pm 8	5.65	34.9	3.7 \pm 0.3	0.75 \pm 0.09	0.80 \pm 0.05	0.77 \pm 0.09
70	High	190 \pm 4	32.1	53.8	2.5 \pm 0.5	0.6 \pm 0.2	0.6 \pm 0.1	0.6 \pm 0.2
120	High	163 \pm 15	49.7	94.7	1.8 \pm 0.2	0.41 \pm 0.05	0.44 \pm 0.03	0.41 \pm 0.04
01	Low	32.1 \pm 6%	0.838	0.419	130 \pm 20	1.7 \pm 0.5	2.5 \pm 1.1	0.6 \pm 0.7
02	Low	35.2 \pm 3	0.930	1.30	26 \pm 6	3.1 \pm 0.2	2.0 \pm 0.1	1.8 \pm 0.3
03	Low	35.0 \pm 4	0.984	2.26	14 \pm 4	3.3 \pm 0.8	2.0 \pm 0.4	1.8 \pm 0.5
06	Low	35.1 \pm 4	2.68	4.09	10 \pm 2	2.2 \pm 0.5	1.6 \pm 0.3	1.5 \pm 0.4
11	Low	35.1 \pm 4	5.27	8.07	6.4 \pm 0.6	0.9 \pm 0.3	0.8 \pm 0.1	0.7 \pm 0.2
32	Low	35.1 \pm 5	21.3	21.3	3.4 \pm 0.4	0.44 \pm 0.07	0.44 \pm 0.05	0.36 \pm 0.04
38	Low	37.5 \pm 5	5.65	34.8	2.5 \pm 0.1	0.34 \pm 0.01	0.39 \pm 0.02	0.36 \pm 0.05
70	Low	36.0 \pm 5	32.1	53.7	2.0 \pm 0.2	0.26 \pm 0.01	0.31 \pm 0.03	0.27 \pm 0.03
120	Low	36.6 \pm 6	49.7	94.6	1.5 \pm 0.1	0.24 \pm 0.03	0.27 \pm 0.03	0.25 \pm 0.04

^a length of each leaching interval^b elapsed time from start of experiment to median of each leaching interval^c ^{95}Zr analysis did not include ^{95}Nb daughter gamma ray (764.5 keV)^d $\bar{X} \pm 1\sigma$ (2 replicates only)^e data from one sample only, $\pm 1\sigma$ counting statistics^f ND = not detected

DATA FOR MELT GLASS #3

$\bar{X} \pm 1\sigma$ (of 3 samples)						
^{60}Co	$^{95}\text{Zr}^c$	^{106}Ru	^{124}Sb	^{125}Sb	^{137}Cs	^{144}Ce
10 ± 4	1.9 ± 0.7	20 ± 7	67 ± 23	30 ± 11	38 ± 16	1.1 ± 0.3
6.0 ± 0.6	1.0 ± 0.3	5 ± 2^d	24 ± 5	9 ± 3	12 ± 7^e	1.1 ± 0.1
3.6 ± 0.4	0.8 ± 0.4	4 ± 2	12 ± 3	6 ± 4	ND ^f	1.2 ± 0.2
2.0 ± 0.2	0.4 ± 0.08	2 ± 0.6	5 ± 1^d	2 ± 1^d	4 ± 2^e	0.97 ± 0.02
1.1 ± 0.2	0.3 ± 0.1	1.7 ± 0.5	4.4 ± 0.4	1.5 ± 0.6	1.5 ± 0.1^d	0.77 ± 0.08
0.70 ± 0.07	0.21 ± 0.05	1.1 ± 0.2	2.4 ± 0.4	0.9 ± 0.6^e	0.74 ± 0.07^d	0.7 ± 0.1
0.70 ± 0.03	0.22 ± 0.08	1.3 ± 0.6	ND	0.6 ± 0.3^e	2.3 ± 0.7^e	0.73 ± 0.08
0.6 ± 0.1	0.2 ± 0.1	0.8 ± 0.2	1.5 ± 0.8^d	0.8 ± 0.2	ND	0.6 ± 0.2
0.39 ± 0.04	0.22 ± 0.01	0.5 ± 0.1	ND ^a	0.4 ± 0.1	3 ± 1	0.48 ± 0.09
2.4 ± 1.1	0.7 ± 0.4	11 ± 2	27 ± 4	19 ± 2	29 ± 7	0.15 ± 0.05
1.6 ± 0.1	0.5 ± 0.2	ND	21 ± 6	12 ± 1	19 ± 1	ND
1.7 ± 0.3	0.6 ± 0.4^d	2.7 ± 1.5^e	12 ± 4	6.7 ± 0.9^d	ND	ND
1.4 ± 0.3	ND	1.5 ± 0.8^e	8 ± 2	2.5 ± 0.4	2.7 ± 0.2^d	ND
0.7 ± 0.1	0.13 ± 0.06^e	1.1 ± 0.4	3.3 ± 0.9	1.0 ± 0.2^d	1.4 ± 0.1^d	0.013 ± 0.005^e
0.36 ± 0.04	0.08 ± 0.01^d	0.6 ± 0.1	4 ± 2	0.6 ± 0.1	0.4 ± 0.3^e	0.03 ± 0.006
0.31 ± 0.04	0.25 ± 0.05^e	0.8 ± 0.4^e	ND	ND	ND	0.08 ± 0.02^d
0.25 ± 0.02	0.076 ± 0.007^d	0.30 ± 0.06	1.4 ± 0.4	0.34 ± 0.01^d	0.4 ± 0.1^d	0.05 ± 0.02
0.23 ± 0.03	0.11 ± 0.02	0.29 ± 0.09	ND	0.24 ± 0.07^d	2.5 ± 0.8	0.07 ± 0.04

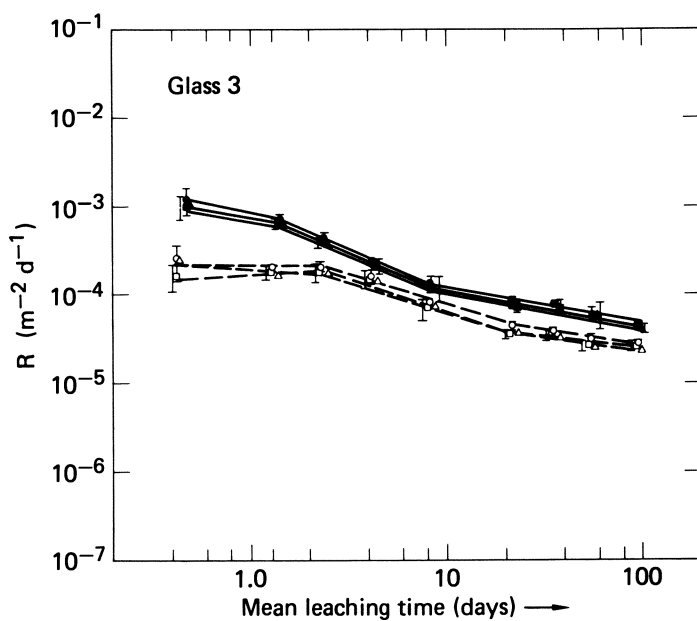


Figure 8. Leaching rates of ^{57}Co , ^{58}Co , and ^{60}Co at high and low flow rates vs. mean leaching time: (\bullet), ^{57}Co hi; (\circ), ^{57}Co low; (\blacksquare), ^{58}Co hi; (\square), ^{58}Co low; (\blacktriangle), ^{60}Co hi; (\triangle), ^{60}Co low.

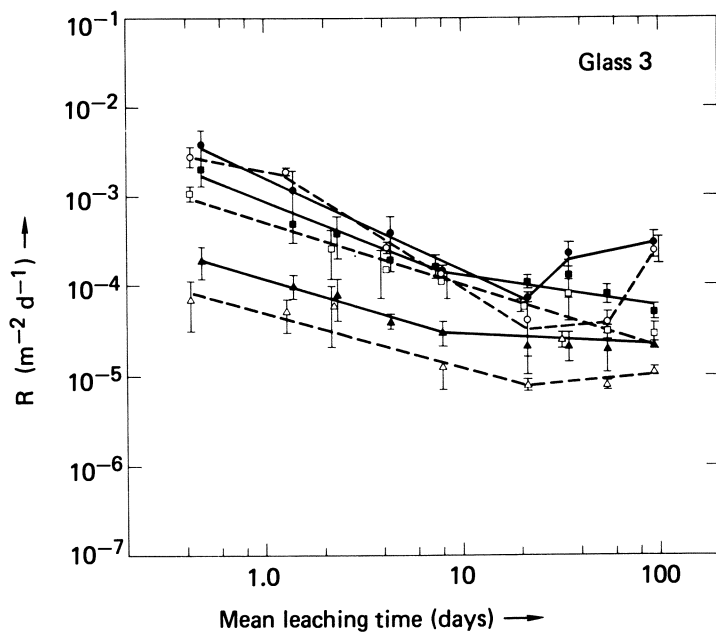


Figure 9. Leaching rates of ^{95}Zr , ^{106}Ru , and ^{137}Cs at high and low flow rates vs. mean leaching time: (\bullet), ^{137}Cs hi; (\circ), ^{137}Cs low; (\blacksquare), ^{106}Ru hi; (\square), ^{106}Ru low; (\blacktriangle), ^{95}Zr hi; (\triangle), ^{95}Zr low.

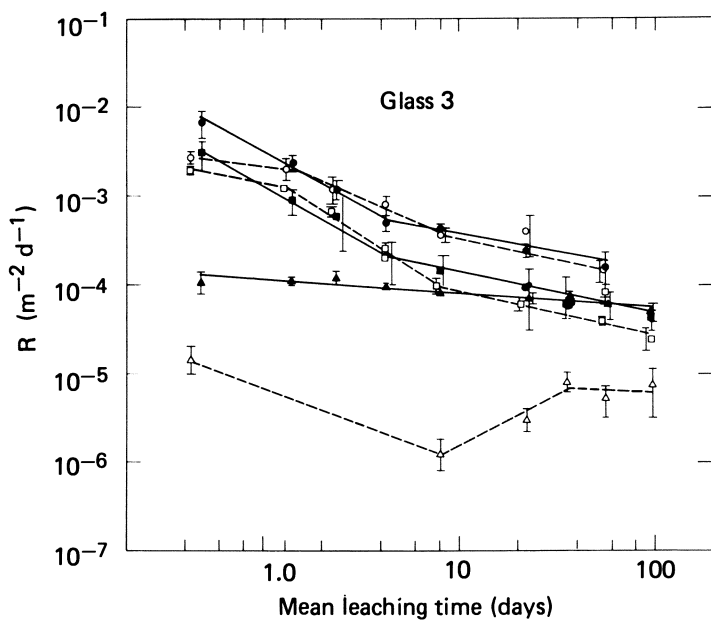
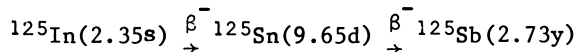


Figure 10. Leaching rates of ^{124}Sb , ^{125}Sb , and ^{144}Ce at high and low flow rates vs. mean leaching time: (●), ^{124}Sb hi; (○), ^{124}Sb low; (■), ^{125}Sb hi; (□), ^{125}Sb low; (▲), ^{144}Ce hi; (△), ^{144}Ce low.

there is not enough experimental evidence to decide between the two, but a knowledge of SiO_4^{--} concentrations in the leachate samples would serve as a check on the glass dissolution rates.

In terms of Equation (2) the leach rate for ^{144}Ce corresponds to a very low value of a and values of b which are very dependent on flow rate. This is consistent with the idea that Ce is so strongly associated with the glass matrix that it is transported into solution almost exclusively by dissolution of the glass.

In the case of the Co and Sb nuclides, there may be some correlation between leaching rate and original mode of production. The leaching rates for ^{57}Co , ^{58}Co , and ^{60}Co are nearly identical. The agreement among these three isotopes of the same element provides some indication of the quality of the experimental data. Since they are all isotopes of Co, immediately upon production ($^{58}\text{Ni}(n,np)^{57}\text{Co}$, $^{58}\text{Ni}(n,p)^{58}\text{Co}$, $^{60}\text{Ni}(n,p)^{60}\text{Co}$, $^{59}\text{Co}(n,\gamma)^{60}\text{Co}$) they should behave similarly through the course of the glass melting and solidification process. Leaching rates for the Sb radionuclides show poorer agreement with each other than those for the Co radionuclides. The radionuclides are produced by the nuclear explosion in quite different ways. Antimony-124 is produced by activation of stable $^{123}\text{Sb}(^{123}\text{Sb}(n,\gamma)^{124}\text{Sb})$ while ^{125}Sb is produced by beta decay along the mass 125 fission product decay chain:



The boiling points of In, Sn and Sb are 2000C, 2270C, and 1380C, respectively, so that the ^{125}Sb precursors should have condensed sooner than ^{124}Sb . Therefore, ^{125}Sb was probably more homogeneously distributed throughout the glass than ^{124}Sb . This in turn suggests that ^{125}Sb should have the lower leach rate of the two. Our experimental results show that ^{125}Sb indeed has a lower leaching rate than ^{124}Sb , but the experimental errors are so large that the difference may not be statistically significant.

According to the theoretical picture corresponding to Equation (2), as protons migrate from solution into the glass and displace cations, the OH^- concentration and solution pH should increase. Our results indicate that when solutions pass over the samples at low flow rates the pH increase is larger (0.52) than at high flow rates (0.27). This suggests that nucleophilic attack on the silicate network should be increased at low flow rates. However, the radionuclide leaching rates at long times indicate that the rate of attack of the silicate network does not change significantly with flow rate, or in the case of ^{144}Ce the rate of attack increases with flow rate. Under the existing flow conditions, the rate-determining step may be transport of dissolved SiO_4^{--} out of the sample cell at low flow rates, and attack on the silicate network at high flow rates. Clearly an independent estimate of the rate of attack on the silicate network would be helpful; it could probably best be made from a

determination of the SiO_4^{--} concentration in the leachate samples.

Conclusions

At this interim stage in the study we conclude as follows:

- Generally, the leaching rates of puddle glass determined by the one-pass dynamic leaching method decrease with time in a similar fashion to those determined on synthetic glasses using various static methods.
- For most of the radionuclides observed, the leaching rates do not depend significantly on the flow rates. Further experiments may be advisable to determine if this is true for the much lower flow rates corresponding to some NTS field conditions.
- Additional analytical work should be done to complete the Pu analyses and to determine the dissolution rates for the silicate network in the glass samples.

Acknowledgements

We are indebted to many people for their help in connection with this investigation. Initially, during the first part of the experiment, Roger Ide provided encouragement and support. We thank P. Bowen for initial fabrication of the water manifolds in the system. Most of the fabrication of the equipment was done by R. Flores who also performed some of the initial flow tests on the peristaltic pumps. J. Bushman and M. Edwards modified and maintained the equipment; W. Beiriger performed the x-ray diffraction analyses; C. Slettevold and A. Biermann performed the particle analysis and determined the surface area on the samples. J. Wittmayer took the SEM photos. We also thank L. Gazlay and D. Hosmer for the gamma-ray spectroscopy analysis. A. Denning helped select the glass samples at NTS. D. Bridges supplied the Well-5B water at NTS. E. Peck performed the spectrochemical analysis on the Well-5B water.

Abstract

Melt glass (fused rock containing fission and activation products and actinides) produced by three underground nuclear explosions has been leached at 25°C with groundwater obtained from a well near the explosion sites. Leaching was carried out in cells with the groundwater passing over glass particles (size range: 40-130 μm) at flow rates of 36 and 6.7 cm/day. With this dynamic flow-through system, the solid sample is continually exposed to fresh leaching solution in an attempt to simulate actual underground conditions. Radionuclide concentrations in

the leachate were obtained at intervals of 1, 2, 3, 6, 11, 32, 38, 70, and 120 days after the leaching began. The fraction of radioactivity leached per day per M^2 surface area varied from 1.5×10^{-2} for ^{22}Na on Day 1 to 7.0×10^{-6} for ^{144}Ce on Day 120. Except for ^{144}Ce , leaching rates did not seem to depend significantly on flow rates.

Literature Cited

1. Borg, I. Y., Stone, R., Levy, H. B., Ramspott, L. D., "Information Pertinent to the Migration of Radionuclides in Ground Water at the Nevada Test Site," Lawrence Livermore Laboratory, Rept. UCRL-52078, Part 1: "Review and Analysis of Existing Information," (May 25, 1976); Part 2: "Annotated Bibliography," (August 31, 1976).
2. Levy, H. B., "On Evaluating the Hazards of Groundwater Contamination by Radioactivity from an Underground Nuclear Explosion," Lawrence Livermore Laboratory, Rept. UCRL-51278, (September 18, 1972).
3. de Marsily, G., Ledoux, E., Barbreau, A., Margat, J., "Nuclear Waste Disposal: Can the Geologist Guarantee Isolation?", *Science*, 197 No. 4303, (August 5, 1977), 519-527.
4. American Physical Society, The Study Group on Nuclear Fuel Cycles and Waste Management, "The Nuclear Fuel Cycle: An Appraisal," *Physics Today*, 30, No. 10, (October, 1977), 32-39.
5. Cowan, G. A., "A Natural Fission Reactor," *Scientific American*, 235, No. 1, (July, 1976), 36-47.
6. Borg, I. Y., Radioactivity Trapped in Melt Produced by a Nuclear Explosion," *Nuclear Technology*, 26, (May, 1975), 88-100.
7. Dupuis, M., "Distribution and Evolution of Radioelements After a Nuclear Explosion," UCRL-Trans-10617-5, Lawrence Livermore Laboratory, (1972), from *Bull. Infor. Sci. Tech.*, 149, 41 (1970).
8. Hoffman, D. C., Stone, R., Dudley, W. W., Jr., "Radioactivity in the Underground Environment of the Cambrian Nuclear Explosion at the Nevada Test Site," Los Alamos Scientific Laboratory, Rept. LA-6877-MS, (July, 1977).

"Work performed under the auspices of the U.S. Department of Energy by the Lawrence Livermore Laboratory under contract number W-7405-ENG-48."

9. Wolfsberg, K., "Sorption-Desorption Studies of Nevada Test Site Alluvium and Leaching Studies of Nuclear Explosion Debris," Los Alamos Scientific Laboratory, Rept. LA-7216-MS, (April, 1978).
10. Paige, B. E., "Leachability of Glass Prepared from Highly Radioactive Calcined Alumina Waste," National Reactor Testing Station, Rept. IDO-14672, (February, 1966).
11. Mendel, J. E., "A Review of Leaching Test Methods and Leachability of Various Solid Media Containing Radioactive Wastes," Battelle Northwest Laboratory, Rept. BNWL-1765, (1973).
12. Hespe, E. D., "Leach Testing of Immobilized Radioactive Waste Solids," Atomic Energy Review, 9, (1971), 195-204.
13. McCarthy, G. J., White, W. B., Roy, R., Scheetz, B. E., Komarneni, S., Smith, D. K., and Roy, D. M., "Interactions Between Nuclear Waste and Surrounding Rock," Nature, 273 (May 18, 1978), 216-217.
14. Morris, J. B., Boulton, K. A., Dalton, J. T., Delve, M. H., Gayler, R., Herring, L., Hough, A., and Marples, J. A. C., "Durability of Vitrified Highly Active Waste from Nuclear Reprocessing," Nature, 273, (May 18, 1978), 215-216.
15. Merritt, W. F., "High-Level Waste Glass: Field Leach Test," Nuclear Technology, 32, (January, 1977), 88-91.
16. Weed, H. C. and Jackson, D. D., "Design of a Variable Flow-Rate, Single-Pass Leaching System," Lawrence Livermore Laboratory, UCID Rept. in preparation, (1978).
17. Diebold, F. E., "Discussions of Glass-Water Interactions," Atlantic Richfield Handford Company, Rept. ARH-2905, Richland, Washington, (September 15, 1973).
18. Paul, A., "Chemical Durability of Glasses: A Thermodynamic Approach," Journal of Materials Science, 12 (1977), 2246-2268.

NOTICE

Reference to a company or product names does not imply approval or recommendation of the product by the University of California or the U.S. Department of Energy to the exclusion of others that may be suitable.

"This report was prepared as an account of work sponsored by the United States Government. Neither the United States nor the United States Department of Energy, nor any of their employees, nor any of their contractors, subcontractors, or their employees, makes any warranty, express or implied, or assumes any legal liability or responsibility for the accuracy, completeness or usefulness of any information, apparatus, product or process disclosed, or represents that its use would not infringe privately-owned rights."

RECEIVED January 16, 1979.

Method for Determining Leach Rates of Simulated Radioactive Waste Forms¹

K. F. FLYNN, L. J. JARDINE, and M. J. STEINDLER

Argonne National Laboratory, Chemical Engineering Division,
9700 South Cass Avenue, Argonne, IL 60439

One of the more important factors affecting the isolation of radioactive waste is the rate of release of the radioactivity from the solid waste form to the environment. The most probable mechanism for release and transport of radioactivity from a solid waste form is by leaching of radioactive isotopes with groundwater. The objective of leach-testing various waste forms is to evaluate the rate at which specific hazardous radionuclides migrate from waste if and when the waste form comes in contact with groundwater. In this paper, measurement of leach rates of radioactive waste by a method which incorporates neutron activation is described.

The radioactive isotopes of most concern in high level waste (HLW) and their estimated toxicities after several decay periods are given in Table I. These data are largely taken from Wallace(1); supplemental estimates from calculations based on ORIGEN code information(2) are included. Other isotopes of the transuranic elements (*e.g.*, ^{240,241,242}Pu, ²⁴³Am, ^{245,246,247}Cm), while present, have not been included since their relative toxicities are negligible compared to the toxicities of the isotopes shown in Table I. Of the isotopes included in Table I, the greatest initial hazard to the public is from ⁹⁰Sr and ¹³⁷Cs. These isotopes represent the greatest hazard during the relative short term (*i.e.*, ~500 y). Plutonium and americium tend to predominate during the next phase (*i.e.*, 500 y to 10⁵ y) with ¹²⁹I and ⁹⁹Tc becoming of comparable importance toward the latter part of this period. Because of either half-life or product yield considerations, the other isotopes have significantly less toxicity and will not be considered here.

Considerable uncertainty exists about the mechanism of leaching of activity from solidified waste by water. The process of dissolution of the solid matrix is important, but ion migration through the matrix to the interface may also play a role. Since

¹ Work performed under the auspices of the U.S. Department of Energy.

Table I. Radioactive Isotopes in Stored High Level Wastes Having Half-Lives Greater than One Year and Their Estimated Relative Toxicities^a (Revision of Wallace Data)

Isotope	Half-Life, y	Relative Toxicity ^b		
		10-y	10 ³ -y	10 ⁵ -y
⁹⁰ Sr	28.8	1.0	---	---
¹³⁷ Cs	30.0	1.5 E-2	---	---
¹⁴⁷ Pm	2.6	5 E-4	---	---
¹²⁵ Sb	2.7	6 E-5	---	---
¹⁰⁶ Ru	1.0	5 E-5	---	---
²³⁸ Pu	89	5 E-5	---	---
²⁴¹ Am	4.3 E+2	4 E-5	8 E-6	---
²⁴⁴ Cm	18.1	3 E-5	---	---
¹⁵¹ Sm	90	2 E-5	---	---
¹⁵⁵ Eu	5.0	7 E-6	---	---
²³⁹ Pu	2.4 E+4	5 E-6	5 E-6	3 E-7
¹²⁹ I	1.6 E+7	8.5 E-7	8.5 E-7	8.5 E-7
⁹⁹ Tc	2.1 E+5	1.5 E-7	1.5 E-7	1 E-7
⁷⁹ Se	7 E+4	6 E-8	6 E-8	2 E-8
¹³⁵ Cs	2 E+6	5 E-8	5 E-8	5 E-8
¹²⁶ Sn	1 E+5	5 E-8	5 E-8	2.5 E-8
⁹³ Zr	9.5 E+5	1.5 E-8	1.5 E-8	1.4 E-8
⁹⁴ Nb	2 E+4	6.5 E-9	6.5 E-9	---
²³⁷ Np	2.1 E+6	6 E-9	6 E-9	6 E-9
¹⁰⁷ Pd	7 E+6	1.5 E-9	1.5 E-9	1.5 E-9

^aRelative toxicity is defined as the ratio of the concentration of a given isotope in the waste to its maximum permissible concentration (MPC) in public zone water (Ref. 1).

^bRelative toxicity values are arbitrarily normalized to ⁹⁰Sr at 10 y as unity. Values may vary from those listed depending on the fission product content of the fuel. The plutonium values are based on the assumption that 98% of the plutonium has been removed by reprocessing of the fuel. Relative toxicities smaller than 1 E-9 have been arbitrarily assumed to be negligible and hence are not included.

the leach rate can vary for different elements, it is most important that the leach rate be determined for specific limits of interest. It is also desirable to measure the leach rates of samples in an undisturbed state since crushing or other destructive measures (usually employed to obtain practical rates) can significantly alter the physical characteristics and hence the leach rate of the material. Neutron activation analysis (NAA) provides a method whereby measurements of specific leached elements can be made in a reasonable time interval without the necessity of physically altering the waste matrix prior to leaching.

Leach rates are generally reported in units of grams of total mass leached per square centimeter of surface area per day of leaching (g/cm^2 day). These units can be misleading in waste management studies since they have been adapted from metallurgical tests for corrosion rates. Loss of volume (or weight) from a surface corresponds to an erosion (or depth) expressed as g/cm^2 day). In waste management, in contrast, the primary interest is the rate at which a specific isotope is separated from the solid matrix into the leaching medium. However, as long as the units measured in any experimental arrangement are clearly defined, at least confusion can be avoided.

Leach rates for borosilicate and phosphate glasses (among the most leach-resistant of all commercially produced glasses) are generally in the range of about 10^{-5} to 10^{-8} g/cm^2 day. The very low leach rates are associated with special experimental glasses. The most likely range of waste glass leach rates center around 10^{-6} g/cm^2 day. Hence, it is important in all radioactive waste forms (*i.e.*, to minimize the surface to volume ratio). The most appropriate shape for this condition is an impervious cylinder. While a spherical shape has the lowest surface-to-volume ratio, the ease of fabrication and handling of a cylindrical shape makes it more desirable.

Laboratory studies of leach rates would most conveniently be done on samples of about 1 g (*i.e.*, 0.1 to 10 g range) of waste. However the measurement of very low leach rates (*e.g.*, $\sim 10^{-6}$ g/cm^2 day) on unground samples of this small size would give tenuous results. A 1-g sphere with a density of 2 would have a surface area of 3 cm^2 . A leach rate of 10^{-6} g/cm^2 day would result in a total weight loss of 3×10^{-6} g per day. Assuming a 30 wt % mixture of HLW (see Table II) in stabilizing additives, (*i.e.*, glass frit, *etc.*), real waste would contain about 3 wt % cesium. If the test material was representative HLW, the cesium loss would be about 10^{-7} g per day. The leaching times necessary to obtain sufficient material in solution so that the concentration exceeds the detection limit for the analysis would be prohibitive (*i.e.*, ~ 1 -y). Neutron activation analysis not only provides the increased sensitivity required for leach rate measurements but also when applied in the manner described in this report, circumvents the background problems caused by the dissolution of container materials.

Table II. Composition of Simulated High Level Radioactive Waste: Revision of Bonner's Data(13)

	Elements in Waste	Relative Molar Abundance	Activation Product (and Half Life) of Naturally Occurring Elements	
<u>Fission Products</u>	Rb	0.015	^{86}Rb	18.7 d
	Cs	0.079	^{134}Cs	2.05 y
	Zr	0.155	^{95}Zr	65.5 d
	Mo	0.139	^{99}Mo	2.8 d
	Tc	0.032	---	---
	Ru	0.086	^{103}Ru	39.5 d
	Rh	0.015	---	---
	Pd	0.047	---	---
	Ag	0.003	$^{110\text{m}}\text{Ag}$	255 d
	Cd	0.003	$^{115\text{m}}\text{Cd}$	43 d
	Sb	0.010	^{124}Sb	60 d
	Te	0.018	$^{129\text{m}}\text{Te}$	34.1 d
	Sr	0.039	^{85}Sr	64 d
	Ba	0.040	^{131}Ba	11.5 d
	Y	0.020	---	---
	La	0.035	^{140}La	1.7 d
	Ce	0.075	^{141}Ce	32.5 d
	Pr	0.034	---	---
	Nd	0.104	---	---
	Pm	0.003	---	---
Sm	0.020	---	---	
Eu	0.004	^{152}Eu	13.2 y	
Gd	0.003	---	---	
<u>Actinides</u>	U	0.016	^{237}U	6.8 d
	Np	0.012	^{239}Np	2.4 d
	Pu	0.000 15	---	---
	Am	0.002 6	---	---
	Cm	0.000 59	---	---

The basic technique established for leach testing involves exposure of a solid sample of known composition and having a premeasured surface area to a leaching medium for a fixed time interval. This is followed by analysis of the leaching medium for the mass of a specific material which has dissolved in the leaching medium. Difficulties arise in trying to duplicate in the laboratory the leaching medium and conditions present in the natural environment. The physical conditions under which the measurements are made differ widely for the various methods.

A survey of leach rate measurements has been made by Mendel(3). As examples of relatively simple procedures, three methods are described below. All such methods require either analyses of bulk liquids for ionic constituents (at low concentrations) after leaching or a drastic increase in the surface area prior to leaching to get higher concentrations that are easier to measure.

Leaching with Soxhlet Apparatus. A Soxhlet leaching apparatus has been used extensively(4) in radioactive waste measurements. The sample is contacted with continuously replenished distilled water. Leaching rates have been shown to be inhibited by ions previously leached from the solid material(5). This technique eliminates interference from ions in solution.

Leaching with Airlift Recirculator. In a similar method (6) used by other investigators, 50 mL of distilled water at room temperature is recirculated over a sample at a rate of 250 mL/min by means of an airlift recirculator. The leach water is sampled and is changed periodically.

Leaching onto Ion-Exchange Resins. A more sophisticated procedure for determining leachabilities of radioactive waste forms has been developed(7). Flowing deionized water is continuously circulated across the sample surface and then through ion-exchange resins where the leached ions are adsorbed. The adsorbed ions are subsequently eluted from the resin columns for atomic absorption analyses. Leachabilities measured by this procedure are claimed to be lower and more consistent than those made in stagnant water in the absence of continuous ionic control(7).

Measurement of Surface Area. The leachability determined by these methods is usually reported as g/cm² day. The total surface area of particulate material can be assessed: 1) by assuming a particle shape (*e.g.*, spherical) and estimating the number of particles, or 2) by measurements using the Brunauer-Emmett-Teller (BET) nitrogen adsorption technique(8). Unfortunately, the BET method measures the area of surfaces to which nitrogen has access; this is not necessarily the same as the area to which a solution has access. Access by solutions requires much larger pore areas,

and even then free transport of ions from the surface to the bulk solution is necessary. Hence, the BET can overestimate the surface area available for leaching.

Accurate determination of the surface area exposed to leaching remains a major uncertainty in the conversion of experimental results to true leach rates. If a simple geometric shape is assumed in determining a lower limit for the surface area, conservative estimates (*i.e.*, upper limits) of the true leach rates are obtained. When there are uncertainties in the leach rate data, upper limits are the most useful for cautious extrapolations to long term storage conditions. In contrast surface areas measured by BET technique lead to errors in the other direction. Surface area measurements by liquid penetration is not a well-developed technique.

Form of Reported Data. The mass of material leached can be determined either by any standard gravimetric method or, in the case of radioactive samples, by measurement of the radioactivity dissolved in the leaching medium. Since different ions are often leached at different rates, it is important to specify the ion when quoting leach rate results. To avoid confusion on this matter, it has been suggested(9) that long-term leaching results be reported as (fraction of A leached)(cm^2/g)⁻¹(day)⁻¹, where A is the specific ion analyzed for.

A standard method for leach-testing immobilized radioactive waste solids and for reporting results has been proposed(10). Other workers, however, consider this proposed method of testing unduly tedious and offer constructive suggestions for accelerating leach tests(4). Many of these proposed methods involve physical destruction of the waste form in order to increase the surface area exposed to the leachant. Such a procedure not only can alter the physical characteristics of the surface exposed to leaching but also can require the measurement of the surface areas of finely divided solids with the concomitant difficulties mentioned above.

Field Leach Tests. Two field leach tests have been successfully conducted(11), using glass blocks containing aged fission products and buried below the surface water table. The groundwater composition and flow rate were accurately determined, the surface area of the block was measured, and the concentration of ⁹⁰Sr in the groundwater was monitored at regular intervals over a 15-y period. This type of experiment is very useful in addressing the questions involved in safe, long-term waste disposal. However, the extensive effort and the need to do fieldtesting for each material make this approach undesirable for development of large scale testing programs.

Neutron Activation Method. Neutron activation analysis for the measurement of trace elements has been used extensively and the literature is replete with papers on this subject. A recent review of this technique as applied to environmental samples has been published by the National Academy of Sciences(12).

The experimental technique devised in this work is based on a NAA method. Neutron irradiation of solid waste forms of simulated HLW (see Table II) produces activation of the elements in the sample. The activation products can be readily measured before and after leaching by radiochemical and/or instrumental techniques. In order to be useful for these purposes, the activation product must have a sufficiently energetic and abundant radiation (either β^- or γ) to be easily detected, as well as a sufficiently long half-life (*i.e.*, several days or more) to be useful for relatively long-term leach studies. The elements in HLW of most concern (see Table I) and their associated measurable radioactive isotopes (see Table II) are strontium (^{85}Sr), cesium (^{134}Cs), the trivalent actinides (^{152}Eu as a standin), and the tetravalent actinides (^{141}Ce as a standin). Trivalent rare earths (^{152}Eu) have been shown to be a satisfactory substitute for the trivalent actinides, and tetravalent cerium (^{141}Ce) substitutes for the tetravalent actinides in waste studies(13). However, if there is uranium present in the waste form, ^{237}U produced by (n,2n) on ^{238}U and ^{239}Np from (n, γ , β) on ^{238}U become useful actinide tracers. In the work described here, ^{85}Sr , ^{89}Sr , ^{131}Ba , ^{141}Ce , and ^{152}Eu in a spray-calcined simulated waste and ^{124}Sb in lead were measured.

analysis using a lithium-drifted germanium (GeLi) detector provides an assay of the gamma-emitting radioisotopes present. After leaching of the solid matrix for a suitable time interval, the leaching medium can be assayed either by gamma ray (*i.e.*, GeLi) or (if greater sensitivity is required) by radiochemical analysis, using conventional radiochemical separation techniques(14) followed by gamma ray analysis (GeLi detector) and/or low-background beta counting of the separated species. From these measurements, the fraction of the element of interest which has been leached from the matrix can be determined with great sensitivity. Because of the sensitivity, these measurements require no destruction of the solid matrix prior to leaching in order to increase the leach rate; also, the concentrations of the ions in solution remain very low, minimizing their effect on the dissolution reaction.

The total mass of the solid matrix can be determined quite accurately by weighing on a standard analytical balance. The surface area of a waste granule exposed to the leachant is more difficult to determine. A conservative estimate (lower limit) can be made by assuming smooth surfaces and measuring the apparent geometric area (*i.e.*, assume an impervious sphere configuration). More accurate measurements of the surface area exposed to the leachant are difficult to obtain with currently available

techniques. On the other hand, since glass monolithic shapes are planned for HLW disposal, test samples that simulate this form, *e.g.*, glass cylinders or beads, can be described by the simple geometric area if the leach reaction does not proceed to change the surface area over the course of the experiment. It is recognized that leach rates of partially reacted surfaces may differ significantly from those determined on smooth, fresh surfaces.

Experimental Results

Leach rate measurements have been made on several waste forms, using the NAA technique. Some results are presented here as examples of the application of this method. Simulated wastes used in these studies consisted of two types of granules obtained from Battelle Pacific Northwest Laboratories. The differential leach rates of the bulk waste matrix were calculated with the equation:

$$L = \frac{A_t}{A_o} \frac{W_o}{St} \quad (1)$$

where A_t = amount of isotope A removed in time t

A_o = initial amount of isotope A in solid

S = surface area of the solid material (cm^2)

W_o = initial weight of the solid material (g)

t = leach period (days)

L = leach rate (g/cm^2 day)

A_t/A_o = fraction of isotope leached.

Gross dissolution of the waste can be measured from the loss of weight of the sample or by determination of the appearance in the leaching medium of the major matrix constituent (*e.g.*, glass). However, the selective leaching of important fission product elements has been observed in this work to be significantly different from that of the bulk waste matrix. The units normally used to describe leach rates, *i.e.*, g/cm^2 day, appear to imply dissolution of the waste. Results quoted as fraction leached per cm^2 day(9) where the fraction leached refers to an identified element or nuclide [*i.e.*, $(A_t/A_o)/St$] may be more descriptive of actual leaching. However it must be remembered that the fraction leached depends on the specific surface area (cm^2/g) of the monolith. Conversion of the data given in these terms to the more conventional form shown in Eq(1) can be easily made if the specific surface area (cm^2/g) is known.

Leaching of Sintered Granules. The initial studies in this work(13) were done in granules consisting of 80% PW-4b spray-calcined simulated waste, 10% silica, and 10% borosilicate glass frit sintered at 1100°C. The granules were about 0.6 cm in diameter and weighed about 370 mg each. The surface area, based on the assumption of an impervious (*i.e.*, "hard") spherical shape, was calculated to 1.1 cm² per 370-mg bead or 3 cm²/g. Distilled water (at 25°C) was the only leachant used in these studies since the wide variability in groundwaters makes it impossible to obtain a single meaningful generic groundwater composition.

Several of these granules were irradiated in the isotope tray (flux $\sim 6 \times 10^{12}$ n/cm² s) of the Argonne CP-5 Research Reactor for 24 h (total neutron fluence, $\sim 5 \times 10^{17}$ n/cm²). After ~ 3 weeks cooling to allow unwanted short-lived activities to decay, neutron-induced radioactivities present in the granules were determined by gamma-ray analysis, using a GeLi detector and a computer-programmed gamma spectrum analysis. Isotopes of particular interest that were identified were ⁸⁵Sr (514-keV γ), ¹³¹Ba (496-keV γ), ¹⁴¹Ce (145-keV γ), and ¹⁵²Eu (1408-keV γ).

After gamma ray analysis was complete, a granule was immersed in 100 mL of room-temperature distilled water for several days with no stirring. (Stirring was generally avoided in these experiments since it was concluded that stagnant water closely approximates slow-moving groundwater in natural situations.) The water was then decanted from the granule and analyzed radiochemically(14) for the elements barium, strontium, cerium, and rare earths (RE). The barium and strontium contents were determined in order to measure leach rates of the alkaline earth metals. Because of chemical (and valence) similarity, the measured cerium leach rates should reflect the leaching characteristics of the tetravalent actinides. The other RE leach rates should reflect the leaching characteristics of the tetravalent actinides and of the RE themselves. The radiochemically separated samples were counted in a low-background (background ~ 0.8 count/min) beta proportional counter, as well as with a GeLi detector. The results with the two different counting methods agreed within experimental error (*i.e.*, about 10%). Two successive seven-day leach tests were performed on each granule. The agreement between these two tests indicated no significant change in leach rate with time on this short time scale, for the particular elements studied (*i.e.*, barium, strontium, cerium, and rare earths). It was not possible to determine the cesium content in these granules because, for economy reasons, cesium was not included in the calcine production. The results of these measurements are given in Table III. Significant differences in the leach rates of the alkaline earths (barium, strontium) the RE (europium), and cerium are observable.

Leach rate measurements using this technique can be made using high-resolution GeLi detectors for gamma counting exclusively (*i.e.*, without radiochemical separations from the leaching medium). This method, while much more rapid, results in a significant

Table III. Leach Rates of Waste Form PW-4 in Distilled Water at 25°C (7 day leaching period)

Isotope	Counting Method	Leach Rate	
		Fraction Leached ^a per day	Equivalent Mass ^b g/cm ² ·day
⁸⁵ Sr	γ	1.1 E-4 ^c	3.8 E-5
⁸⁹ Sr	β	9.8 E-5	3.3 E-5
¹³¹ Ba	β	1.0 E-4	3.5 E-5
¹⁴¹ Ce	γ	3.3 E-6	1.1 E-6
	β	2.9 E-6	1.0 E-6
Rare Earths (¹⁵² Eu)	γ	1.3 E-5	4.4 E-6

^aFraction of indicated isotope.

^bMass of solid waste that would have been leached if the total mass had been leached at the same rate as the indicated isotope.

^cRead 1.1×10^{-4} .

decrease in sensitivity, as well as some increase in uncertainty, as a consequence of analyzing extremely complex gamma spectra containing many overlapping gamma rays. Low-energy gamma rays such as those associated with ¹⁴⁷Nd (91-keV) and ¹⁷⁰Tm (84-keV) are particularly difficult to resolve as is ⁸⁵Sr (514-keV) whose gamma ray energy is very close to the usually abundant annihilation radiation (511-keV). Low-abundance gamma rays also tend to get lost in the Compton continuum from the more abundant high-energy gamma rays which are always present. For these reasons, and to improve sensitivity, radiochemical separations, though time-consuming, represent an important part of the procedure for quantitative measurements. For qualitative measurements, application of the technique without radiochemical separations is simple, straightforward, and quick.

The counting techniques described in this paper are also readily applicable to studies of "hot" radioactive waste (*i.e.*, radioactive waste from reprocessed nuclear fuel). With this type of material, the cesium can be analyzed as 30-y ¹³⁷Cs (662-keV γ), the RE as 13-y ¹⁵²Eu (964-keV and 1408-keV γ), the strontium as 28-y ⁹⁰Sr (after chemical separation and beta counting), and the actinides by group separation and alpha counting.

Leaching of Lead Matrix Materials. The use of a metal matrix for waste encapsulation is being studied. The neutron activation method was used to evaluate the leaching characteristics of potential metal matrix materials. Lead was selected for initial studies. Reagent grade lead beads (2.2-mm diameter, weighing 75 mg

each) having a specific surface area of about $2 \text{ cm}^2/\text{g}$ were irradiated (as described above) for 24 h at a thermal neutron flux of about $6 \times 10^{12} \text{ n/cm}^2\text{s}$. After an appropriate cooling time to allow short-lived gamma activities to decay (about 2 weeks), the gamma radiation from the beads was measured. Sufficient ^{124}Sb activity was produced from neutron capture by the antimony impurity in the lead to serve as a tracer for the bulk lead during the leach studies.

The irradiated lead beads were immersed in 25°C air-saturated quiescent distilled water (pH, ~ 6) for one week, after which the leaching medium was analyzed for ^{124}Sb by gamma counting. The lead beads were also weighed before and after leaching to assess the total weight loss. Fifty beads were used in order to increase the sensitivity of the measurement. The leach rates (grams of lead/ cm^2 day) as calculated from Eq(1) were $3.6 \text{ E-}4$ from the weight loss and $3.2 \text{ E-}4$ from the ^{124}Sb determination. These two numbers agree within estimated experimental uncertainties and hence indicate that ^{124}Sb is a representative tracer to measure the total mass leach rates for lead. Also, this agreement serves to verify that this method of leach rate determination gives results comparable to those obtained with more standard methods such as weight loss measurements.

Discussion and Conclusions

The neutron activation testing procedure is most useful for the measurement of very low leach rates. The leach rates delineated in Table III were each based on one granule weighing 370 mg and having 1.1 cm^2 ($\sim 3 \text{ cm}^2/\text{g}$) surface area. These conditions easily permitted the measurement of leach rates of the order of 10^{-6} g/cm^2 day for one-week leach tests without radiochemical separations being necessary. If gamma counting is supplemented with radiochemistry and low-background beta counting, at least two orders of magnitude more sensitivity (*i.e.*, 10^{-8} g/cm^2 day) can be achieved. This sensitivity can be increased further by increasing the sample size and/or neutron fluence (each can readily be increased by a factor of 10). With such modifications, measurement of leach rates of less than 10^{-10} g/cm^2 day would be readily available.

Leach rates for elements other than those listed in Table II can also be determined by this method. In fact, any element in the periodic table that is solid at room temperature and has an activation product with a half-life sufficiently long to allow leach testing can be studied with this technique. This method can also be applied to the study of the leach rates of alpha emitting actinides present in waste. In this case, standard carrier-free radiochemical procedures, coupled with low background alpha counting, would be invoked.

The classical leach test methods currently in use, (the Soxhlet, Paige, Kelley, procedures described above in Description of Leach Rate Measurement Procedures as well as those described in

Ref 3) give at best qualitative results. Although these results may be adequate for comparing the leach rates of various waste forms, they tend to be unsuitable for extrapolation to final repository or accident conditions. This deficiency has been pointed out by Mendel(3) and Sheffler *et al.* (15), among others.

The technique described in this paper allows leach rates to be measured without physically altering the waste form being studied hence, the results are more amenable to extrapolation to final conditions.

Our method for measuring leach rates is thought superior to other methods currently in use. Meaningful leach rate data can be obtained using relatively simple laboratory scale equipment coupled with standard NAA techniques. More detailed information can be procured by applying radiochemical separations and more sophisticated counting methods. The experimental technique described here is applicable to the measurement of leach rates for the elements of interest, from any solid waste form, in any potential storage environment.

Literature Cited

1. Wallace, R. M. *et al.*, "High Level Radioactive Waste Management," *Advan. Chem.*, Ser. 153, M. H. Campbell (ed.), American Chemical Society, Washington, D. C. (1976).
2. Bell, M. J., "ORIGEN - The ORNL Isotope Generation and Depletion Code," Oak Ridge National Laboratory Report ORNL-4628 (1972).
3. Mendel, J. E., "A Review of Leaching Test Methods and the Leachability of Various Solid Media Containing Radioactive Wastes," Battelle Pacific Northwest Laboratories Report BNWL-1765 (1973).
4. Mendel, J. E. and Warner, I. M., "Waste Glass Leaching Measurements," Battelle Pacific Northwest Laboratories Quarterly Report BNWL-1741 (1973).
5. Weyl, W. A. and Marloe, E. C., "The Constitution of Glasses, a Dynamic Interpretation," Vol. II, Part 2, pp. 1118-1119, Interscience Publishers, New York (1964).
6. Paige, B. E., "Leachability of Glass Prepared from Highly Radioactive Calcined Alumina Waste," Phillips Petroleum Co., Atomic Energy Division, Report IDO-14672 (1966).
7. Kelley, J. A. and Wallace, R. M. *Nucl. Technol.* (1976), 30, 47.

8. Brunauer, S., Emmett, P. H., and Teller, E., *J. Am. Chem. Soc.* (1938), 60, 309.
9. Godbee, H. W., Clark, C. W., and Fitzgerald, C. L., *Physical Properties of Solids Incorporating Simulated Radioactive Wastes*, p. 565, "Proceedings of the Symposium on the Solidification and Long Term Storage of Highly Radioactive Wastes," Richland, Washington, CONF-660208 (1966).
10. Hespe, E. D., *Atomic Energy Review* (1971), 9, 195.
11. Merritt, W. F., *Nucl. Technol.* (1977), 32(1), 88.
12. Robertson, D. E. and Carpenter, R., "Neutron Activation Techniques for the Measurements of Trace Metals in Environmental Samples," National Academy of Sciences-National Research Council Report NAS-NS-3114 (1974).
13. Bonner, W. F., Blair, H. T., and Romero, L. S., "Spray Solidification of Nuclear Waste," Battelle Pacific Northwest Laboratories Report BNWL-2059 (August 1976).
14. Flynn, K. F., "Radiochemical Procedures and Techniques," Argonne National Laboratory Report ANL-75-24 (1975).
15. Scheffler, K., Riege, U., Louwrier, K., Mabzke, H., Ray, I., and Thiele, H., "Long Term Leaching of Silicate Systems: Testing Procedure, Actinides Behavior and Mechanism," Karlsruhe Report KFK-2456 (1977).

RECEIVED January 16, 1979.

Ceramic Forms for Nuclear Waste¹

R. G. DOSCH

Sandia Laboratories, Albuquerque, NM 87185²

Options for disposal of high level liquid radioactive waste, a by-product of the nuclear fuel cycle, range from controlled surface storage in remote areas to storage in deep geologic formations and injection into outer space. Features or operations common to all these options are the production of a solid waste form, transportation, and disposal, with the ultimate goal of isolating the waste from the biosphere. Since some of the long-lived radionuclides are extremely toxic to man, isolation must be assured over long periods of time.

Any solid waste form should serve to reduce waste volume and provide short term stabilization under conditions such as fracture, fire, or water immersion which could result from a transportation mishap. In the geologic storage scenarios currently receiving the most scrutiny, the most likely path to the biosphere has been identified as aqueous transport of nuclides via groundwater. Thus an acceptable waste form would also resist dissolution under ambient repository conditions, with the obvious benefit of assuring a sufficiently low nuclide release rate into an aquifer to preclude a significant threat to health and safety.

At the present time, glass waste forms which have been under development for many years in the United States and elsewhere, are considered the reference materials in high level waste management (1,2). A vitrified waste form will almost certainly be employed in the initial waste disposal programs. Their use in deep geologic storage, however, involves some potential problems. For example, vitrified wastes which are relatively insoluble in water or brine under normal conditions, undergo modification and/or dissolution quite rapidly at temperatures of 250°C, a condition that is expected under the lithostatic pressures associated with the principal geologic repositories considered to date (3,4). In addition, as metastable glasses inevitably devitrify,

¹ This work supported by the United States Department of Energy (DOE), under Contract AT(29-1)-789.

² A U.S. DOE Facility.

0-8412-0498-5/79/47-100-129\$05.00/0

© 1979 American Chemical Society

significant changes in properties such as leachability can be expected.

Parallel waste form development programs on a much smaller scale have been and are being conducted in a few laboratories. Most are addressing the development of ceramic waste forms, which are inherently more stable in a thermodynamic sense than glasses. Some of these include: 1) Glass ceramics (5) - these materials are prepared from glasses by using special heat treatments to promote crystallization; 2) Supercalcine - the product of a process whereby chemical constituents are added to liquid waste with the intent of forming stable crystalline hosts for specific nuclides during calcination and subsequent consolidation (6); 3) Metal or graphite encapsulated waste oxides (6); and 4) Atomically dispersed waste oxides in a ceramic titanium dioxide matrix (7,8).

An overview of the process of incorporating radioactive waste in a titanium dioxide ceramic form will be presented. The process goals were to produce a stable, crystalline waste form and a process effluent which did not require remote handling, or preferably could be treated as a chemical waste. The nuclide waste, up to 25% by weight, is introduced into a titanate material by an ion exchange process. The loaded titanates are converted to a theoretically dense (4.5 g/cc) ceramic by pressure sintering. Characterization studies of the final ceramic form have been performed using transmission electron microscopy, non-dispersive x-ray analysis, and other techniques in order to identify some of the important properties of these complex materials. The long term leachability of the ceramic has been studied and compared to a glass waste form. This work is summarized along with the initial results of some high temperature-high pressure leaching studies.

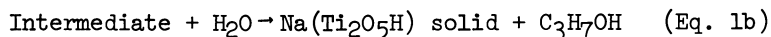
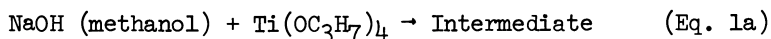
The overall development program included the study of other exchange materials such as niobates, zirconates, and tantalates, some of which had superior ion exchange and leaching properties, but were initially economically unattractive as compared to the titanates. These alternate materials will be briefly discussed along with applications to nuclide stabilization in other areas of nuclear processing.

Ion Exchange Material Preparation and Chemistry

The titanate material used in the waste solidification process is one of a group of materials of the general formula $M [M_x O_y H_z]_n$ where M is an exchangeable cation of charge +n and M' may be Ti, Nb, Zr, or Ta (9). In the initial work with these materials M was a quaternary ammonium ion, generally the tetramethylammonium ion, in compounds with a stoichiometry of the type $(CH_3)_4N(Ti_2O_5H)$ and $(CH_3)_4N(Nb_2O_6H)$ which were highly water soluble. These formulas are empirical, but if one considers the compounds as simple salts which dissolve to form $(CH_3)_4N^+$ and

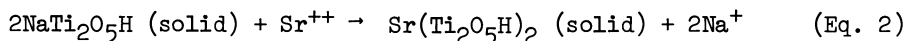
$(M_x^i O_y H_z)^-$ species, the formulas adequately describe their chemistry.

The anionic species react quantitatively with metal cations in solution to form precipitates with combining ratios of one $(M_x^i O_y H_z)^-$ per unit positive charge on the cation. These precipitates, such as $\text{Na}(\text{Ti}_2\text{O}_5\text{H})$ or $\text{Ca}(\text{Ti}_2\text{O}_5\text{H})_2$, act as ion exchange materials in which the Na^+ and Ca^{++} ions are replaced by cations with a greater affinity for the material. The earliest exchange materials were prepared by this method, but for the waste solidification work, a more direct and economical method was used involving reaction of the appropriate metal alkoxide, $\text{Ti}(\text{OC}_3\text{H}_7)_4$, $\text{Nb}(\text{OC}_2\text{H}_5)_5$, $\text{Ta}(\text{OC}_2\text{H}_5)_5$, or $\text{Zr}(\text{OC}_4\text{H}_9)_4$ with an alcohol solution of a base containing the desired exchangeable cation, e.g. a solution of 10-20 w/o sodium hydroxide in methanol. In the first step (Eq. 1a), an exothermic ester interchange reaction takes place followed by reaction with the hydroxide ion to form a product which is soluble in the alcohol solution. The second step (Eq. 1b) is a hydrolysis reaction resulting in a precipitate which is filtered and dried under vacuum at ambient temperature.

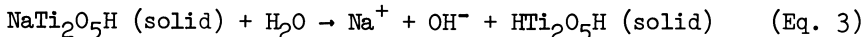


The overall yield is essentially 100% by any of the preparation methods, but the physical characteristics of the ion exchangers are dependent on preparation conditions. For example, sodium titanate prepared by Eqs. 1a and 1b with hydrolysis in one liter of water per mole of $\text{Ti}(\text{OC}_3\text{H}_7)_4$ has a bulk density of 0.45 g/cm^3 and a specific surface area of $10\text{-}40 \text{ m}^2/\text{g}$. The same material prepared by Eqs. 1a and 1b and hydrolyzed in a solution of 100 ml of water in 1000 ml of acetone for each mole of $\text{Ti}(\text{OC}_3\text{H}_7)_4$ has a bulk density of 0.35 g/cm^3 and a specific surface area of $200\text{-}400 \text{ m}^2/\text{g}$. In all cases, the materials consist of agglomerates of $50\text{-}100 \text{ \AA}$ particles with the degree of aggregation of the particles determining both the bulk density and surface area. A program to characterize the sodium titanate material has verified that the chemical and physical properties are reproducible from batch to batch for any of the preparation methods. As expected, the materials with the highest surface areas are most reactive and have been studied most extensively for solidification of aqueous wastes. Attempts to determine structure of the complex anion in the exchange material were unsuccessful with the exception of the niobate for which a crystalline form of the tetramethylammonium niobate salt was obtained (10,11,12).

The principal reaction with aqueous waste solutions is believed to cation exchange as illustrated in Eq. 2.



Another reaction of the titanate which has an important effect in waste solidification is the reaction with hydrogen ion, as in the hydrolysis reaction shown in Eq. 3.



This reaction is significant for sodium titanate ($K_{\text{eq}} \approx 10^{-6}$ moles²/l²) and sodium zirconate, but is negligible for sodium niobate and some other "titanates" such as $\text{Mg}(\text{Ti}_2\text{O}_5\text{H})_2$. Gelatinous hydroxide precipitates which would appear likely based on Eq. 3 were not observed in the reaction of sodium titanate with aqueous waste, and stoichiometric loading was achieved with polyvalent cations which form insoluble hydroxides as well as for those forming soluble hydroxides.

Hydrogen ion was found to be much less exchangeable than Na; hence, the overall capacity of $(\text{Na,H})\text{Ti}_2\text{O}_5\text{H}$ for cation exchange is nearly proportional to the Na content. However, the affinity for various cationic species varies widely with Na content. For example, in tests with stoichiometric amounts of several $(\text{Na,H})\text{Ti}_2\text{O}_5\text{H}$ compounds batch equilibrated with 0.015 M Cs solutions, distribution coefficients (K_d) were found to vary from 4 for $\text{HTi}_2\text{O}_5\text{H}$ (hydrated TiO_2) to >1000 for $(\text{Na}_{0.5}\text{H}_{0.5})\text{Ti}_2\text{O}_5\text{H}$ ($K_d = [\text{Cs}] \text{ solid} / [\text{Cs}] \text{ solution} \times \text{Solution volume, ml} / \text{Weight solid, g}$). The K_d for standard sodium titanate, $\text{NaTi}_2\text{O}_5\text{H}$, was ~200. For purposes of comparison, sodium niobate has a high affinity for Cs ($K_d > 1000$) and a high overall capacity, while sodium zirconate has a very low affinity for Cs ($K_d < 10$). Like the titanate, both the niobate and zirconate have very high affinities for polyvalent cations.

High Level Waste Solidification

The effectiveness of various sodium titanate, sodium niobate, and sodium zirconate materials for solidifying high level waste solutions has been investigated extensively using non-radioactive and tracer-level solutions simulating the composition expected at the Allied-General Nuclear Services, Barnwell, S.C., plant (Table I). The testing was extended to demonstrations conducted at Oak Ridge National Laboratory using high level waste generated using Purex chemistry to reprocess small (0.5-1 Kg) batches of typical spent light water reactor fuel. Two methods for contacting the ion exchange materials with the waste solutions were evaluated: 1. Batch equilibration in which the ion exchanger was added directly to the waste solution to form a product with the consistency of a "damp sand," and 2. A downflow fixed bed ion exchange contactor.

The batch contact consisted of equilibrating stoichiometric quantities of waste and ion exchanger for 15 to 30 minutes. The solid product was then washed with water to remove most of the sodium ions. This step was necessary as high sodium content in

Table I. Compositions of AGNS Barnwell^a High Level Liquid Waste and the Simulant Used in the Titanate Solidification Studies

Constituent	Total Abundance g/tonne of U	Concentration moles/liter	Simulant moles/liter
Fission Products			
Se	14.4	0.0003	0.0003
Br	13.7	0.0003	0.0003
Rb	347	0.0071	0.0071
Sr	828	0.0166	0.0163
Y	416	0.0082	0.0082
Zr	3710	0.072	0.0701
Mo	3560	0.065	0.0643
Tc	822	0.016	----
Ru	2330	0.041	0.0201 ^b
Rh	505	0.0086	0.0080
Pd	1520	0.025	0.0254
Ag	82	0.0013	0.0013
Cd	136	0.0021	0.0021
In	1.2	0.00002	----
Sn	25.7	0.00038	----
Sb	10.8	0.00016	----
Te	535	0.0074	0.0074
Cs	2600	0.034	0.034
Ba	1750	0.022	0.0224
La	1320	0.0167	0.0167
Ce	2540	0.032	0.032
Pr	1280	0.016	0.0160
Nd	4180	0.051	0.0507
Pm	35.6	0.0004	----
Sm	1010	0.0118	0.0119
Eu	174	0.002	0.002
Gd	122	0.0014	0.0014
Tb	1.8	0.00002	----
Actinides			
U	10,000	0.074	0.074
Np	482	0.0036	----
Pu	100	0.0007	----
Am	525	0.0038	----
Cm	24	0.0002	----
Soluble Nuclear Poison			
Gd	9000	0.1007	0.1007

Table I (con't.)

Constituent	Total Abundance g/tonne of U	Concentration moles/liter	Simulant moles/liter
Impurities and Corrosion Products			
Na	100	0.0077	----
Fe	2000	0.063	0.05
Cr	200	0.0068	0.0067
Ni	80	0.0024	0.0025
TBP Decomposition			
PO_4^{-3}	2000	0.037	----

- a) Based on one tonne of 35,000 MWD/MTU fuel processed after 150 day cooling period, and a volume of 150 gal/tonne.
- b) Concentration of Ru in simulant was limited to 50% of that expected for economic reasons.

the solids had a deleterious effect on the leaching properties of the final consolidated waste form. The results obtained from batch equilibrations of sodium titanate or sodium niobate with aliquots of the high level waste solution are listed in Table II. Although the "feed" waste solution contained all radionuclides expected in spent fuel, only data for certain key radionuclides are reported. The "blank," which gives an estimate of the magnitude of contamination by the cell environment, was a sample of de-ionized water placed beside the samples in the hot-cell for the duration of the test. As expected from the earlier work with simulants, the decontamination factors (DF) for Cs were modest, with values of about 5 and 30 for the titanate and niobate, respectively (DF as used here is the ratio of feed concentration to effluent concentration of a radionuclide), while those for polyvalent cations were large. Using sodium titanate, DF's $\geq 10^2$ were achieved for rare earths and $\sim 10^5$ for Pu. The values for the rare earths may have been higher, but analytical limitations prevented this determination. As expected, very little of the Tc was removed by either material since it occurred principally as TcO_4^- .

The fixed bed ion exchange column provided a much higher level of decontamination and since the goal was to produce an effluent with minimum contamination, it was eventually considered to be the baseline process. In this approach, the waste solutions, which were approximately 1M in HNO_3 , were adjusted to a pH of 0.5-1 by addition of sodium hydroxide and flowed through a titanate bed at one column volume per hour. The columns were subsequently washed with water to remove excess sodium.

Table II. Activities of Principal Radionuclides Remaining in High-Level Waste After One Batch Equilibration

Sample	Activity (Ci/ml) (a)					
	$^{99}\text{Tc}(\beta)$	$^{106}\text{Ru}(\gamma)$	$^{137}\text{Cs}(\gamma)$ (b)	$^{144}\text{Ce}(\gamma)$	$^{154}\text{Eu}(\gamma)$	$\text{Pu}(\alpha)$
Feed	3×10^{-6}	2×10^{-2}	9×10^{-2}	4×10^{-2}	3×10^{-3}	7×10^{-5}
Blank	$<(9 \times 10^{-8})$	$<(3 \times 10^{-8})$	2×10^{-7}	$<(2 \times 10^{-8})$	$<(5 \times 10^{-9})$	$<(9 \times 10^{-11})$
ST	2×10^{-6}	$<(3 \times 10^{-4})$	2×10^{-2}	4×10^{-6}	$<(2 \times 10^{-5})$	3×10^{-10}
SN	2×10^{-6}	$<(1 \times 10^{-4})$	3×10^{-3}	2×10^{-3}	1×10^{-4}	$<(2 \times 10^{-9})$

(a) For cases where radionuclides were undetected, the detection limits are given in parentheses.

(b) Ratio of ^{137}Cs to ^{134}Cs was about 3.5.

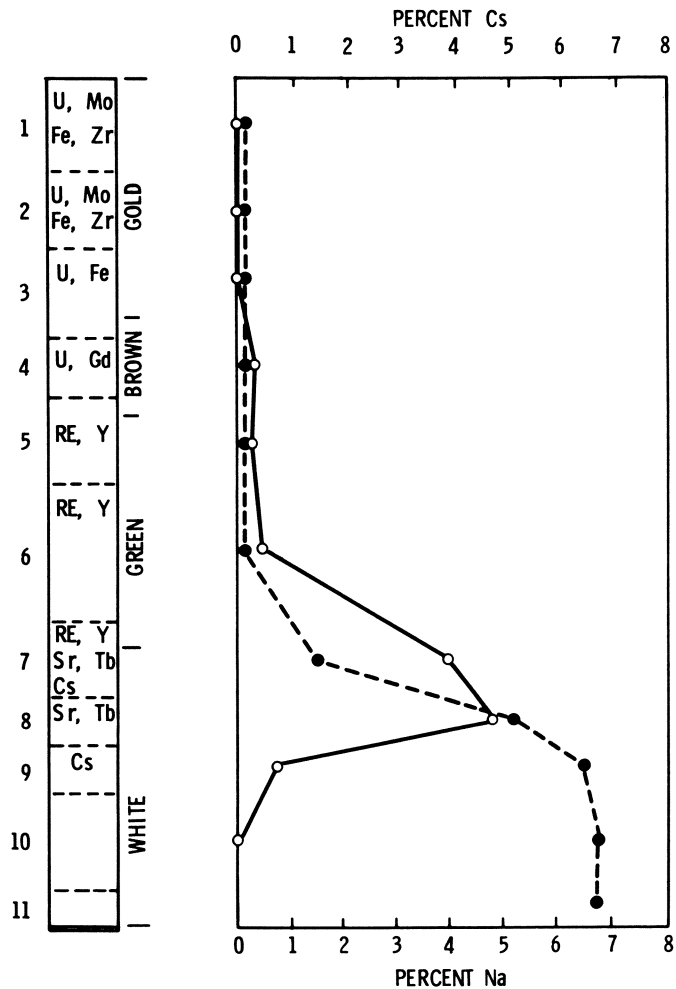


Figure 1. Elemental distribution of fission waste nuclides on a sodium titanate column. The distribution shown on the left was determined from qualitative analyses of the numbered column segments. The Cs and Na distributions on the right were obtained by quantitative analyses of each numbered segment. (○), Cs; (●), Na.

The waste nuclides were fractionated on the column into several bands as shown in Fig. 1 for a sodium titanate column. The distribution of the elements are based on qualitative emission spectrographic analyses of the numbered segments. The Cs and Na distributions are based on quantitative analyses of each segment. Since Cs is concentrated in the leading band, the ^{137}Cs DF was dependent on the degree of column loading, i.e., for columns loaded to 50% capacity and washed with one column volume of water, ^{137}Cs was not detected in the effluent ($\text{DF} > 3 \times 10^8$); however, when the column was loaded to 90% capacity and washed, the DF dropped to 1.5×10^2 . In the niobate column, the Cs band was preceded by the Sr and the leading edge of the rare earth band, and higher loading could be realized prior to radionuclide breakthrough. The effluent from both of the columns contained essentially 100% of the Tc, present as the TcO_4^- ion, and approximately 0.2% of the original ^{106}Ru activity.

More efficient use of the titanate material was achieved by passing the column effluent through a synthetic zeolite bed (Zeolon 900 Na from the Norton Co., Akron, Ohio) to sorb Cs which "leaked" from the column. A zeolite bed equal to 20% by weight of the titanate was sufficient to produce a Cs $\text{DF} > 10^8$ in the effluent from a titanate column loaded to slightly more than 100% of the calculated capacity. The use of the zeolite does not effect the overall process conditions since it can be incorporated directly into the sodium titanate during preparation. A Dowex 1-X8 resin bed was used to remove the ^{99}Tc from the effluent and also served to remove additional ^{106}Ru , leaving 0.002% of the original Ru activity in the effluent. Finally, the effluent was passed through a ferric titanate bed (13) which reduced the ^{106}Ru concentration by an additional factor of 120.

A comparison of the activity in the effluent from the above process with the activity in the "feed" solution is shown in Table III for an experiment in which a titanate column was used at approximately 100% capacity. Only ^{106}Ru and a small amount of residual alpha activity were detected in the effluent.

A single test of a batch procedure was done using magnesium titanate instead of the sodium form. Since no sodium was present, a washing/filtering step was not required. After addition of the magnesium titanate to the liquid waste, the solid product was calcined in the reaction vessel at 650°C to remove water and destroy nitrates, and the resulting material was pressure sintered under the same conditions used for column material. The density and leaching characteristics of the product were comparable to or better than those found in the same qualifying tests applied to any of the titanates produced by other methods.

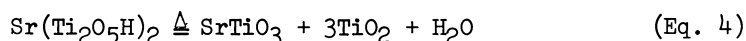
The advantage of the $\text{Mg}(\text{Ti}_2\text{O}_5\text{H})_2$ batch equilibration process would be its simplicity. Secondly, an off-gas stream from this process would be almost identical with that produced in existing flowsheets for direct calcination of liquid wastes. A potential disadvantage would be the inclusion of anions such as phosphate,

sulfate, and fluoride in the final waste form. The project ended before further investigations into the batch process and the effects of the anions on the properties of the titanate waste form could be initiated.

Consolidation and Characterization of the Ceramic Waste Form

The use of ion exchange resins and natural or synthetic inorganic exchange materials in the nuclear industry is well documented (14). In the waste solidification application, the titanates or niobates offer no unique sorption properties. They do, however, provide a relatively high overall sorption capacity for a variety of nuclides in materials which can be converted into a stable ceramic host for the sorbed ions. After the sorption process, the column bed must be consolidated to reduce surface area. The project emphasis was directed toward a stable waste form and a considerable effort was devoted to producing and characterizing a highly dense form with favorable physical, chemical and thermal properties (15).

At temperatures of 600°-650°C, the waste form dehydrates and crystallizes to form a mixture of titanates (niobates, zirconates) and titania (niobia, zirconia) as illustrated for the case of Sr⁺⁺ by Eq. 4.



Both cold pressing / sintering and pressure sintering were studied as consolidation methods. Residual pellet porosity could not be reduced, however, below 30 vol% by the former method at temperatures up to 1000°C and with the addition of up to 30% by weight of a glass binder. More favorable results were obtained by pressure sintering methods. This process was carried out in vacuum in graphite dies where conditions ranged from 900 to 1100°C and 6.9 to 13.8 MPa (1000 to 2000 psi). In general, the latter technique was highly successful for samples with less than 2% residual porosity were obtained routinely. Addition of a glass consolidation aid to the waste allowed for a significant reduction in the pressing parameters. For example, titanate waste forms with 5, 15 and 30% by weight of glass binder were successfully consolidated to near maximum density at temperatures of 1000, 950 and 900°C, respectively. Cylindrical pellets up to 5 cm in diameter were produced and the feasibility of a semi-continuous pressure sintering process was demonstrated.

Wide variations in Cs and Na leaching observed in some of the first samples produced were found to result from the formation of the corresponding molybdate compounds which are highly water soluble. This problem was eliminated by the addition of 1-2% by weight of elemental silicon which served as a reducing agent and prevented molybdate formation. The silicon was added during the preparation of the sodium titanate material.

During development, evaluation of the consolidated materials was based primarily on two criteria, leachability and the concentration factor, i.e., the concentration of waste oxides on a volume basis. The concentration factor is directly affected by the residual porosity in a consolidated waste as well as by the dilution caused by the addition of consolidation aids. This factor can be as high as 1.2 g/cm^3 for a fully dense (4.5 g/cm^3) titanate waste prepared from the projected Barnwell plant solution composition. The factor is slightly lower for a titanate waste containing silicon and zeolite additions, which has a typical density of 4.2 g/cm^3 . The leachability was determined by an "instantaneous" leach test developed for fast, comparative evaluations of materials, the details of which are described elsewhere (16).

The consolidated titanate waste pellets are similar in appearance to their glass counterparts, i.e., both are dense, black and apparently homogeneous. Microscopic analyses, however, reveal important differences between these two waste forms. While little definitive work has been done with glassy waste forms, it is apparent that several readily soluble oxide particulates of various nuclides are simply encapsulated in the glass matrix. The titanate waste form has undergone extensive analyses which includes optical microscopy, x-ray, scanning electron microscopy, microprobe, and transmission electron microscopy (17). The samples of titanate examined were prepared by pressure sintering and consisted of material from a fully loaded titanate column. Zeolite and silicon additions were also present in the samples.

A solid solution titanate is not produced by pressure sintering, but rather a complex assemblage of phases. Optical microscopy showed that a few percent of closed porosity remains in the pellets, and on this scale no gross inhomogeneities are apparent. X-ray analysis clearly showed that the dominant phase is rutile (TiO_2) and that several other background lines are also detectable. Scanning electron microscopy generally confirmed the absence of inhomogeneities, but the microprobe clearly indicated that some degree of elemental segregation exists.

Transmission electron microscopy provided a completely different impression of the material (Fig. 2) and was used to identify eight different phases in the waste which are summarized in Table IV. The major phase was rutile, which made up approximately 50% of the solid, and to within the limits on the x-ray detector ($\sim 1 \text{ At}\%$), no other elements were in the solution in the rutile. The second most abundant crystalline compound (estimated volume fraction ~ 0.1) was gadolinium titanate, $\text{Gd}_2\text{Ti}_2\text{O}_7$. There is evidence that U, Zr, Y, and possibly Sm and Eu are in solid solution with this gadolinium phase. Elemental silicon crystals remaining in the waste were found to be surrounded by SiO_2 .

Two types of metallic globules were observed in the waste form. These were principally elemental molybdenum with trace elements in solution and elemental palladium with other trace elements in solution. In the case of molybdenum, the silicon

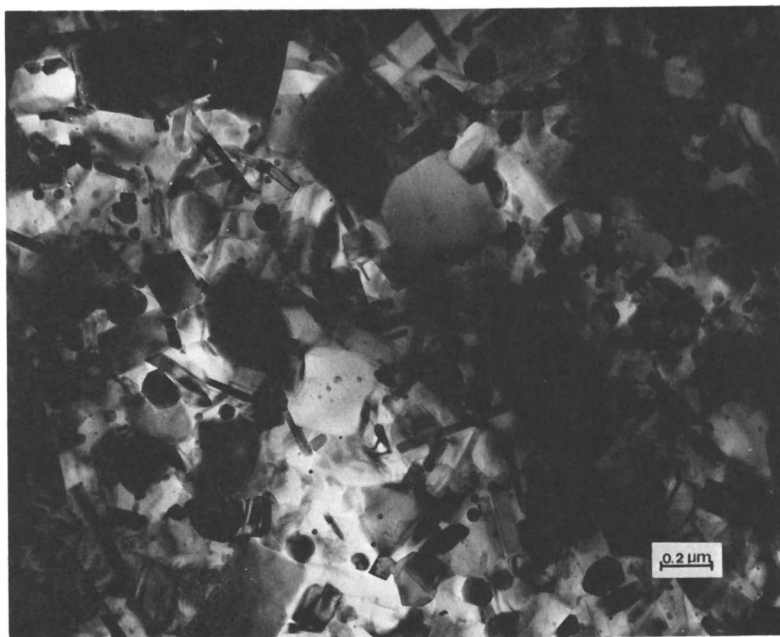


Figure 2. Transmission electron photomicrograph of a ceramic titanate waste form. The sample was prepared by pressure sintering a titanate fully loaded with fission waste oxides and includes zeolite and silicon additions.

Table III. Comparison of the Radionuclide Activity in Effluent from Titanate Solidification Process with the Activity in the High Level Waste Feed Solution

<u>Nuclide</u>	<u>High Level Waste Feed (dpm/ml)</u>	<u>Titanate Process Effluent (dpm/ml)</u>
^{90}Sr	6.6×10^{10}	$\leq 6 \times 10^2$
^{99}Tc	$\sim 1 \times 10^2 \text{ ug/ml}$	$\leq 8 \times 10^{-4} \text{ ug/ml}$
^{106}Ru	1.9×10^{10}	8.4×10^4
^{134}Cs	3.8×10^{10}	$\leq 3.2 \times 10^2$
^{137}Cs	1.3×10^{11}	$\leq 1.8 \times 10^2$
^{144}Ce	5.7×10^{10}	$\leq 1.4 \times 10^3$
^{154}Eu	4.8×10^9	$\leq 3.4 \times 10^2$
Gross Alpha	$5 \times 10^8 \text{ cpm/ml}$	3 cpm/ml

Table IV. Phases Identified in Ceramic Titanate Waste

<u>Phase¹</u>	<u>Energy Dispersive Analysis</u>
TiO_2 (Rutile)	Ti
Amorphous Silica (SiO_2)	Si (Trace U, Al, Na)
$\text{Cs}_2\text{O} \cdot \text{Al}_2\text{O}_3 \cdot 4\text{SiO}_2$ (dehydrated pollucite)	Si, Al, Cs (Trace Ti, Rb)
$\text{Gd}_2\text{Ti}_2\text{O}_7$	Ti, Gd, U, Nd (Trace Zr, Y)
Elemental Mo	Mo (Trace Fe, Ti)
Elemental Pd	Pd - Some Te and Ti (Trace Fe, Mo)
Cubic ZrO_2	Zr (Trace U, Si)
Amorphous Zeolite (Na,Cs) Alumino Silicate	Na, Cs, Al, Si (Trace Ti, U, Fe, Mo, Gd, Sr)

1) At least eight more distinct phases have been detected by electron diffraction and/or x-ray energy dispersive analysis. These have not been identified but most appear to be titanates.

additions were effective in reducing the oxidation state as evidenced by globular regions of the metal formed in the amorphous layers of SiO_2 adjacent to the residual Si particles. Traces of iron were also detected in the metallic globules. The elemental palladium spheres occurred in the rutile crystals and frequently appeared to contain tellurium, iron, molybdenum, and uranium in solution. Several amorphous phases were indicated in the waste form. The first, mentioned earlier, was amorphous SiO_2 which was estimated at approximately 5 vol% and which contained possible traces of Ti, Al, U, and Na. Another amorphous phase resulted from the cesium bearing zeolite added to the waste before consolidation. A single, small crystal of pollucite ($\text{Cs}_2\text{O} \cdot \text{Al}_2\text{O}_3 \cdot 4\text{SiO}_2$) was also identified suspended in the amorphous zeolite. In addition, six minor crystalline phases were observed but have not been identified.

The characterization work has shown that, although the titanate ceramic appears to be homogeneous on a macro scale, it is actually quite heterogeneous on an atomic scale and contains at least 14 different phases and possibly more. Since interactions of the waste form with any environment surrounding it will also occur on an atomic scale, it is important that this type of information be available when speculating on the long term stability of any waste form.

Leachability of Waste Forms

An evaluation of leaching properties is necessary in proposing waste forms for high level waste management, as this property is important in the source term for modeling radionuclide transport to the biosphere as a function of time. In discussing leaching properties of various waste forms, care must be exercised in defining the purpose of the test as well as the experimental conditions used to avoid confusion as to the significance of the results. Qualitative comparisons of the leaching properties of different materials under identical experimental conditions has been suggested as a valid means of using leaching data (18) and that philosophy has been applied to the titanate waste leaching work.

A long term leaching study to compare the behavior of a titanate waste with glassy waste forms and to attempt to elucidate a leaching mechanism has been in progress for 16 months (19). The glass wastes include a zinc borosilicate glass prepared at Battelle Northwest Laboratories and a glass prepared at Sandia Laboratories using zinc borosilicate frit supplied by Battelle. Both glasses contain approximately 25% by weight of fission waste oxide simulant and are believed to differ only in that phosphate, at the level expected in actual waste, was included in the Sandia glass. The titanate was a pressure sintered material also containing approximately 25% by weight of fission waste oxide simulant. Monolithic samples of each waste form are being contacted

with water at 95°C in a Soxhlet apparatus and the release rates of Na, Sr, Cs, Mo, Si, and Zn have been monitored over the past 16 months. After one to two months, the glasses were visually attacked as evidenced by the formation of a surface film, which periodically sloughed off and reformed. The titanate appearance has remained unchanged over the duration of the test.

Based on dissolved ions only, the titanate waste showed an overall leach rate of 3.4×10^{-5} g/cm²·day and a rate of 5.3×10^{-7} g/cm²·day for the fission waste oxides only. The results indicate that the leaching which is occurring is associated with the silicate phases in the ceramic, i.e., the SiO₂ formed from the silicon and the zeolite. The glass samples showed overall leach rates of $6-15 \times 10^{-5}$ g/cm²·day and fission waste oxide leach rates of $1.8-2.7 \times 10^{-6}$ g/cm²·day, where the higher rates in both cases were observed in the phosphate-containing glass. The above leach rates are the average rates over a period of 15 months. However, significant variations in weekly or monthly rates show that leaching is a cyclic process for both the glass and ceramic materials. The apparent effect of the phosphate on the leaching properties of the glass is not of concern for the titanate waste, as anionic species such as phosphate and sulfate are not retained by the material during the ion exchange solidification process.

Deep geologic disposal imposes more severe conditions relative to leaching than those generally employed in laboratory studies. A leaching study has been initiated to compare the leaching behavior of the ceramic and glass wastes under conditions which would apply to high level waste stored in bedded salt at the proposed site of the Waste Isolation Pilot Plant (WIPP) in the Southeastern part of New Mexico (3). These include contacting monolithic samples with two "standard" brines (20) characteristic of the WIPP site at 250°C and 16.6 MPa. Deionized water and seawater are also included in the experimental matrix. A period of seven days was used in the initial experiments to be discussed. The waste forms were a fully loaded, pressure sintered titanate waste containing zeolite and silicon additions, a copper borosilicate glass prepared from Frit #199 supplied by Battelle Northwest Laboratories, and a copper borosilicate glass prepared from the same frit and containing 30% by weight of waste oxides.

The most severe attack on all the materials occurred in the deionized water where weight losses of 1-2%, 18-19% and 9-37% were observed for the titanate waste, glass, and glass wastes, respectively. In near-saturated and saturated brines, the attack was less severe. Surprisingly, small weight gains were observed for some of the titanate samples. Summarizing the work in brines, the titanate results ranged from a 0.5% weight increase to a 0.25% weight decrease whereas the glass lost 4 to 13%, and the glass waste 1 to 3% in weight, respectively. In seawater, the weight change in the titanate was below detection limits (0.1%) while the glass waste lost 5% by weight.

Applications to Other Waste Streams

The work on high level waste solidification has led to applications of the same materials to other areas of waste management. These include decontamination of defense wastes currently in tank storage at Richland, WA, selective separation of Cs for beneficial uses, and development of a process flowsheet for conversion of Zircaloy fuel cladding hulls to sodium zirconate for use in waste stabilization. Each is briefly described below.

Sodium titanate has been found to be very effective in removing Sr from defense waste typified by a $6M$ $NaNO_3$ - $0.6M$ $NaOH$ solution also containing the sodium salts of aluminate, nitrite, phosphate, carbonate, sulfate, and chromate in the range of 0.14 to 0.007 N and Sr in the analytical concentration range of 0.04 to 0.4 ppm (21). Sodium titanate columns have provided a Sr decontamination factor of greater than 10^3 for 2500 column volumes of the waste at flow rates of 2 to 6 column volumes per hour. The material has also been shown to remove residual actinide contamination from the same and similar waste streams (22).

The fact that Cs in high level waste is found in the leading chromatographic band on both the titanate and zirconate columns suggests the feasibility of recovering a significant fraction of relatively pure Cs as a by-product of solidification. In studies aimed at beneficial uses of selected isotopes, a simulated liquid high level waste was passed through a zirconate column to the extent that only the Cs band is allowed to breakthrough. Up to 85% of the Cs can be isolated in this manner in a solution that is, for all practical purposes, free of actinides and other radio-nuclides (23). The process was also demonstrated with high level waste in hot cell tests.

The Zircaloy Conversion Process (24, 25, 26) is a concept whereby one waste stream, Zircaloy fuel hulls, can be utilized in the stabilization of a second waste stream. The process flowsheet, which is conceptual in nature, details the steps required to convert the fuel hulls to sodium zirconate to be used in the solidification of liquid high level waste.

Summary

The preparation, composition, structure and leaching characteristics of a crystalline, ceramic radioactive waste form have been discussed, and where applicable, compared with vitrified waste forms. The inorganic ion exchange materials used such as sodium titanate were prepared from the corresponding metal alkoxide. The alkoxides were reacted in methanol with a base containing the desired exchangeable cation and the final powder form was produced by hydrolysis in an acetone-water mixture followed by vacuum drying the precipitate at ambient temperature.

The baseline solidification process involves contacting an inorganic titanate ion exchange material with liquid waste in a

downflow, fixed bed column configuration. Approximately 100% of the exchange capacity can be realized by using a zeolite, either incorporated in the titanate or as a separate bed, to prevent Cs contamination of the effluent. The Tc, present as the TcO_4^- anion, is found in the column effluent along with approximately 0.2% of the ^{106}Ru initially in the feed. A Dowex 1-X8 anion exchange column can be used to quantitatively remove the Tc and in combination with a ferric titanate bed, lowers the ^{106}Ru by an additional three orders of magnitude.

After loading, the materials are dried at 100°C and pressure sintered. Optimum conditions were established as 1100°C and 6.9 MPa, as no improvement in the product was achieved by increasing either temperature or pressure. Cylindrical pellets up to 5 cm in diameter were produced and the feasibility of a semi-continuous pressure sintering process was demonstrated. Temperatures could be decreased as far as 900°C by the addition of a glass binder to the titanate waste. Elemental silicon at a level of 1-2% by weight was incorporated in the material during the preparation of the sodium titanate to prevent the formation of water soluble molybdate phases during the consolidation process.

The baseline process, including the pressure sintering step, was demonstrated with both simulated high level waste and under hot cell conditions using a waste solution prepared from typical spent light water reactor fuel. A batch contacting method using sodium titanate was also evaluated, but the overall decontamination factor was much lower than obtained in the column process. A batch procedure using magnesium rather than sodium titanate appeared promising based on a single set of experiments. The magnesium titanate was added directly to the waste solution producing a product of the consistency of damp sand. Since no sodium was added to the waste, a washing/filtering step was not required, and the waste was directly calcined at 650°C to destroy the nitrates, and pressure sintered under the same conditions used for the column materials. The density and leaching characteristics were comparable to or better than any of the titanate waste forms produced by other methods. The simplicity made the process look attractive; however, the project ended before further investigation could be completed.

The baseline product was a ceramic waste form with a density range of 4.2 to 4.5 g/cm^3 , containing approximately 25% by weight of fission waste oxides. The lower end of the density range reflects the addition of zeolite to the material. Although the pellets were visually homogeneous, microstructural analyses showed them to be a very complex material consisting of an assemblage of crystalline phases along with amorphous phases due to zeolite and silicon additions. The matrix material was rutile in which were contained a minimum of thirteen other crystalline phases, seven of which have been identified. Neither of the basic process steps, solidification and consolidation, were found to be sensitive to changes in liquid waste composition.

The leaching characteristics of the ceramic waste were compared with some vitrified waste forms under identical experimental conditions. The results are complex due to different leaching rates for various elements and the attack on the glass surface which results in the formation of a surface film which periodically sloughs off, however, some general comparison can be made. In long term (16 month) leaching studies using monolithic samples in distilled water at 95°C, both the ceramic and glass wastes showed a high resistance to attack. Based on dissolved ions (Sr, Cs, Mo, Zn, Si, and Na) only, the ceramic waste had an overall average leach rate over a 15 month period of 3.4×10^{-5} g/cm²·day and a rate of 5.3×10^{-7} g/cm²·day for the fission waste oxides (Sr, Cs, and Mo). The glass samples showed overall leach rates of $6-15 \times 10^{-5}$ g/cm²·day, and fission waste oxide leach rates of $1.8-2.7 \times 10^{-6}$ g/cm²·day. The higher rates in both cases were observed in the phosphate-containing glass. The results indicate that the leaching which did occur in the ceramic materials was associated with the silicate phases present.

In leaching studies with monolithic samples at 250°C in water, salt brines and seawater, the attack on both forms was more severe. After seven days, weight changes in the titanate waste form were a 1-2% loss, 0.5% increase to 0.25% loss, and not detected (<0.1%) in deionized water, brines and seawater, respectively. A copper borosilicate-based vitrified waste showed 9-37%, 1-3% and 5% weight losses in the same solutions. Significant attack on the glass waste in the form of a surface film was again observed and the weight loss data may be biased in some cases depending on the degree to which the film had sloughed off prior to weighing. The surfaces of the titanate waste were visibly unaltered, however, which may indicate that the attack was localized and occurred primarily on silicate phases associated with zeolite and silicon additions.

The use of inorganic ion exchangers to solidify liquid radioactive waste followed by pressure sintering to produce a ceramic waste form appears to be a viable alternative to calcination/vitrification processes. Both the process and waste form are relatively insensitive to changes in the composition of the waste feed. The stability of the ceramic waste form has been shown to be superior to vitrified wastes in leaching studies at elevated temperatures. Further studies on the effects of radiation and associated transmutation and the influence of temperature regimes associated with potential geologic repositories are needed for a more definitive comparison of crystalline and amorphous waste forms.

Acknowledgements

The author expresses appreciation to all those who contributed to this project with special thanks to Drs. B. T. Kenna and J. K. Johnstone, whose work in the areas of leaching and consolidation/characterization, respectively, is liberally summarized in this review.

Literature Cited

1. Alternatives For Managing Wastes from Reactor and Post-Fission Operations in the LWR Fuel Cycle, ERDA - 76 -43, May (1976).
2. Mendel, J. E., Palmer, C. R., and Eschback, E. A., "Preliminary Assessment of Potential Effects of Alternate Fuel Cycles on High-Level Waste Vitrification Processing," Symposium on Waste Management and Fuel Cycles '78," Edited by R.G. Post and M. E. Wacks, Tucson, AZ, March (1978).
3. Braithwaite, J. W. and Johnstone, J. K., Sandia Laboratories, Unpublished Research.
4. McCarthy, G. J., White, W. B., Roy, R., Scheetz, B. E., Komarneni, J., Smith, D. K., Roy, D. M., "Interactions Between Nuclear Waste and Surrounding Rock," *Nature*, Vol. 273, 18 May (1978).
5. De, A.K., Luckscheiter, B., Malow, G., and Schiewer, E., "Fission Products in Glasses Part II: Development of Glass Ceramics," HMI-B 218, Sept. (1977).
6. McElroy, J.L., "Quarterly Progress Report Research and Development Activities in Waste Fixation Program," PNL - 2264/UC-70, Nov. (1977).
7. Lynch, R.W., Editor, "Sandia Solidification Process Cumulative Report," SAND76-0105 (1976).
8. Lynch, R.W., Dosch, R.G., Kenna, B.T., Johnstone, J.K., and Nowak, E.J., "The Sandia Solidification Process - A Broad Range Aqueous Waste Solidification Method," Proc. IAEA Symposium on the Management of Radioactive Wastes," IAEA - SM 207/15, Vienna, Austria, March 22-26 (1976).
9. Dosch, R.G., "Ceramics from Ion Exchangers: An Approach to Nuclear Waste Solidification," *Trans. Amer. Nucl. Soc.*, 22, (1975).
10. Morosin, B. and Percy, P.S., "Structural Studies of the Hydrolysis Products of Ti, Nb and Zr Alkoxides," *Chem. Phys. Letters* 40(2), 263 (1976).
11. Percy, P.S., Dosch, R.G., and Morosin, B., "Preparation and Structural Studies of the Hydrolysis Products of Titanium, Niobium and Zirconium Alkoxides," SAND76-0556, Sandia Laboratories, Albuquerque, NM (1976).
12. Graeber, E.J., and Morosin, B., "Molecular Configuration of the Decaniobate Ion ($\text{Nb}_{10}\text{O}_{28}^{-6}$)," *Acta. Cryst.* B33, 2137 (1977).
13. Kenna, B.T., Sandia Laboratories, Unpublished Research.
14. Brownell, L.E., Kindle, C.H., and Theis, T.L., "Review of Literature Pertinent to the Aqueous Conversion of Radionuclides to Insoluble Silicates with Selected References and Bibliography (Revised)," ARH-2731REV, Dec. (1973).

American Chemical Society
Library

15. Johnstone, J.K., "The Sandia Solidification Process: Consolidation and Characterization Part I. Consolidation Studies," SAND78-0663, May (1978).
16. Lynch, A.W., "A Short Duration Leach Test for Radioactive Waste," Nucl. Tech. 34, No. 8, p. 463 (1977).
17. Johnstone, J. K., Headley, T.J., Hlava, P.F., and Stohl, F.V., "The Sandia Solidification Process: Consolidation and Characterization Part II. Characterization," SAND78-1669, Sept. (1978).
18. Mendel, J.E., "A Review of Leaching Test Methods and the Leachability of Various Solid Media Containing Radioactive Waste," BNWL-1765. July (1973).
19. Kenna, B.T., Murphy, K.D., and Levine, H.S., "Studies of Waste Form Leaching: Part I. Long Term Elevated Temperature Leaching," to be published in J. Amer. Cer. Soc.
20. Dosch, R.G., and Lynch, A.W., "Interactions of Radionuclides With Geomedia Associated with the Waste Isolation Pilot Plant (WIPP) Site in New Mexico," SAND78-0297, June (1978).
21. Dosch, R.G., "The Use of Titanates in Decontamination of Defense Waste," SAND78-0710, June (1978).
22. Schultz, W.W., Rockwell Hanford Operations, Personal Communication.
23. Kenna, B.T. and Murphy, K.D., "Separation of ^{137}Cs From Nuclear Waste," Nuclear and Cosmological Chemistry Symposium, ACS Meeting, Anaheim, CA, 1978. Submitted for publication in J. Inorg. Nucl. Chem.
24. Levine, H.S., "An Assessment of Processes for Conversion of Zircaloy Cladding Waste to Zirconate Ion Exchange Material," SAND75-0643, July (1976).
25. Levine, H.S. and Nowak, E.J., "Conversion of Waste Zircaloy Hulls to Zirconate Ion Exchange Materials for Waste Stabilization," Nucl. Tech. 36 (Nov.) 106 (1977).
26. Levine, H.S., "Conversion of Fuel Hulls to Zirconate Ion Exchanger for Stabilization of Wastes from the Thorium Fuel Cycle," Symposium on Waste Management and Fuel Cycles "78," Edited by R.G. Post and M.E. Wacks, Tucson, AZ, March (1978).

RECEIVED January 16, 1979.

A Field Study of Radionuclide Migration¹

DARLEANE C. HOFFMAN

Los Alamos Scientific Laboratory, Los Alamos, NM 87545

In the first phase of the field studies which have been described in detail in another report (1), the site of the 0.75-kt nuclear test, Cambric, detonated on May 14, 1965, was investigated by re-entry drilling, and sampling of both solid and water. The Cambric test was fired beneath the water table in tuffaceous alluvium in Frenchman Flat (See Figure 1). It was chosen for study for the following reasons. Sufficient time had elapsed so that the ground water had refilled the cavity and chimney regions to the preshot level of 73 m above the detonation point. Thus, water which had been in contact with the radioactive debris for some time could be obtained for analysis of radionuclide content. The Cambric detonation point was only 294 m below the ground surface which made re-entry drilling and sampling less difficult and expensive than for some of the deeper tests. The tritium (T) present from the test was sufficient to provide a readily measurable tracer for water from the region of the test. The postshot debris also contained enough plutonium, uranium, and fission products so that measurements of their relative concentrations in rubble and ground water from various regions could be made. A summary of the intensity of the radionuclide source term at the time of re-entry is given in Table I. The ratios of the concentrations of the radionuclides relative to T are given in Table II. It was believed that this relatively low yield test would have had little effect on the local hydrology. The alluvium was judged to be a good medium for hydrologic studies because of its permeability and the absence of large cracks or fissures, and the very small natural hydraulic gradient in the region. Finally, the Cambric site was far enough removed from the areas of active nuclear testing so that damage or interruption of drilling and sampling operations was unlikely.

¹ Work conducted under the auspices of the U.S. Department of Energy.

0-8412-0498-5/79/47-100-149\$05.00/0
©1979 American Chemical Society

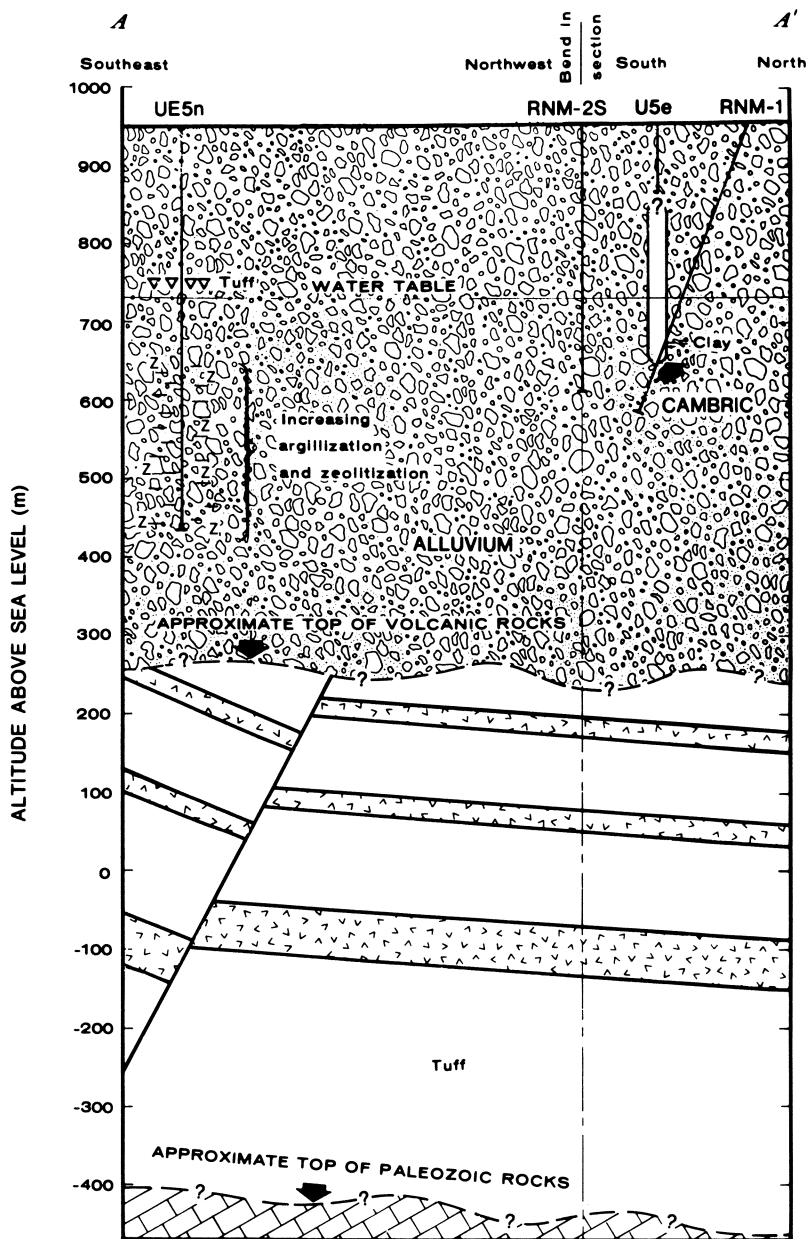


Figure 1. Geologic section at Cambric site (1)

TABLE I
CAMBRIC SOURCE TERM AT 10 YEARS

<u>Nuclide</u>	<u>Half-Life (Years)</u>	<u>Activity (Curies)</u>
^3H	12.3	3.4×10^4
^{85}Kr	10.7	4.4
^{90}Sr	29	34
^{106}Ru	1.0	2.8
^{125}Sb	2.8	3.2
^{137}Cs	30	99
^{144}Ce	0.78	0.4
^{147}Pm	2.6	33
^{155}Eu	5.0	6.4

Cambric Re-entry Well RNM-1

Field Operations. Safety considerations dictated that re-entry would be by means of slant drilling rather than vertical drilling from the ground surface directly above the detonation point. The Cambric re-entry hole, designated RNM-1, was drilled in May, 1974, nine years after Cambric had been fired. A satellite well, RNM-2S, was constructed in April, 1974. It was to be pumped later in order to induce an artificial gradient so that water could be drawn from RNM-1 and provide an opportunity for the study of radionuclide migration under field conditions. RNM-2S was drilled prior to RNM-1 to avoid the possibility of cross contamination from Cambric. A schematic diagram of the placement of RNM-1 and RNM-2S is shown in Figure 2. A total of 67 sidewall core samples was taken in RNM-1 as drilling progressed from the surface to about 50 m below the original detonation point. These sampling points are shown in Figure 3. One core from each depth was placed immediately in a nitrogen-flushed, gas-tight, stainless-steel container for subsequent analyses of ^{85}Kr , HT, HTO, and for γ -spectral analyses. Other core samples were sealed in water-tight plastic bags for later γ -spectral and radiochemical analyses of the cores and contained fluids, and for lithologic examination of the alluvium.

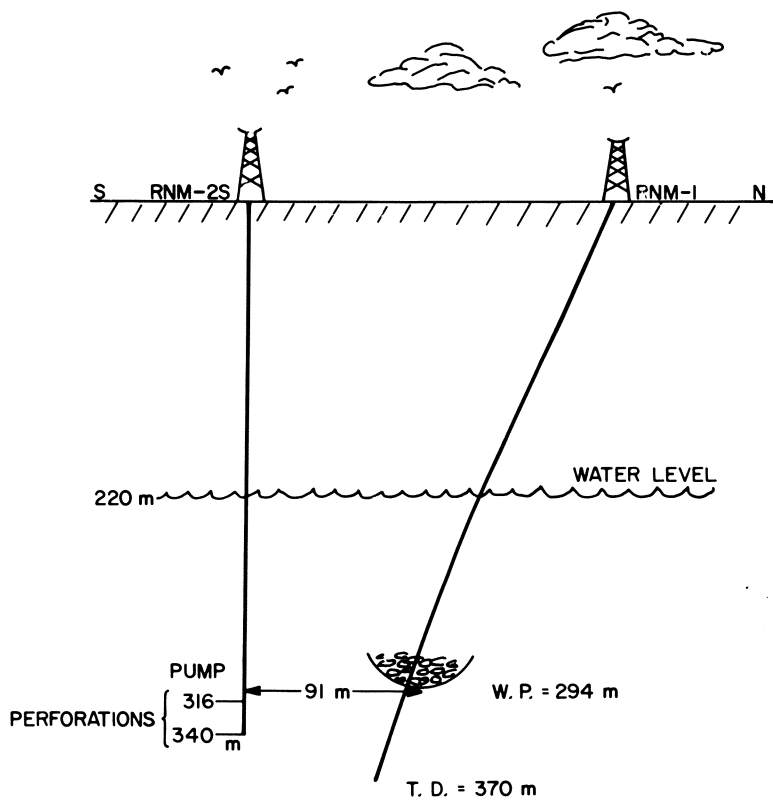


Figure 2. Schematic of RNM-1 and RNM-2S.

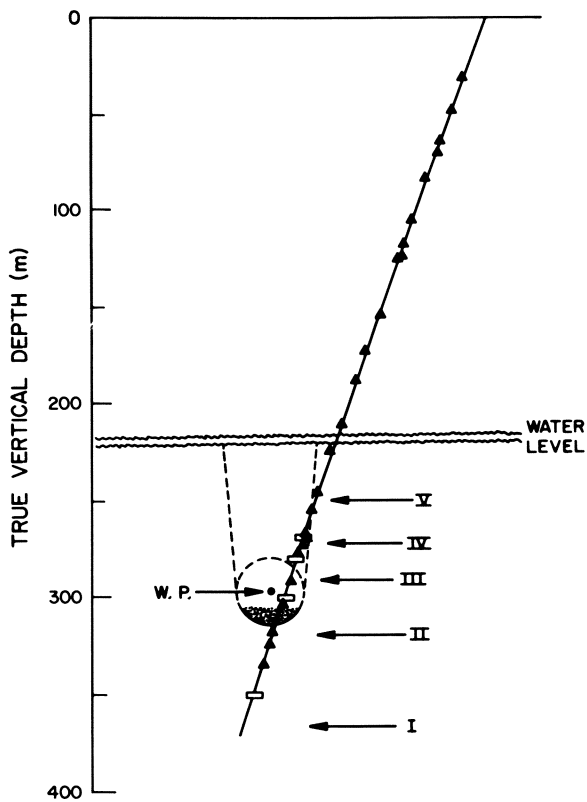


Figure 3. Sampling points at RNM-1: (▲), core samples (67).

TABLE II
RATIOS FOR RNM-1 SOURCE AT t_0 (5-14-65)

Nuclide	Half-Life (Years)	$(N_x/N_T)^a$	$(A_x/A_T)^b$
T	12.26	1.00	1.00
^{85}Kr	10.74	1.22×10^{-4}	1.38×10^{-4}
^{90}Sr	28.9	1.66×10^{-3}	7.05×10^{-4}
^{106}Ru	1.010	3.68×10^{-3}	4.46×10^{-2}
^{125}Sb	2.77	1.52×10^{-4}	6.73×10^{-4}
^{137}Cs	30.0	5.03×10^{-3}	2.05×10^{-3}
^{144}Ce	0.779	2.84×10^{-3}	4.47×10^{-2}
^{147}Pm	2.62	1.65×10^{-3}	7.74×10^{-3}
^{155}Eu	5.00	1.73×10^{-4}	4.24×10^{-4}
^{238}U	4.5×10^9	1.78×10^2	4.90×10^{-7}
^{239}Pu	2.44×10^4	6.28	3.16×10^{-3}
^{241}Am	4.2×10^2	$\approx 2.5 \times 10^{-2}$	$\approx 7.7 \times 10^{-4}$

^aThis is the atom ratio of the indicated nuclide to the post-detonation tritium of ≈ 6.3 g or 1.25×10^{24} atoms.

^bThis is the ratio of the disintegration rate for each nuclide relative to tritium calculated from the indicated half lives.

After completion of sidewall sampling and cleaning the hole, 14-cm diameter casing with appropriately placed, inflatable external packers was installed to a vertical depth of 355 m. The packers were used to minimize external movement of the water in the annular space between the casing and hole wall. The hole was then drilled to a total depth of 370 m. The drilling mud and fluids used in drilling and developing the well were labeled with 20 ppm of Li so that the Li content of water samples taken later could be used as an indication of the degree of contamination from added fluids. (No other water was added.) Two types of water samples were removed from each zone. "Pressurized" water samples were obtained by lowering evacuated, gas-tight, 2-liter samplers into the well. These were opened at depth to allow the water to enter and after closing the valve were brought to the surface. Water was also removed to the surface by a submersible pump. Upon completion of sampling the lower uncased region, a packer was placed at the top of the zone, the casing in the next zone was perforated, and water was sampled as before. In this way, each of the five zones shown in Figure 4 was sampled successively.

Results. The γ -spectral and radiochemical analyses of the various kinds of core and water samples removed from RNM-1 provided a good picture of the distribution and concentration of the radioactivity in the environment around the Cambrian nuclear test.

Ten years after the test, most of the radioactivity and the highest specific activities of all radionuclides were still found in the region of the original explosion cavity. No activity above background was found 50 m below the cavity. Measurements of HT and HTO removed from the cores and pressurized water samples showed that more than 99.9% of the T was present as HTO. Although some ^{85}Kr and T were found in the chimney, they were concentrated in the cavity region. The measured $^{85}\text{Kr}/\text{T}$ ratios were consistent with the calculated ratio for Cambrian and the ^{85}Kr seemed to be dissolved in the water. Comparison of the specific activities of the solid and water from a core taken from the lower cavity region gave effective distribution coefficients of 10^4 , $\geq 10^4$, and $\approx 10^8$ for ^{90}Sr , ^{137}Cs , and ^{239}Pu , respectively.

Water was pumped from each zone until the T concentration was relatively constant as illustrated in Figure 5 for Zone II, the lower cavity region. The pH and conductivity were measured in the field and standard water analyses were performed later. A summary of these data is given in Table III. Representative activity levels of the radionuclides detected in water from each zone are given in Table IV. Water from the region of highest radioactivity at the bottom of the cavity contains only T and ^{90}Sr at levels higher than the recommended (2) concentration guides (CG) for drinking water in uncontrolled areas.

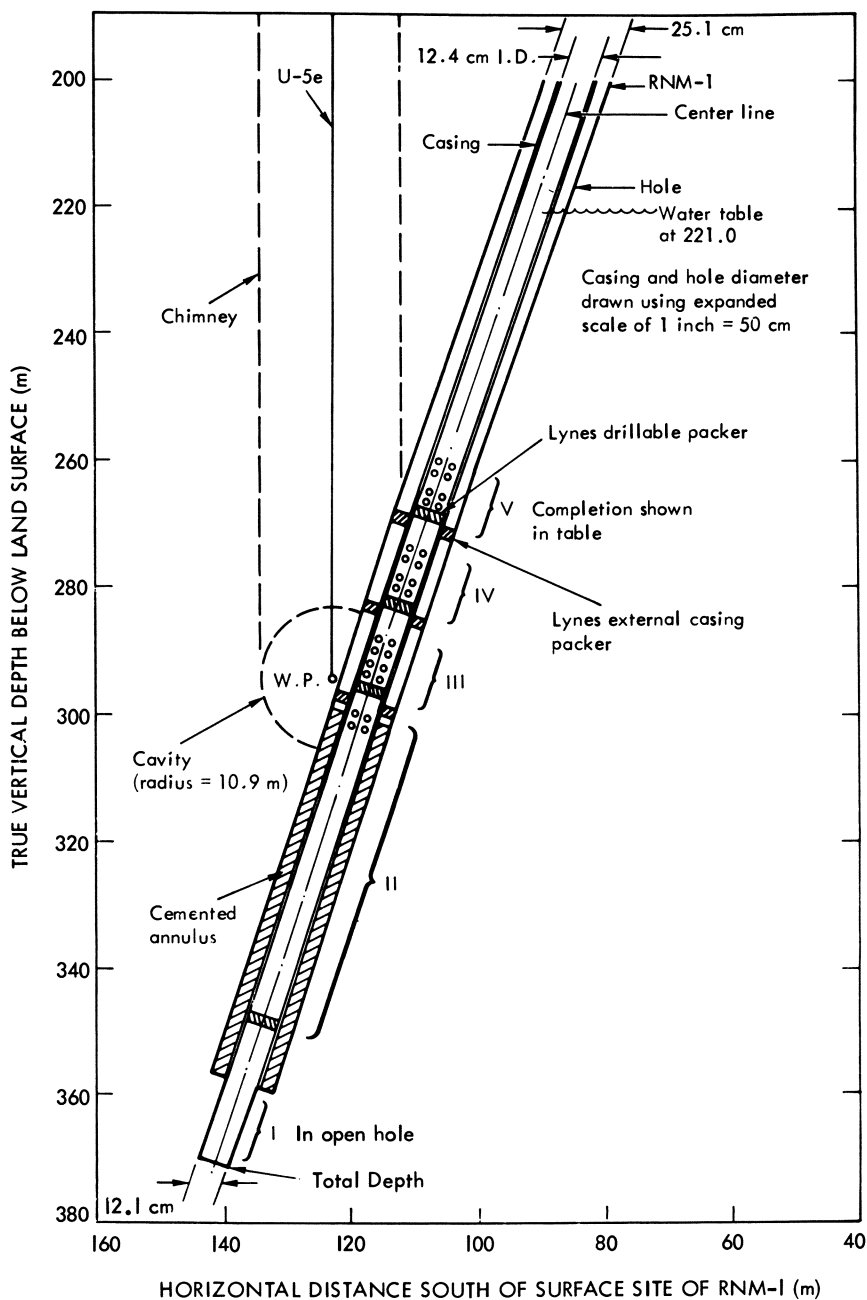


Figure 4. Construction details of RNM-1 (1)

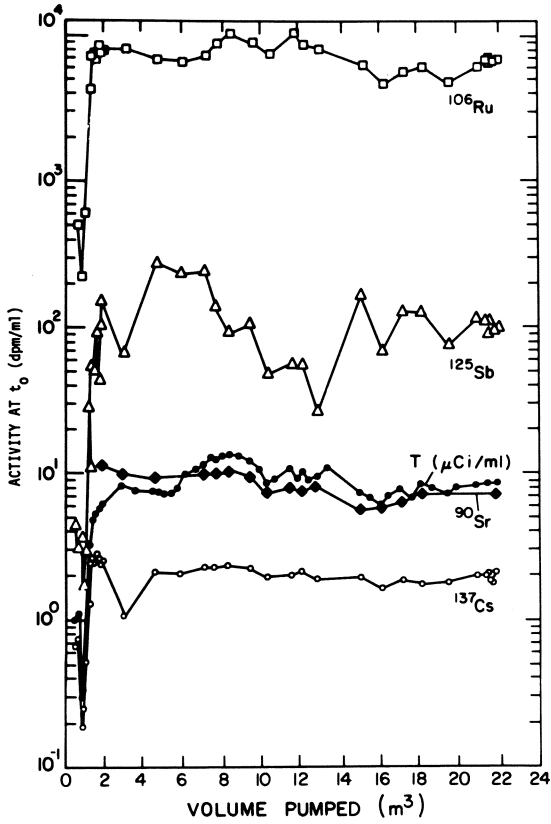


Figure 5. Analyses of water samples from Cambric, Zone II (1)

TABLE III
ANALYSES OF REPRESENTATIVE WATER SAMPLES PUMPED FROM RNM-1^a

Zone	Cl	HCO ₃	SO ₄	Volume Pumped (m ³)	Conductivity (umho/cm)	pH	Ca (ppm)	Li (ppm)
I	≈ 20	≈ 170	≈ 30	≈ 53	≈ 420	8.1	≈ 15	≤ 0.05
II	≈ 100	≈ 140	≈ 200	23.7	≈ 1000	8.3	≈ 50	0.4
III	≈ 40	≈ 470	≈ 110	18.9	≈ 1100	7.2	≈ 70	0.2
IV	≈ 30	≈ 550	≈ 110	45.7	≈ 1100	7.1	≈ 90	≈ 1.5
V	≈ 20	≈ 350	≈ 65	18.6	≈ 670	7.4	≈ 50	0.4

^aData from Reference 1, p. 66.

TABLE IV
 REPRESENTATIVE ACTIVITY LEVELS IN WATER SAMPLES

Zone	T	⁸⁵ Kr	⁹⁰ Sr	¹⁰⁶ Ru	¹²⁵ Sb	¹³⁷ Cs	²³⁹ Pu
	($\mu\text{Ci}/\text{ml}$)	Bg	Bg	Bg	Bg	Bg	Bg
Below Cavity	Bg ^a	Bg	Bg	Bg	Bg	Bg	Bg
Lower Cavity	6.1	800	8	11	5	1.6	≤ 0.0029
Upper Cavity	3.8	1200	5	4	2	1.4	≤ 0.0026
Chimney	0.084	70	5	n.d. ^b	n.d.	0.8	n.d.
Adjacent to Chimney	0.028	20	0.2	n.d.	n.d.	0.2	n.d.
CG ^c	0.003	--	0.67	22.2	222	44.4	11.1

^aBg = no activity detectable above background levels.

^bn.d. = not detected.

^cCG = Recommended (Ref. 2) concentration guide (CG) applicable to water in uncontrolled areas.

By comparing the measured ratio of each nuclide detected in the water to the T in the water with the calculated ratio for the Cambric source term (Table I), an effective retention factor, E_d , for each nuclide on the solid debris was estimated as follows. (It was assumed that all the T and radionuclides are contained below the water table and that the fraction of each nuclide not in the water is in the solid debris.)

$$E_d = \frac{(A_X/A_T)_{\text{Cambric}}}{(A_X/A_T)_{\text{water}}} = \frac{(A_X \text{ Cambric})(A_T \text{ water})}{(A_X \text{ water})(A_T \text{ Cambric})}$$

$$\frac{A_T \text{ water}}{A_T \text{ Cambric}} \geq 0.999 \approx 1.$$

$$A_T \text{ Cambric}$$

$$\text{Thus, } E_d \approx \frac{A_X \text{ Cambric}}{A_X \text{ water}} \approx \frac{A_X \text{ solid}}{A_X \text{ water}}.$$

The retention factors for each zone are shown in Table V. They range from $> 10^7$ for ^{239}Pu and $> 10^6$ for ^{147}Pm to 10^2 to 10^4 for ^{90}Sr , ^{106}Ru , ^{125}Sb , and ^{137}Cs . The very high values for ^{239}Pu and ^{147}Pm may be related to their low solubility at these pH's as well as to low leaching rates from the fused debris. The values for ^{90}Sr and ^{137}Cs appear to be significantly lower in the chimney than in the cavity region, perhaps reflecting their movement from the cavity as the gaseous species ^{90}Kr and ^{137}Xe and subsequent adsorption on the surface of the alluvium rather than in the fused debris in the cavity region.

Satellite Well RNM-2S

The satellite well designated RNM-2S was drilled 91 m south of RNM-1. After completion of sampling operations at RNM-1, the packer between zones IV and V was drilled out and pumping was begun at RNM-2S in October, 1975 at a rate of 250 to 300 gallons (0.95 to 1.14 m^3) per minute. This pumping was expected to overcome any natural gradient and induce a sufficient artificial gradient to draw water from the Cambric cavity to RNM-2S. Detection of T would signal the arrival of water from Cambric. By August 1977, more than 1.14 million m^3 of water had been removed without detection of T. An estimate based strictly on the volume of water in a sphere 91 m in radius (the distance between RNM-1 and 2S) using a porosity of ≈ 0.3 for the alluvium and the assumption of equal transmissivity in all directions, indicates that $\approx 10^6 \text{ m}^3$ of water must be pumped to draw T to RNM-2S. Pumping was suspended and RNM-1 was resampled to see if the radionuclide levels had changed. Pressurized and pumped water

TABLE V
E_d's FROM WATER SAMPLES

Zone	E _d					
	90Sr	106Ru	125Sb	137Cs	147Pm	239Pu
Below Cavity	Bg ^a	Bg	Bg	Bg	Bg	Bg
Lower Cavity	2.1x10 ³	1.0x10 ²	2.9x10 ²	2.5x10 ⁴	≥10 ⁶	≥3.2x10 ⁷
Upper Cavity	1.6x10 ³	1.9x10 ²	3.6x10 ²	1.8x10 ⁴	n.d.	≥1.9x10 ⁷
Chimney	3.9x10 ¹	n.d. ^b	n.d.	6.6x10 ²	n.d.	n.d.
Adjacent to Chimney	3.1x10 ²	n.d.	n.d.	1.1x10 ³	n.d.	n.d.

^aBg = no activity detectable above background levels.

^bn.d. = not detected.

samples were obtained from RNM-1 and analyses showed that the T level had decreased by a factor of 50 or more (see Table VI) relative to the original values for Zone IV. (Although water can enter from perforations in both Zones IV and V, most of the water production is believed to be from Zone IV). The ^{90}Sr and ^{137}Cs levels shown in Table VII are not too different from the original values. This seems to indicate that the distribution ratios (activity per gram solid divided by activity per ml water) are relatively high (> 100). The source term will then not be rapidly depleted and a more or less constant equilibrium value should be maintained in the water.

In October, 1977 a higher capacity pump was installed in RNM-2S and pumping was resumed at a rate of about 2.27 m^3 per minute. Significant amounts of tritium were finally detected after a total of about 1.44 million m^3 of water had been pumped. The concentrations are still rising rapidly as shown in Figure 6. A number of pressurized samples have been taken and show ^{85}Kr as well as HTO and HT. These data are summarized in Table VIII. The observed $^{85}\text{Kr}/\text{T}$ atom ratios are very similar to that of 1.2×10^{-4} calculated for the Cambrian source term, consistent with the hypothesis that the ^{85}Kr is dissolved in the water and moves along with the HTO.

TABLE VI
REPRESENTATIVE ACTIVITY LEVELS IN RNM-1 WATER SAMPLES

	Activity at t_0		Atom Ratio
	T ($\mu\text{Ci}/\text{ml}$)	^{85}Kr (dpm/ml)	$^{85}\text{Kr}/\text{T}$
Original:			
Zone IV (8-8-75)	0.15	70	1.8×10^{-4}
Zone V (8-14-75)	0.038	13	1.3×10^{-4}
Re-entry:			
I (10-4-77) ($1.17 \times 10^6 \text{ m}^3$ pumped from 2S)	0.0032	75	9.4×10^{-3}
II (11-30-77) ($1.34 \times 10^6 \text{ m}^3$ pumped from 2S)	0.0020	6	1.3×10^{-3}

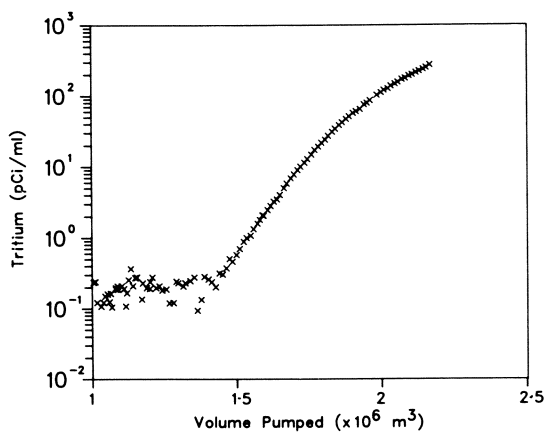


Figure 6. Tritium concentration as a function of volume of water pumped

TABLE VII
ACTIVITY LEVELS OF ^{90}Sr AND ^{137}Cs IN WATER
FROM RE-ENTRY OF RNM-1

	Activity at t_0			
	(dpm/ml)		Atom Ratio	
	^{90}Sr	^{137}Cs	$^{90}\text{Sr}/\text{T}$	$^{137}\text{Cs}/\text{T}$
Original:				
Zone IV (8-8-75)	≈ 6	≈ 1	1.8×10^{-5}	3.1×10^{-6}
Zone V (8-14-75)	≈ 0.25	≈ 0.2	2.3×10^{-6}	1.8×10^{-6}
Re-entry:				
I (10-4-77)	≈ 1	≈ 0.2	1.4×10^{-4}	3.0×10^{-5}
II (11-30-77)	≈ 0.6	≈ 0.5	1.4×10^{-4}	1.2×10^{-4}

TABLE VIII
ANALYSES OF PRESSURIZED WATER SAMPLES FROM RNM-2S
(All activities corrected to zero time.)

Sample	Volume Pumped (m^3)	T ($\mu\text{Ci}/\text{ml}$)	^{85}Kr (dpm/ml)	Atom Ratio $^{85}\text{Kr}/\text{T}$
1	1.702×10^6	1.69×10^{-5}	0.48×10^{-2}	1.11×10^{-4}
2	1.702×10^6	1.62×10^{-5}	1.06×10^{-2}	2.58×10^{-4}
3	1.852×10^6	3.64×10^{-5}	1.15×10^{-2}	1.24×10^{-4}
4	1.852×10^6	3.65×10^{-5}	0.91×10^{-2}	0.98×10^{-4}

Future

Pumping at RNM-2S will continue and large volumes of water will be analyzed for other radionuclides. Simple calculations (R. Stone, private communication, 1978) show that it will take more than 1500 years for nuclides from RNM-1 having distribution ratios of 100 or more to reach RNM-2S. Laboratory experiments (3) indicate that the ratios for Sr, Ru, Cs, Ce, Pm, and Pu are larger than 100. Those for Sb and U are much smaller and isotopes of these elements might be detectable in the water. Non-equilibrium effects or the presence of colloidal or non-sorbed species might allow other nuclides to move more rapidly than expected. Pumping and monitoring of radionuclide levels will be continued at least until a maximum in the tritium concentration has been reached and the shape of the T concentration curve has been defined.

It is hoped that studies similar to those conducted at Cambric can be carried out for nuclear devices tested in other media such as tuff. Re-entry drillback and sampling sooner after detonation would be desirable so that the behavior of shorter-lived species such as ^{95}Zr , ^{99}Mo - ^{99}Tc , ^{103}Ru , ^{131}I , ^{147}Nd , and ^{237}U can be studied. Although these nuclides have such short half lives that they are not apt to be transported off-site, they would provide sensitive monitors of the behavior of longer-lived activities of the same elements, such as 9.5×10^5 -year ^{93}Zr , 2.1×10^5 -year ^{99}Tc , 1.6×10^7 -year ^{129}I , and $^{235,238}\text{U}$ which are of interest on a long time scale.

Acknowledgments

I wish to acknowledge the many people from the Los Alamos Scientific Laboratory, the Lawrence Livermore Laboratory, the U. S. Geological Survey, and the Desert Research Institute who have contributed to the studies which have been briefly reviewed here. R. W. Newman, NV, is Project Manager, and J. E. Sattizahn (LASL), R. H. Ide (LLL), L. D. Ramspott (LLL), and D. C. Hoffman (LASL) have served as Technical Directors.

Abstract

The radionuclide distribution in both the water and aggregate around a 0.75-kt nuclear test which was detonated below the water table at the Nevada Test Site has been investigated. An extensive suite of sidewall core samples was obtained from near the surface to below the original cavity region. Representative water samples were pumped from five different zones in the cavity and rubble regions. Most of the radioactivity was found in solid material contained in the lower cavity region. Water pumped from the region of highest radioactivity showed only tritium and strontium-90 at

levels higher than the recommended concentration guides for drinking water. Water is being pumped from a satellite well some 90 m away to induce an artificial gradient and draw water from the test zone.

Literature Cited

1. Hoffman, Darleane C., Stone, Randolph, and Dudley, Jr., William W., Los Alamos Scientific Laboratory Report LA-6877-MS (1977), "Radioactivity in the Underground Environment of the Cambrian Nuclear Explosion at the Nevada Test Site".
2. ERDA-0524, Standards for Radiation Protection, April 8, 1975, Appendix A, Table II, p. 13; Code 10 Federal Regulations, January 1, 1975, Appendix B, Table II, p. 177.
3. Wolfsberg, Kurt, Los Alamos Scientific Laboratory Report LA-7216-MS (1978), "Sorpton-Desorption Studies of Nevada Test Site Alluvium and Leaching Studies of Nuclear Test Debris".

RECEIVED January 16, 1979.

Nuclide Migration in Fractured or Porous Rock

P. G. RICKERT, R. G. STRICKERT,¹ and M. G. SEITZ

Argonne National Laboratory, Argonne, IL 60439

Repositories built in geologic bodies are being considered for permanent disposal of nuclear wastes. In the context of deep geologic repositories, the rock formation itself may be considered as part of the mechanism retaining the wastes within the immediate neighborhood of the repository. The interactions of nuclear wastes with geologic materials are being studied in laboratory experiments to evaluate geologic media as barriers to nuclide migration. Migration caused by flowing water is considered the most credible mechanism for moving wastes from a repository in a well chosen site. The extent and rate of migration of wastes under the influence of groundwater, of course, depend on several parameters; including the type and extent of the chemical reaction of the radionuclides with the geologic media.

In previous work (1,2,3) it was found that the kinetics of sorption was an important parameter affecting the migration of nuclides in geologic media. For example, in experiments designed to measure the kinetics of reaction for radionuclides in solution with tablets of rock, it was found that periods from several minutes to several hours were required for the radionuclides to reach steady state concentrations on the rock tablets and in the solutions. Figure 1 shows the reaction curves found for the sorption of plutonium and americium from solution by a tablet of granite. The reaction rates for the sorption of plutonium and americium from solution are not the same, and both require a number of hours to reach steady state concentrations.

The observation that the sorption process progresses as a function of time implies that under conditions of solution flow through geologic media, there may not be instantaneous or local equilibrium between a nuclide bearing solution and geologic media, but rather, the nuclide would be sorbed from solution through a length or zone of the media. Following adsorption, the nuclide would desorb after an amount of water passed over the media. The nuclide would again be re-adsorbed downstream a distance dependent

¹ Current address: Battelle Pacific Northwest Laboratories, Richland, Washington 99352.

0-8412-0498-5/79/47-100-167\$06.00/0

© 1979 American Chemical Society

upon the rate of adsorption and the flow rate of the solution. Desorption and readsorption would continue in this manner and the migration of the nuclide would be defined in terms of the rate of adsorption, the rate of desorption, and the equilibrium distribution of the nuclide between solution and geologic media.

To quantify this treatment of migration as influenced by kinetics, a model has been developed in which instantaneous or local equilibrium is not assumed. The model is called the Argonne Dispersion Code (ARDISC) (4). In the model, adsorption and desorption are treated independently and the rates for adsorption and desorption are taken into account. The model treats one dimensional flow and assumes a constant velocity of solution through a uniform homogeneous media.

This paper describes an experimental study of the applicability of the ARDISC model to laboratory studies of nuclide migration in geologic media.

Basic Description of Model

The model assumes a one dimensional column divided into an arbitrary number (LEND) of units or zones. Each zone can sorb a given species such that at equilibrium the distribution of the species between the surface of the zone and the volume of solution (initially at unit concentration of the species) is

$$\alpha/\beta \quad (1)$$

where

α = amount of species sorbed on the surface

and

$\beta = 1 - \alpha$

If after this distribution is established, a second cycle occurs in which the solution from the initial zone is transferred to a second zone with the same characteristics as the first zone and a fresh solution containing none of the species is placed in the first zone, another equilibration, this time in both zones will occur. This process is continued by the model for additional cycles and zones.

The description of the model up to this point is analogous to a description of a chromatographic model which incorporates the concept of the theoretical plate (5).

If, however, the movement from zone to zone is fast enough that equilibrium does not occur, the fraction sorbed from solution can be calculated if the rate of sorption is known (or can be estimated). A parameter, F , is therefore defined

$$F = \frac{\text{fraction of species sorbed from soln. during one cycle time}}{\text{fraction of species sorbed from soln. at equilibrium}} \quad (2)$$

which can be related to the rate of adsorption of the species.

The parameter, F , gives directly the amount adsorbed in a zone in which the species initially is present only in the solution.

For any species adsorbed on the surface of a zone, the fraction of the sorbed species which desorbs during the time of a cycle can be measured (or estimated). Another parameter, G , is therefore defined

$$G = \frac{\text{fraction of species desorbed from surface during 1 cycle time}}{\text{fraction of species desorbed from surface at equilibrium}} \quad (3)$$

to account for desorption under non-equilibrium conditions. The parameter, G , gives directly the amount desorbed in a zone where the species is initially present only on the surface of a zone.

Thus for each zone, during a given cycle, the adsorption-desorption process is separated into two distinct events with F or G describing the kinetics of each event. Such an approach is of course valid only for first order rate reactions. In the limit of low concentration, (such as that resulting from slow leaching from a repository) the reaction sites on the rock will not approach saturation and the number of reaction sites can be considered to remain constant during adsorption. Therefore, for a single species in solution at tracer concentrations the reaction should approximate a first order reaction (i.e., where no complications such as concentration effects, step-wise dehydration, dissociation, etc., are present).

If a calculated cycle is defined as a partial equilibration between the species on the surface of a zone and the species in the solution of a zone, and is followed by an instantaneous transfer of the solution to the next zone, the following recursive formulae apply:

$$R(\ell, Z) = \alpha R(\ell-1, Z) + (1-G)R(\ell-1, Z) + F\alpha S(\ell-1, Z) \quad (4)$$

$$S(\ell, Z+1) = \beta S(\ell-1, Z) + (1-F)S(\ell-1, Z) + G\beta R(\ell-1, Z) \quad (5)$$

or rearranging

$$R(\ell, Z) = [G\alpha + 1 - G]R(\ell-1, Z) + F\alpha S(\ell-1, Z) \quad (6)$$

$$S(\ell, Z+1) = [\beta + 1 - F]S(\ell-1, Z) + G\beta R(\ell-1, Z) \quad (7)$$

where $R(\ell, Z)$ = amount of species sorbed on the surface in the Z th zone after the ℓ th cycle.

$S(\ell, Z+1)$ = amount of species in solution in the $(Z+1)$ th zone after the ℓ th cycle. (the solution in the Z th zone is transferred to the $(Z+1)$ th zone at the end of the ℓ th cycle.)

Thus if α , F , and G are known and if ℓ and Z are specified, the distribution of the species both in solution and on the media can be calculated by the model. For equations 6 and 7, one must have

an initial amount of species present.

Experimental

If the rate of adsorption, the rate of desorption, and the equilibrium partitioning of a nuclide between a solid medium and solution are known, then the rate of migration of a nuclide through the medium can be predicted with the ARDISC model.

The rate of adsorption and the rate of desorption are assumed to be dependent on the geometric relationship of the rock and solution (i.e., dependent upon the volume of solution and on the shape and area of the solid medium in contact with the solution). Because the dependence of sorption kinetics on the geometric relationship is not known, the rates for sorption are determined by experiment for the particular geometry (surface area of rock to volume of solution) for which the prediction of nuclide migration is desired.

The applicability of the ARDISC model to laboratory migration experiments was studied in two sets of experiments. In the first set of experiments, the rate of adsorption, the rate of desorption, and the equilibrium partitioning of americium III between solution and simulated fissures were measured in static and batch experiments. The measured parameters were used in the model to predict the migration of americium III through simulated fissures. The predictions were compared with experimental results. In the second set of experiments, strontium was eluted through a column of glauconite at six solution flow rates ranging from 14.4 to 721 centimeters per hour. To obtain input data for the ARDISC model the equilibrium partitioning of strontium between solution and glauconite was determined from the resulting curves and the rate for adsorption and the rate for desorption were determined by curve fitting the results of one of the column infiltration experiments. The parameters that were determined in this way were used in the model to predict the migration of strontium through the column of glauconite for four of the solution flow rates. The predictions were compared with experimental results.

Fissures

Fissures were fabricated by cutting slabs of rock from a core of gray hornblende schist. X-ray diffraction analysis of gray hornblende schist identified chlorite and an amphibole (hornblende) as the major mineral phases present and feldspar as a minor constituent. The slabs were cut into rectangles approximately 2.54 cm wide by 5.08 cm long. Each piece was polished on one side with successively finer sized abrasive with the final abrasive size being 600 mesh. To form a fissure, two rectangular pieces were put together. Wax gaskets were placed along the long edges of the rectangular pieces to form a 0.027 cm gap between

the two pieces. The surface area to volume ratio produced was 74 cm² to 1 mL and the surface area to volume ratio was constant for all the fissures used.

Fissure Adsorption Experiments. To perform fissure sorption experiments, one end of each fissure was connected via small bore tubing to a microliter pipetter as is shown in Figure 2. Rock-equilibrated water, described below, was injected into each fissure and the fissure walls were allowed to equilibrate with the solution for a period of two days before the adsorption experiments were performed.

Rock-equilibrated water was produced by allowing distilled water to be in contact with granulated gray hornblende schist for a period of several days. The solution produced was filtered through a 0.4 μm NUCLEOPORE filter before use. Analysis of the resulting solution showed that rock equilibrated-water contained 48 mg/L total solids (dried at 180°C). The E_h of the solution was measured to be 0.275 V. The pH of the gray hornblende schist equilibrated water was measured to be 7.6 at the time of the first adsorption experiment. Thereafter the solution pH was maintained at 7.5-7.7.

Adsorption experiments were performed by removing rock-equilibrated water from the fissures and injecting stock solution which was made by dissolving tracer amounts of americium-241 in rock equilibrated water. The stock solution was allowed to equilibrate within the fissures for different periods of time and was then removed from each fissure. The stock solution was assayed before injection and after removal from the fissures so that the change in americium concentration was determined for a different time in each fissure. Ten adsorption experiments were performed in this manner and the results are presented in table I. Figure 3 is a graphical representation of the initial part of the adsorption curve.

Equilibrium Partitioning Experiments. The equilibrium partitioning of americium-III between gray hornblende schist and rock equilibrated water was determined in batch partitioning experiments with rectangular blocks of gray hornblende schist (5). The surface area sorption coefficient, K_s, was determined to be 4.5 ± .5 mL/cm² where

$$K_s = \frac{\alpha}{\beta} \frac{\text{volume of solution}}{\text{surface area of sample}} \quad (8)$$

α from equation 1 is the fraction of nuclide concentration adsorbed from solution.

β from equation 1 is the fraction of nuclide concentration remaining in solution; 1 - α.

Solving equation 8 for the geometric surface area to volume ratio

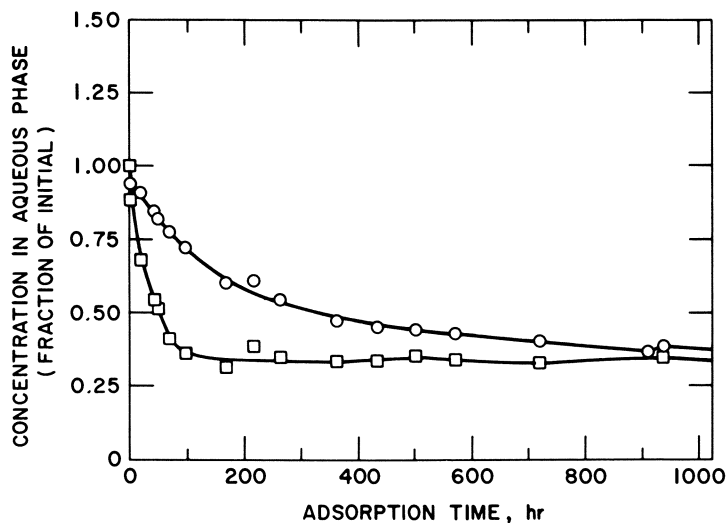


Figure 1. Sorption of plutonium IV and americium III from solution by a tablet of granite. Experiment No. 16; granite LI-6152; (\square), ^{237}Pu ; (\circ), ^{241}Am .

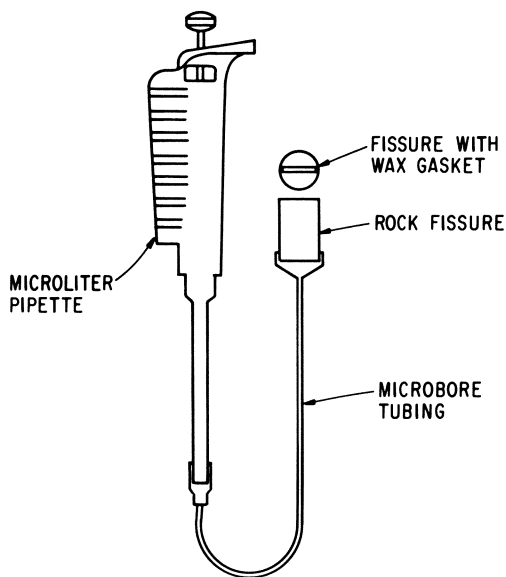


Figure 2. Apparatus used in static fissure adsorption experiments

found in the fissures, the fraction of the nuclide concentration predicted to be adsorbed by the fissure surfaces at equilibrium in fissure sorption experiments is 0.997.

Fissure Desorption Experiments. Desorption experiments were performed with two fissures by injecting rock equilibrated water into the fissures immediately after removing the americium-bearing solution from the fissures in adsorption experiments. After injection, the rock-equilibrated water was allowed to react within the fissures for a period of time before removal. The rock-equilibrated water was assayed after removal from the two fissures and the amount of nuclide desorbed as a function of contact time was determined. Between five and seven desorption experiments were performed for each of six time periods between ten seconds and sixty minutes for each of the two fissures. The results of the desorption experiments are presented in table 2 as the percent of β (at equilibrium) that desorbed from the fissures in a period of time.

Because most of the americium remains on the rock even after desorption is completed, the ratio of activity desorbed to that expected at equilibrium is subject to large uncertainty. The results of the desorption experiments are so varied that no quantitative conclusion can be drawn about the rate for desorption. However, the results do indicate that desorption may occur with a rate equal to or less than the rate for adsorption.

Fissure Elution Experiments. The migration characteristics of americium by water transport in fissures fabricated from gray hornblende schist were determined. Fissures not used in the previous sorption experiments were used for these elution experiments. A diagram of the experimental apparatus is shown in Figure 4. Solution reservoirs were attached above the fissures and the small bore tubes affixed to the bottom of the fissures were connected to solution metering pumps.

Before the elution experiments were performed, the "schist"-equilibrated water was pumped through the fissures for two days to allow the fissure walls to interact with the rock-equilibrated water.

Two sets of fissure elution experiments were performed. In the first set of experiments, the rock equilibrated water contained in the reservoirs above three fissures was first replaced with americium bearing stock solution. The solution metering pumps were left running in order not to interrupt the flow while the exchange was made. The flow was slow enough that air was not drawn into the fissures during the exchange. Flow was continued until an arbitrary volume, 0.67 fissure volumes, of stock solution were drawn into each fissure and then the solution metering pumps were turned off. This volume was chosen to permit the observance of a leading edge of activity, if it existed, moving with the water front. Stock solution was drawn into the fissures at linear

Table I. ^{241}Am Adsorption by Gray Hornblende Schist:
Fissure Experiments (static)

Adsorption Time, Seconds	Fissure Number	Activity Applied in 152 λ	Percent Remaining in Solution
15	1	65 nCi	84.6 \pm .1
54	5	0.98 nCi	71 \pm 1
150	8	0.97 nCi	63.1 \pm .9
300	2	1.1 nCi	50.7 \pm .8
600	7	1.7 nCi	36.3 \pm .5
3600	4	56 nCi	32.3 \pm .1
60120	2*	173 nCi	25.0 \pm .1
60120	8*	184 nCi	17.4 \pm .1
86400	5*	111 nCi	2.20 \pm .02
250200	6	0.84 nCi	0.05 \pm .25

*Cores #2, #5, and #8 were used twice for adsorption experiments. The activity applied during the first adsorption experiments was insignificant when compared to the activity applied in the second experiment. The reported errors are for counting statistics.

Table II. Am^{+3} Desorption from Gray Hornblende Schist:
Fissure Experiments (static)

Desorption Time, Seconds	Desorption Runs	Percent of β^* (at equilibrium) Desorbed	
		Core #2	Core #8
10	5	8 \pm 5	4 \pm 2
20	7	13 \pm 10	13 \pm 4
60	7	31 \pm 47	19 \pm 6
360	6	8 \pm 6	13 \pm 5
1200	5	13 \pm 8	6 \pm 2
3600	7, 6 (core #8)	14 \pm 19	22 \pm 16

* β is the fraction of a nuclide in solution at equilibrium. The desorption values were determined assuming that 0.003 of the nuclide would be in solution at equilibrium. The values that are presented are the arithmetic mean and standard deviations found for the number of experiments performed for each time interval.

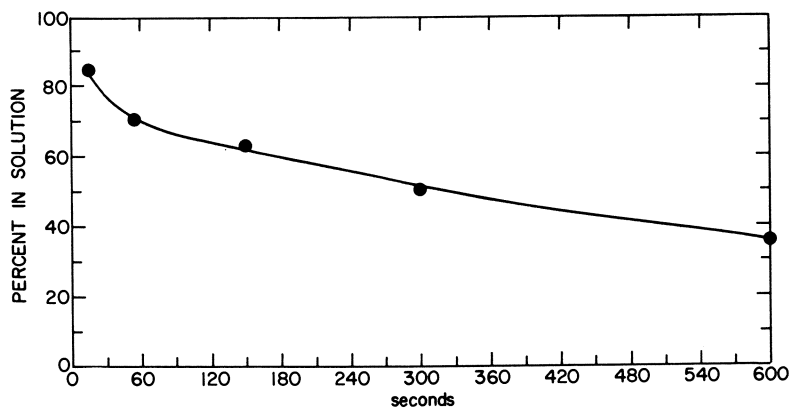


Figure 3. Adsorption curve obtained for the static fissure adsorption experiments

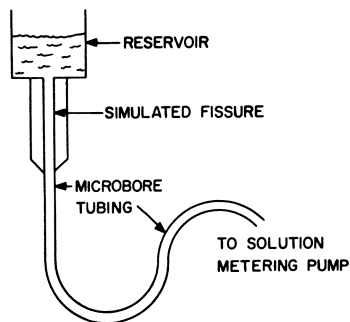


Figure 4. Diagram of apparatus used for fissure elution experiments

flow rates of 1.13, 2.29, and 4.77 cm/hr respectively. After stopping the flow of stock solution into the fissures, it was removed from the reservoirs above the fissures and the solution in each fissure was left stagnant for a period of twenty-four hours. Based on the kinetic data in table 1, it is believed that the americium in the stock solution becomes equilibrated with the surface of the fissures during the twenty-four hour period that the stock solution remained stagnant. At equilibrium 0.997 of the americium is adsorbed; it is therefore expected that the americium distribution on the fissure walls, after the twenty-four hour period, represents the migration of americium into the fissures during the 0.67 fissure volume elutions.

After the twenty-four hour period of contact, the solution in the fissures was rapidly withdrawn. The surfaces of the fissures were dried under vacuum at 25°C and then dismantled. The distributions of americium on the fissure surfaces were determined first qualitatively using autoradiographs of the fissure surfaces with POLAROID LAND black and white 3000 ASA type 47 film. The autoradiographs are shown in Figures 5, 7, and 9. The lighter areas on the autoradiographs represent areas of americium adsorption.

The distributions of americium on the fissure surfaces were then quantitatively determined by scanning the face of each fissure with a NaI scintillation crystal through a 0.3 cm slit in lead shielding. The 59 keV gamma ray emitted by ^{241}Am was monitored. Histograms of the americium distributions on the fissure surfaces were produced and are presented in Figures 5, 7, and 9.

The second set of fissure-elution experiments was performed in the same manner as described for the first set of fissure-elution experiments. The difference in the second set of experiments was that after 0.67 fissure volumes of stock solution were drawn into the fissures at their respective flow rates, the stock solution in the reservoirs was replaced with rock-equilibrated water. The solution metering pumps were not turned off during the exchange. Subsequently, a total of twenty fissure volumes of solution was drawn through each fissure before the metering pumps were turned off. After the metering pumps were stopped, the rock-equilibrated water was removed from the reservoirs and the solution in the fissures was rapidly drawn off.

The fissures were dried under vacuum at 25°C and were dismantled. The distributions of americium on the fissure surfaces in the second set of experiments were determined as they were in the first set, that is: first qualitatively by autoradiography and then quantitatively by gamma scanning the fissure faces through a 0.3 cm slit.

Autoradiographs of the fissure surfaces from the second set of experiments are presented in Figures 6, 8, and 10. Histograms representing the quantitatively determined distribution of americium on the fissure surfaces are also presented in Figures 6, 8, and 10.

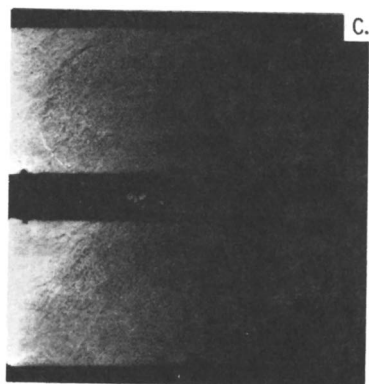
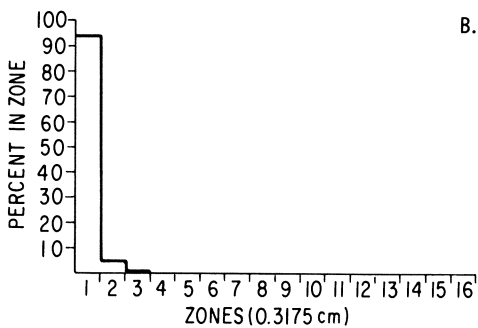
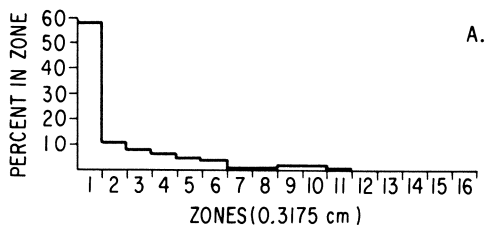


Figure 5. Distribution of americium on fissure surface, experimental and predicted, after 0.67 fissure volume elution. Flow rate of 1.13 cm/hr. (A), Americium distribution on surface of fissure; (B), model prediction of americium on surface of fissure; (C), autoradiograph of fissure surface showing americium distribution.

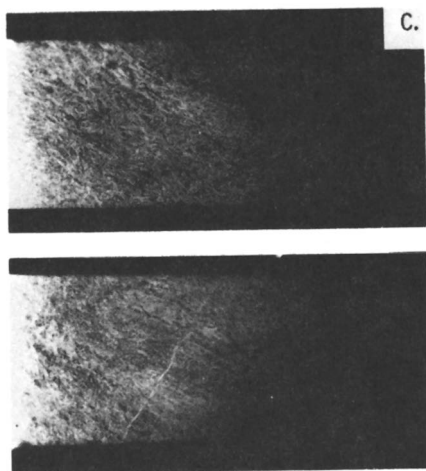
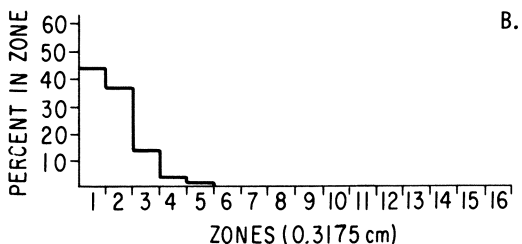
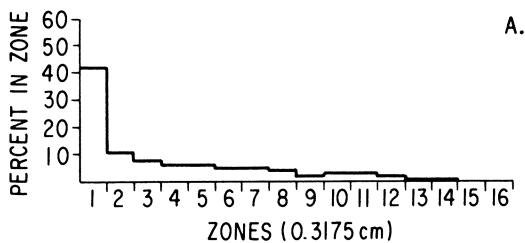


Figure 6. Distribution of americium on fissure surface, experimental and predicted, after 20 fissure volume elution. Flow rate of 1.13 cm/hr. (A), Americium distribution on surface of fissure; (B), model prediction of americium on surface of fissure; (C), autoradiograph of fissure surface showing americium distribution.

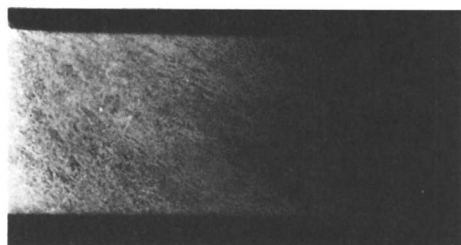
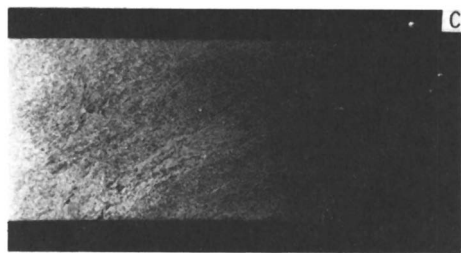
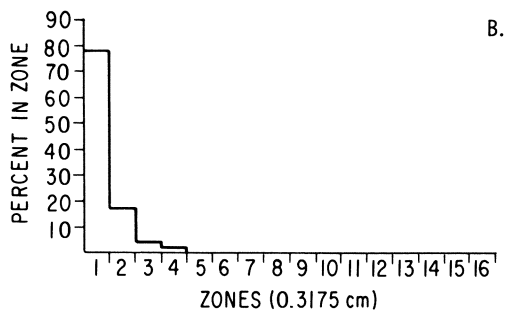
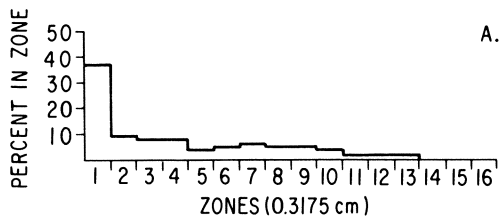


Figure 7. Distribution of americium on fissure surface, experimental and predicted, after 0.67 fissure volume elution. Flow rate of 2.29 cm/hr. (A), Americium distribution on surface of fissure; (B), model prediction of americium on surface of fissure; (C), autoradiograph of fissure surface showing americium distribution.

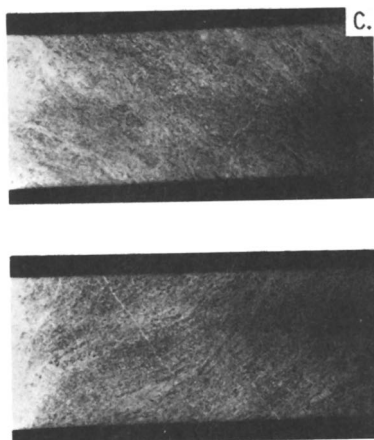
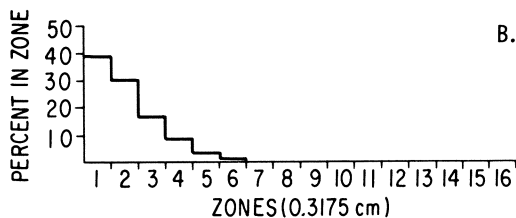
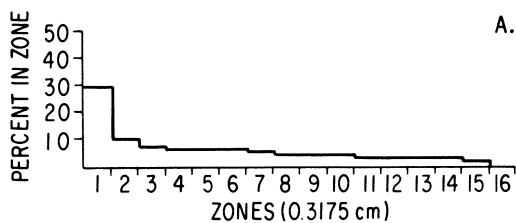


Figure 8. Distribution of americium on fissure surface, experimental and predicted, after 20 fissure volume elution. Flow rate of 2.29 cm/hr. (A), Americium distribution on surface of fissure; (B), model prediction of americium on surface of fissure; (C), autoradiograph of fissure surface showing americium distribution.

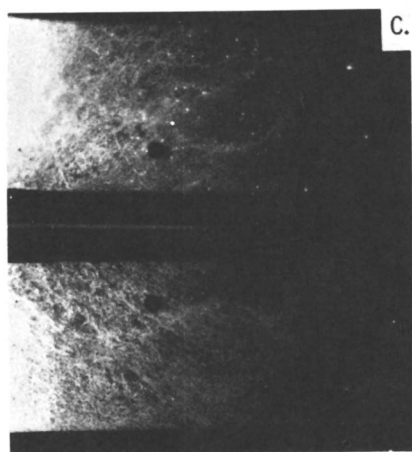
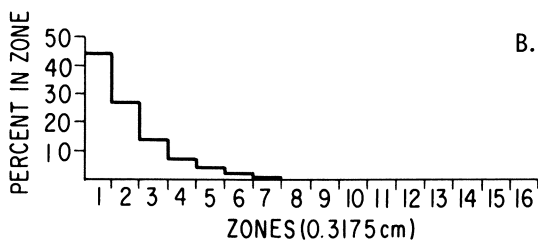
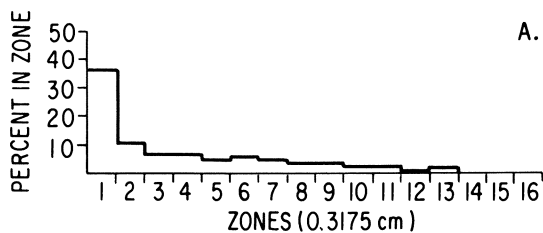


Figure 9. Distribution of americium on fissure surface, experimental and predicted, after 0.67 fissure volume elution. Flow rate of 4.77 cm/hr. (A), Americium distribution on surface of fissure; (B), model prediction of americium on surface of fissure; (C), autoradiograph of fissure surface showing americium distribution.

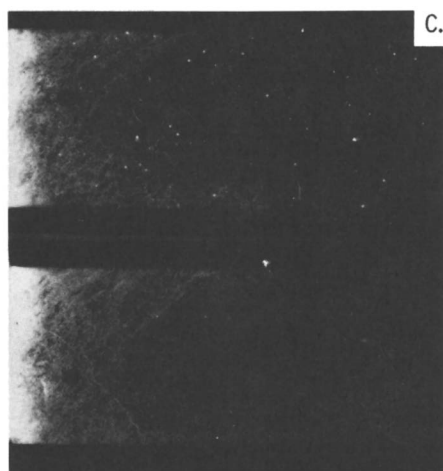
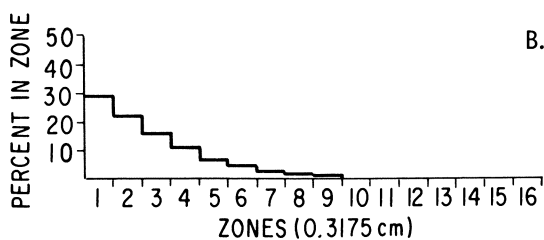
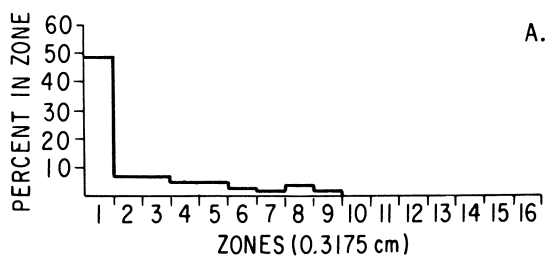


Figure 10. Distribution of americium on fissure surface, experimental and predicted, after 20 fissure volume elution. Flow rate of 4.77 cm/hr. (A), Americium distribution on surface of fissure; (B), model prediction of americium on surface of fissure; (C), autoradiograph of fissure surface showing americium distribution.

Model Predictions. The rate for desorption of americium from the fissure surfaces into solution was assumed to equal the rate for the adsorption of americium from solution by the fissure surfaces. The sorption rate and the equilibrium fractionation of americium that were determined in the static experiments were used to determine input parameters to the ARDISC model. The ARDISC model predictions for the distributions of americium on the fissure surfaces in both sets of experiments are presented in Figures 5 through 10 along with the autoradiographs and the experimental histograms representing the various distributions of americium on the fissure surfaces.

Strontium Migration Experiments in Glauconite

The work that was performed in this set of experiments was an extension of work performed by Inoue and Kaufman (7). In the previous work, the migration of strontium in glauconite was modeled using conditions of local equilibrium for flows up to 6.3 kilometers per year (72 cm/hr). The differences between the predicted and experimental results in the experiments performed by Inoue and Kaufman may be due to the existence of non-equilibrium behavior.

Column Infiltration Experiments. Six infiltration experiments, each at a different flow, were performed with one column of glauconite. The apparatus used in the infiltration experiments consisted of a mineral column contained in a stainless-steel tube connected to a sample-injection valve and a solution-metering pump. Glauconite [a hydrous silicate, nominally $(K,Na)(Al,Fe^{+3},Mg)_2(Al,Si)_4O_{10}(OH)_2$] was prepared by sifting glauconite sand to obtain a fraction of uniform size (<40 and >70 mesh size). The sand was washed repeatedly in distilled water to remove dust adhering to the particles and was packed in a stainless-steel tube to form a column 15 cm long by 1.0 cm diameter with 53 percent porosity.

The column was conditioned by eluting it with a solution of 0.01 M $CaSO_4$ and 0.0001 M $SrCO_3$. The solution used in this set of experiments was produced to simulate the solution used by Inoue and Kaufman.

Strontium-85 with $SrCl_2$ carrier was added to an aliquot of the calcium-strontium solution to form a radioactive solution with $\sim 1 \times 10^{-6}$ M ^{85}Sr . At the start of an experiment, a small quantity (20 $\mu\ell$) of the radioactive solution was injected into the solution stream above the glauconite column and the column was eluted with solution until all the radioactive strontium had moved through the column. The eluent was collected in fractions and each fraction was analyzed to determine the migration characteristics of the strontium in the column.

The radioactive strontium in solution vs. the eluate fractions for each flow rate is plotted in Figure 11. The strontium

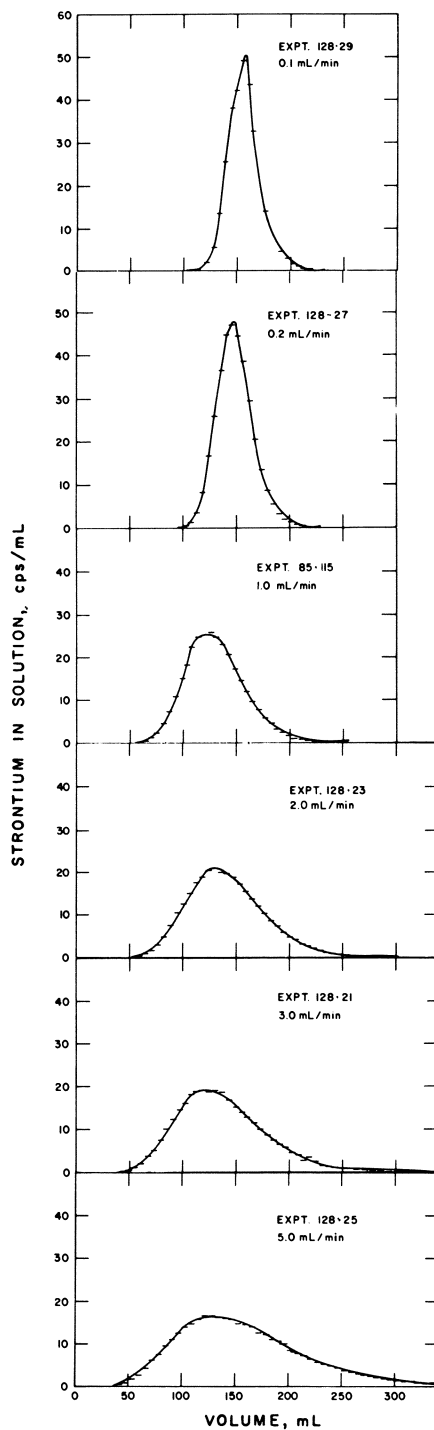


Figure 11. Elution of strontium from the column of glauconite. Peak width increases with flow (top to bottom) indicating nonequilibrium behavior. Slowest flow rate is 0.1 mL/min or 14 cm/hr; fastest flow rate is 5 mL/min or 720 cm/hr.

peaks have a shape that is dependent on the flow rate of the eluent. The sharpest peak is produced with the slowest flow rate; the widest peak is produced with the fastest flow rate. The strontium peaks were delayed relative to the advancing water front (which would traverse the column in the first 6.5 mL of eluent). Moreover, each of the strontium peaks seen in Figure 11, even the one produced with the slowest flow is wider than predicted by the peak width (2 mL full width at half maximum) that was seen for peaks of tritiated water that were eluted through the column (8). Therefore, the strontium has interacted with the glauconite column and, as indicated by the different peak shapes, interacted differently at each flow. The flows given in Figure 11 were measured by collecting eluate over specific periods of time. In each experiment, all the radioactive strontium was eluted in the single peak seen in the figure.

To relate the six curves obtained experimentally with the ARDISC model, the rate for adsorption, the rate for desorption and the equilibrium distribution of the nuclide between glauconite and solution had to be determined.

The relative migration rate of the peak concentration of strontium at a solution flow rate of 0.1 mL per minute was used to calculate the equilibrium fractionation of strontium between glauconite and solution. It was determined that at equilibrium 0.958 of the strontium would be adsorbed by the glauconite and 0.042 of the strontium would be in solution (mobile phase).

The rate for adsorption and the rate for desorption were determined by curve fitting with ARDISC. It was assumed that the rate for desorption equaled the rate for adsorption. The α and β parameters were held constant at 0.958 and 0.042 respectively. The F, G, and zone length input parameters to the ARDISC model were varied to fit the strontium migration data at a flow rate of 2 mL per minute.

Assuming first order reaction kinetics, the sorption rate that was determined for adsorption and desorption was 0.187 sec^{-1} . A reaction rate of 0.187 sec^{-1} implies a half time of reaction of 3.7 seconds.

The curves predicted by the model for four of the six flow rates are presented in Figure 12.

Discussion and Conclusions

Figures 5, 7, and 9 show the americium distributions on fissure surfaces after the administration of 0.67 fissure volumes of stock solution at flow rates of 1.13, 2.29, and 4.77 cm/hr. The peak concentrations of americium were adsorbed at the top of the fissures and leading edges of americium were extended into the fissures. In general, at faster flow rates the relative quantities of americium sorbed at the top of each fissure decreased and the length and relative amount of the leading edge extending into each fissure increased.

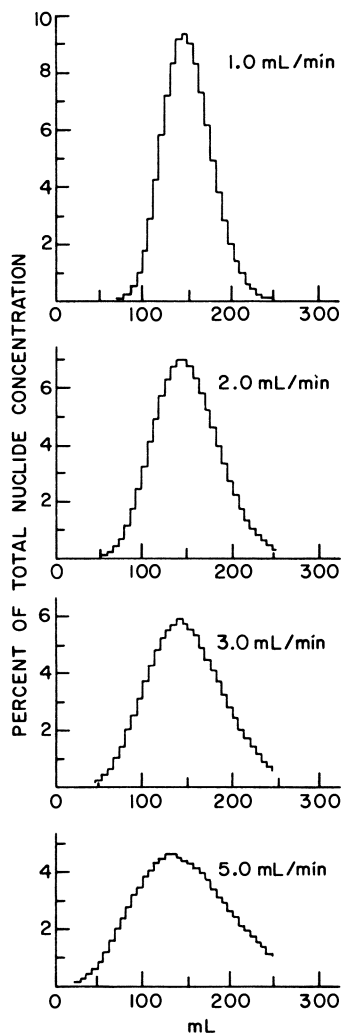


Figure 12. Model predictions for the elution of strontium from the column of glauconite at four flow rates

The ARDISC model predictions for 0.67 fissure volume additions of stock solution into fissures at the three flow rates also show that the peak concentrations of americium will be sorbed at the top of each fissure. The leading edges of the nuclide are predicted to extend into the fissures. The ARDISC model also predicts that at faster flow rates, the relative amount of americium sorbed in the peak concentration at the top of each fissure should decrease. Also, the length and relative amount of the leading edge extending into each fissure is shown to increase.

Figures 6, 8, and 10 show that the distributions of americium on the fissure surfaces after the addition of 0.67 fissure volumes of stock solution followed by the elution of 20 fissure volumes of "schist"-equilibrated water through the fissures at flow rates of 1.13, 2.29, and 4.77 cm/hr. A comparison was made between the americium distributions found on the fissure surfaces after the addition of americium stock solution and that found after elution of the americium by 20 fissure volumes of "schist"-equilibrated water. It was found that after the initial loading of americium into the fissures in the first 0.67 fissure volumes of solution, the peak concentrations of americium that were sorbed at the top of the fissures decreased in their relative concentration. The leading edges of the detectable nuclide concentration extending into the fissures had increased in length and relative concentration with subsequent elution by rock equilibrated water through the fissures. The ARDISC model predicted the same relationships.

The ARDISC model qualitatively predicted the shape of the curves representing the distribution of americium on the fissure surfaces. However, the model was not able to predict accurately the distribution of americium on the fissure surfaces in each experiment. A plot of the natural logarithm of the fraction of the nuclide remaining in solution vs. the absorption time does not produce a straight line (Figure 13) for the first five data points obtained in the static fissure absorption experiments. A plot of the natural logarithm of the fraction remaining in solution vs. time should produce a straight line if the reaction were first order. The ARDISC model assumes that the sorption reactions are first order. The discrepancy between the experimental and predicted results may be due to higher order sorption kinetics. In addition, differences between the predicted and the experimental results may also be due to a number of factors such as non-homogeneous media, non uniform flow through the fissures, small pH fluctuations, precipitation reactions, and colloid formation by some of the nuclide.

In the column infiltration experiments with strontium, the model predictions closely resemble the experimental curves for the four flow rates compared. The input parameters to the ARDISC model were derived from experimental data obtained in infiltration experiments. The model predictions were based on the assumptions that the rate for adsorption and the rate for desorption were equal and that the sorption reactions were both first order.

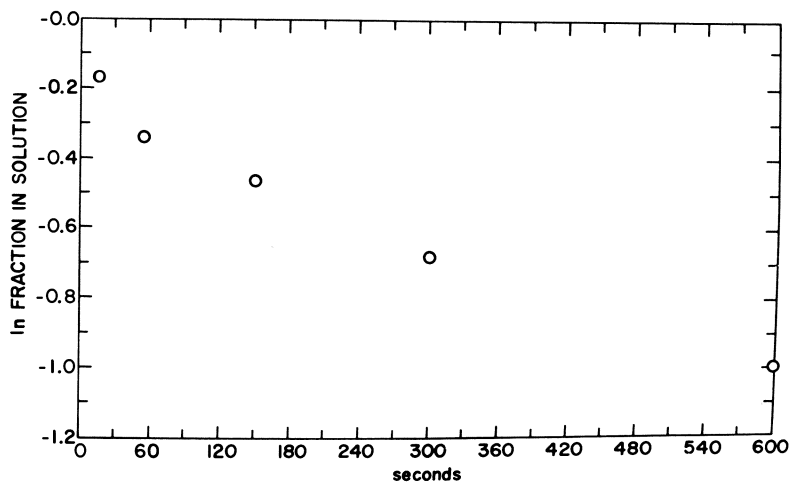


Figure 13. Plot of \ln fraction of americium in solution vs. time for the data obtained in the static fissure absorption experiments

The results of the experiments presented in this paper demonstrate that the migration of nuclides in geologic media can be studied experimentally and treated in at least a semiquantitative fashion using kinetic and partitioning data. The ARDISC model is a useful aid in analyzing nuclide migration data obtained in laboratory experiments. But the ARDISC model is limited to first-order sorption kinetics.

Phenomena such as nuclide transport by particles or nuclide transport in colloidal form will interfere with a kinetic approach to predicting nuclide migration. The results indicate that the measurement of kinetic parameters may be as important to understanding the migration of a nuclide through a geologic media as the measurement of the equilibrium-sorption value (K_d).

Literature Cited

1. Seitz, M. G., Rickert, P. G., Fried, S. M., Friedman, A. M., and Steindler, M. J., "Studies of Nuclear-Waste Migration in Geologic Media," Annual Report November 1976 - October 1977, ANL-78-8 (1978).
2. Strickert, R., Friedman, A. M., and Fried, S., "The Sorption of Technetium and Iodine Radioisotopes by Various Minerals," Nuclear Technology, in press (1978).
3. Friedman, A. M., Ed., "Actinides in the Environment," Am. Chem. Soc. Symposium Series No. 35, Washington, D.C., 1976.
4. Strickert, R. G., Friedman, A. M., and Fried, S. M., "ARDISC: A Program to Calculate the Distribution of a Radioisotope in Pores of Partially Equilibrated Rock," Argonne National Laboratory Report, in print (1978).
5. Snyder, L. R., Principles of Adsorption Chromatography, Marcel Dekker, Inc., New York, pp. 12-16, (1968).
6. Rickert, P. G., Seitz, M. G., Fried, S. M., Friedman, A. M., and Steindler, M. J., "Transport Properties of Nuclear Waste in Geologic Media," report to the Waste Isolation Safety Assessment Program, March, ANL program code 85249-00 (1978).
7. Inoue, Y., and Kaufman, W., "Prediction of Movement of Radio-nuclides in Solution Through Porous Media," Health Physics, 9, pp. 705-715 (1963).
8. Seitz, M. G., Rickert, P. G., Fried, S. M., Friedman, A. M., and Steindler, M. J., "Transport Properties of Nuclear Waste in Geologic Media," report to the Waste Isolation Safety Assessment Program, April, ANL program code 85249-00 (1978).

RECEIVED January 16, 1979.

Kinetic Effects in Migration

A. M. FRIEDMAN and S. FRIED

Argonne National Laboratory, Argonne, IL 60439

The usual basis of predictions of migratory behavior of ions in geological strata is the treatment of this behavior as an equilibrium chromatographic elution (1,2). This then leads to the following expression for the migratory velocity (v) of a species:

$$V = v_w \frac{1}{1 + K_d \frac{\rho}{\epsilon}} \quad (1)$$

where v_w = velocity of the water front

K_d = concentration ratio of adsorbed and dissolved solute

ϵ = porosity of the strata

ρ = bulk density of the strata.

This expression will predict the movement of a solute whose adsorption is in equilibrium with the surrounding strata. This equilibrium chromatographic motion will result in the migration of a band of activity whose concentration profile is gaussian and whose deviation will be a function of the hydrodynamic dispersion, T_h (due to statistical variations in path length) and absorptive dispersion T_a (due to statistical variations in the absorption and desorption process). While these dispersions are interactive and do not sum in a simple fashion they both depend on path length.

The longitudinal hydrodynamic dispersion is given (3, 4, 5) by:

$$T_h^2 = \frac{1}{3} (\lambda + 0.173) d_w \ell \quad (2)$$

where λ is related to the mean migration distance and grain size, d_w is the average distance of water flow and ℓ is the pore size.

The absorptive dispersion is given by:

$$T_a = A d \sqrt{\frac{8}{N}}$$

where A is the area of the column

0-8412-0498-5/79/47-100-191\$05.00/0

© 1979 American Chemical Society

\bar{d} is the distance absorbing species is moved
 N is the number of theoretical plates (% number of pores)
 If we take $N = \bar{d}/\ell$,

$$\text{then: } T_a^2 = 8A^2(\ell)(\bar{d}) \quad (4)$$

Therefore both types of dispersion will be proportionate to the square root of the distance migrated. If they add as a simple vector sum, (which may be a gross simplification) then:

$$T^2 = T_a^2 + T_h^2 = \bar{d}(\ell) \left[8A^2 + \frac{1}{3} (\lambda + 0.173) \right] \quad (5)$$

This type of behavior would produce distributions of activity shown in Figure 1 where the various peaks are symmetric gaussians of increasing width.

However, in many cases involving geological materials these normal behavior patterns are not observed. Figures 2-A and 2-B are illustrations of this for Pu (6) and Cs (2) ions. As can be seen in the figures the distributions are neither symmetric (or gaussian) and tend to form a "plume" in the direction of flow. This plume can, of course, lead to higher concentrations than normal at distances downstream from the main body of activity and thus are important to models of waste migration.

There are several types of mechanisms that could account for this behavior. (A) There could be abnormal flow paths, such as fissures which allow a small amount of activity to migrate more quickly than the main body. (b) This activity could be carried on colloidal, non-absorbing particles. Or (C) the flow rate could be too fast for equilibrium to occur for the adsorption and desorption processes. These possibilities can be examined to determine which appears the most important.

Figure 3 illustrates the distributions found for ^{237}Pu and ^{241}Am when a mixed sample of these tracers was infiltrated into a large (30 cm x 30 cm) block of Bandelier tuff (6). The nuclide activities were determined simultaneously by coring sections of the tuff and represent the activity distributions in the rock. It is obvious that although the activities are both normalized at 100% at the surface the increased dispersion of the plutonium concentration during elution leads to an increase of almost an order of magnitude in its activity relative to Am at the 5-6 cm depth. It is highly unlikely that abnormal flow paths or movement of colloidal clay particles would discriminate between americium and plutonium; therefore this experimental result tends to discount these possible types of mechanisms. However, a pure Pu polymer could carry the Pu more rapidly downstream.

A further useful piece of information can be obtained from data such as is illustrated in Figure 4 (2). In this experiment a simulated groundwater solution traced with Pu and Am was shaken with a sample of basalt and the concentration of ions in

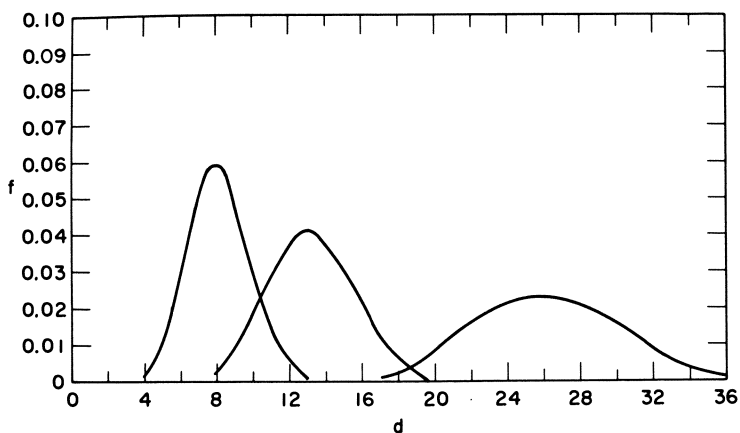


Figure 1. Predicted movement of elution peaks calculated by the use of Equation 5 for the dispersion and a linear absorption isotherm solution

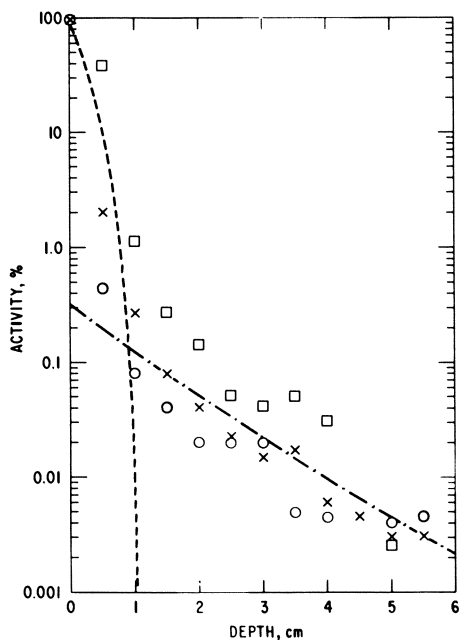


Figure 2a. Concentrations of activity observed for ^{238}Pu (originally in the IV oxidation state) when eluted into a (30 \times 30-cm block of) Bandelier tuff and washed with various amounts of water: (---), the distribution calculated for a gaussian shape; (- · -), the residual activity; (O), 150 mL rainfall; (\times), 500 mL rainfall; (\square), 7000 mL rainfall.

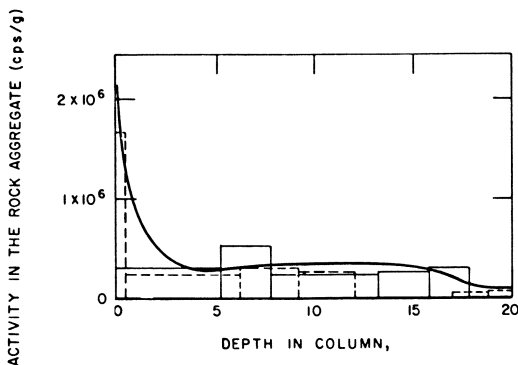


Figure 2b. Activity curve for concentrations of $^{134}\text{Cs}^+$ absorbed on a column of Selma chalk. Two series of samples of chalk were analyzed after the experiment and their radioactivities are indicated by the histograms. The smooth curve is the distribution inferred from these results. Column 24-3, selma chalk, Cs-134. (—), First series of samples; (---), second series of samples.

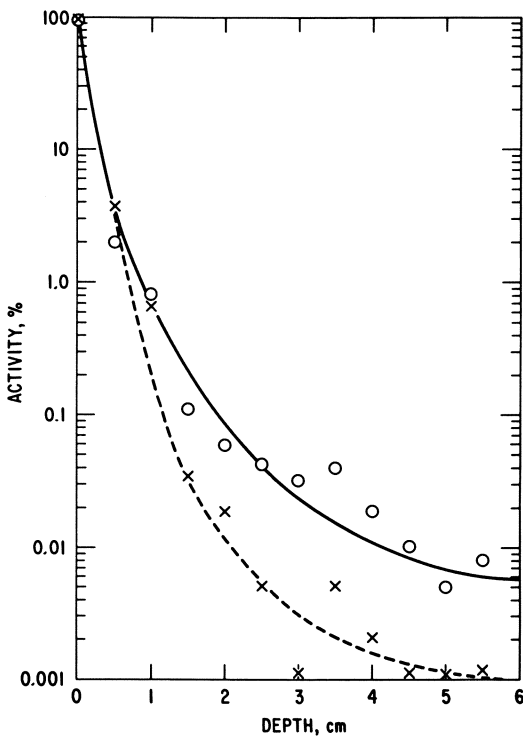


Figure 3. Relative activities of $^{237}\text{Pu}^{+4}$ and $^{241}\text{Am}^{+3}$ found in Bandelier tuff after simultaneous elution. Values are normalized to 100 at the surface. (○), ^{237}Pu ; (×), ^{241}Am ; 1.0 L rainfall.

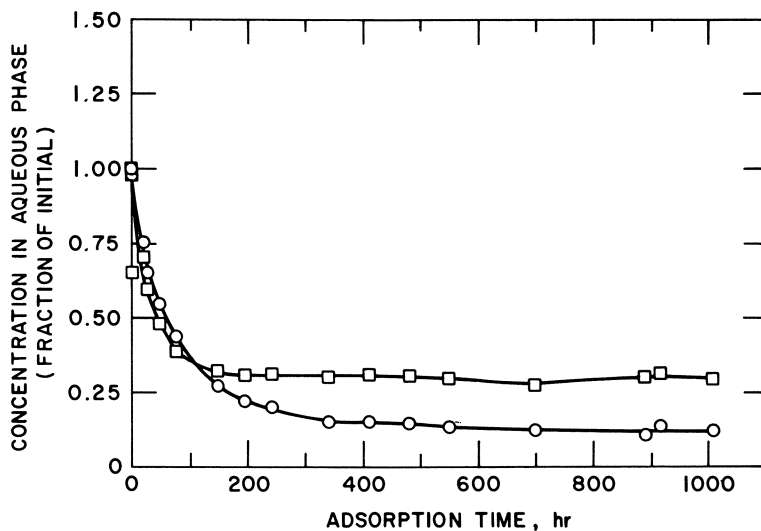


Figure 4. Relative absorption rates of $^{241}\text{Am}^{+3}$ and $^{237}\text{Pu}^{+4}$ on basalt. Experiment No. 19, Columbia River basalt; (\square), ^{237}Pu ; (\circ), ^{241}Am .

Table I

Static Absorption Experiments with Plutonium and Americium Added Simultaneously to Each Solution at Ambient Temperature. The experiments were each run for 900 h or more.

Rock Type	Expt.	Characteristic Reaction Time, h		Partition Coefficient, K_D	
		Pu	Am	Pu	Am
Limestone, Salem Formation	13-A	40	10	>150 ^a	~160 ^a
Granite, LI-6152	16	25	160	30 ^a	5
Columbia River Basalt	19	60	150	230 ^a	320
Tuff, Nevada Test Site	22	180	5	39	370 ^a
Low-Temperature Metamorphic	25	450	~20	130	2.6
Magenta	28	50	400	41 ^a	47

^aIn these experiments, a considerable amount (>50%) of the radio-nuclide associated with the solution was retained on the walls of the polyethylene tube. The activity in the solution was determined by subtracting the activity on the walls from the activity of the tube plus solution. The corrections are large and may have led to errors in the calculated partition coefficients.

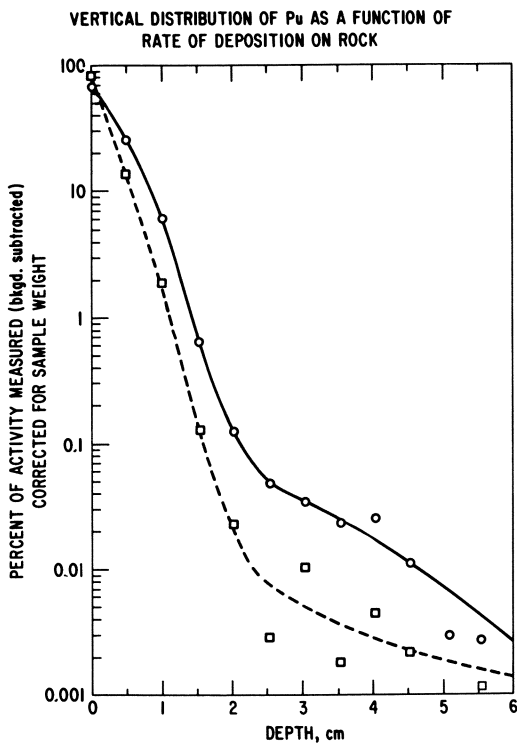


Figure 5. Vertical distribution of $^{237}\text{Pu}^{+4}$ as a function of rate of deposition on Bandelier tuff. Total deposit: approximately 2×10^6 d/m; (—), Site A, Pu applied at rate of 2 mL/min; (---), Site B, Pu applied at rate of 0.02 mL/min.

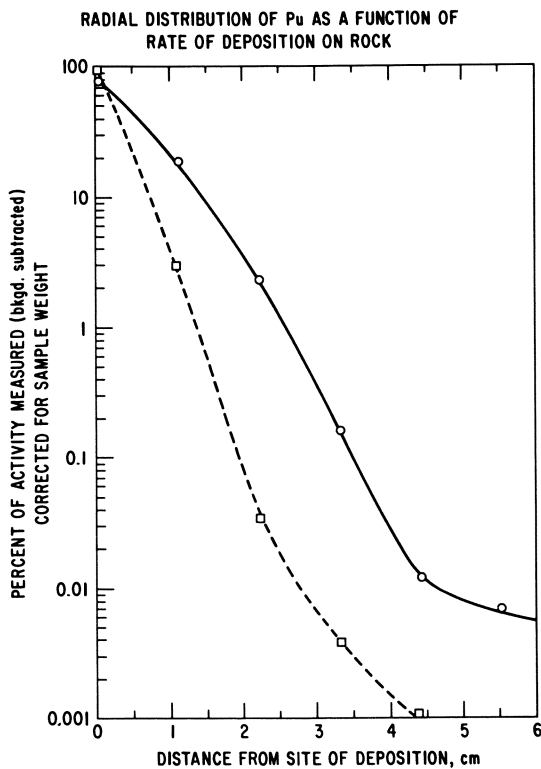


Figure 6. Radial distribution of $^{237}\text{Pu}^{+4}$ as a function of the rate of deposition on Bandelier tuff. Total deposit: approximately 2×10^6 d/m; (—), Site A, Pu applied at rate of 1 mL/min; (---), Site B, Pu applied at rate of 0.01 mL/min.

the aqueous phase was determined at various intervals of time. As can be seen the time dependence of absorption is different for the two elements. This is generally true, and in Table I are given a few of the values found in reference (2). As can be seen in Table I the time for equilibration of Pu in tuff is much longer than that for Am. Furthermore, the time needed for equilibration is much longer than the transit time of the solution through the pores of the rock (less than 1 hour). For example, if the average pore size is 1 mm and if the flow rate is as low as 10 meters per year, then the average residence time for solutions in the pores will be 0.88 hours, and equilibrium would not be attained. Further evidence that this kinetic effect is important can be seen in Figures 5 and 6 (6). These figures demonstrate the results of further experiments on the infiltration of Pu into Bandelier tuff. It is seen in these figures that both the radial and longitudinal dispersion of the Pu distributions are increased with increasing flow rate.

This set of observations, then, leads to the conclusion that the kinetics of adsorption and desorption may severely effect the dispersion of nuclides in geomedial. The following paper in this symposium will describe in detail further experiments aimed at quantifying these effects.

References

- (1) "Actinides in the Environment," p. 16, A. M. Friedman, Ed., Amer. Chem. Soc. Sympos. Series #35, ACS, Washington, D.C., 1976.
- (2) "Studies of Nuclear-Waste Migration in Geologic Media," p. 34, M. G. Seitz, P. G. Rickert, S. M. Fried, A. M. Friedman, and M. J. Steindler, Argonne National Laboratory Report ANL-78-8, 1978.
- (3) J. Bear in "Flow Through Porous Media," R. J. M. DeWiest, Ed., Chap. 4, p. 140, Acad. Press, N.Y., 1969 (see ref. 4,5 for corrections to Bear's formula).
- (4) "Migration of Plutonium in Rock: Incorrect Dispersion Formula," H. Krugmann, *Science*, 200, 88 (1978).
- (5) "Comment," A. M. Friedman and S. Fried, *Science*, 200, 88 (1978).
- (6) "Migration of Plutonium and Americium in the Lithosphere," S. Fried, A. M. Friedman, J. J. Hines, R. W. Atcher, L. A. Quarterman, and A. Volesky, Argonne National Laboratory Report ANL-76-127, 1976.

RECEIVED January 16, 1979.

Sorption Behavior of Trivalent Actinides and Rare Earths on Clay Minerals¹

G. W. BEALL, B. H. KETELLE, R. G. HAIRE, and G. D. O'KELLEY

Oak Ridge National Laboratory, Oak Ridge, TN 37830

Much interest in the past few years has been generated in connection with problems of radioactive waste isolation in a growing nuclear economy. Many studies have been initiated to find the most suitable sites for waste repositories, and the environmental impact if breaches occur in such repositories. These studies must ultimately result in safe methods of storage for nuclear waste for the present and for times that are measured on a geologic scale.

Salt mines have been suggested as possible sites for such repositories owing to their geologic stability and limited presence of water. The experiments which we wish to report in this paper were fashioned with this type of repository in mind. Clay minerals are potentially useful in several applications of exchange of radionuclides. They have been shown to be quite useful in removal of specific nuclides from waste streams (1). In connection with the Swedish waste isolation program they are being considered for secondary containment (2). A special case of secondary containment occurs if waste material should escape from their casks and from the surrounding salt beds. They can be expected to be held by geologic formations surrounding such beds. Therefore, studies of rates of exchange and equilibrium constants are important.

Experimental

Distribution coefficients were measured employing batch methods. The solution (ml) to clay (mg) ratios were approximately as follows: 1:5 attapulgite; 1:60 montmorillonite; and 1:25 kaolinite. The solutions were brines (NaCl) buffered with pH 5 acetate solution. The original stock solution contained 3 M NaCl and 1 M Na acetate buffer. The lower [Na] solutions were made by

¹ Research sponsored by the Office of Basic Energy Sciences, Division of Nuclear Sciences, U.S. Department of Energy, under contract (W-7405-eng-26) with the Union Carbide Corp.

0-8412-0498-5/79/47-100-201\$05.00/0

© 1978 American Chemical Society

appropriate dilution of this stock solution. The clays employed were obtained from Source Clay Minerals Repository (3). Attapulgite and kaolin were used as received. A 2% dispersion montmorillonite was prepared and centrifuged to remove approximately 80% of the sand. The remaining suspended clay was converted to the sodium form by passing it through a Dowex-50 cation exchange column (Na form) at 60°C. The tracers employed in the exchange studies were ^{241}Am , ^{244}Cm , ^{249}Cf , $^{253-254}\text{Es}$, ^{140}La , ^{157}Sm , ^{169}Yb , ^{134}Cs , ^{86}Rb , ^{42}K and ^{85}Sr . The actinides and most of the other isotopes were made at the High Flux Research Reactor at Oak Ridge National Laboratory. The ^{169}Yb , ^{134}Cs , ^{86}Rb , and ^{85}Sr isotopes were obtained from New England Nuclear.

Results

The three clays used in this study have different morphologies. The montmorillonite and kaolinite are typical sheet or plate-like clays, whereas the attapulgite exhibits a needle-like morphology (4).

The distribution coefficients (D) in units liters/kg have been measured as a function of concentration of sodium varying from .25 M to 4 M. They were studied as a function of [Na] because from the ion exchange equilibrium (5) the equation relating D to [Na] is given by:

$$d \log D = -M/N d \log [\text{Na}]$$

where: N = charge of cation on the exchanger

M = charge of cation exchanging with cation of charge N.

The distribution coefficients (D) in units liters/kg for the rare earths and actinides studied are listed in Tables 1, 2, and 3. Graphical representation of the data for typical rare earths and actinides, contained in Tables 1, 2, and 3, can be seen in Figures 1 and 2, where log D's vs. log [Na] are plotted. Under a given set of conditions there is very little difference between the rare earths and actinides in any of the clays. All the clays exhibit slopes of -1.1 to -1.7, which is in better agreement with a monoacetate complex that would be expected to yield slopes of -2 than the bare Am^{+3} ion. There are no good activity coefficients available for NaCl, Na acetate and AmCl_3 mixtures; therefore, no attempt was made to correct the experimental numbers. The D values for kaolinite and montmorillonite are in reasonable agreement when normalized by their respective capacities of 3.0 and 78 m.e./100 gm, indicating that the mechanism of exchange for the two clays are quite similar. In contrast, the D values for attapulgite are completely out of proportion with its respective 13 m.e./100 gm capacity.

Another striking difference can be seen in the kinetics of exchange between the clays. Kaolinite and montmorillonite have very rapid exchange reactions that take less than fifteen minutes to come to equilibrium. Attapulgite in contrast takes as long as nine days to come to equilibrium (Figure 3). The D values for ^{241}Am in a 0.5 M [Na] solution are given as a function of time in Figure 4. It can be seen that there is a very rapid initial re-

Table 1

Distribution Coefficients ($\mu\text{g}/\text{kg}$) for M(III)/Na(I)
Exchange on Kaolinite at pH 5

Molarity [Na]	Am	Cm	Cf	Es(pH 4)	La	Sm	Yb
4	0.22	0.3	0.16	0.5	0.2	0.15	0.07
2	0.45	0.5	0.5	2.0	0.33	-	0.11
1	1.07	0.7	1.1	1.4	0.44	0.44	0.32
0.5	1.9	1.5	2.2	2.4	0.85	-	0.63
0.25	4.3	3.2	5.3	4.9	3.0	3.95	1.83

Table 2

Distribution Coefficients ($\mu\text{g}/\text{kg}$) for M(III)/Na(I) Exchange
on Montmorillonite at pH 5

Molarity [Na]	Am	Cm	Cf	Es(pH 4)	La	Sm	Yb
4	2.2	2.4	1.6	3.1	1.7	1.5	1.7
2	2.9	3.6	3.8	3.5	2.2	3.1	2.5
1	6.4	6.6	7.7	9.1	4.0	5.5	5.4
0.5	11.5	14	18.0	25.0	12.2	18.2	13.7
0.25	33.9	37	43.5	54.0	38.5	48.7	39.2

Table 3

Distribution Coefficients ($\mu\text{g}/\text{kg}$) for M(III)/Na(I) Exchange
on Attapulgite at pH 5

Molarity [Na]	Am	Cm	Cf	La	Sm	Yb
4	163	251	310	98	99	103
2	550	600	778	201	194	177
1	1,700	1,600	2,300	306	437	248
0.5	6,600	4,000	9,500	680	1000	490
0.25	20,400	13,800	24,600	1670	1490	830

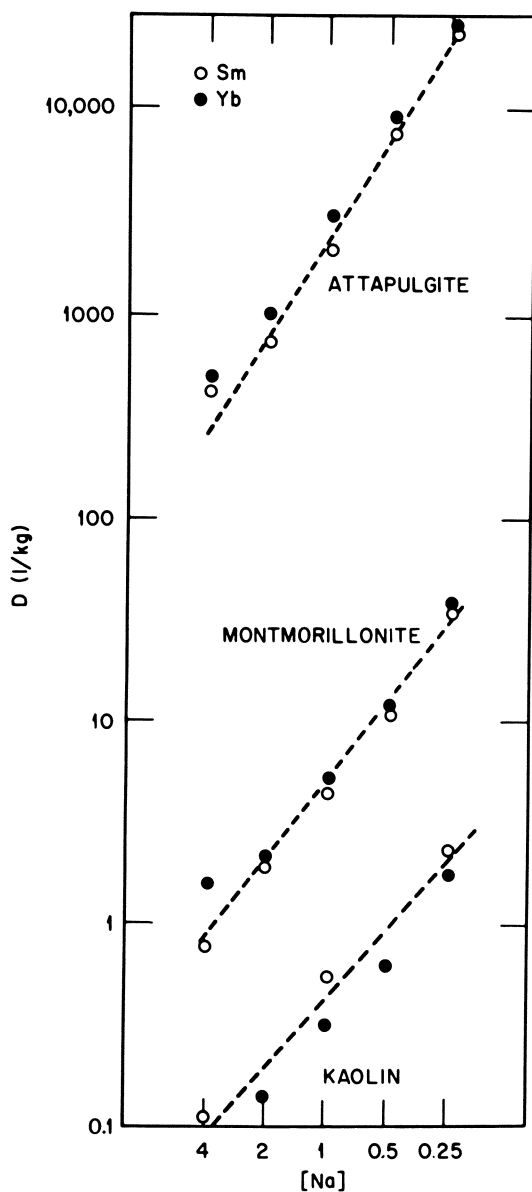


Figure 1. Plot of Sm and Yb exchange on kaolin, montmorillonite, and attapulgite: $\log D$ vs. $\log [Na]$.

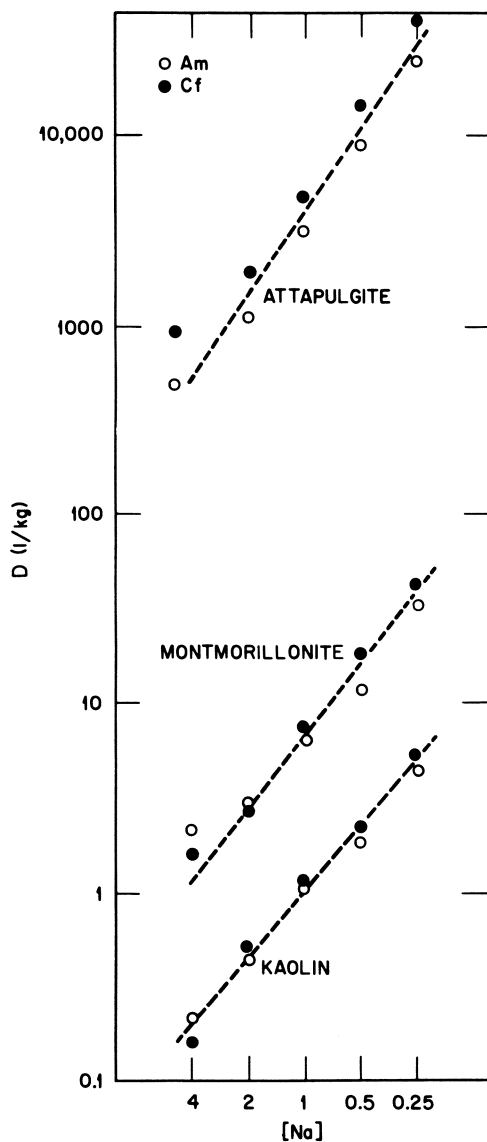


Figure 2. Plot of Am and Cf exchange on kaolin, montmorillonite, and attapulgite: $\log D$ vs. $\log [Na]$.

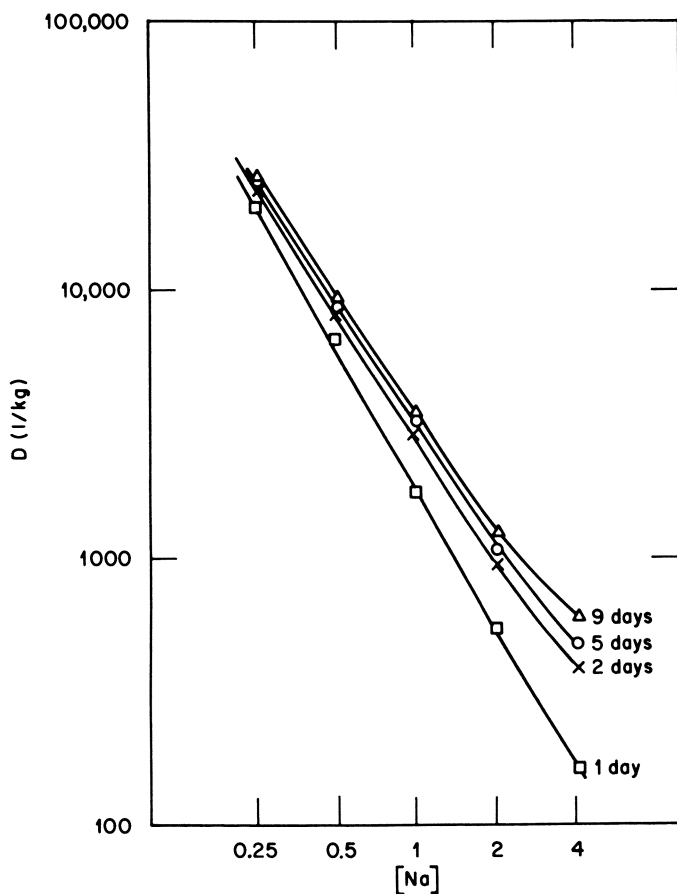


Figure 3. $\log D$ vs. $\log [Na]$ for Am on attapulgite as a function of time of equilibrium

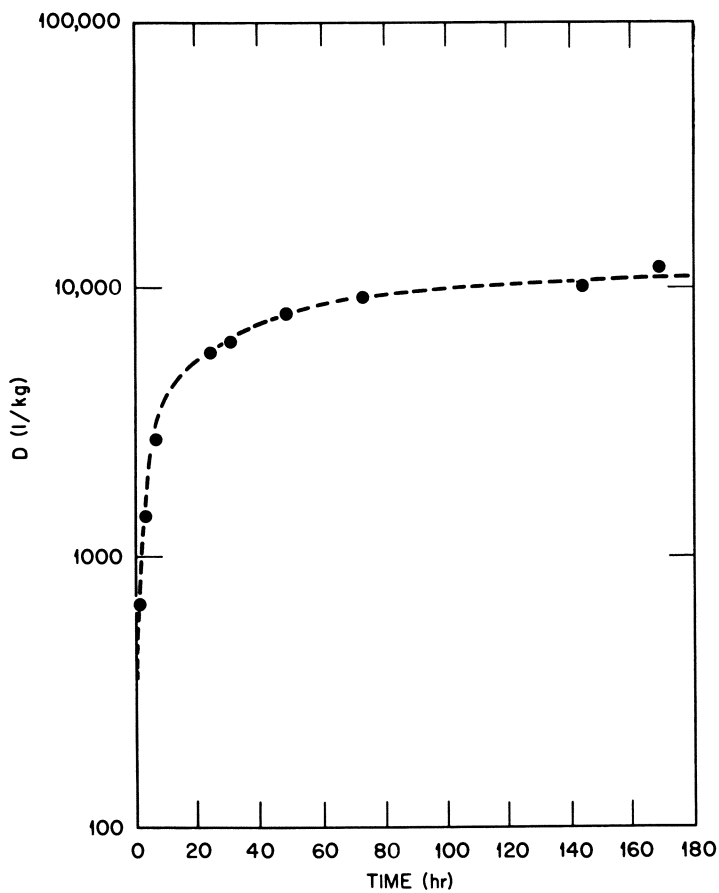


Figure 4. Kinetics of exchange of Am on attapulgite

action requiring less than a day for equilibrium, with a second very slow reaction requiring days to come to equilibrium.

The D values for Am, Cs, Rb, K and Sr on attapulgite are plotted in Figure 5. The D values increase from K to Rb and finally Cs. The Cs behavior has been previously reported (7,8). The rates of exchange also follow this order. The K and Rb are quite rapid reactions while Cs has a two component reaction, one rapid requiring approximately thirty minutes with a second requiring almost a day. All of the preceding data indicate some highly unusual and specific reactions of attapulgite for the rare earths, actinides, and Cs. These highly specific reactions cannot be explained satisfactorily by analogy to the comparable reactions of kaolin and montmorillonite.

The most striking difference between these three clays has already been mentioned previously. The morphological differences deserve more scrutiny as to their structural origins. Structural representation of kaolin, montmorillonite, and attapulgite are given in Figures 6, 7 and 8, respectively. It can be seen that kaolin and montmorillonite do derive their morphologies largely from their structures. These two clays are basically layered structures consisting of aluminum oxygen octahedra, and silicon oxygen tetrahedra, differing only in the order of stacking of the components. Attapulgite likewise is built up of these basic units, but the major difference occurs in the arrangement of these units. The first two clays were extended layers of alternating planes of Al and Si. Attapulgite has this same layered structure on a microscopic level. These microscopic units are then linked across a single oxygen shared between two Si tetrahedra. This linking bond exhibits prominent cleavage which results in the needle-like morphology of attapulgite. This linking of the microscopic layered structures also result in a very open channeled structure which contains about 8 zeolitic waters per unit cell. These channels could possibly be sources of the high specificity for the rare earths and actinides. It can be speculated that the size of the channels must also be the reason for the differences in both the kinetics and D values seen for Cs, Rb, and K. The two rates of reaction seen for Am and Cs could be explained by these channels also, since the needles would contain two types of channels. The first would be channels that are quite open resulting from the prominent cleavage exhibited across the weak bond shown in Fig. 8. The second type of channel would be internal having only ends exposed to exchange. The rapid reaction could result from interaction with these highly exposed channels, with the second slower reaction limited by diffusion into the inner channels.

The D values on the three clays studied indicate very little difference between the rare earths and actinides. The D values also indicate that there is a small increase in D when going from low atomic number to higher atomic number in agreement with results of (9). The most unexpected results are that geometric or structural considerations can cause high specificity for some

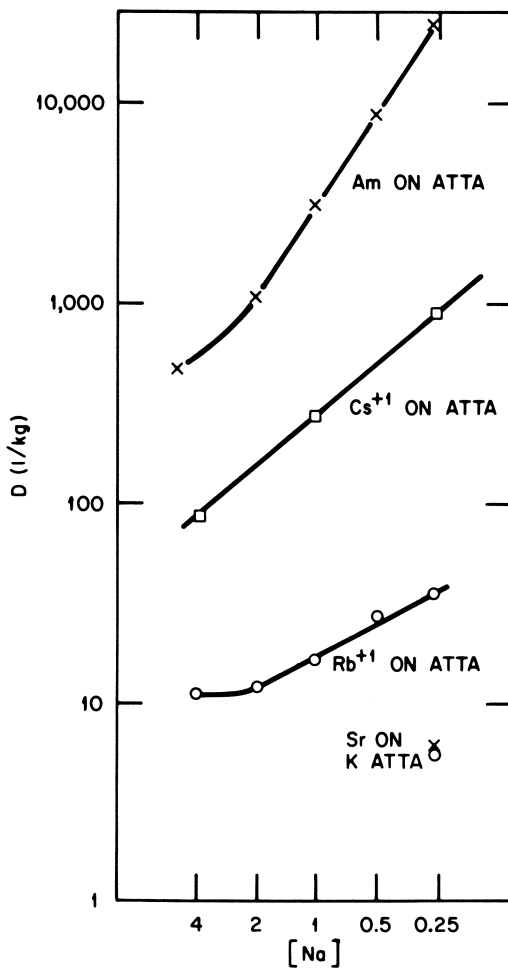


Figure 5. Comparison of the exchange of Am, Cs, Rb, K, and Sr on attapulgite

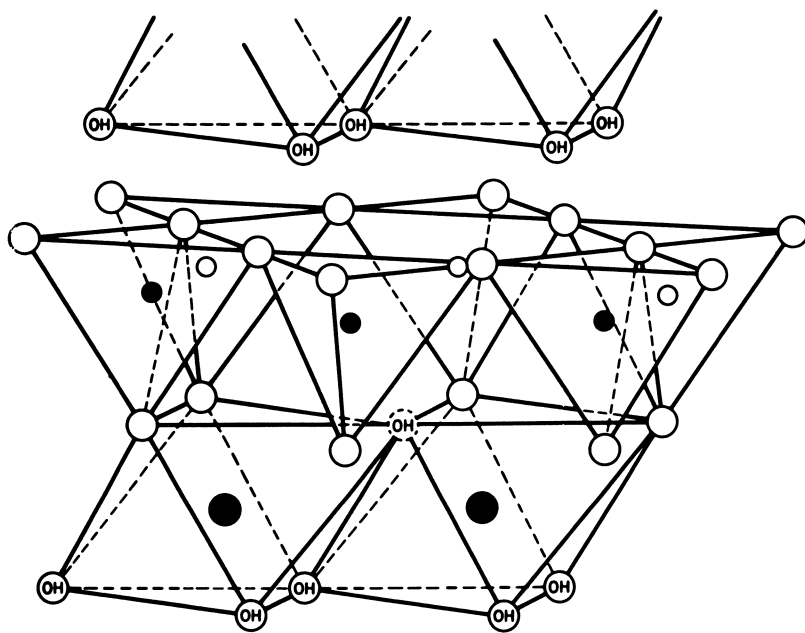


Figure 6. Structural representation of kaolin

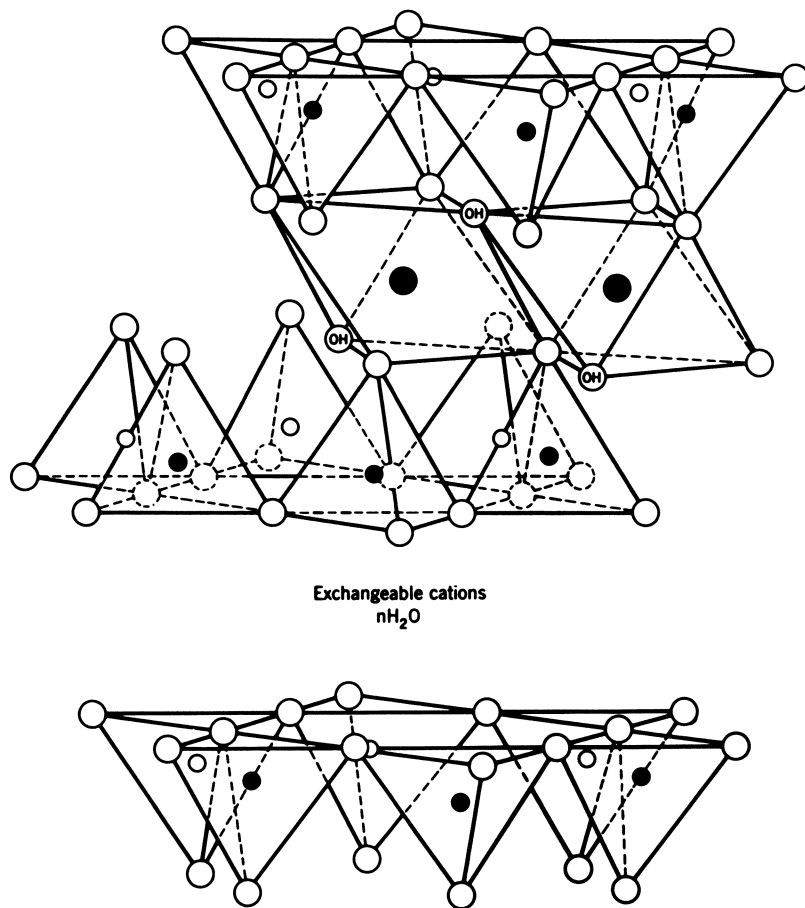


Figure 7. Structural representation of montmorillonite

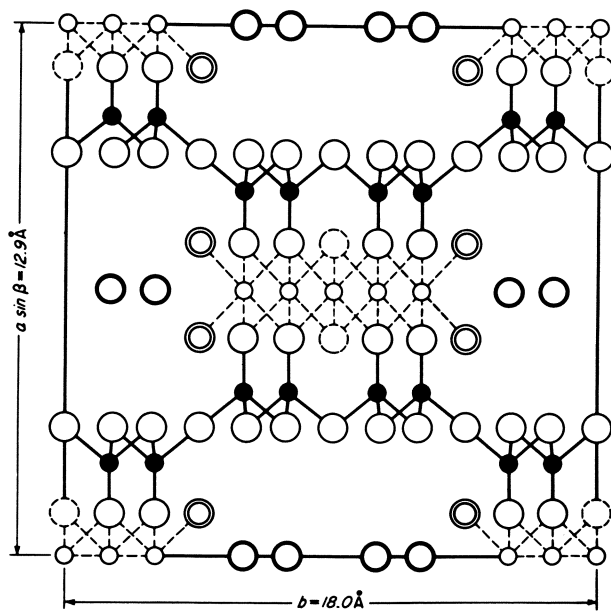


Figure 8. Structural representation of attapulgite

ions. This high specificity for the actinides in particular has important implications for waste isolation, since in the long term these elements present the greatest hazards in nuclear waste. This behavior of attapulgite toward the actinides could also have possible applications in purification of waste streams or in cleanup of radioactive spills.

Literature Cited

1. Tamura, T and Jacobs, O. G., *Health Phys.* 5, 149-154 (1961).
2. "Handling of Spent Nuclear Fuel and Final Storage of Vitri-fied High Level Waste," Technical Reports by the Swedish Nuclear Fuel Safety Project (KBS), 1978.
3. Source Clay Mineral Repository, University of Missouri, Rolla, Mo.
4. Grim, Ralph E., "Clay Mineralogy," 2nd Ed., McGraw-Hill, N. Y., New York (1968).
5. Nelson, F., Murase, T., and Kraus, K., *J. Chromatog.* 13, 503-535 (1963).
6. Choppin, Gregory R., and Schneider, Joan K., *J. Inorg. Nucl. Chem.*, 32, 3283-3288 (1970).
7. Chandra, Umesh, Master's Thesis, University of Bombay (1969).
8. Merriam, C. Neale, and Thomas, Henry C., *J. Chem. Phys.*, 24, 993-995 (1956).
9. Adgaard, P., *Bull. Groupe franc. Argiles*, 26, pp 193-199.

RECEIVED January 16, 1979.

Studies of Actinide Sorption on Selected Geologic Materials

R. J. SILVA, L. V. BENSON, and J. A. APPS

Earth Sciences Division, Lawrence Berkeley Laboratory, Berkeley, CA 94720

The long term objective of this program is to establish a basis for the prediction of radionuclide sorption in geologic environments of the type anticipated for terminal radioactive waste storage. In order to begin to identify parameters which should be incorporated in a predictive sorption model, a study of the interaction of U, Np, Pu, Am, and Cm with basalt, shale and granite was initiated. The following discussion covers the experimental results to date. The mineral makeup of the rocks and the composition of the solutions were determined so that as the dependence of nuclide adsorption on these parameters becomes better known, the results of these experiments may be understood in greater detail.

The sorption/desorption processes were studied by a batchtype technique. Aqueous solutions were prepared by mixing rock powders with distilled-deionized water. For the sorption experiments, portions of these aqueous solutions were loaded with tracer quantities of a single radioactive nuclide and contacted with wafers of a given rock type. For the desorption experiments, wafers from the sorption experiments were contacted with the remaining portions of the aqueous solutions.

The progress of the contact experiments was monitored by gamma-ray counting of solutions. Actinide tracer concentrations on the wafers and in the solutions were measured at the end of the contact period by alpha and gamma-ray counting. These data were used to calculate sorption coefficients. Autoradiography of the wafers is being performed to gather information on sorption specificity.

Selection of Rock Samples and Tracers

Radionuclides. Isotope selection was based primarily on three experimental requirements: (1) both alpha and gamma emitters present for counting purposes; (2) alpha emitter present for autoradiography; (3) approximately equal

0-8412-0498-5/79/47-100-215\$06.50/0

© 1979 American Chemical Society

molar concentration of the elements at the start of sorption experiments. Table I shows the isotopic compositions of the tracer solutions and the photons used for gamma counting of samples. In the case of U, Np, and Am, the single isotopes ^{233}U , ^{237}Np , and ^{243}Am were used for both alpha and gamma counting. In the case of Pu, the isotope ^{237}Pu was used for gamma counting, while ^{242}Pu was used for alpha counting and for adjusting the molar concentration. The ^{243}Cm was used for both alpha and gamma counting and ^{248}Cm to adjust the molar concentration. Small amounts of other isotopes made during the production processes were also present in most of the samples.

Rock Samples. Three rock types were selected as substrates: basalt from the Umtanum unit in the Pasco Basin in Washington state, quartz monzonite from the Climax Stock of the Nevada Test Site, and shale (metashale) from the Eleana Formation of the Nevada Test Site. Since both the basalt and the quartz monzonite exhibited different kinds and amounts of alteration within the same rock type, two samples from each rock type were used in the experiments. However, there was insufficient material to study the interaction of the more altered of these rock types with all five actinides, therefore, only the interaction with Pu was studied.

Sample Characterization

Physical and chemical analyses of the samples were made in order to interpret the results of the sorption experiments and to provide basic data for the calculation of mass transfer which occurred in the rock dissolution experiment. Cores, 3.2 cm in diameter, were taken from each of the rock samples and sectioned in tap water for subsequent analyses (Figure 1).

Petrographic Studies. Polished thin sections were examined by optical methods to determine original mineralogy and alteration phases. The sections were taken and oriented in such a manner to allow comparison of the microscopic mineralogy with the results of the autoradiography experiments. The shale was too fine-grained to be characterized in detail.

Both basalt samples (DC3-3600 and DH5-2831) are composed primarily of glass (40-50 percent) and plagioclase feldspar (35-40 percent). They contain in addition minor amounts of clinopyroxene (3-5 percent) orthopyroxene (1 percent), and opaques (1-2 percent). The relatively unaltered basalt (DC3-3600) possesses several intersecting fractures filled with clay. There are dark gray alteration zones adjacent to certain fractures where a smectitic clay has replaced

Table I. Isotopic Abundances of Actinide Tracers

Element	Isotope	% by alpha activity	% by weight	Photon used for γ counting
Uranium	^{233}U	99.57	99.99+	Th L X-rays
	^{232}U	0.43	0.0002	
Neptunium	^{237}Np	100	100	86 and 29 keV γ -rays
Plutonium	^{242}Pu	84.08	99.91	
	^{240}Pu	4.58	0.091	
	^{238}Pu	11.32	0.003	
	^{237}Pu	0.02	~ 0.0002	Np K X-rays
Americium	^{243}Am	97.42	99.84	75 keV γ -rays
	^{241}Am	2.54	0.15	
Curium	^{248}Cm	1.86	95.76	
	^{246}Cm	5.45	3.87	
	^{244}Cm	0.51	0.0014	
	^{243}Cm	92.17	0.38	Pu K X-rays

glass and feldspars. Both plagioclase and clinopyroxene have been replaced by secondary minerals (clay, chlorite) along crystal faces and cleavage planes. In the vesicular basalt, (DH5-2831) approximately 40-50 percent of the vesicles remain unfilled; the rest are usually filled with cristobalite.

The quartz monzonite samples (U15E-7 and U15E-7a) were originally composed of 70-80 percent feldspar, 10-15 percent biotite, 3-8 percent quartz, and 2-8 percent opaques. Both samples have been hydrothermally altered; U15E-7a being the more altered. The original feldspars in both samples have been sericitized and/or altered to clinozoisite. Secondary calcite also occurs in both samples. Pyrite is an abundant secondary mineral and minor amounts of both epidote and chlorite replace biotite and fill fractures.

Scanning electron microscopy (SEM). SEM studies of the shale and the quartz monzonite samples were not feasible since the morphology of secondary minerals could not be explicitly identified by this technique. Energy dispersive analysis by x-rays (EDAX) of the clay in fractures of the DC3-3600 basalt sample indicated the presence of Fe, Mg, Ca, K, Al, and Si which suggests that the clay is an Fe- and Mg-rich smectite (nontronite). SEM and EDAX studies of DH5-2831, the amygdalic basalt, indicated the presence of a pure silica phase coated by small clay (smectite) particles. Other vesicles "floored" with pure silica were covered with a relatively thick coating of the smectite. In addition, one vesicle was filled with gypsum fibers intermixed with an irregularly-shaped aluminosilicate containing Na, K, and Ca.

X-ray diffraction studies. The highly-altered quartz monzonite (U15E-7a) was examined with x-ray diffraction techniques. Four regions, distinguishable in hand specimens by their color, (metallic, pink, dark-gray, and yellow-gray) were sampled and analyzed. The results (Table II) support the petrographic observations and indicate that the original calcic feldspars have been altered to potassium-bearing phases (potassium feldspar or sericite) or to other secondary calcium-bearing minerals (calcite and clinozoisite).

Bulk chemical analysis of the solids. The three rock types were chemically analyzed by neutron activation (NAA) and x-ray fluorescence (XRF). The resulting data (not included in this report) were used for depth-of-leaching calculations given below. With the measurement of volatile components in the basalt and shale, the total measured abundances in all three samples was close to 100 percent.

Characterization of physical properties. A variety of physical properties were measured including density, specific

TABLE II. X-ray Diffraction Data for Highly Altered
Quartz Monzonite (U15E-7a)

METALLIC SAMPLE	DARK-GREY SAMPLE
Pyrite	Pyrite
Calcite	Calcite
Muscovite/Sericite	Muscovite/Sericite
Quartz	K-feldspar
YELLOW-GREY	
PINK SAMPLE	
Pyrite	Muscovite/Sericite
Calcite	K-feldspar
Muscovite/Sericite	Quartz
Quartz	
K-feldspar	
Clinzoisite	

surface area, permeability, and pore characteristics (Table III). Pore volume was determined by the mercury injection method on a Micromeritics Model 900/910 Porosimeter and also by measuring the volume of gas which flowed into the sample under ambient conditions. Specific surface area was determined both on a Model 2100 Orr Analyzer and on a QUANTASORB Surface Area Analyzer by the standard multipoint BET technique using krypton and nitrogen adsorption. Permeability was measured by introducing a gas pressure pulse and monitoring pressure decay (transient method).

Certain of the physical data (Table III) appear to be less than satisfactory. In general, agreement between the two types of porosity measurements is not good and the values for DC3-3600, UE15-7 and UE15-7a appear excessively large. The densities of the quartz monzonite appear unusually low, i.e., values in the range 2.6 to 2.7 were expected (1).

Purification and Characterization of Actinide Tracers

Before the tracer solutions were used, it was necessary to insure elemental purity and freedom from other contaminants. In addition, one oxidation state was selected for each element as the starting point for the experiments. The 6+ oxidation state for U, 5+ for Np, 4+ for Pu, and 3+ for both Am and Cm were used. These selections were accomplished through the use of cation-exchange chromatography. A given radionuclide was first sorbed on the top of a cation-exchange resin column from a dilute hydrochloric acid solution and, after washing, selectively eluted with a hydrochloric acid solution appropriate for the given oxidation state. The column characteristics and chemical form of each radionuclide are shown in Table IV. After column elution, all tracers were made up to nearly equal molar concentration in 2M HCl.

The Dissolution Experiment

It was necessary to prepare an aqueous electrolyte solution for the sorption study. To simulate sorption processes which occur in natural systems, the electrolyte solution should fulfill two criteria:

- (1) The composition of the solution should closely approximate the natural aqueous phase so that the effects of ion pairing and complexation are accounted for.
- (2) The solution should be in equilibrium with the solid's surface with respect to all chemical processes excepting sorption/desorption. If the solid dissolves, the surface energy distribution and the composition of the aqueous phase will constantly change. If precipitation occurs, the surface of the solid may become coated with pre-

TABLE III. Physical Property Data

LAB	DC3-3600	DH5-2831	U15E-7	U15E-7a	UE-17E	DC3-3600 (powder)	U15E-7 (powder)	UE-17E (powder)
Recovery Depth (m)								
Hg Bulk Density (g/cc)	MM ⁽²⁾	2.94	2.17	2.16	2.18	2.49	-	-
Hg Density at 50,000 psi (g/cc)	MM	3.43	2.60	2.38	2.39	2.68	-	-
Average Pore Diameter (μm)	MM	0.0044	0.0106	76	40	0.0104	-	-
Net Pore Volume (cc/g)	MM	0.016	0.057	0.42	0.041	0.019	-	-
Porosity, Hg Injection (%)	MM	14.3	16.7	9.2	8.8	7.1	-	-
Porosity, Gas Volume (%)	TT ⁽³⁾	6.4	8.3	6.4	6.5	7.7	-	-
Specific Surface Area (ORR Analyzer) m^2/g	MM	8.36	16.4	0.376	0.123	8.54	8.01	4.76
Specific Surface Area (Quantasure Analyzer) (m^2/g)	LBL ⁽⁴⁾	4.57	-	-	-	6.44	-	-
Gas Permeability (Darcies)	TT	7×10^{-3} ⁽¹⁾	3×10^{-4} ⁽¹⁾	$< 1 \times 10^{-7}$	$< 1 \times 10^{-7}$	$< 1 \times 10^{-7}$	-	-

(1) Fracture permeability

(2) Analysis done by Micromeritics

(3) Analysis done by Terra Tek

(4) Analysis done by Lawrence Berkeley Laboratory Molecular Materials Research Division

precipitate, thus altering the character of the sorptive substrate.

In order to produce an aqueous solution which fulfills these criteria, 120 g each of basalt, quartz monzonite, and shale were ground to powders less than 37 μ m in diameter. Each of the samples was placed in two liters of distilled-deionized water which had been pre-equilibrated with an atmosphere containing 10 percent CO₂, 90 percent Ar, and 10 ppm O₂. The experiment was carried out in an inert atmosphere box at room temperature (26 \pm 2°C). Samples of the fluid (10 ml) were extracted at various times over a 35-day period and filtered (0.05 μ m). Analyses for Na, K, Mg, Ca, Fe, Al, SiO₂ (aq), Eh, and pH were made on each sample. The experiment was terminated at the end of 846 hours and analyses for HCO₃, SO₄, and Cl were made on each of the fluids.

Reaction rates. The molar concentrations of Na, K, Ca, Mg, and SiO₂, as well as pH, plotted as a function of elapsed time are shown in Figures 2 to 7. With some variation, a similar pattern is displayed by all three rock types: an initial steep portion followed by an approximately linear region with small positive slope. Exceptions to this can be seen in Figure 2 where Na in the shale solution has a slightly negative slope, in Figure 3 where K in the shale solution has essentially zero slope, and in Figure 6 where the overall dissolution pattern of SiO₂ appears roughly parabolic.

The release of cations is interpreted to have resulted chiefly from two processes: an initial release caused by rapid exchange of surface cations for hydrogen followed by a slow release due to structural attack and disintegration of the aluminosilicate lattice. Other processes which could complicate the form of the dissolution curves are: adsorption of cations released by structural breakdown, ion exchange on interlayer sites of cations released by structural breakdown and surface exchange (shale only), precipitation of amorphous or crystalline material, and dissolution rate differences among the various crystalline phases.

Structural breakdown. Calculations of the depth of leaching/dissolution were made using the following assumptions:

- (1) The rock powder was assumed to have a homogeneous distribution of elements;
- (2) All atomic sites were equivalent in size and had a cubic geometry;
- (3) The most mobile cation (the cation which showed the largest concentration increase in the solution relative to its concentration in the solid) did not participate in precipitation or adsorption processes.

These calculations were made for the basalt and quartz

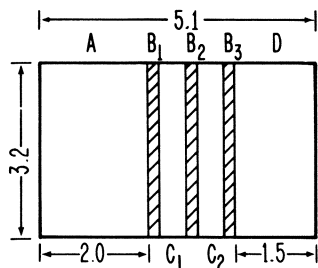


Figure 1. Core processing (scale in cm). Samples taken for area and pore-size distribution measurements (A), petrographic thin sections (B_1 , B_2 , and B_3), sorption experiments (C_1 and C_2), and permeability measurements (D).

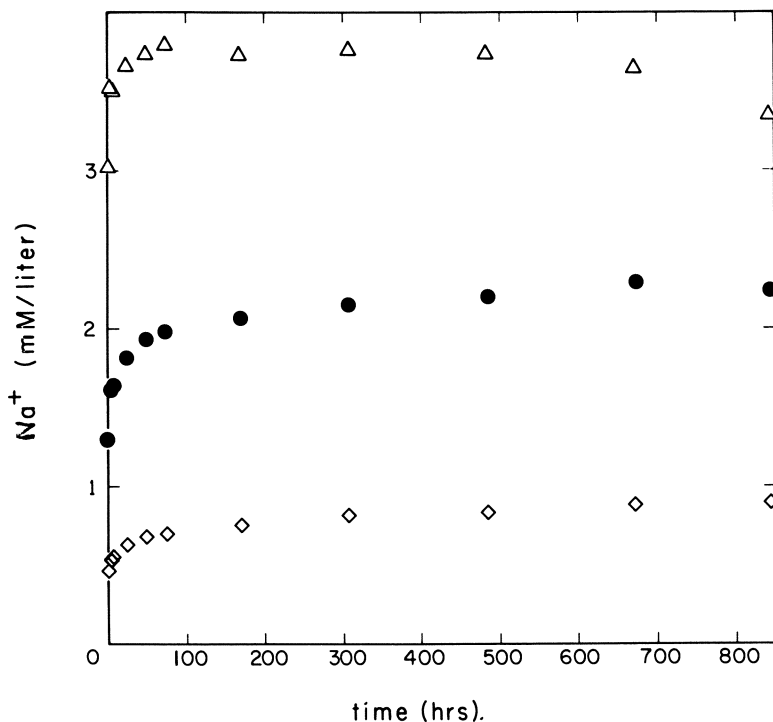


Figure 2. Sodium released to the aqueous solution during the dissolution of powders from three rock types. (Δ), Eleana shale (UE-17e); (\diamond), quartz monzonite (U15e-7); (\bullet), umtanum basalt (DC 3-3600).

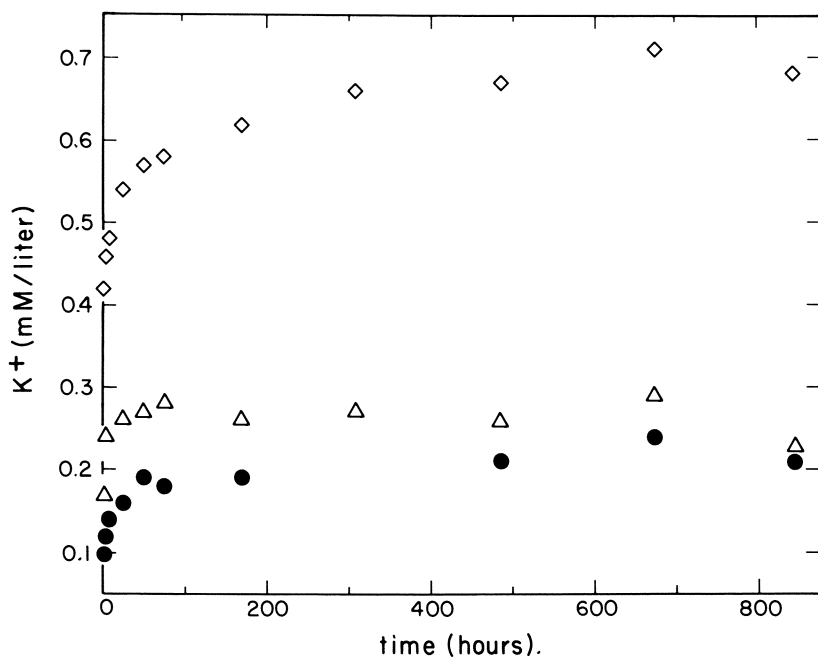


Figure 3. Potassium released to the aqueous solution during the dissolution of powders from three rock types. (Δ), Eleana shale (UE-17e); (\diamond), quartz monzonite (U15e-7); (\bullet), umtanum basalt (DC 3-3600).

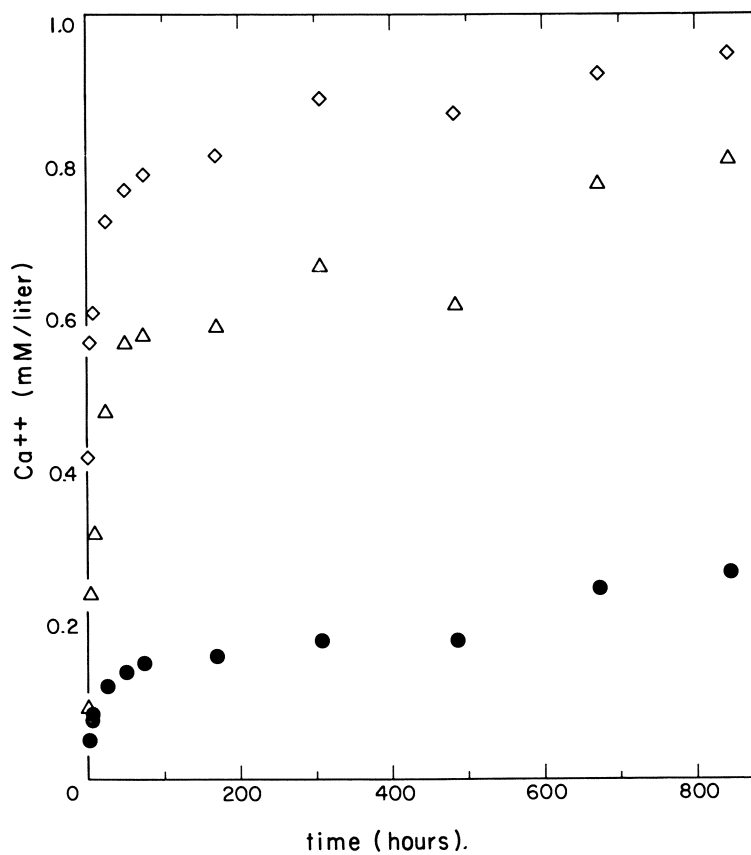


Figure 4. Calcium released to the aqueous solution during the dissolution of powders from three rock types. (Δ), Eleana shale (UE-17e); (\diamond), quartz monzonite (U15e-7); (\bullet), umtanum basalt (DC 3-3600).

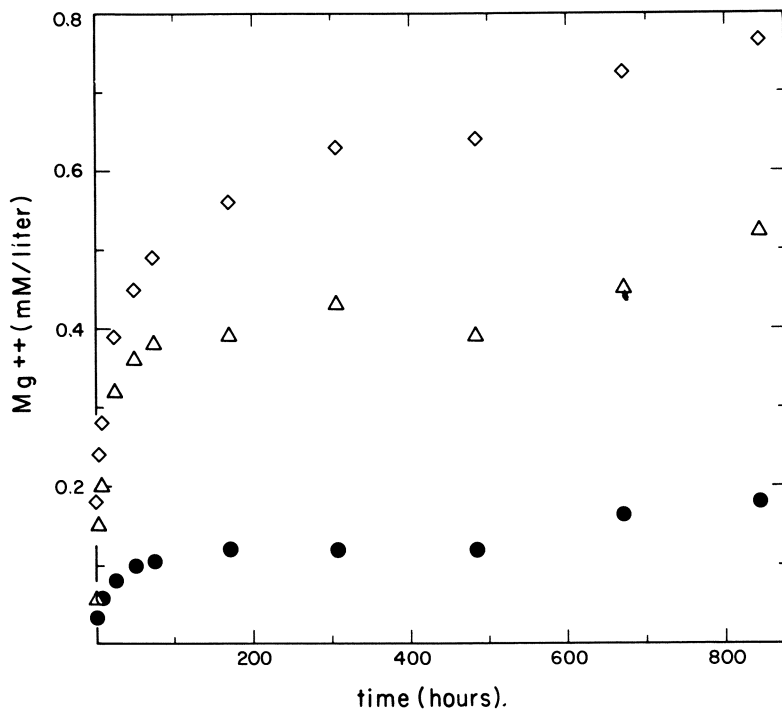


Figure 5. Magnesium released to the aqueous solution during the dissolution of powders from three rock types. (Δ), Eleana shale (UE-17e); (\diamond), quartz monzonite (U15e-7); (\bullet), umtanum basalt (DC 3-3600).

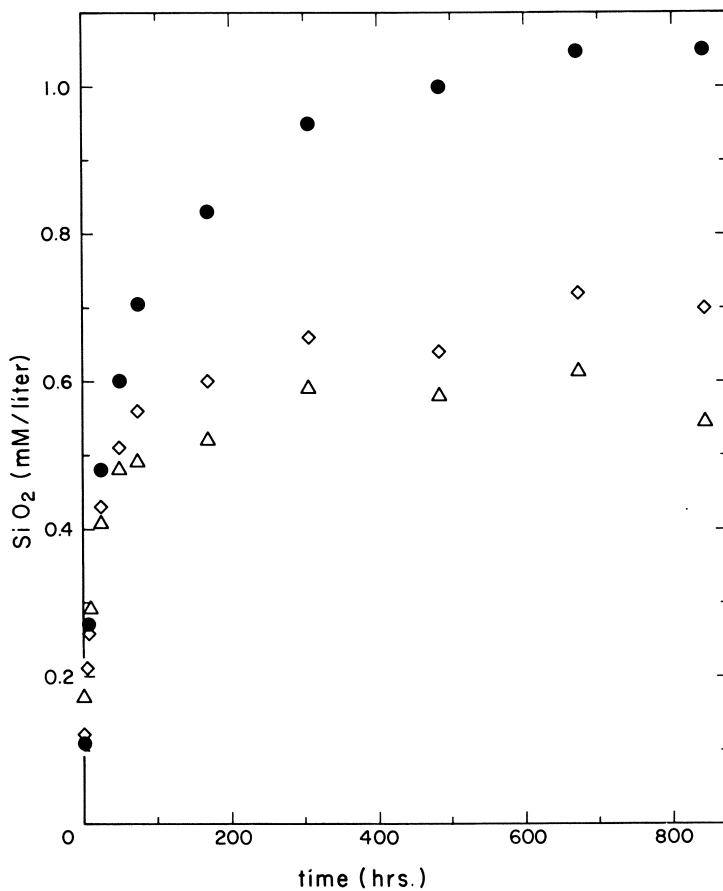


Figure 6. Aqueous silica released to the aqueous solution during the dissolution of powders from three rock types. (Δ), Eleana shale (UE-17e); (\diamond), quartz monzonite (U15e-7); (\bullet), umtanum basalt (DC 3-3600).

monzonite experiments only, since the shale experiment may have involved other complicating processes such as ion exchange between the aqueous phase and interlayer sites. Both the depth of leaching/dissolution that occurred during the entire experiment and the rate of leaching during the approximately linear portion of the experiment were determined. The results of these and other calculations are summarized in Table V. The data indicate that several atomic layers have been either totally stripped or have experienced diffusional processes (leaching) during the course of the experiment. The rate of release of cations during the linear region of the experiment was smaller than the initial release rate; however, the linear rate is still sufficient to have affected the solids to a depth of 0.4 (basalt) to 1.8 (quartz monzonite) atomic layers during the subsequent adsorption experiment which ran approximately six weeks (1006 hr). These calculations serve to point out the difficulties in eliminating interference effects during a long-term sorption experiment.

Final composition of the aqueous phase. The final compositions of the waters resulting from the three dissolution experiments have been summarized and listed together with compositions of waters from natural systems (Table VI). The experimental and natural basalt waters have very similar compositions. However, the experimental quartz monzonite water has a higher than natural K content while the shale water has higher than natural K and Na contents. The HCO_3 content of each of the experimental waters is higher than the content of its natural counterpart while the opposite is true for SO_4 .

The differences in cation compositions are probably due to the fact that phases containing these ions (illite, smectite, etc.) have sufficient time to form in natural systems but did not form in the experimental system. The high HCO_3 content of the experimental system is due to contact with an infinite reservoir of CO_2 having a partial pressure of 0.1 atmosphere.

Rock/Tracer Contact Experiments

Procedure. The rock wafers were gently cleaned three successive times with methanol in an ultrasonic bath, dried and placed in the inert atmosphere box. Two wafers of each rock type were inserted horizontally in stainless steel holders and placed in linear polyethylene containers holding 150 ml of the appropriate prepared water. The wafers were allowed to equilibrate with the water for three days and then 5 λ of tracer solution was added. The resultant solutions contained $\sim 5 \times 10^{-8}$ M of each element. The pH of each solution was measured before and after the addition of the tracer and did not change sign-

TABLE IV. Tracer Purification and Oxidation State Selection

Method: Cation Exchange Column

HCl Elution

Dowex 50 x 8 Resin

0.5 cm diam x 12 cm long - 26°C

Elution Conc. HCl	Species
3 M	UO ₂ ⁺⁺
0.5 M	NpO ₂ ⁺
9 M	Pu ⁴⁺
6 M	Am ³⁺
6 M	Cm ³⁺

TABLE V. Depth-of-Leaching Calculations

	BASALT (DC3-3600)	QUARTZ MONZONITE (U15E-7)
total moles per gram of sample	.0411	.0473
unit cell edge (A)	2.28	2.45
most mobile ion	Na	Mg
mobile ion mole fraction	.0249	.00535
surface sites in 120 g sample	1.85x10 ²²	1.61x10 ²²
layers leached (846 hr)	5.9	11
leach depth (A) (846 hr)	13	26
linear region leach rate (layers hr ⁻¹)	0.35x10 ³	1.75x10 ⁻³

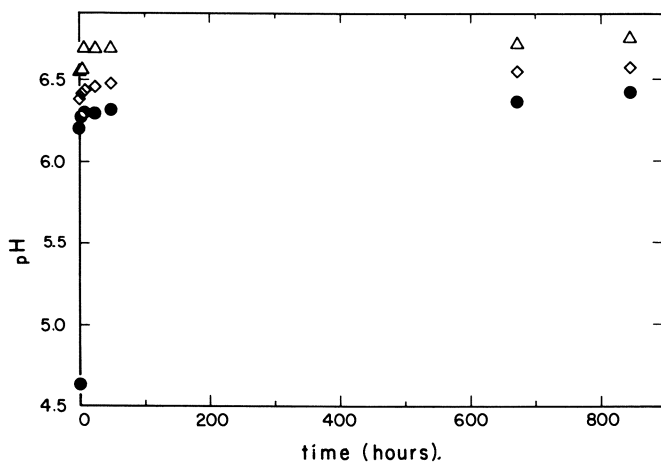


Figure 7. Changes of pH during the dissolution experiments. Note the rapid initial decrease in the hydrogen ion concentration. (Δ), Eleana sale (UE-17e); (\diamond), quartz monzonite (U15e-7); (\bullet), umtanum basalt (DC 3-3600).

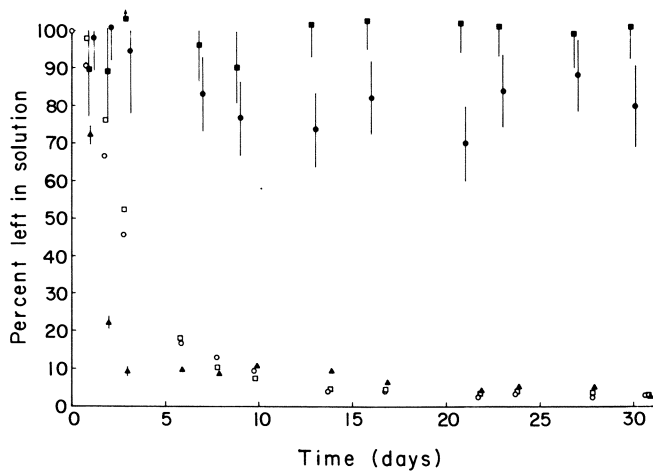


Figure 8. Percentage of initial concentrations of tracers left in solution as a function of time for the sorption experiments with the blank containers. (\bullet), U; (\blacksquare), Np; (\blacktriangle), Pu; (\square), Am; (\circ), Cm.

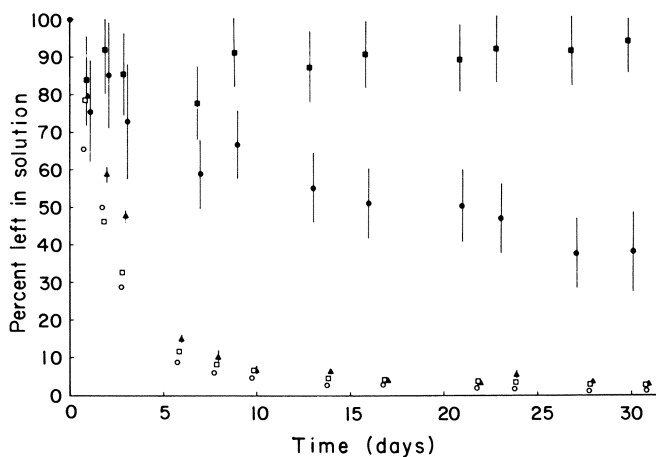


Figure 9. Percentage of initial concentrations of tracers left in solution as a function of time for the sorption experiments with the basalt samples. (●), U; (■), Np; (▲), Pu; (□), Am; (○), Cm.

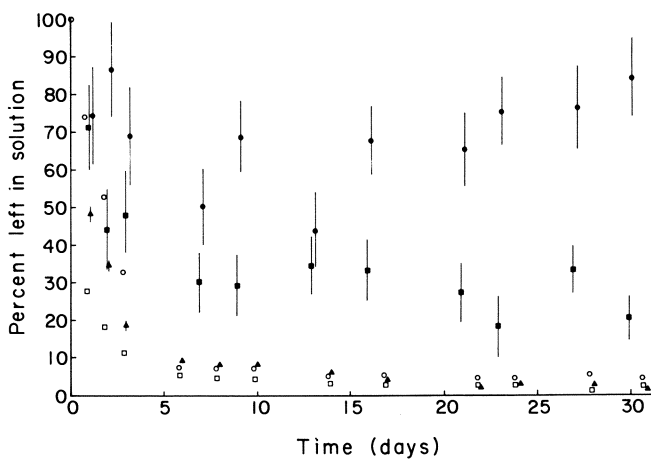


Figure 10. Percentage of initial concentrations of tracers left in solution as a function of time for the sorption experiments with the shale samples. (●), U; (■), Np; (▲), Pu; (□), Am; (○), Cm.

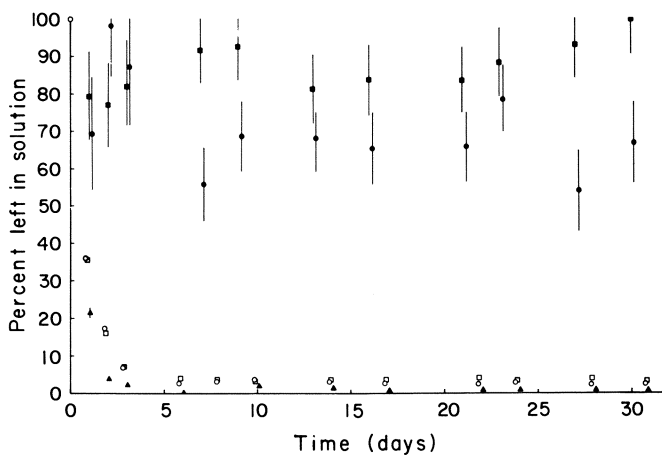


Figure 11. Percentage of initial concentrations of tracers left in solution as function of time for the sorption experiments with the quartz monzonite samples. (●), U; (■), Np; (▲), Pu; (□), Am; (○), Cm.

TABLE VII. Adsorption Coefficients, $K = \frac{d/m/gm}{d/m/ml}$

I = Basalt, II = Shale, III = Quartz monzonite, A = Altered

Sample	$\frac{Up}{Down}$	K(alpha)	K(filter)	K(gamma)
I - U	1.51	1.87	2.01	2.80
II - U	7.78	0.761	0.797	6.65
III - U	2.33	0.316	0.343	0.287
I - Np	1.09	0.416	0.394	0.459
II - Np	0.797	1.53	1.29	48.7
III - Np	1.53	0.199	0.204	0.471
I - Pu	4.33	48.9	423	60.1
I - Pu - A	7.00	137		139
II - Pu	3.50	188	729	145
III - Pu	7.37	261	2973	225
III - Pu - A	11.0	113		143
I - Am	7.73	1270	14300	1033
II - Am	3.02	97.8	394	962
III - Am	6.02	1290	12700	1323
I - Cm	4.35	746	4900	525
II - Cm	2.78	44.2	724	219
III - Cm	3.29	164	6460	171

TABLE VIII. Desorption Coefficients, $K = \frac{d/m/gm}{d/m/ml}$

I= Basalt, II= Shale, III= Quartz monzonite, A= Altered

Sample	$\frac{Up}{Down}$	K(alpha)	K(filter)
I - U	3.65	2.57	3.50
II - U	3.83	1.04	1.10
III - U	2.52	2.26	1.82
I - Np	1.35	1.45	1.19
II - Np	1.20	0.675	0.570
III - Np	1.10	3.86	2.90
I - Pu	5.20	67.3	777
I - Pu - A	2.18	345	
II - Pu	1.32	201	122
III - Pu	2.98	108	103
III - Pu - A	11.07	779	
I - Am	4.33	274	5331
II - Am	1.01	480	798
III - Am	4.71	186	1664
I - Cm	5.57	850	12672
II - Cm	1.75	187	1118
III - Cm	4.08	561	2676

TABLE VI. Comparison of Prepared Waters With Waters From Natural Systems (mg/l)

	DC3-3600	(1)	U15E-7	(2)	(3)	UE-17E	(4)	(5)
Na	52	37	20	93	6.0	77	12	18
K	8.0	7.0	26	3.0	1.6	9.0	1.1	1.5
Mg	4.4	8.0	19	18	1.7	13	16	19
Ca	11	19	38	117	10	32	29	96
Fe	1.2	0.2	2.3	0.2	.01	1.4	.02	1.0
Al	.12	-	.01	0.2	.02	.01	0	0
SiO ₂	63	55	42	33	25	33	16	15
pH	6.4	7.8	6.6	7.6	6.8	6.8	4.9	7.8
HCO ₃	190	150	290	214	57	380	126	133
Cl	1.5	10	1.5	32	1.1	0.8	12	25
SO ₄	2	20	2	337	2.4	3	22	208

- (1) Average composition of groundwaters from Columbia River basalts (525 samples).
- (2) Seepage waters from climax stock (quartz monzonite).
- (3) Average composition of perennial springs in quartz monzonites and granodiorites of the Sierra Nevadas (56 samples).
- (4) Groundwater from the Brunswick Shale of New Jersey.
- (5) Groundwater from the Chicopee Shale of Massachusetts.

ificantly. A blank solution not containing wafers was prepared in a similar manner for each of the five actinides by mixing 50 ml of each of the three water types. The containers were sealed, removed from the inert atmosphere box, and gently agitated with an Eberbach variable-speed shaker for six weeks.

The concentrations of tracers in solutions were determined periodically. The polyethylene containers were constructed in such a way that, when inverted, 50 ml of solution passed from the wafer compartment into a second compartment. The second compartment of the container was inserted through a hole in a lead shield which housed a 3.5 cm diameter by 1.2 cm deep high-purity Ge gamma-ray detector. The other compartment containing the solution and wafers was shielded from the detector by the lead housing.

At the end of the six weeks, the containers were returned to the inert atmosphere box and the wafers removed. One wafer was immediately placed in a new container with 50 ml of aqueous solution for the desorption study. The other wafer was rinsed lightly, allowed to dry and counted.

Aliquots of the solutions (50 ml) were placed in polyethylene bottles for gamma-ray counting and 0.5 ml samples were evaporated on platinum plates for alpha counting. In addition, 10 ml of each of the solutions were passed through 0.05 μm Nucleopore filters. Aliquots (0.5 ml) of the last 2 ml passing through filters were evaporated on platinum plates for alpha counting. Both alpha and gamma count rates on the wafers were measured.

Results and Discussion. Changes in concentrations of the actinides in solution in the blank containers are shown in Figure 9. A large fraction of the Pu, Am and Cm was removed from solution while only a small amount of the U and none of the Np was lost from solution. Since the starting concentration of Pu exceeds the solubility for the hydroxide (or hydrated oxide), the Pu probably precipitated as colloidal-size particles (2); the behavior of Am and Cm cannot be explained by a similar mechanism. However, there is recent experimental evidence that indicates the solubility products for Am and Cm carbonates may be of the order 10^{-41} (3). If this is the case, there was sufficient carbonate ion concentration in the solutions to cause precipitation of these compounds.

Figures 10, 11 and 12 show the results of the contact experiments for the basalt, shale and quartz monzonite samples. The rate of adsorption was rapid during the first two weeks and changed slowly thereafter. In these experiments Pu, Am and Cm exhibited behavior similar to the results obtained in the blank experiments. Uranium showed moderate adsorption (~ 50 percent) on the basalt but only slight adsorption (10-20 percent) on the shale and quartz monzonite wafers. Neptunium showed strong adsorption (70-80 percent) on the shale and slight adsorption (~ 10 percent) on the basalt and quartz monzonite.

The calculated adsorption coefficients (K) are presented in Table VII. K (alpha) refers to results from alpha counting the wafers and solutions, while K (gamma) refers to results from gamma counting. K (filter) refers to results from the alpha counting of wafers and filtered solutions.

Measurement precision of the K values is $\pm 5-10$ percent for K (alpha) and K (filter). Precision of the K (gamma) measurements are $\pm 5-10$ percent for Am and Cm; ± 20 percent for Pu; and $\pm 30-35$ percent for Np and U. These values represent only errors associated with the counting.

Except for Np, alpha counting showed that wafer surfaces facing upward consistently had higher counting rates than surfaces facing downward. The up/down ratios are also presented in Table VII. This behavior suggests that a process such as settling may be involved.

Comparisons of K (α) and K (γ) show good agreement for each given rock type and element except for the shale samples. With the exception of Pu, K (γ) values for the shale samples were considerably larger than K (α) values. Since alpha counting detects only material on the surface while gamma counting detects both surface and bulk-adsorbed material, adsorption on the basalt and quartz monzonite samples represents a surface process while the shale samples exhibit a diffusional effect in addition to surface sorption. Differential migration of the actinides into the samples was not expected since the measured permeabilities and porosities for the three rock types were nearly equivalent. However, as was noted above, the permeability and porosity data may be substantially in error.

Finally, a comparison of K (α) and K (filter) for each rock type and element show that, while the values for U and Np agree quite well, the values differ substantially for Pu, Am and Cm. Apparently, there were still considerable amounts of filterable or adsorbable species left in solution after the six weeks contact time.

The observed differences between the elements could presumably be attributed to differences in sorption properties of the chemical species present. Unfortunately, with the possible exception of Np, the lack of a complete set of thermodynamic data precludes a quantitative prediction of the concentrations of the various possible species in solution or of the conditions for the formation of solid phases. However, our data suggest that precipitation or colloid formation were the major reactions of Pu, Am and Cm in our solutions and, perhaps, a minor reaction of U.

The data obtained from the filtered solutions can be used to estimate an upper limit to the concentrations of soluble U, Pu, Am and Cm under the conditions of our experiments. These concentrations were approximately $4 \times 10^{-8} \text{M}$ for U, $2 \times 10^{-10} \text{M}$ for Pu, and $2 \times 10^{-11} \text{M}$ for Am and Cm. Estimates of the concentrations of possible chemical species in solution for the four actinides were made using measured or estimated solubility, complexation and hydrolysis constants (4-8), and the measured OH^- , CO_3^{2-} , SO_4^{2-} , and Cl^- concentrations given in Table VI. The results showed that hydroxide and carbonate are the ligands that need to be considered; chloride and sulfate concentrations are sufficiently low that their effects may be neglected. The hydroxide and carbonate concentrations in our solutions were about $4 \times 10^{-8} \text{M}$ and $1 \times 10^{-6} \text{M}$, respectively.

Solubility product constants of 10-11.73 and 10-22.4 have been reported (8) for uranyl carbonate and hydroxide, respectively. The hydroxide was calculated to be the stable solid phase under the conditions of our experiments. For

the uranium concentrations used in our experiments, the dominant hydrolysis product was most likely $\text{UO}_2(\text{OH})_2^0$; $K [\text{UO}_2^{2+} + 2\text{OH}^- = \text{UO}_2(\text{OH})_2^0] = 10^{15.98}$ (8), saturated solution concentration = 10^{-7}M . The dominant carbonate complex was estimated as UO_2CO_3^0 ; $K [\text{UO}_2^{2+} + \text{CO}_3^{2-} = \text{UO}_2\text{CO}_3^0] = 10^{10.3}$ (8), saturation concentration = $5 \times 10^{-4}\text{M}$. Since the starting concentration of U was $5 \times 10^{-8}\text{M}$, precipitation was not expected to occur. Therefore, the reasons for the behavior of U in our experiments is not understood.

The hydroxide was expected to be the stable solid phase for Pu^{4+} under the conditions of our experiments. Reported and estimated solubility product constants range from 10^{-52} (7) to 10^{-62} (6). The major hydrolysis product for Pu^{4+} was estimated to be $\text{Pu}(\text{OH})_4^0$; $K [\text{Pu}^{4+} + 4\text{OH}^- = \text{Pu}(\text{OH})_4^0] = 10^{46.5}$ (6), saturation concentration range = 10^{-7}M to 10^{-16}M . Using this hydrolysis constant, an apparent solubility product quotient of 10^{-56} was calculated from our data. Unfortunately, reliable information does not exist for estimating the effects of carbonate complexing on the system. In addition, it has been suggested that PuO_2^+ is the major soluble species in equilibrium with the hydroxide precipitate under conditions similar to our experiments (9). Since neither of these effects were included, the calculated solubility quotient could be in error, i.e., too large.

In general, the chemical behavior of Am and Cm in solution are quite similar and similar to that of the trivalent lanthanides. The americium hydroxide and carbonate solubility product constants were estimated as $10^{-23.3}$ (6) and 10^{-33} (10), respectively, from published values on lanthanide compounds. The values for Cm would be expected to be nearly the same. The carbonate was calculated to be the stable solid phase. Because of the lack of experimental data on the hydrolysis and carbonate complexation constants, it is not possible to calculate the concentrations of the major species in our solutions. However, $\text{Am}(\text{OH})_2^{2+}$ has been estimated (11) as the dominant hydrolysis product; $K [\text{Am}^{3+} + \text{OH}^- = \text{Am}(\text{OH})_2^{2+}] = 10^{8.08}$ (4). A saturation concentration of 10^{-7}M was calculated for this species in equilibrium with the solid carbonate. Since the starting concentration of Am was $5 \times 10^{-8}\text{M}$, precipitation was not anticipated. However, as mentioned previously, the assumed carbonate solubility may be high by eight orders of magnitude. From our data, solubility product quotients for the possible compounds, $\text{Am}_2(\text{CO}_3)_3$ and AmOHCO_3 were estimated as 10^{-41} and 10^{-25} , respectively. The values for Cm should be similar.

Rock/Tracer Desorption Experiments

Procedures. One of the rock wafers from each of the containers used in the adsorption experiments was placed in a new polyethylene bottle containing 50 ml of the appropriate aqueous solution. The containers were removed from the inert atmosphere box and gently agitated for six weeks. Tracer concentrations in the solution were measured periodically as described previously. At the end of six weeks, the experiments were terminated, the wafers removed from the containers, and the tracer concentrations of the components of the system determined in the same manner as in the adsorption experiments.

Results and Discussion. The data obtained from the gamma-ray spectra taken during the course of the desorption experiments were not useful for monitoring the rates of desorption. For the samples containing U and Np, only a small amount of activity appeared in solution and therefore the counting errors precluded a meaningful analysis. Though the counting errors for samples containing Pu, Am and Cm were small, large fluctuations in the measured values again made detailed analysis fruitless. However, there were some general trends that should be mentioned: most of the material that appeared in solution did so in 2 to 3 days; in general, the basalt and quartz monzonite wafers desorbed 3 to 5 times more tracer than the shale wafers; and the Pu, Am, and Cm values fluctuated a factor of 2 to 3 about the mean.

The distribution coefficients calculated from the alpha counting data are given in Table VIII. The gamma counting of the solutions is still in progress. The symbols are the same as used previously. For K (alpha), the counting precision is ± 10 percent for the U, Am and Cm samples and ± 20 -30 percent for the Np and Pu samples. For K (filter), the counting precision is ± 10 percent for U, ± 10 -20 percent for Np, Am and Cm and ± 30 -40 percent for the Pu samples.

The up/down effect was also apparent in the data of the desorption experiment (Table VIII). However, only desorption data for shale differ significantly from the sorption data, i.e., the up/down ratios are closer to unity in the desorption experiments. A comparison of K (alpha) and K (filter) show substantial differences for Am, Cm, and Pu (basalt) samples.

Autoradiography of Rock Wafers

Procedure. At the completion of the sorption and desorption experiments, the rock wafers were placed in

contact with Kodak AR.10 nuclear emulsion films to obtain alpha particle induced autoradiographs. Due to the low concentrations of tracers on many of the wafers, rather lengthy exposure times (up to three months) are needed to obtain autoradiographs that can be readily studied under low magnification (X5). The autoradiographs will be compared with the microstructure and mineral phases of the wafer surfaces and correlations made between sorption and these parameters. Individual mineral phases exhibiting selective uptake will be used as sorptive substrates in future experiments.

Literature Cited

1. Izett, G. A., U. S. Geol. Surv. TEM-836-C 1960.
2. Lloyd, M. H. and Haire, R. G., "Studies on the Chemical and Colloidal Nature of Pu (IV) Polymer" the XXIV th International Union of Pure and Applied Chemistry Congress", Hamburg, Germany, September, 1973.
3. Private Communication from Gary Beall (Oak Ridge National Laboratory) at the WISAP Contractors Information meeting, Seattle, Oct. 1-5, 1978.
4. Rai, D. and Serne, R. J. , "Solid Phases and Solution Species of Different Elements in Geologic Environments", Pacific Northwest Laboratory Report - 2651, March 1978.
5. Apps, J. A., Lucas, J., Mathur, A. K., and Tsao, L., "Theoretical and Experimental Evaluation of Waste Transport in Selected Rocks: 1977 Annual Report of LBL Contract No. 45901AK". Lawrence Berkeley Laboratory Report - 7022, p. 8, September 1977.
6. Baes, C. F. and Mesmer, R. E. "The Hydrolysis of Cations", p. 169, Wiley-Interscience Publications, N. Y., 1976.
7. Cleveland, J. M. "The Chemistry of Plutonium", p. 81, Gordon and Breach Science Publications, N. Y., 1970.
8. Sillen, L. G. and Martell, A. E., "Stability Constants of Metal Ion Complexes", Spec. Publ. No. 17, The Chemical Society, London, 1964.
9. Rai, D., Serne, R. J. and Swanson, J. L., "Solution Species of ^{239}Pu in Oxidizing Environments: II. Plutonyl (V)", Pacific Northwest Laboratory Report - 7027, June, 1978.
10. Smith, R. M. and Martell, A. E., "Critical Stability Constants", vol. 4: Inorganic Complexes, p. 37, Plenum Press, N. Y., 1976.
11. Allard, B. and Beall, G. W., "Predictions of Actinide Species in the Groundwater", Workshop on the Environmental Chemistry of the Actinide Elements, Warrington, Virginia, October 9, 1978.

RECEIVED January 16, 1979.

Biogeochemistry of Actinides: A Nuclear Fuel Cycle Perspective

E. A. BONDIETTI, J. R. TRABALKA, C. T. GARTEN, and G. G. KILLOUGH
Oak Ridge National Laboratory, Oak Ridge, TN 37830¹

Nuclear fuel cycles based on U, Th and Pu produce long-lived α -emitting isotopes of the actinide elements. Man-made actinide element releases to the biosphere occur primarily through weapons testing, nuclear fuel reprocessing, fuel fabrication, and nuclear waste disposal activities. While the global inventory of dispersed Pu and Am, for example, is largely of military origin, the advent of nuclear fuel reprocessing and waste disposal activities associated with nuclear power will inevitably lead to localized contaminated landscapes.

Because of their physiological property of concentrating primarily in bone and the low penetrating power of the α particle, internal deposition from ingestion and inhalation intakes are the most important exposure modes to man. Most of the actinides show low water solubilities and consequently drinking water typically will not dominate over diet with respect to ingestion.

The purpose of this paper is to compare the biogeochemical behavior of the actinides which are important constituents of nuclear fuel cycles. To the extent possible, the environmental behavior of the essentially man-made elements Pu, Am, Cm and Np will be compared to Th and U, which are ubiquitous in the environment. By comparing the man-made actinides to naturally occurring actinides, a generic perspective of the potential hazard of the synthetic actinides to people is obtainable.

Natural U and Th Intakes by People

Through inhalation and ingestion, people assimilate small quantities of natural U and Th. The U and Th which is assimilated from the lung and gastrointestinal tract (G.I. tract) tends to deposit the skeleton (1,2,3).

¹ Research sponsored by the Division of Ecological Research, U.S. Department of Energy under Contract W-7405-eng-26 with Union Carbide Corporation. ESD Publication No. 1284.

0-8412-0498-5/79/47-100-241\$06.50/0
© 1979 American Chemical Society

The literature suggests that the concentrations in bone which result from environmental exposure are about 1 to 30 ng U/g bone ash and about 10 ng Th/g bone ash (2,3,4). Thus U may become more concentrated in bone than thorium. However, Th is more abundant in the lithosphere than U; this is exemplified by average abundances in soil of 6 μg Th/g and 2 μg U/g (4,5,6).

Modeling Intakes. To determine the significance of diet and inhalation as sources of internally deposited U and Th, dietary and inhalation estimates for the general population were used in an Oak Ridge National Laboratory (ORNL) model, INREM II (7). A schematic of the intake and deposition pathways considered by the model are depicted in Fig. 1. Uranium in the typical diet is about 1.3 $\mu\text{g}/\text{day}$ (2,8). Thorium, while more abundant in soil than U, is not as available to plants and consequently a dietary contribution of 0.8 $\mu\text{g}/\text{day}$ has been estimated (2). The inhalation of U approximates 7 ng/day in New York (2). Assuming a soil Th/U ratio of 3, the Th inhalation is about 21 ng/day. For inhalation, two activity median aerodynamic diameters (AMAD) of aerosol particulates were considered. In addition, two ICRP (9) solubility classes of U and Th aerosols were considered. The resulting predictions of Th and U bone concentrations after 70 years of exposure to environmental U and Th were then compared to literature values (Table 1).

For natural Th, the inhalation of 21 ng/day and ingestion (via the diet) of 0.8 $\mu\text{g}/\text{day}$ results in bone ash concentrations of about 13 ng/g for the class W solubility case and about 6 to 9 ng/g for the class Y case. Ingestion contributes 50% or less of this bone-deposited Th. Because an absorption coefficient of 0.1% from the G.I. tract was used, the contribution from ingestion is probably overestimated. Nevertheless, the estimated bone concentrations agree with literature means (2).

For natural U, the situation is different. The amount in bone after 70 years is about 1 ng U/g bone ash. Ingestion dominates inhalation as the contributing intake mode. The inhalation value (7 ng/day) is based on a New York study (10), and would need to be raised substantially in the model to make a significant contribution of U to bone. However, the Th inhalation value, which was derived from the U value, would need to be adjusted (upward) accordingly, significantly altering the subsequent estimate of bone Th. However, measured Th-232 concentrations in surface air under arid conditions (11) do not suggest that the U-Th inhalation value is low. The daily U intake via ingestion (1.3 μg) appears to be a reasonable estimate since it is based on numerous studies in several countries (8).

The G.I. tract assimilation coefficient for natural U may be higher than the 1% assumed here. Two studies over a 3 year period on a number of Japanese hamlets (12,13) suggested that the amount of U excreted daily in the urine of the sampled population ranged from between 1 to 3% of the amount in the diet. Since both urine and feces are potential routes for excretion of assimilated U, the urinary data are minimum values for daily U assimilation assuming

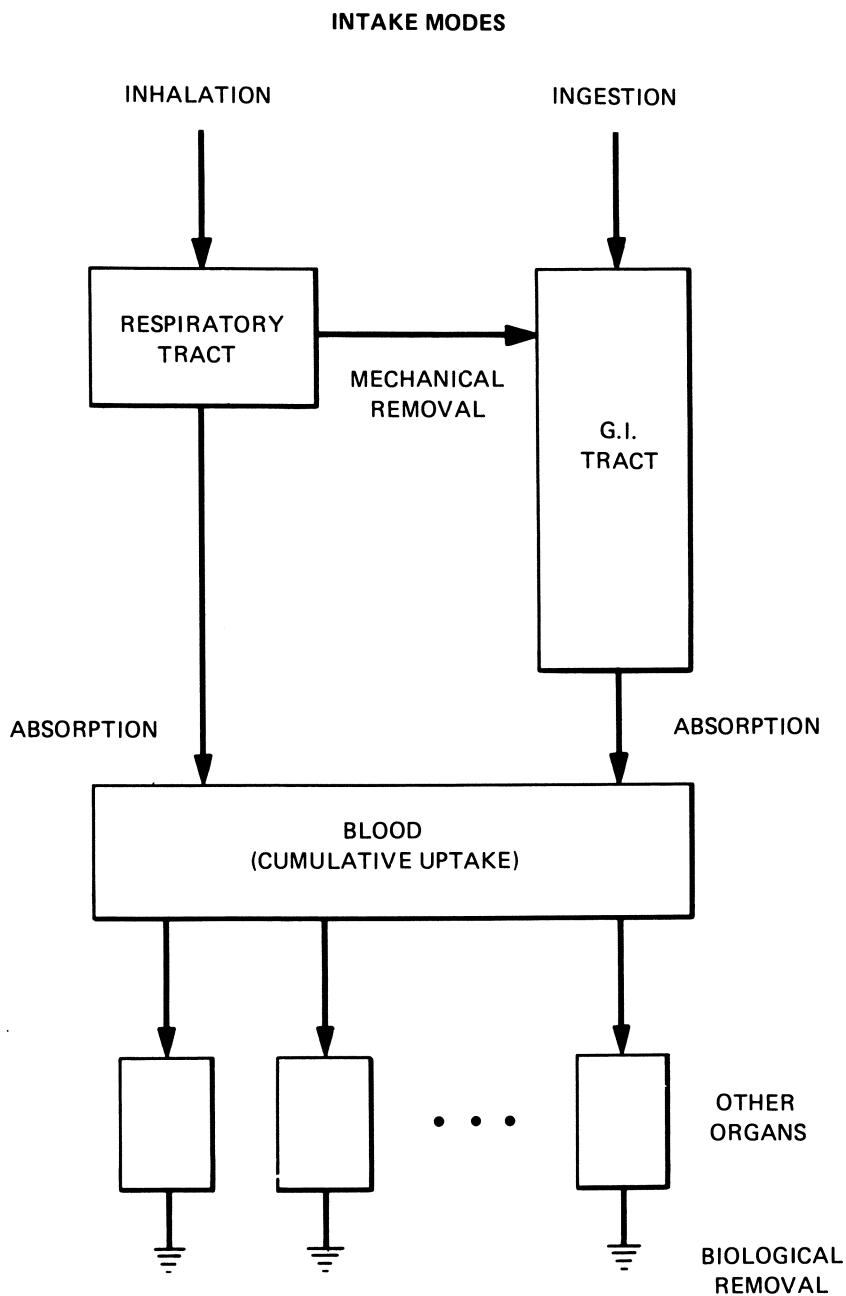


Figure 1. Schematic representation of radioactivity movement as modeled by the INREM II code

Table I. Estimated Th-232 and U-238 Contents of Human Bone Ash After 70 Years of Exposure to Naturally-Dispersed Th-232 and U-238 via inhalation and diet

Assumed Solubility Class [†]	Intake Mode		Bone ash, (ng/g)*
	Inhalation (ng/day)	Ingestion (μg/day)	
Thorium			
W • [Th(NO ₃) ₄]	21	0.8	13(3)**
Y • [ThO ₂ ; Th(OH) ₄]	21	0.8	9(3)
Uranium			
D • [UO ₂ (NO ₃) ₂ ; UO ₃]	7	1.3	1.0(0.8)**
W • [UF ₄ ; UCl ₄]	7	1.3	0.9(0.8)

*Literature mean is 12 ng Th/g bone ash; 1 to 30 ng U/g bone ash.

**Contribution from diet, assuming 0.1% (Th) and 1% (U) absorption, is shown in parenthesis.

[†]ICRP solubilities for inhaled aerosols incorporated into model; soil-bound element may not be similar.

that bone and other organs are at equilibrium with respect to U intakes.

A Site-Specific Application. Welford *et al* (14) have estimated the skeletal U content at 3.2 μg based on analyses of 63 vertebrae samples from New York residents. This U concentration is equal to about 1.1 ng/g bone ash, assuming 28% ash in the skeleton (10 kilograms) of reference man (15).

The agreement between the model results and the New York bone data is significant because the inhalation and ingestion parameters are from New York studies. Considering the apparent uniformity of dietary U contribution (8), reported U values of 20 to 30 ng/bone ash (2,8) appear high, suggesting that drinking water contributes significantly to U in some diets (14). Since a 1% G.I. tract assimilation coefficient (as used here) results in a good approximation of the New York bone values, the use of a 32% value (8) is questionable.

Modeling Conclusions. This exercise indicates that Th and U span the interface between the case where inhalation appears to dominate in the contribution of actinides in bone, and the case where ingestion is the more important pathway. The reasons for these differences lie in two important transfers: The soil/sediment to organism transfer (as it affects dietary concentrations) and the assimilation from the vertebrate GI tract. While terrestrial-derived foodstuffs dominate our diet, other components of the diet (i.e., aquatic-derived foods) may also make a contribution to intakes. Exceptions to the inhalation case may therefore occur in special populations where certain aquatic foods are consumed in greater amounts, i.e., shellfish (16).

In attempting to understand the biogeochemical behavior of the transuranium elements, it may be convenient to compare their behavior to U and Th. Although we have meager, but important, data on U and Th accumulations from lifetime exposure, our ability to assess transport pathways of transuranium elements to people will be enhanced if a body of comparative literature is established.

Plant Uptake of the Actinides

To the extent that diet contributes to internal body burdens, a comparison of the relative plant uptake of actinides from soil is of interest. Several studies have compared the uptake of various transuranium elements by plants (17,18,19). However, studies which include U and Th are not as available. Figure 2 presents recent results for field-grown vegetation of soil originally contaminated in 1944 with soluble forms of U, Th and Pu (and daughter Am) (20,21). The crops examined include soybeans, snapbeans, Japanese Millet, squash, tomatoes, carrots, and radishes. All plant samples were washed in a manner approximating food preparation (although the leaves and stems of these crops are not usually eaten). Data set 1 comes from a study of U, Th and Pu comparisons, while

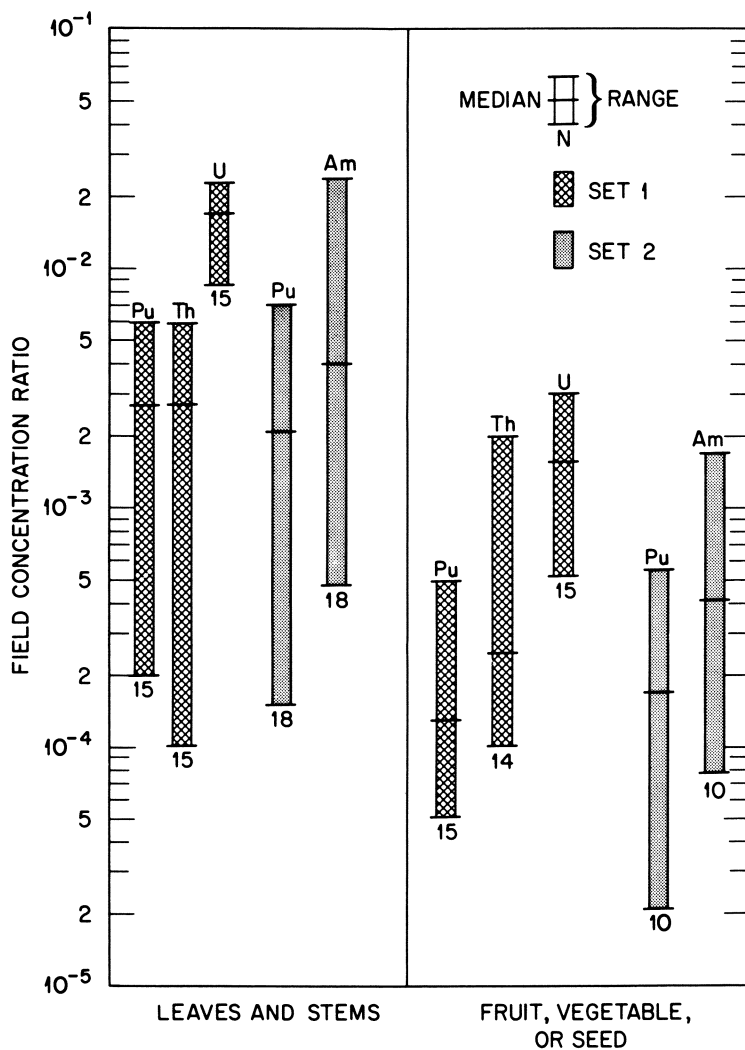


Figure 2. Actinide field concentration ratios ($[plant]/[soil]$) for plants grown on a floodplain soil contaminated with soluble U, Th, and Pu (Am) in 1944 (21). Up to six species were analyzed; N refers to total harvest composite samples examined from three growing seasons.

set 2 is derived from Pu and Am comparisons. Different analytical methods (isotope dilution mass spectrometry for Th and U; α -spectrometry for Pu and Am) are the reason for the separate groups of data. Each set represents analyses on the same plant materials. The number of samples analyzed (N) is found below each range bar. As illustrated by Figure 2, the relative order of plant uptake (based on concentration ratios, C.R.*) is $U > Am > Pu \approx Th$, although substantial overlap occurs. The ranges associated with each element C.R. primarily reflect plant species variation. The figure therefore represents a composite view of all plants analyzed, much as a value for diet would reflect its diverse constituents.

Not included in this example are Cm and Np. Curium is very similar to Am with respect to plant uptake (17,22). Neptunium represents a peculiar case since it can be argued that both Np(IV) and Np(V) are important oxidation states in the environment (20). Several investigators (17,19) have demonstrated that in alkaline soils, Np (probably Np(V)) shows a higher plant availability than either Pu or Am. On the other hand, our studies (unpublished) indicate that reduction to Np(IV) can occur in acid to neutral soils, resulting in plant uptake values characteristic of Pu. The high uptakes noted for alkaline soils (i.e., Np(V)) is probably due to the low charge characteristic of the NpO_2^+ cation, possibly coupled with the formation of a carbonate complex analogous to U(VI). The low specific activity of Np-237 and low nuclear production rates, however, minimizes its potential as a radiological hazard.

Based on an earlier hypothesis (20), we can expand the actinide ranking with respect to plant uptake to the following: $Np(V) > U(VI) > Am(III) \approx Cm(III) > Pu(IV) \approx Th(IV) \approx Np(IV)$. This ranking reflects the dominant chemical states we expect in the environment.

Comparative Terrestrial Transport of Actinides to Mammals

Actinides in soil reach people and other animals via inhalation of resuspended soil particles and ingestion of contaminated food. Absorption from the lung depends heavily on physical properties of the inhaled particles and the chemical form of actinides sorbed to particulates. As a rule, assimilation of actinides via inhalation is greater than assimilation from food via the intestines. For example, the absorption of Pu(IV) citrate and Pu(IV) nitrate from the rat lung was 60% and 12% of the administered dose, respectively, while the corresponding absorption via ingestion was 0.03% and 0.003% (23). Regardless of the pathway, animal experiments show that 75 to 100% of the internal Pu body burden is usually deposited in liver and skeleton (23). For long term assessments of health hazard to the general public from actinides in the terrestrial environment, we will initially emphasize ingestion as the route of

* C.R. = [plant (dry weight)]/[soil (dry weight)]

exposure to people because field studies show a decreasing susceptibility of plutonium-contaminated soil particles to resuspend with time, resulting in air concentrations over contaminated soil declining by half every one to two years (24). The extent to which ingestion will dominate inhalation depends on many factors, many of which have not been investigated. Since our previous example of U and Th transport to people gives some perspective on the relative importance of ingestion, attention to this pathway is justified.

Assimilation from the Gastrointestinal Tract. There are several sources of variation in the assimilation of actinides from the mammalian intestine. Among the most important are chemical form and age of the animal. The comparative metabolism of different actinides administered to rats as nitrates has been studied by Sullivan and Crosby (25,26). The consistency of experimental technique in their administration of actinides to adult and newborn rats permits comparisons between the assimilation of different actinides. The fractional assimilation, expressed as the amount in liver and carcass together, 7 days post-dose, was approximately 10^{-4} for isotopes of U, Pu, Am and Cm in adult rats. In young rats, the assimilation was about two orders of magnitude greater.

On a comparative basis, Pu, Am and Cm tend to be assimilated from the G.I. tract into the internal body in the following order: Pu < Am < Cm (Figure 3). When Pu-nitrate is inhaled in aerosol form by dogs (27), daughter Am-241 tends to be transported more from lung and lymph nodes to liver than does plutonium (Fig. 3). Another example of potential Am enrichment is that when the rumen contents of fistulated cattle grazing on the Nevada Nuclear Test Site were leached with simulated gastric fluids, Am-241 was more soluble than Pu-239 (28).

The administration of actinides in nitric acid solutions to animals lacks biological realism from the standpoint of food-chains. Uranium has been studied best in this regard. The calculated assimilation of U from food by domestic animals ranges from 0.6% in cattle (2) to 2% in swine (2). In people, estimated values for the assimilation of U from food vary from approximately 2% to 12% and 32% (2). These estimates are greater than the measured assimilation of nitrate forms and illustrate the errors which can be incurred by extrapolating data from rat experiments to man. In laboratory experiments, the chemical form which probably simulates the intake of actinides from natural foods best is citrate. This is because citric acid is a fundamental compound in plant metabolism. Baxter and Sullivan (29) have shown that when Pu is intragastrically administered to rats in citrate form, the assimilation is approximately 2×10^{-3} , about 2 orders of magnitude greater than assimilation of the nitrate form (1×10^{-5}). A more significant study (30), indicated that about 1% of plant (tumbleweed) incorporated Pu fed

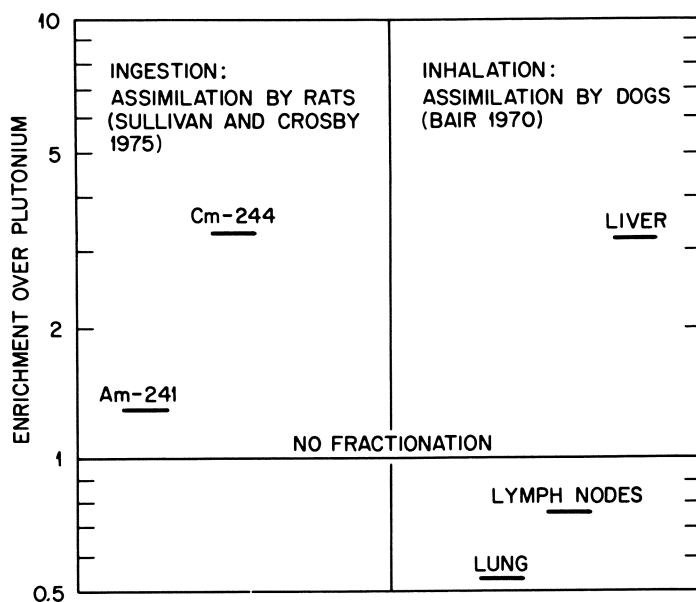


Figure 3. Enrichment of trivalent actinides over Pu(IV) across biological membranes. The assimilation of Am-241 and Cm-244 from the rat GI tract is greater than for plutonium. When plutonium nitrate is inhaled by dogs, daughter Am-241 is preferentially transported to the liver, resulting in depletion in lung and lymph nodes.

to rats was found in internal tissues 24 hours after feeding. However, Am and Cm uptake was lower than for Pu, possibly due to insoluble oxalates in the plant.

Field Studies. We have attempted to compare the relative availability of actinides to small mammals living in contaminated environments near ORNL. Shrews, rats and mice have been collected from a 30 year old contaminated floodplain forest ecosystem (21). Cotton rats (*Sigmodon hispidus*) have been collected from the banks of a former liquid radioactive waste pond which contains Pu, Am and Cu in sediments and shoreline vegetation. Analyses were performed by isotope dilution mass spectrometry (U, Th and Pu) or by alpha spectrometry (Pu, Am and Cm).

In shrews and mice, U tends to be more available than Pu or Th (Fig. 4). These comparisons are based on concentration ratios: the concentration of actinides in the internal body (bone, muscle and internal organs) of shrews, mice and rats ratioed to their respective concentrations in soil or sediment.

Due to differences in analytical technique, species differences, and different collecting sites, direct comparisons between the availability of Th, U and Am, Cm are not valid. However, Am and Cm tend to be more available than Pu to the rats examined (Fig. 4) although the differences are not significant when sample variability is considered. Evidence for Am enrichment in the field may in fact be totally obscured by biological variability. Field studies at the Nevada Test Site with cattle exemplify this problem. When 5 tissue types from up to 20 animals which had grazed on contaminated soil were examined for Pu and Am, Pu/Am ratios varied by almost 2 orders of magnitude (31).

The outstanding limitation of observations such as these which are based on field studies is the lack of control of animal exposure. Although laboratory experiments can be criticized for a lack of biological realism, they are more carefully controlled than observations based on animals collected under field conditions where accumulation is via inhalation as well as ingestion. By ratioing the concentrations in the body to soil concentrations, this analysis bypasses the question of whether inhalation or ingestion is the more important route of exposure.

Comparative Actinide Behavior in Aquatic Food Chains

The major repository of transuranic elements entering aquatic systems is the bed sediment (1-4). A significant portion is thought to arrive at the bed sediment surface as a result of association with, and subsequent settling of, suspended particulate matter. Concentrations of plutonium and americium in sediments relative to those in water reportedly range from 1×10^4 to 3×10^5 (32,33,34). Little information is currently available for other actinides of interest relative to nuclear fuel cycle wastes (Th, U, Cm and Np).

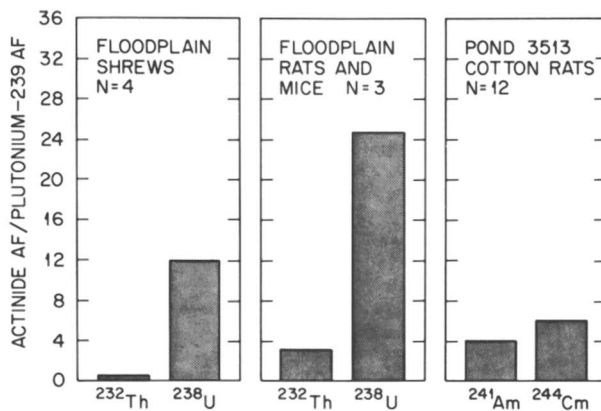


Figure 4. Comparative accumulation of actinides by small mammals from contaminated soil or sediment relative to the accumulation of plutonium-239. Accumulation factor (AF) = concentration of nuclide in the internal small mammal body \div concentration of nuclide in dry soil. Twelve shrews and seven rats and mice from a floodplain forest were composited to yield four and three separate analyses, respectively. Twelve cotton rats inhabiting the banks of a liquid waste pond (3513) also were analyzed.

Until relatively recently, data on aquatic food chain behavior of the actinides was relatively scarce. Recent reviews have pointed to the fact that most of the available information was limited to the marine environment (35,36). This is still the case for data on distribution of actinides in tissues of aquatic organisms, particularly vertebrates. The available data suggest that patterns are similar to those reported for terrestrial animals; highest concentrations were found in the gastrointestinal tract (G.I. tract) and mineralized tissues (bone and liver in vertebrates and shells and exoskeletons in invertebrates). Recent data from studies in fresh-water environments suggest that gills may contain an additional important component of the body burden for plutonium (37,38). Laboratory studies on the channel catfish using a Pu-237 tracer indicate that the G.I. tract skeleton, liver, and kidney should contain most of the body burden resulting from environmental exposure (39,40). Edible muscle has been found to contain the lowest actinide tissue concentrations (33,35,37,38,40,41) in aquatic organisms studied to date.

Surface Phenomena. Non-metabolic associations appear to play a major role in food chain behavior of the actinides (32-35,42). Noshkin (35) pointed out that marine organisms associated with the sediment-water interface contain 100 times higher plutonium burdens than marine free-swimming vertebrates. This has also been shown to be true for plutonium and americium in the vicinity of Windscale (33). Thus some association with the sedimentary actinide pool, whether by surface sorption to plant cell walls, exoskeletons, G. I. Tract linings, or perhaps by direct uptake from sediments (and associated interstitial water) consumed during feeding, is indicated in many instances. Laboratory gavage studies using Pu-237 fulvate (an organic chelating agent found in sediments) indicated that channel catfish could deposit a small (1×10^{-3}), but not insignificant, fraction of ingested plutonium into edible tissues (39). Plutonium-239 concentrations in chironomids (important fresh-water fish food organisms) held in simple laboratory environments (microcosms) were approximately 1×10^{-3} that of the sediments on which they fed (G.I. tract removed to eliminate external contamination) (43). When G.I. tract contents were included, the fraction present rose to 7% of the sediment concentration. Concentrations in emergent portions of aquatic plants have been shown to be an order of magnitude less than submerged plants in the same system (Pu-237 in complex laboratory microcosms, 42, and Pu-239 and Am-241 in field studies at Hanford's U-Pond (37)). Thus the sedimentary pool cannot be ignored as the potential direct source of actinide elements for a major fraction of the aquatic biota which reaches the human diet.

Transuranic elements (and other actinides) have a very high affinity for particulate matter (and surfaces in general) in aquatic ecosystems. It is difficult to use the traditional concentration ratio referenced to water (often assumed to be the source without support) as a measure of the tendency of biota to accumulate

these elements in tissues. As will be seen, concentration ratios based on water decline up the trophic ladder. This behavior, coupled with the known limited tendencies of the actinides to penetrate biological membranes, suggests that discrimination against actinide uptake occurs at each food chain transfer - leading to dilution of actinide concentrations the further along a food chain the element is transferred. We believe that it may be more useful to relate the observed concentrations of actinides in aquatic biota to that in the primary biotic source in the system: sediment (both suspended and bottom). The underlying hypothesis is that due to the high sediment concentration ratios relative to water, observed element accumulation in tissues of higher trophic levels will be dominated by G. I. tract discrimination rather than by direct uptake from water. External contamination on surface and G. I. tract loadings with sedimentary particulates are not considered to be true uptake and should be considered separately. This may be considered analogous to contamination of the pelt and G. I. tract by soil activity in terrestrial mammals.

Comparative Actinide Behavior. The data from existing fresh-water actinide radioecology studies have been digested and condensed for presentation in Tables II (radium and uranium) and III (transuranics). Information on thorium in fresh-water environments is extremely fragmented; hence its omission. Concentration ratios were calculated and averaged for relatively broad ecological groups in order to facilitate generalized comparisons between data from different water bodies and between different elements. There are rather apparent gaps in existing data sets (ours included) which make some comparisons difficult. Concentration ratios have been calculated relative to both sediment and water wherever existing data permitted.

Environmental studies on the behavior of actinide elements in fresh-waters have been conducted at a variety of sites throughout the world. These range from large, deep natural lakes, such as Lake Michigan and Lakes Issyk-kul and Sevan in the Soviet Union, to relatively small, shallow ponds (Pond 3513, former final radioactive waste settling basin at Oak Ridge National Laboratory (ORNL) and U-Pond, on the Hanford Reservation) and impoundments (White Oak Lake at ORNL and those at the Jaduguda uranium mining and milling complex, Bihar, India). Higher actinide concentrations are observed in the aquatic environments at nuclear fuel cycle facilities, while the levels in the natural lakes are extremely low by comparison, derived primarily from weapons-testing fallout and natural sources. Lake Issyk-kul has been intensively studied because its watershed lies in an area whose soils have a naturally high uranium content.

Some generalizations are applicable to virtually all data sets presented. As noted earlier, concentration ratios decline with increasing trophic level: herbivores < littoral flora; piscivores < planktivores < zooplankton < phytoplankton. Perhaps

Table II. Radium and Uranium Concentration Ratios in Fresh-Water Organisms
 Referred to Both Sediment and Water*

Organism	India (43,44,45)		U.S.S.R. (41,47,48)	
	Jaduguda Mine Area	Lake Michigan (34)	Lake Issyk-Kul	Moscow Ponds
	238U			
	226Ra			
Phytoplankton		(2.2)		
Zooplankton		(1.4)	-0.8 (1.9)	
Littoral Flora	-0.3 (3.4)	(1.6)	-0.1 (2.6)	
Littoral Fauna	-3.1 rice			
Vertebrates-herbivores	-1.9 rice	(0.7)	-1.1 (1.6)	
bone	(1.6)		-1.2 (1.5)	(2.0)
muscle	(1.8)		-1.4 (1.3)	(2.7)
-planktivores	-2.1 (1.6)		-3.3 (-0.6)	
bone	-2.9 (0.8)	(1.0)		(0.4)
-piscivores		(-0.4)	-1.8 (0.9)	(0.8)
		(-0.3)		

*Expressed as the \log_{10} [organism (dry wt.)]/[sediment, water] to facilitate comparisons; values based on water shown in parentheses.

Table III. Transuranic Concentration Ratios in Fresh-Water Organisms Referenced to Both Sediment and Water*

Organism	Lake Michigan (34,49)		Oak Ridge National Laboratory Pond 3513		White Oak Lake		Lake Michigan (34,39)		Hanford U-Pond (37,50)	
	241Am		244Cm		239Pu					
Phytoplankton	-2.2(4.1)		-1.1(3.4)	-1.5(2.3)	-1.8(3.7)		-1.5(4.0)		-0.3	
Zooplankton	-3.4(2.9)		-1.8(2.7)	-1.7(2.1)	-2.0(3.5)	-1.4(3.0)	-3.0(2.5)		-0.7	
Littoral Flora	-2.1(4.2)	-0.4	-1.9(2.6)	-2.0(1.8)	-2.0(3.5)	-1.5(2.9)	-1.8(3.7)		-0.8	
Littoral Fauna	-2.4(3.9)	-0.3	-2.7(1.8)	-3.0(0.8)	-3.4(2.1)		-2.3(3.2)		-0.9	
Vertebrates-herbivores		-1.0							-1.5	
bone										
muscle		-2.3								-3.1
-planktivores	<-4.1(<2.2)									-4.1(1.4)
-piscivores	<-4.6(<1.7)									-4.9(0.6)

*Expressed as the \log_{10} [organism (dry wt.)]/[sediment, water] to facilitate comparisons; values based on water in parentheses.

because of the surface contamination/GIT loading problems alluded to previously, differences between the littoral flora and fauna are not always apparent. However, in our experience, when such contributions are taken into account, trophic level differences between littoral organism groups are readily apparent (51). Concentration ratios for zooplankton from shallow aquatic systems are higher than corresponding values from large, deep lakes (trivalent actinides in Pond 3513 vs. Lake Michigan and plutonium in Pond 3513 and U-Pond vs. Lake Michigan in Table III, for example) because of a closer association with sedimentary particulates. The utility of calculating a concentration ratio relative to the sediment values is also seen. Concentration ratios calculated on this basis are less than unity, declining by approximately an order of magnitude with each intervening trophic step. Since actinides are only poorly transferred across biological membranes, i.e., discriminated against in transfers, these values seem to provide a more realistic description of actinide behavior in food chains. Further, ratios (based on radioactivity concentrations) of the trivalent actinides to plutonium in sediments (or interstitial water) are much closer to the same quotients in biota than are the corresponding ratios in water from Hanford's U-Pond (37,52) and ORNL's Pond 3513. Thus Am/Pu (biota) or Cm/Pu (biota) are closest in value to the same ratios calculated for sediment than for water. For Hanford's U-Pond, Am/Pu (biota) Am/Pu (sediment or interstitial water) ranges from 1.7 to 2.8; the same value for water ranges from 0.002-0.003. The ratios of Cm/Pu in Pond 3513 biota (primarily invertebrates and plants) average about 2.5:1, the sediment mean is 0.8:1, however, the corresponding water value is 40:1. Thus, it appears that a sound basis exists for presentation of actinide concentration ratios calculated relative to a sedimentary source rather than water.

Comparisons between the relative availability of the actinide elements are not as obvious. Data for more than one element are not often available from the same environment and there exist numerous gaps in data sets, particularly for higher vertebrate trophic levels. Comparisons between trivalent actinide concentration ratios in zooplankton and herbivorous vertebrates from Pond 3513 at ORNL vs. corresponding values for plutonium (Table III) indicate higher availability for Am and Cm by factors of 2 to 5. Comparisons between ^{241}Am and ^{239}Pu ratios from Hanford's U-Pond suggest higher availability for Am by factors of 3 to 5. Comparisons between ^{241}Am and ^{239}Pu based on Lake Michigan data (Table III) are inconclusive due to limited information, but suggest no substantial differences (e.g., order of magnitude) between the two elements.

Uranium and Radium vs. Transuranics

Data bases for the naturally-occurring actinides, ^{226}Ra and ^{238}U , are more fragmentary. Thus, one has to make some assumptions in order to attempt a meaningful comparison between the

availability of the natural actinides and the transuranic elements. Using the data set for Lake Issyk-kul (most complete, Table II), uranium appears to be more available than the transuranics in all systems save the Hanford U-Pond, an environment which appears to have unusually elevated concentrations. If the Lake Michigan data set is used, uranium appears less available than the transuranics, but the differences would probably be much smaller if sediment concentration ratios were available. This is a consequence of the greater solubility of uranium (also radium) than the transuranics, particularly under the slightly alkaline conditions found in most fresh-water environments. If whole-body concentration ratios in herbivorous vertebrates are used as an estimate of the tendency of the actinides to deposit in bone tissue, then uranium appears to be more available than the transuranics (save ^{241}Am in U-Pond). This assumption is probably reasonable since whole-body concentration ratios for U in vertebrates (Table II) are comparable to those for bone tissues. This should also be the case for the transuranic elements since, as we observed earlier, the major fraction of the body burden resides in the skeleton and other mineralized tissues. The limited data for ^{226}Ra (Table II) appear to fall within reported values in data sets for the transuranics (Table III). In the one instance where radium uptake may be directly compared with uranium, i.e., the data for rice in Table II, radium is apparently less available. Because of the limitations presented by the data sets on natural actinides, our conclusion about biological availability relative to the transuranic elements must be conservative. We believe that, when more information on relative actinide availability in fresh-water environments is obtained, uranium may be shown to be more available than the transuranics generally, but that substantial differences in the reverse direction are not likely. Based on the information provided by the present data sets, we can suggest the following scheme for relative actinide bio-availability:
 $\text{U} > \text{Am}, \text{Cm} > \text{Pu}.$

An indication of what one might eventually expect to obtain for a generalized pattern of relative bio-availability for the actinides of interest in nuclear fuel cycles is shown in Table IV. This represents a recent data set in which concentration ratios have been obtained for all five actinides in tissues of a vertebrate (used as human food) from a single aquatic ecosystem (Pond 3513 at ORNL); comparisons are thus facilitated. The values for bone (Table IV) suggest a pattern of bio-availability as follows: $\text{U} > \text{Am}, \text{Cm} > \text{Th}, \text{Pu}$. Taken in its entirety, the data set in Table III indicates essentially the same pattern.

Exposure Pathways to People: Summarizing Importance

From the preceding sections, the greater tendency for U to transfer to both people and small mammals when compared to Pu, Th, Am and Cm is evident. Availability comparisons for vertebrates in

Table IV. Comparisons of the Actinide/Pu Concentration Ratios in the Bullfrog (*Rana catesbeiana*) from Former Waste Settling Basin at Oak Ridge National Laboratory

Specimen	$^{239,240}\text{Pu}^*$	$^{238}\text{U}/\text{Pu}$	$^{241}\text{Am}/\text{Pu}$	$^{244}\text{Cm}/\text{Pu}$	$^{232}\text{Th}/\text{Pu}$
immature-carcass without G.I. tract	1.9×10^{-3}	8.1	5.0	3.0	0.32
adult- bone (male)	2.6×10^{-4}	40.0	3.3	3.8	0.42
bone (female)	7.0×10^{-5}	64.0	1.9	1.2	2.7
muscle (male)	2.5×10^{-4}	7.4	7.8	3.7	5.7
muscle (female)	1.0×10^{-4}	30.0	4.9	6.0	3.0

*Concentration in tissue (ash wt.) \div Concentration in sediment (ash wt.). Plutonium determined by both mass spectrometry and solvent extraction-alpha spectrometry techniques; Th and U by mass spectrometry, and Am and Cm by solvent extraction-alpha spectrometry.

aquatic food chains, although more limited, suggest no substantial alteration in this pattern. For natural Th and U, ingestion is the dominant environmental route to people, although not necessarily the important contributor of internally-deposited elements. A similar statement can be made for fallout Pu since atmospheric testing has almost ceased (16).

Both Pu and Th will probably enter the skeleton and other internal tissues predominantly from inhalation. This statement is based on the fact that in the field, Pu and Th demonstrate similar transfers from soil to small mammals and laboratory studies demonstrate similar metabolic characteristics (1,3,23). Soil chemical behavior is also similar (20). As demonstrated in Table I, natural Th in human bone originates largely from inhalation, even assuming that adsorption from the diet is 0.1%. Another strong argument for the importance of inhalation is found in tissue distributions of Th-232 and Th-230 in humans. Table V summarizes work by Wrenn, et al. (53) which shows that lungs of non-occupationally exposed individuals contains burdens of Th isotopes comparable to the skeleton. Thorium-228 distributions are different from Th-230, 232 distributions and reflect assimilation of parent Ra-228 from the diet.

As the relative transfer coefficients from soil to plants and from diet to the blood increase, ingestion takes on more importance. This certainly appears to be the case for U. It may be that ingestion will be more important for Am and Cm than for Pu or thorium. Neptunium remains in enigma because of the paucity of data.

Table V. Distributions of Th-232, Th-230, and Th-228 in selected non-occupationally exposed human organs*

Organ	Distribution (%)**		
	Th-232	Th-230	Th-228
Lung	20	21	1.8
Lymph nodes	6	6	0.7
Spleen, liver, kidney	13	17	2.6
Skeleton	62	56	94.9

* After Wrenn, et al. (53).

** Median values for 5 individuals normalized to standard man masses.

Assessing Hazards of Environmentally-Dispersed Actinides to People

The U.S. Environmental Protection Agency has proposed that "The annual alpha radiation dose rate to members of the critical segment of the exposed population as the result of exposure to transuranium elements in the general environment should not exceed either 1 millirad per year to the plumonary lung, or 3 millirad per year to the bone" (54). The USEPA also derived a soil contamination level of $0.2 \mu\text{Ci}/\text{m}^2$ (1 cm depth, soil particles less than 2 mm) as a reasonable "screening" level for which the resultant dose rates to the critical segment of the exposed population could be reasonably predicted to be less than the guidance recommendations.

Current estimations of dose rates to critical organs from environmentally-dispersed transuranics rely on environmental transport and metabolic models (9,15,54). The rather short time period that these elements have been in the biosphere (from the activities of people) makes validation of environmental transport models extremely difficult. To approximate the maximum possible lifetime accumulation in the skeletons of people exposed to actinides in the general environment, one approach would be to use a bone/soil accumulation factor. A principal advantage of this method is that it is independent of the exposure pathway. However, it assumes that aquatic components of the diet are insignificant, and thus would not apply to circumstances where only sediments are contaminated. Bone is a critical tissue because the deposition of actinides in bone is initially high after entry into the bloodstream, and retention times are long. For example, in rats more than 70% of the body burden is found in the skeleton 16 days after oral administration of Pu-citrate or Pu-nitrate (23). The Cm content of rat bone, 256 days after intramuscular injection, was 20 times greater than the amount in any other internal tissue excluding the injection site (54). Approximately 81% of the $86.3 \mu\text{g}$ of natural U estimated to be in man is in the skeleton (56).

Of the actinides we have considered here, only U comes to equilibrium in bone in man's lifetime (3). The amount of Pu, Th, Am, Cm and Np in human bone continually accumulates. Because of this, the bone/soil ratio is time dependent. However, it is interesting to note that existing data sets on Th-232 (57,58) in human bone do not show a strong age-dependent trend. This probably reflects the diversity of inhalation exposures people are subject to.

Bone-Soil Ratios. In man, the typical concentration of natural U in bone has been considered to be about 20 ng/g bone ash (8) although a comprehensive data set (10) suggests a substantially lower value (1 ng). Thorium is present at concentrations near 10 ng/g bone ash. The concentration of U and Th in terrestrial soils is approximately 2 and 6 $\mu\text{g}/\text{g}$ respectively (2,4,5). The calculated adult human bone ash/soil ratio for U is therefore greater than that for Th (Table VI). This comparison is consistent with observed differences in the accumulation of U

and Th in small mammals (Fig. 4) and frogs (Table IV).

For purposes of comparison, the bone/soil ratio has been calculated for Th, U, and Pu in small mammals collected from the previously mentioned contaminated floodplain forest near ORNL. A bone/soil ratio for Am was also calculated from published data (59). These ratios are listed in Table VI. The variability around the average ratios in small mammals is great with coefficients of variation near unity. Nevertheless, the relative ranking of average values indicates the following order of availability: $Pu \sim Th < Am < U$ for small mammals.

Table VI. The accumulation of actinides by small mammals and man from soil expressed as the concentration ratio of element in internal small mammals bodies (skeleton and internal organs) or the concentration in human bone ash to a measured soil concentration. Thorium, U, Pu data from ORNL floodplain studies; Am data from (59). Human data calculated from information in (2).

Group	Nuclide	N ^a	Average	CV ^b
Small mammals	Th	7	0.0003	0.66
	U	7	0.004	0.92
	Pu	7	0.0003	0.83
	Am	2	0.001	0.80
People	Th	1	0.002	—
	U	1	0.01	—

^aNumber of values averaged.

^bCV = standard deviation ÷ average

From the calculated bone/soil ratios in man for the naturally-occurring actinides as well as the laboratory and field studies on small mammals, the availability of Pu, Am, and Cm relative to U and Th can be deduced. First, the field studies indicate a similar degree of uptake by mammals for Pu and Th (Fig. 4, Table VI) which are both characterized by the tetravalent state in the terrestrial environment (20). Second, the trivalent actinides, Am and Cm, tend to exhibit similar (Fig. 3) or slightly greater (Fig. 4) uptake by mammals than Pu. Last, U exhibits consistently greater uptake in mammals than Th or Pu (Fig. 4, Table VI). On the basis of available data, the following rank order of bone ash/soil ratios for

people might be used for evaluating lifetime accumulation:

$$\begin{array}{l} \text{Th, Pu} < \text{Am, Cm} < \text{U} \\ 0.002 \quad 0.005 \quad 0.01 \end{array}$$

This ranking suggests that about 2.5 times as much Am and Cm may accumulate in bone than Pu or Th assuming identical chemical and physical forms in the soil. Uranium may show about a 5-fold greater relative accumulation.

Estimating Dose to Bone from Chronic Exposure. Using these accumulation factors, the maximum amount of Pu, U, and Am in bone after 70 years exposure to soil contaminated at the proposed EPA screening level might be estimated. Since Pu-238 and U-232 contribute the most α -activity in breeder fuels (U-233 and Pu-239), they were chosen for dose comparisons. For a soil with a bulk density of 1.3 g/cm³, 0.2 $\mu\text{Ci}/\text{m}^2$ (1 cm depth) corresponds to about 15 pCi/g soil (top 1 cm). Using the 0.002 accumulation factor for Pu and the reference man value of 54% ash in bone (as differentiated from skeleton), the lifetime accumulation of Pu is calculated to be 0.016 pCi/g in situ bone. Assuming uniform distribution in bone and converting the activity concentration to dose (3) results in a dose rate for Pu-238 of about 1.7 mrad/year. This estimate, which is based on an independent methodology, suggests that the proposed EPA soil screening level is not unreasonable if the projected dose rate to bone is not to exceed 3 mrad/year.

The same exercise applied to an identical U-232 activity concentration in soil would result in 0.08 pCi/g bone or 8.2 mrad/year contribution from U-232 alone. This value may be high considering the uncertainties of what the typical natural U content of bone is. However, the α -emitting daughters of U-232 (Th-228, Ra-224, Rn-220, and Po-216) would raise this dose rate by about a factor of 4 (60). If the estimate of the trivalent actinide bone ash/soil accumulation factor is valid, then 15 pCi Am-241/gram of soil would contribute 0.04 pCi/g bone and a 4 mrad/year dose rate at age 70. Because Am-241 may accumulate in the skeleton to a greater degree than Pu, it would be a greater contributor of transuranic activity to bone even though its activity level in soils contaminated with Pu-239, 240, etc., may be lower. The physical form of the Pu will be very important in this instance. For example, lung inhalation data has shown little Am-241 enrichment from inhaled PuO₂ but substantial enrichment from Pu-nitrates.

Summary. Through an examination of the comparative behavior of the actinide elements in terrestrial and aquatic food chains, the anticipated accumulation behavior of the transuranium elements by people was described. The available data suggests that Pu, Am and Cm will not accumulate to a greater degree than U in the skeletons of individuals exposed to environmentally dispersed activity. The nature of the contamination event, the chemical and physical associations in soils and sediments, the proximity to the

contamination site - all will influence observed behavior.

Because of the establishment of regulatory guidelines for limiting chronic exposure to transuranium elements, research on environmental behavior must address the question of accumulation by people. In the absence of lifetime accumulation data and the paucity of contaminated sites, approaches such as those documented in this paper may aid in understanding and evaluating the hazards of releasing actinide elements to the biosphere.

Literature Cited

1. Durbin, P. W., *Health Phys.*, (1960), 2, 225-238.
2. Bondietti, E. A., Garten, C. T., Jr., Francis, C. W. and Eyman, L. D. *J. Environ. Qual.* (1979), in press.
3. Wrenn, M. E., International Symposium on Areas of High Natural Radioactivity, T. L. Cullen and E. Penna Franca, (Eds.), pp. 131-158, Academia Brasileira de Ciencias, 1975.
4. Beninson, D. J., Bouville, A., O'Brien, B. J., and J. O. Snihs, *Ibid*, pp. 75-106.
5. Klement, A. W., Jr., *Radioactive Fallout, Soils, Plants, Foods*, Man, E. B. Fowler (Ed.), pp. 113-156, Elsevier, New York, 1965.
6. Bowen, H. J. M., *Trace Elements in Biochemistry*, pp. 39-40, Academic Press, New York, 1966.
7. Killough, G. G., Dunning, D. F., Jr., Plesant, J. C., ORNL/NUREG/TM/84, National Technical Information Service, 1978.
8. Hursh, J. B. and Spoor, W. L., *Uranium, Plutonium, Transplutonia Elements*, H. C. Hodge, J. N. Stannard, and J. B. Hursh (Eds.), pp. 197-239, Springer-Verlag, New York, 1973.
9. International Commission on Radiological Protection, ICRP Publication 19, Pergamon Press, Oxford, May 1972.
10. Welford, G. A. and R. Baird, *Health Phys.*, (1967) 13, 1321-1324.
11. Thomas, C. W., Young, J. A., BNWL-1751 (pt. 2), pp. 42-45, National Technical Information Service, 1973.
12. Yamamoto, T., Yunoki, E., Yamakawa, M., Shimizu, M. and Nukada, K., *J. Radiat. Res.*, (1974), 15, 156-162.
13. Masuda, K., *Japanese J. Hyg.*, (1971), 26.
14. Welford, G. A., Baird, R., Fisenne, I. M., in *Proc.*, 12th Mid-year Topical Symposium, Health Phys. Soc., Saratoga, New York, 1976.
15. International Commission on Radiological Protection, ICRP Publication 6, Pergamon Press, Oxford, 1964.
16. Bennett, Burton, G., IAEA-SM-199/40, pp. 367-383, IAEA, Vienna, 1976.
17. Price, Keith, R., BNWL-1688, Battelle Northwest Laboratory, Richland, Wash., Oct. 1972.
18. Adams, W. H., Buchholz, J. R., Christenson, C. W., Johnson, G. L., and Fowler, E. B., LA-5661, Los Alamos Scientific Laboratory, Los Alamos, New Mexico, 1975.
19. Schreckhise, P. G., Cline, J. F., Abstract P/184, Twenty-Third Annual Health Physics Society Meeting, 1978.

20. Bondiotti, E. A. and Sweeton, F. H. Transuranics in Natural Environments, (NVO-178), M. G. White and P. B. Dunaway (Eds.), pp. 499-476, National Technical Information Service, 1977.
21. Dahlman, R. C. and McLeod, K. W., Transuranics in Natural Environments," (NVO-178), M. G. White and P. B. Dunaway (Eds.), pp. 303-320, National Technical Information Service, 1977.
22. Weimer, W. C., Laul, J. C., Kutt, J. C., Bondiotti, E. A., in Proceedings, Third International Conference on Nuclear Methods in Environmental and Energy Research, 1978, in press.
23. Durbin, P. W., Health Phys., (1975), 29, 495-510.
24. Volchok, H. L., Schonberg, M., Toonkel, L., Health Phys., (1977), 33, 484-485.
25. Sullivan, M. F. and A. L. Crosby, BNWL-1950 (Pt. 2), pp. 105-108, 1975.
26. Sullivan, M. F. and A. L. Crosby, BNWL-2000 (pt. 1), pp. 91-94, National Technical Information Service, 1976.
27. Bair, W. J., BNWL-1221, pp. 7.7-7.10, National Technical Information Service, 1970.
28. Barth, J., Transuranics in Natural Environments (NVO-178), M. G. White and P. B. Dunaway, (Eds.), pp. 419-434, National Technical Information Service, 1977.
29. Baxter, D. W., and Sullivan, M. F., Health Phys., (1972), 22, 785-786.
30. Ballou, J. E., Price, K. R., Gies, R. A., Proctor, P. G. Health Phys., (1978), 34, 445-450.
31. Smith, D. D., Bernhart, D. E., Transuranics in Desert Ecosystems, (NVO-181), M. G. White, P. B. Dunaway, Wireman, (Eds.), National Technical Information Service, 1978.
32. Eyman, L. D., and Trabalka, J. R., Transuranics in Natural Environment, (NVO-178), pp. 477-488, Nevada Applied Ecology Group, Las Vegas, Nevada (1977).
33. Hetherington, J. A., Jefferies, D. F., Mitchell, N. T. Pentreath, R. J., and Woodhead, D. S., IAEA-SM-199/11, pp. 139-153, IAEA, Vienna, 1976.
34. Wahlgren, M. A., Alberts, J. J., Nelson, D. M., and Orlandini, K. A., IAEA-SM-199/144, pp. 9-23, IAEA, Vienna, 1976.
35. Noshkin, V. E., Health Phys., (1972), 22, 537-549.
36. Hanson, W. C., Health Phys., (1975), 28, 529-537.
37. Emery, R. M., Klopfer, D. C., and Weimer, W. C., BNWL-1867, Battelle Northwest Laboratory, Richland, Wash., 1974.
38. Alberts, J. J., Bartett, G. E., and Wayman, C. W., ANL-78-88, Part III, pp. 40-42, 1976.
39. Eyman, L. D. and Trabalka, J. R., Health Phys., 32 (1977), 475-478.
40. Trabalka, J. R., Eyman, L. D., Bergman, H. L., and Frank, M. L., Health Phys., (1978), in press.
41. Kovalsky, V. V., Voronitskaya, I. Ye., and Lekarev, V. S., USAEC Conf. Proc., CONF-660405, pp. 329-332, 1966.
42. Trabalka, J. R. and Eyman, L. D., Health Phys., (1976), 31, 390-393.

44. Viswanathan, R. Bhatt, Y. M. Sreekumaran, C., Doshi, G. R., Cogate, S. S., Bhagwat, A. M., and Unni, C. K., *Indiana Acad. Sci.*, (1966), 64B, 301-313.
45. Iyengar, M. A. R. and Markose, P. M., *USAEC Conf. Proc.*, CONF-701227, pp. 143-153, 1970.
46. Markose, M. P., Eappen, K. P., Venkataraman, S., and Kamath, P. R., *Proceedings, Third International Symposium on the Natural Radiation Environment*, Houston, Texas, April 23-28, 1978, in press.
47. Kovalsky, V. V. and Voronitskaya, I. Ye., *Geochem. Internat.* (1965), 2, 544-552 (Engl. Translation of *Geokhimiya*).
48. Kovalsky, V. V. and Voronitskaya, I. Ye., *Ukr. Biokhim, Zh.*, (1966), (4), 419-424.
49. Edgington, D. N., Alberts, J. J., Wahlgren, M. A., Karttunen, J. O., and Reeves, C. A., *IAEA-SM-199/47*, 493-516, IAEA, Vienna, 1976.
50. Emery, R. M., Klopfer, D. C., and McShane, M. C., *Health Phys.*, (1978), 34, 255-269.
51. Auerbach, S. I., *et al.*, ORNL-5257, pp. 66-67, Oak Ridge National Laboratory, Oak Ridge, Tennessee, 1977.
52. Healy, J. W., Eyman, L. D., and Trabalka, J. R., *Transuranic Uptake by Aquatic Organisms, (Appendix I) in an Examination of Possible Limits for the Shallow Earth Burial of Transuranic Wastes*, Los Alamos Scientific Laboratory, Los Alamos, New Mexico, in press.
53. Wrenn, M. E., Singh, N. P., Ibrahim, S. A. Cohen, N., Saccomanno, G., in *Proc. Third International Symposium on the Natural Radiation Environment*, Houston, Texas, April 23-28, 1978, in press.
54. United States Environmental Protection Agency, EPA 520/4-77-016, USEPA, Washington, D. C., 1977.
55. Scott, K. G., Axelrod, D. J., Hamilton, J. G., *J. Biol. Chem.*, (1949), 177, 325-335.
56. Hamilton, E. I., *Health Phys.* (1972), 22, 149-153.
57. Lucas, H. F., Edington, D. N., Markum, F., *Health Phys.*, (1970). 19, 739-742.
58. Clifton, R. J., M. Farrow, Hamilton, E. I., *Ann. Occup. Hyg.* (1971), 14 303-308.
59. Bradley, W. G., Moor, K. S. Naegle, S. R., *Transuranics in Natural Environments, (NVO-178)*, M. G. White and P. B. Dunaway (Eds.), pp. 385-406, National Technical Information Service, 1977.
60. Till, J., ORNL/TM-5049, National Technical Information Service, 1976.

RECEIVED January 16, 1979.

Radionuclide Sorption Studies on Abyssal Red Clays¹

KENNETH L. ERICKSON

Sandia Laboratories², Albuquerque, NM 87185

In order to provide data required by the U.S. Seabed Disposal Program to assess the feasibility of emplacing radioactive wastes in sub-seafloor geologic formations, the radionuclide sorption properties of a widely distributed abyssal red clay are being experimentally investigated. These properties are extremely important and should be investigated in detail since the adequacy of the sediment to serve as a barrier to the migration of nuclides away from the waste form should largely be determined by the sorption behavior of those nuclides. In this regard, sorption of the actinide elements is generally considered to be of principal concern. However, before pursuing an extensive experimental program involving the actinides, a preliminary investigation was conducted to examine the sorption of several nuclides having relatively much less complicated solution chemistries. The generalizations being developed to describe the sorption of the preliminarily investigated nuclides will then be used in planning an efficient program for investigating the sorption and complex chemistry of the actinide elements.

In most mathematical analyses used to establish bounds for radionuclide migration rates through the abyssal red clays, the sorption properties of the sediment are generally represented mathematically by the sorption equilibrium distribution coefficients for each of the species involved. These coefficients are usually denoted by K_{D_i} and are defined by

$$K_{D_i} = \bar{C}_i / C_i$$

where \bar{C}_i = the equilibrium solid-phase concentration of species i , mg-atom/gm

¹ This work supported by the United States Department of Energy (DOE), under Contract AT(29-1)-789.

² A U.S. DOE facility.

C_i = the equilibrium solution-phase concentration of species i , mg-atom/ml

For a given material, the distribution coefficients are functions of temperature, pressure, the concentration of species i , and the concentrations of all other competing species.

In the sediments being studied, it is believed that nuclide migration away from the waste form will primarily be due to molecular diffusion. The simpler mathematical analyses of diffusion which yield analytical solutions show that, to a first approximation, the migration rate of species i should generally be inversely proportional to the magnitude of K_{D_i} (1). Hence, the adequacy of the sediment to serve as a barrier to nuclide migration depends, in an inversely proportional manner, on the values of the various distribution coefficients, which, depending on species and conditions, could be expected to vary from near zero to 10^5 ml/gm or greater.

Therefore, the preliminary investigation described herein examined several aspects of the behavior of the equilibrium distribution coefficients for the sorption of rubidium, cesium, strontium, barium, silver, cadmium, cerium, promethium, europium, and gadolinium from aqueous sodium chloride solutions. These solutions initially contained one and only one of the nuclides of interest. For the nuclides selected, values of K_{D_i} were then determined as functions of the concentration of species i in the equilibrium solution and to a limited extent as functions of solution pH. The data used to calculate the values for K_{D_i} were obtained from batch equilibration experiments. The experimental procedures used are discussed later and were considered to be such that the values obtained for the various distribution coefficients provided a reasonable representation of the sorption properties of the sediment at locations sufficiently distant from the waste form so that the clay remains physically and chemically essentially unaltered.

Red Clay

Samples of the red clay having uniform physical and chemical characteristics were provided by G. R. Heath of the University of Rhode Island. The samples were obtained from core LL44-GPC-2, collected on October 11, 1976, at $30^\circ 20.9'N$, $157^\circ 50.85'W$, water depth 5821 meters, and are representative of the smectite-rich region of the red clays which occurs in the sediment at depths below about ten meters. In this region, the sediment appears to contain about five to six percent by weight leachable iron and manganese in the form of hydrous oxides. The remaining material appears to be dominated by iron-rich smectite and lesser, varying amounts of phillipsite (2). The results of a semi-quantitative (precision in data is within a factor of 2) elemental analysis

performed on the red clay (by emission spectroscopy) are given in Table I.

Table I. Semi-quantitative Analysis of Red Clay
(Done by Emission Spectroscopy)

Element	Concentration	
	(ppm)	(mg-atom/gm)
Rb	80	0.0009
Sr	810	0.0092
Ba	630	0.0046
Na	810	0.035
K	13000	0.33
Ca	10000	0.25
Mg	25000	1.0
Fe	63000	1.1
Mn	13000	0.24
Al	81000	3.0
Si	160000	5.7
Li	16	0.023
Ni	1300	0.022
Cu	1600	0.025
Ti	3300	0.069
Cr	130	0.0025
V	250	0.0049
Zr	200	0.0022
Be	50	0.0056

The nature of the solid-phase concentrations of rubidium, strontium, and barium given in Table I are of some concern since those concentrations must be appropriately accounted for when distribution coefficients and solution-phase concentrations are calculated from experimental data. Since the average concentrations (given in Table II) of rubidium, strontium and barium in seawater are relatively substantial, the concentrations given in Table I could certainly be the solid-phase concentrations of rubidium, strontium and barium which are in sorption equilibrium with the concentrations of the respective elements in the original interstitial seawater.

Table II. Average Concentrations of Rubidium, Strontium and Barium in Seawater (3)

Element	Average Concentration in Seawater
	(mg-atom/ml)
Rb	2.4×10^{-6}
Sr	1.5×10^{-4}
Ba	3.6×10^{-7}

The concentrations of rubidium, strontium and barium given in

Table I could also represent the presence of salts of those elements. However, for the reasons given below, it was concluded that the solid-phase concentrations of rubidium, strontium and barium were probably the result of sorption rather than the presence of salts

The principal rubidium salts which would probably have been present in the sediment (chloride, sulfate, bicarbonate, etc.) are all soluble in water. As discussed later, the red clay was thoroughly dialyzed prior to use (including prior to analysis by emission spectroscopy). Any rubidium salts initially present in the clay samples would, therefore, have been removed by the dialyzing solution. Hence, it was assumed that the rubidium concentration given in Table I represented sorbed rubidium which had been in equilibrium with the rubidium in the original interstitial seawater. Then when calculating distribution coefficients from experimental data, the concentration given in Table I was used as the initial clay-phase rubidium concentration, rather than zero as used with most of the other species studied.

Many of the principal compounds of strontium and barium which could have been present in the sediment are also soluble in water, but the carbonates and sulfates are relatively insoluble. In solutions of low ionic strength the solubility product constants for strontium carbonate and sulfate are 1.1×10^{-10} and 3.2×10^{-7} , respectively, and for barium carbonate and sulfate are 5.1×10^{-9} and 1.1×10^{-10} , respectively (4). Again, any soluble salts should have been removed by the dialyzing solution. Furthermore, when the dialyzing solution from the first dialysis was concentrated by a factor of about one hundred, no precipitate was observed. After the first dialysis, the carbonate concentration in the dialyzing solution should have been sufficiently small (due to the near-neutral conditions existing in the solution) so that the corresponding saturation concentrations of strontium and barium should have been large enough to yield noticeable precipitates when the solution was concentrated. However, the sulfate concentration (resulting from the sulfate in seawater) was probably sufficiently large so that only the corresponding saturation concentration of strontium would have been great enough to yield a noticeable precipitate. Therefore, the bulk dialyzing solution was probably undersaturated with respect to strontium carbonate and sulfate and with respect to barium carbonate. Since each dialysis was conducted for at least twenty-four hours, and the dialysis bags were only about two centimeters in diameter, the concentrations of nonsorbing species in the interstitial and bulk dialyzing solutions should not have been greatly different. Hence, the interstitial solution was also probably undersaturated, and any strontium initially present as a carbonate or sulfate and any barium present as a carbonate should have been removed by the dialyzing solution or sorbed by the clay (due to the favorable equilibria for strontium and barium sorption, which are discussed later). The dialyzing

solution from the next to last dialysis was concentrated by a factor of about twenty and did not yield a noticeable precipitate. The sulfate concentration (as a result of the sulfate in seawater) in that solution should have been sufficiently small so that the corresponding saturation concentration of barium would have yielded a noticeable precipitate. The bulk dialyzing solution and the interstitial solution were, therefore, probably undersaturated with respect to barium sulfate. Then after the last dialysis, the maximum interstitial solution-phase concentration of barium sulfate was probably much less than 10^{-5} mg-atom/ml. Since the ratio of the volume of interstitial solution to mass of clay was on the order of 5 ml/gm, the maximum concentration of barium sulfate which should have been possible in the dried solid would have been on the order of only 10^{-5} mg-atom/gm, which is considerably less than the barium concentration given in Table I. It was, therefore, assumed that the strontium and barium concentrations given in Table I represent sorbed strontium and barium which had been in equilibrium with the strontium and barium, respectively, in the in situ interstitial seawater or which had been sorbed during dialysis. Again when calculating distribution coefficients from experimental data, the concentrations given in Table I were used as the initial clay-phase strontium and barium concentrations, rather than using a value of zero.

Experimental

It was felt that the presence of residual salts in the clay would complicate the analysis of experimental data. Therefore, in order to remove such salts prior to using the clay, the samples of sediment were dialyzed (using deionized water) until a twenty-fold concentration of the dialyzing solution did not yield a precipitate upon addition of silver nitrate. (Also, no precipitate was observed upon concentration of the solution.) The solids were then dialyzed once more, vacuum dried, and stored in sealed containers in a desiccator until needed. (The preceding procedure may have resulted in some alteration of the sorption properties of the red clay, particularly with regard to the hydrous oxides. It is intended to assess the extent of such alteration, if any, during the course of future work.)

As discussed later, it was suspected and later experimentally determined that cation exchange is a major mechanism responsible for radionuclide sorption. Therefore, the cation-exchange capacity of the clay (defined here as the total milliequivalents of exchangeable cations per gram of clay) was evaluated using both cesium and barium exchange. (For a given species, the cation-exchange capacity of the clay should be reasonably constant, independent of solution-phase concentrations of that species, as long as the physical and chemical characteristics of the solid remain unaltered, particularly the charge distribution which determines the nature of the electrical double layers in the

regions of the solid-liquid interfaces.)

The cation-exchange capacity for cesium was determined from the isotopic redistribution of Cs^{137} between 0.01 M CsCl solutions and cesium-saturated clay. The cesium-saturated clay was prepared by contacting 0.25 to 0.55 grams of clay with 50 to 100 ml of 1.0 M CsCl solution (stable Cs). After allowing sufficient time for equilibration (48 to 96 hours), the original 1.0 M solution was reduced to 0.01 M by repeated centrifuging of the suspension followed by decanting of the supernatant and then diluting of the remaining solution. An appropriate amount of Cs^{137} was then added to the suspension, and 3.0-ml samples were periodically removed and analyzed for Cs^{137} (by gamma counting) until isotopic redistribution of the cesium isotopes was apparently complete. Then, for reasonably complete isotopic redistribution, the distribution coefficient calculated for Cs^{137} (from the change in the solution-phase concentration of Cs^{137}) should have been essentially the same as the distribution coefficient for both stable and radioactive cesium. Also since the solution-phase concentration of Cs^{137} was much less than the concentration of stable Cs and since the clay was saturated with cesium, the cation-exchange capacity for that element should be equal to its solid-phase concentration (which should have remained essentially constant upon dilution of the CsCl solution) and was calculated from

$$\text{Cs Exchange Capacity} = K_{D_{\text{Cs}^{137}}} \times 0.01 \text{ mequiv/ml}$$

The cation exchange capacity for barium was determined in an analogous manner.

The data used to calculate the values of K_{D_i} for each nuclide studied were obtained from batch equilibration experiments in which 0.68 N NaCl solutions (or occasionally other solutions) having various concentrations of the nuclide of interest were contacted with the red clay at 4°C (occasionally at 11°C) and ambient pressure. The 0.68 N NaCl solutions were used instead of artificial seawater in order to provide somewhat simpler systems for study. A temperature of 4°C was generally used since this is approximately the ambient temperature in the sediment. Since sorption phenomena are generally little affected by pressure, it further was assumed that any effects due to differences between the pressure on the seafloor and the ambient laboratory pressure would generally be small. (The validity of this assumption should be verified, and it is intended to do so during future experimentation.)

The general procedure for the batch equilibration experiments was as follows. About 0.25 to 0.55 grams of clay and 45 to 70 ml of 0.68 N NaCl solution were added to a 125-ml polyethylene bottle. Next 2.5 ml of a 0.68 N NaCl solution, buffered with predetermined amounts of sodium bicarbonate and/or boric acid, were added. (In order to obtain data at low values of the solution pH, addition

of the buffer was omitted and 0.25 ml of 1.0 N HCL was added to the bottle.) The pH buffering or adjustment was followed by addition of 2.5 ml of a 0.68 N NaCl solution containing predetermined amounts of stable and/or radioactive isotopes of the nuclides of interest. (The radioactive isotopes used were Cs¹³⁷, Sr⁸⁵, Ba¹³³, Eu¹⁵², Gd¹⁵³, Pm¹⁴⁷, Ce¹⁴⁴, and Ag^{110m}.) The polyethylene bottles were then placed in a shaker bath maintained at 4 ± 1 or 11 ± 1 °C. Samples were then periodically removed for analysis by atomic absorption (only stable isotopes present) or by gamma or beta counting. Samples were removed until the analyses indicated that the solution-phase concentration of the nuclide was no longer changing with time. The sampling procedure consisted of allowing the clay to settle from suspension and then removing a liquid sample (of known volume) which was filtered through a 0.2 μ m Gelman filter. At the conclusion of several of the equilibration experiments, samples of the solid were removed and analyzed for the nuclide of interest. For each such experiment, the nuclide concentration associated with the solid generally accounted for the change in nuclide concentration observed in the solution. The relative difference between the total amount of nuclide determined as lost from solution and the total amount determined as gained by the solid was usually less than $\pm 10\%$. Also, for most nuclides and most sets of experimental conditions, "blank" experiments were conducted in order to determine if nuclides were lost from solution due to phenomena other than sorption by the clay. The "blank" experiments were done similarly to the sorption experiments (to include sample removal and analysis) except that the clay was omitted.

For reasons given later, it was believed that the hydrous iron and manganese oxides in the sediment were of major importance in determining the sorption properties of the clay. As an initial attempt to assess the significance of those hydrous oxides, equilibration experiments were performed in which, to the extent possible the hydrous iron and manganese oxides were removed from the clay. The method used for removing the hydrous oxides was that recommended by Mehra and Jackson (5), and involved a reduction-complexation-extraction process (using a dithionite-citrate-bicarbonate solution) followed by washing and centrifuging of the solid. The procedure removed about ten percent by weight of the solids, the remaining portion of which was green colored. Hereafter, the samples prepared using the above method are generally referred to as "deferrated."

Results and Discussion

General. The abyssal red clays were, in part, originally selected for study because previous investigations of their sorption properties had been encouraging (6,7), and because generally the types of minerals occurring in the sediment exhibit very favorable ion-exchange and adsorption properties. In

particular, the ion-exchange equilibria associated with smectite minerals (which constitute a major portion of the sediment) have been found to show strong preferences for cesium, strontium, barium, yttrium, and cerium (8-13). These equilibria, at least in the case of cesium, appear to depend little on pH in the range of 3 to 10 (7,11). Also, the smectites generally have relatively large ion-exchange capacities, on the order of 0.8 to 1.5 milliequivalent per gram (14). Furthermore, hydrous iron and manganese oxides (which constitute a reasonably significant portion of the sediment) have been found to strongly adsorb strontium, barium and various transition metals (15,16,17). It has also been proposed that these hydrous oxides control the concentrations of cobalt, nickel, copper and zinc in soils and fresh water sediments (18). The adsorption equilibria associated with the hydrous iron and manganese oxides have been found very dependent on solution pH (15,16,17), and ion exchange has been suggested as one of the dominating sorption phenomena. The sorption capacities of the hydrous oxides are also dependent on pH and appear to be considerably less than the capacities of the smectite minerals (17,19).

Therefore, based on available literature, the following sorption results were expected: (1) as a result of the smectite minerals, the sorption capacity of the red clay would be primarily due to ion exchange associated with the smectites and would be on the order of 0.8 to 1.5 milliequivalents per gram; (2) also as a result of the smectite minerals, the distribution coefficients for nuclides such as cesium, strontium, barium, and cerium would be between 10 and 100 ml/gm for solution-phase concentrations on the order of 10^{-3} mg-atom/ml; (3) as a result of the hydrous oxides, the distribution coefficients for nuclides such as strontium, barium, and some transition metals would be on the order of 10^4 ml/gm or greater for solution-phase concentrations on the order of 10^{-7} mg-atom/ml and less; (4) also as a result of the hydrous oxides, the solution-phase pH would strongly influence the distribution coefficients for most nuclides except the alkali metals; (5) as a result of both smectites and hydrous oxides being present, the sorption equilibrium data would probably reflect the influence of multiple sorption mechanisms. As discussed below, the experimental results were indeed similar to those which were expected.

Sorption Capacity. The average sorption capacity of the clay determined from isotopic redistribution of Cs^{137} between aqueous 0.01 M CsCl solutions and cesium-saturated clay was 0.91 mequiv./gm. The average sorption capacity similarly determined by isotopic redistribution of Ba^{133} was 0.74 mequiv./gm. The maximum relative error in these capacities was estimated at $\pm 10\%$.

If those sorption capacities were due to ion exchange, it would be expected that preparation of the cesium- and barium-saturated clays would have caused various counter ions such as those of sodium, potassium, magnesium, and calcium to be desorbed from the clay and to appear in the 1.0 M solutions. The total

amount of desorbed species (in milliequivalents) per gram of solid should be approximately equal to the measured ion exchange capacities. Furthermore, since the clay had been extensively dialyzed before use, the amounts of any salts of sodium, potassium, magnesium, and calcium which might have been present should have been negligible (for reasons similar to those given when discussing salts of rubidium, strontium, and barium), and it is reasonable to expect that the concentrations given for those elements in Table I represent concentrations of exchangeable counterions or (especially in the case of magnesium) constituents of the clay mineral lattices. The amount of each desorbed species (in mg-atoms) per gram of clay should then be approximately equal to the corresponding concentrations given in Table I. Such behavior was, in fact, observed experimentally as discussed below.

When preparing the cesium- and barium-saturated clays, the 1.0 M solutions used were decanted (after centrifuging) and analyzed semiquantitatively by emission spectroscopy. From those analyses, it appears that the following species were desorbed: sodium, potassium, calcium, magnesium, and strontium. It further appeared that desorption of potassium was almost unique to cesium sorption; whereas, desorption of the other species appeared to be common to both cesium and barium sorption. Small amounts of other elements such as nickel and copper were also detected by the analyses. However, to what extent the observed concentrations may represent desorption and to what extent they may represent the dissolution of sparingly soluble substances (particularly hydroxide species) is as yet uncertain. The apparent concentrations of the desorbed species per gram of clay are given in Table III.

Table III. Apparent Concentrations of Desorbed Species

Element	Concentration	
	(mequiv./gm)	(mg-atom/gm)
K (Cs sorption)	0.21	0.21
K (Ba sorption)	0.01	0.01
Na	0.06	0.06
Ca	0.44	0.22
Mg	0.11	0.06
Sr	0.02	0.01
Total (Cs sorption)	0.84	
Total (Ba sorption)	0.64	

For both cesium and barium sorption, there is reasonable agreement between the total concentrations of desorbed species and the ion-exchange capacities determined by isotopic redistribution. The small differences which exist could easily be due to the precision in the elemental analyses. (Also, the experimental technique would not have detected desorption of hydrogen ions.) The solid-phase concentrations of sodium, potassium, magnesium, calcium,

and strontium from Tables I and III are compared in Table IV.

Table IV. Comparison of Initial Solid-Phase Concentrations and Solid-Phase Concentrations of Desorbed Species

Element	Solid-Phase Concentration (mg-atom/gm)	
	Initial (Table I)	Desorbed (Table III)
K (Cs sorption)	0.33	0.21
Na	0.04	0.06
Ca	0.25	0.22
Mg	1.0	0.06
Sr	0.01	0.01

In the case of potassium (cesium sorption), calcium, and strontium, the agreement is fairly good and in the case of sodium, somewhat poorer but well within the precision of the analyses. In the case of magnesium, the agreement is very poor. However, the magnesium concentration given in Table I could, to a large extent, be due to incorporation of magnesium into the lattice structure of the clay minerals (20). Therefore, at solution-phase concentrations (on the order of 10^{-4} mg-atom/ml or greater) at which the solid-phase concentration of the nuclide of interest would be a significant fraction of the sorption capacity of the clay, it appears reasonable to conclude that sorption does result from ion exchange. The extension of this conclusion to lower solution-phase concentrations at which the solid-phase concentration of the nuclide of interest would be a negligible fraction of the ion-exchange capacity of the clay may or may not be justified.

The ion-exchange capacities discussed above (and the identification of the principal desorbing species) appear consistent with capacities of about 0.4 to 0.8 mequiv./gm (principal desorbing species being sodium, potassium, calcium and magnesium) reported for a related pacific red clay (7). The sorption capacities given above also appear reasonably consistent with capacities of about 0.8 to 1.5 mequiv./gm, which have been reported for related clay minerals found within the continental United States (8,9,10,12,14).

Distribution Coefficients. The distribution coefficients determined for rubidium (at 11°C) and for cesium (at 11°C for $-\log C_i$ less than 5 and at 4°C for $-\log C_i$ greater than 5) are summarized in Figure 1. Over the range of solution-phase concentrations in which both rubidium and cesium were studied, the rubidium coefficients appear to behave very similarly to those for cesium. For solution-phase concentrations on the order of 10^{-3} mg-atom/ml, the coefficients are on the order of 100 ml/gm, as was expected. Furthermore, the distribution coefficients obtained for cesium generally appear consistent with the corresponding coefficients obtained for similar oceanic sediments and related clay minerals found within the continental United States (6,7,8,9,10,12,13). In the pH range of 6.3 to 8.0, the cesium coefficients appear to

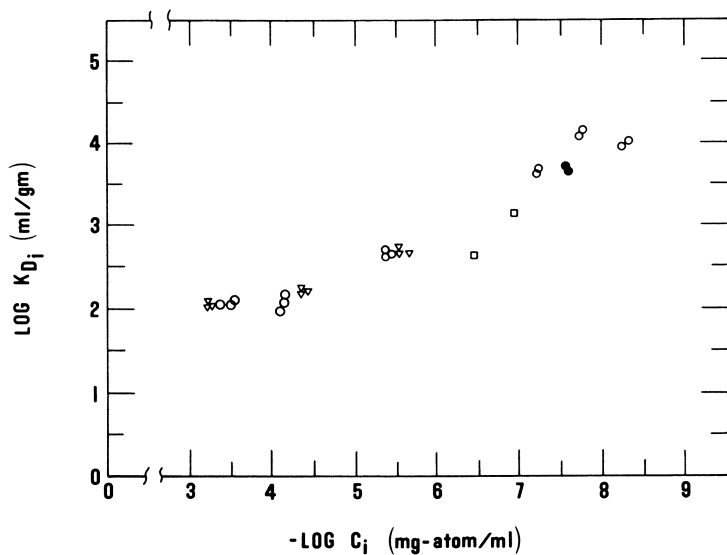


Figure 1. Distribution coefficients for Cs and Rb in 0.68N NaCl solutions: (□), Cs (pH 6.5, deferrated); (●), Cs (pH 2.7); (○), Cs (pH 6.3-8.0); (▽), Rb (pH 7.0-7.6).

increase rather gradually as the solution-phase concentration decreases from about 3×10^{-4} to 3×10^{-6} mg-atom/ml. The coefficients then undergo a fairly sharp increase as the concentration decreases from 3×10^{-6} to about 3×10^{-8} mg-atom/ml and then appear to be approaching constant values as the solution-phase concentration decreases further. Also, lowering the solution pH to 2.7 and treating the clay to remove hydrous iron and manganese oxides do not appear to greatly affect the cesium distribution coefficients. (Furthermore, the coefficients for cesium at $-\log C_i$ of about 4.1 were obtained from desorption data and appear consistent with the other coefficients obtained from sorption data.)

The sharp increase observed in the distribution coefficients for cesium between concentrations of about 3×10^{-6} and 3×10^{-8} mg-atom/ml suggests that sorption of cesium may result from at least two different mechanisms. If so, apparently one mechanism dominates at lower solution-phase nuclide concentrations (on the order of 3×10^{-6} mg-atom/ml or less) because of a relatively much more favorable equilibrium constant for the corresponding sorption phenomena. However, this mechanism has a relatively small sorption capacity which essentially becomes exhausted at higher solution-phase concentrations. The other mechanism involves a relatively less favorable equilibrium constant, but has a relatively much greater sorption capacity and, therefore, dominates at higher solution-phase concentrations. The mechanism dominating at higher concentrations is probably an ion exchange phenomena having a sorption capacity essentially equal to that which was determined by isotopic redistribution of Cs^{137} . The mechanism dominating at lower concentrations may or may not be an ion-exchange phenomena. Furthermore, the fact that solution pH and removal of hydrous oxides do not appear to appreciably affect the cesium distribution coefficients suggests that both mechanisms are associated with the silicate phases (rather than at least one mechanism being associated with the hydrous iron and manganese oxides.)

The distribution coefficients determined for strontium (at $4^\circ C$) and for barium (at $11^\circ C$ for $3.0 < -\log C_i < 4.5$ and at $4^\circ C$ for all other values of $-\log C_i$) are summarized in Figure 2. Due to the relatively high concentration of strontium in seawater (and hence the relatively high concentration initially in the clay-phase) only limited data for strontium were obtained. The distribution coefficients which were obtained appear to behave similarly to the respective coefficients for barium but are somewhat smaller in magnitude. For solution-phase concentrations on the order of 10^{-3} mg-atom/ml, the barium coefficients appear to be between 10 and 100 ml/gm, and for solution-phase concentrations on the order of 10^{-7} , the barium coefficients appear to be on the order of 10^4 , as was expected. Furthermore, the coefficients for both strontium and barium are generally consistent with the corresponding data obtained for similar oceanic sediments and related clay minerals found within the continental United States (6,7,8,13). The

distribution coefficients for barium increase steadily as the solution-phase concentration decreases from about 10^{-2} to about 10^{-7} mg-atom/ml. At solution-phase concentrations of about 10^{-4} mg-atom/ml, there appears to be little difference between the barium distribution coefficients at pH 2.6 and those at pH 7.0 and greater. However, at concentrations less than 10^{-5} , the distribution coefficients at pH 2.6 are significantly reduced relative to the coefficients at pH 7.0 and greater. (No appreciable dissolution of the hydrous oxides was observed at pH 2.6.) Also, the chemical removal (to the extent possible) of the hydrous iron and manganese oxides appears to have drastically reduced the (deferrated) distribution coefficients (at values of C_i of about 10^{-7} mg-atom/ml) relative to the coefficients for untreated clay. Furthermore, it appears that the effect of low pH and hydrous oxide removal are similar, since the data for both situations appear to nearly lie along the same horizontal line. (However, such close agreement may be fortuitous.) These results seem reasonable. The isoelectric points determined for hydrous iron and manganese oxides are generally on the order of pH 4 or greater, although lower pH values have been reported (17,21). Therefore, at a solution pH of 2.6, the hydrous iron and manganese oxides would probably have lost their cation-exchange capacity, and the net result of a low solution pH would be similar to chemically removing the hydrous oxides. (Also, the coefficients for barium at $-\log C_i$ of about 4.1 were obtained from desorption data and appear consistent with the other coefficients calculated from sorption data.)

The strong dependence (at lower solution-phase nuclide concentrations) of the distribution coefficients on solution pH and on the removal of the hydrous iron and manganese oxides suggests the existence of at least two separate sorption mechanisms. Again, apparently one mechanism dominates at lower solution-phase nuclide concentrations (probably on the order of 10^{-3} mg-atom/ml or less) because of a relatively much more favorable equilibrium constant for the corresponding sorption phenomena. However, this mechanism has a relatively small sorption capacity which essentially becomes exhausted at higher solution-phase concentrations. The other mechanism involves a relatively less favorable equilibrium constant but has a relatively much greater sorption capacity and, therefore, dominates at higher solution-phase concentrations. The mechanism dominating at higher concentrations is probably an ion-exchange phenomena which is associated with the silicate phases and which has a sorption capacity essentially equal to that which was determined by isotopic redistribution of Ba^{133} . The mechanism dominating at lower concentrations is probably an ion-exchange or other sorption phenomena which is associated with the hydrous iron and manganese oxides.

Finally, as discussed below, the clay-phase concentrations given for strontium and barium in Table I appear to provide a very limited "field verification" of the strontium and barium

distribution coefficients obtained experimentally. It was mentioned previously that when the values of C_i and K_{D_i} shown in Figure 2 were calculated, the initial clay-phase concentrations given in Table I were used. For convenience below the concentrations and coefficients so calculated have been referred to as "corrected." For each set of corrected values of C_i and K_{D_i} given in Figure 2, a corresponding set of "uncorrected" values of C_i and K_{D_i} were also calculated using the same experimental data but assuming an initial clay-phase concentration of zero. Some typical uncorrected values of C_i and K_{D_i} and the corresponding values from Figure 2 are shown in Table V.

Table V. Uncorrected Versus Corrected Values of C_i and K_{D_i} .

Element	Uncorrected Data		Corrected Data (Figure 2)	
	$-\log C_i$	$\log K_{D_i}$	$-\log C_i$	$\log K_{D_i}$
Sr	4.28	1.85	3.97	1.85
	5.40	2.11	4.36	2.11
Ba	4.15	2.39	4.15	2.49
	8.06	4.09	6.12	4.09
	9.01	4.23	6.57	4.23

The data for barium corresponding to the value of $-\log C_i$ (uncorrected) of 4.15 was obtained from changes in solution-phase concentrations determined by atomic absorption. The uncorrected value of C_i is, therefore, the best available value for C_i and was used in Figure 2. However, the uncorrected value of K_{D_i} does not account for any barium initially present in the clay-phase and should represent the minimum value which the distribution coefficient would have. All other data given in Table V were obtained from changes in solution-phase concentrations of radioactive tracers (determined by gamma counting). Assuming reasonably complete isotopic redistribution, the experimental data should have given the distribution coefficients for all strontium or barium present, both that initially in the clay-phase and that which was subsequently sorbed from solution. The uncorrected values of K_{D_i} obtained from the experimental data should, therefore, be the best available values for K_{D_i} and were used in Figure 2. But, the values of C_i calculated only from changes in solution-phase concentrations would be less than or equal to the actual values of C_i when strontium or barium was initially present in the clay. The uncorrected values of C_i should, therefore, represent minimum values for the actual solution-phase concentrations.

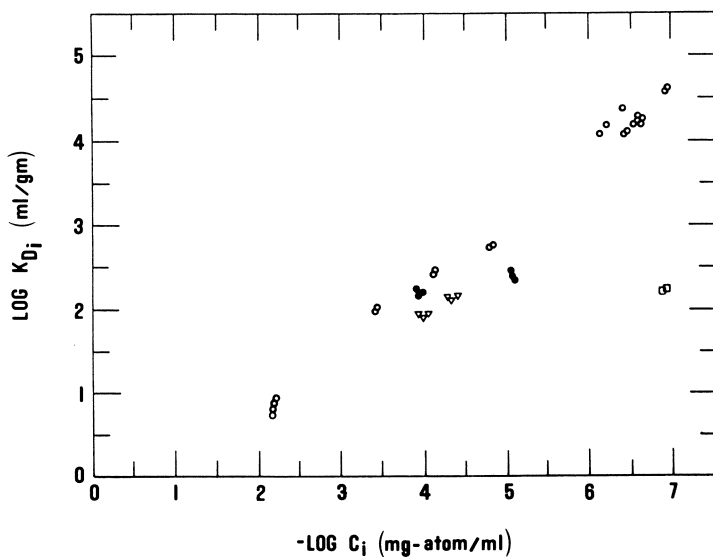


Figure 2. Distribution coefficients for Sr and Ba in 0.68N NaCl solutions: (□), Ba (pH 8.3, deferrated); (●), Ba (pH 2.6); (○), Ba (pH 7.0-8.1); (▽), Sr (pH 7.1-7.3).

The average concentrations of strontium and barium in seawater are 1.5×10^{-4} mg-atom/ml ($-\log C_i = 3.82$) and 3.6×10^{-7} mg-atom/ml ($-\log C_i = 6.44$), respectively. For strontium (referring to Table V) the minimum value of $\log K_{D_i}$ corresponding to a solution-phase concentration of 1.5×10^{-4} would be about 1.74 (obtained by linear extrapolation of the uncorrected data), and the maximum value of $\log K_{D_i}$ would be about 1.85. Therefore, the clay-phase strontium concentration which would be in equilibrium with the average concentration of strontium in seawater would be about 10^{-2} mg-atom/ml, which is very nearly the clay-phase concentration given in Table I. For barium, the minimum value of $\log K_{D_i}$ corresponding to a solution-phase concentration of 3.6×10^{-7} would be about 3.4 (obtained by linear interpolation between uncorrected data), and the maximum value of $\log K_{D_i}$ would be about 4.1. Therefore, the clay-phase barium concentration which would be in equilibrium with the average concentration of barium in seawater would be between about 0.001 and 0.004 mg-atom/ml, which is in reasonable agreement with the clay-phase concentration given in Table I. Assuming that the average concentrations given for strontium and barium in seawater are not greatly different from the concentrations of those elements in the in situ interstitial seawater, then the concentrations given in Table I appear to be in reasonable agreement with the concentrations of strontium and barium which the experimentally determined distribution coefficients indicate would be in sorption equilibrium with the in situ interstitial seawater. Therefore, to a limited extent, the data given for strontium and barium in Table I appear to provide a "field verification" of the strontium and barium distribution coefficients which were obtained in the laboratory.

The distribution coefficients determined for cadmium (at 11°C) are given in Figure 3. The coefficients appear somewhat less than the corresponding data for strontium and barium. Such results could be due to either anionic complex formation (22) and/or a less favorable sorption equilibrium.

The distribution coefficients evaluated for silver (at 4°C) are also given in Figure 3. The silver coefficients determined in 0.68 N NaCl solutions are somewhat less than the corresponding coefficients for cesium and rubidium, and also for strontium and barium. Such results are probably due to either anionic complex formation (22) and/or a less favorable sorption equilibrium. (Furthermore, the experiments done using silver in sodium chloride solutions required equilibration times on the order of 90 days, as opposed to two to four days for most other experiments, and it appears that processes, which may or may not be important, are involved which are not understood.)

In order to obtain a better understanding of the behavior of silver, distribution coefficients were evaluated using deionized water and 0.68 N NaNO_3 solutions. The coefficients obtained from

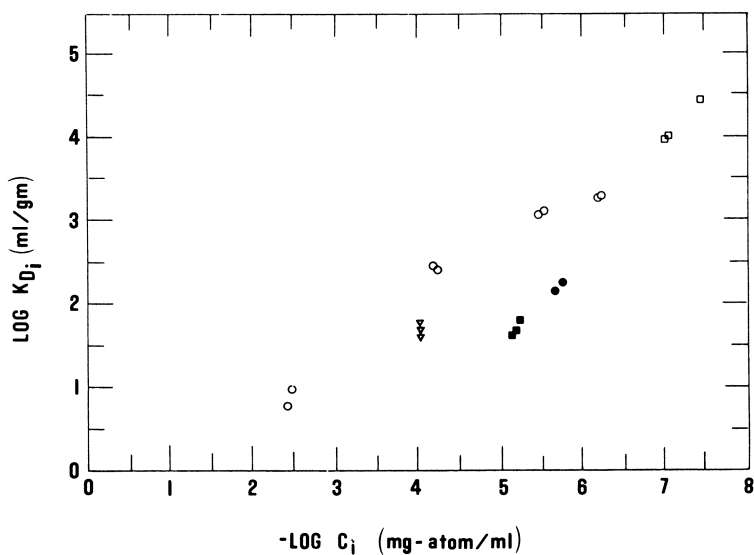


Figure 3. Distribution coefficients for Ag and Cd in various solutions: (○), Ag (0.68N NaNO₃, pH 6.8-7.8); (●), Ag (0.68N NaNO₃, pH 3.3); (□), Ag (deionized H₂O, pH 7.3); (■), Ag (0.68N NaCl, pH 7.3); (▽), Cd (0.68N NaCl, pH 5.3).

the limited experiments done using deionized water indicated that, at least under certain conditions, very favorable equilibria for the sorption of silver could be obtained. A more extensive series of experiments using the sodium nitrate solutions was, therefore, conducted. The distribution coefficients obtained for silver in 0.68 N NaNO_3 solutions are similar in magnitude to the corresponding coefficients for rubidium and cesium and for strontium and barium in 0.68 N NaCl solutions and are significantly greater than the coefficients for silver in 0.68 N NaCl solutions. (Also, the experiments done using deionized water and 0.68 N NaNO_3 solutions required equilibration times of only about two to four days.) Therefore, it appears that the relatively low silver distribution coefficients obtained using sodium chloride solutions were probably due to the existence of competing reactions for the formation of anionic complexes. The coefficients for silver in sodium nitrate solutions also show a strong pH dependence and generally appear to behave similarly to barium (rather than cesium and rubidium) in sodium chloride solutions except that the silver coefficients appear to be approaching a constant value of about 2000 ml/gm as the solution-phase concentration decreases below about 10^{-6} mg-atom/ml. The strong influence of pH suggests the existence of at least two separate mechanisms for silver sorption, which are probably essentially the same as those discussed for barium. Furthermore, the fact that silver appears to behave more like barium than rubidium or cesium tends to indicate that sorption equilibria are determined by the type of cation and the electrical configuration of the cation as well as by the electrical charge of the cation.

The distribution coefficients obtained for the lanthanides cerium, promethium, europium, and gadolinium (at 4°C) are summarized in Figures 4 and 5. For solution-phase concentrations on the order of 10^{-3} mg-atom/ml, the lanthanide coefficients appear to be between 10 and 100 ml/gm, and for solution-phase concentrations on the order of 10^{-7} or less, the lanthanide coefficients appear to be on the order of 10^4 or greater, as was expected. Furthermore, the distribution coefficients given for the lanthanides in Figures 4 and 5 appear to be generally consistent with other lanthanide data which have been obtained for similar oceanic sediments and related clay minerals found within the continental United States (6,7,11). The coefficients given in Figure 4 were determined from the analysis of initial and final solution-phase concentrations of radioactive tracers. However, significant decreases in solution-phase tracer concentrations also occurred in "blank" samples (prepared similarly to the sorption equilibration samples but without addition of clay). Some typical data from those "blank" samples are given in Table VI. If the decreases in solution-phase concentrations observed in the blank samples reflect errors in the literature values for the hydroxide solubility products for the nuclides studied (23), then the data given in Figure 4 may be reasonably correct (since the final solution-phase nuclide

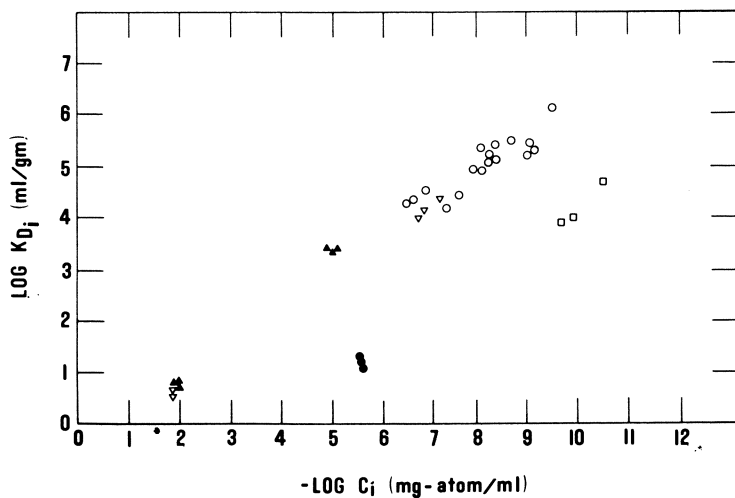


Figure 4. Uncorrected distribution coefficients for Ce, Pm, Eu, and Gd in 0.68N NaCl solutions: (∇), Ce (pH 5.0-8.0); (\square), Pm (pH 7.2-7.3); (\blacktriangle), Gd (pH 6.2-7.9); (\circ), Eu (pH 5.9-8.2); (\bullet), Eu (pH 2.7).

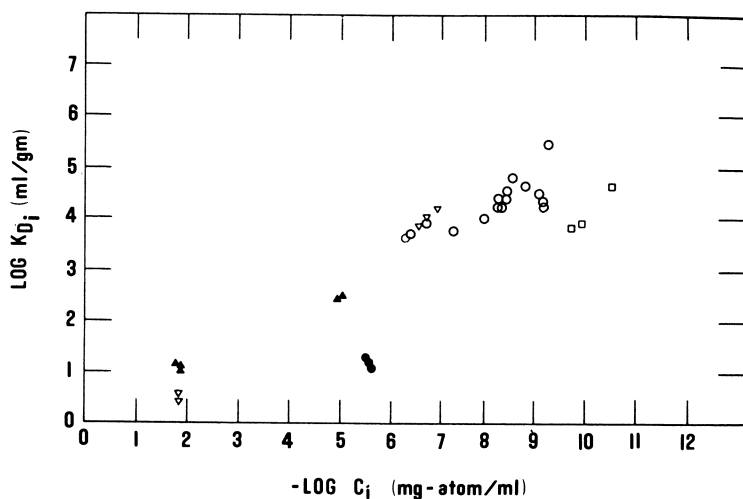


Figure 5. Corrected distribution coefficients for Ce, Pm, Eu, and Gd in 0.68N NaCl solutions: (▽), Ce (pH 5.0-8.0); (□), Pm (pH 7.2-7.3); (▲), Gd (pH 6.2-7.9); (○), Eu (pH 5.9-8.2); (●), Eu (pH 2.7).

concentrations in the sorption experiments were always less than the final concentrations in the corresponding blanks.) However, if the decreases in solution-phase concentrations represent the effects of competing hydrolysis or other chemical reactions or represent the effects of sorption on the walls of the container, then the distribution coefficients given in Figure 4 would, to some extent, be in error. As a primitive attempt to account for such errors, the coefficients given in Figure 4 were corrected by using the final solution-phase tracer concentrations in the corresponding blank samples as the initial solution-phase tracer concentrations from which to calculate the "corrected" values of the distribution coefficients. The data so obtained are shown in Figure 5 and are probably conservative. The coefficients given in Figure 5 are probably smaller than the actual distribution coefficients.

Table VI. Typical Data from "Blank" Samples.

Element	Final pH	Initial Solution	Final Concentration
		Concentration (mg-atom/ml)	<u>Initial Concentration</u>
Eu	4.61	2.2×10^{-6}	0.87
	8.07	2.2×10^{-6}	0.23
	8.44	2.2×10^{-6}	0.02
Gd	7.42	5.3×10^{-4}	0.12
Ce	6.49	1.6×10^{-5}	0.65

The distribution coefficients for europium also appear to be strongly influenced by low values of the solution pH. Such behavior is similar to that of barium and silver and again suggests that the sorption of the lanthanides may be due to at least two separate mechanisms, which are also probably essentially the same as those discussed for barium.

Based on the experimental techniques, the maximum relative error in the values of both C_i and K_{D_i} was estimated as being on the order of $\pm 10\%$ for values of C_i greater than 10^{-6} mg-atom/ml and on the order of $\pm 20\%$ for lesser values of C_i . However, some rather large deviations were observed between data points obtained from identically prepared experiments (especially at values of C_i less than 10^{-6} mg-atom/ml). This tends to indicate that very subtle variations in the nature of the clay samples did occur between the individual experiments. The values of C_i and K_{D_i} given in Figures 1 through 5 should, therefore, be considered as representative values which (especially at values of C_i less than 10^{-6} mg-atom/ml) might be subject to variations on the order of ± 0.5 log units. Furthermore, the assumption that the solid-phase concentrations of rubidium, strontium and barium given in Table I represented the concentrations of sorbed species introduces further

uncertainties into the values of C_i and K_{D_i} for those elements.

If the assumption were totally invalid, the data for barium should involve the worst errors since some of the values of C_i given as being equal to about 10^{-7} mg-atom/ml might then be as small as about 10^{-10} mg-atom/ml.

Conclusions

For the nuclides studied (rubidium, cesium, strontium, barium, silver, cadmium, cerium, promethium, europium, and gadolinium) the distribution coefficients generally vary from about 10 ml/gm at solution-phase concentrations on the order of 10^{-2} mg-atom/ml to 10^4 and greater at concentrations on the order of 10^{-7} and less. These results are encouraging with regard to the sediment being able to provide a barrier to migration of nuclides away from a waste form and also appear to be reasonably consistent with related data for similar oceanic sediments and related clay minerals found within the continental United States.

For each nuclide studied, the sorption distribution coefficients appeared to result from a minimum of two separate mechanisms. In all cases, one mechanism appears to be an ion-exchange phenomena associated with the silicate phases and appears to have a relatively much larger sorption capacity than the other mechanism. In the case of cesium (and probably rubidium) the second mechanism appears to also be related to the silicate phases and may or may not be an ion-exchange phenomena. However, for the other elements studied, the second mechanism appears to be related to the hydrous iron and manganese oxides and again may or may not be an ion-exchange process.

The results of this preliminary investigation (particularly the general behavior of the distribution coefficients and the identification of multiple sorption mechanisms) will provide a basis from which plans can be developed for studying the sorption and complex chemistry of the actinides. The results will also provide a basis from which plans can be developed for studying sorption equilibria involving several competing nuclides.

Abstract

The radionuclide sorption properties of a widely distributed abyssal red clay are being experimentally investigated using standard batch equilibration techniques. These measurements provide data required by the U.S. Seabed Disposal Program to assess the feasibility of emplacing radioactive wastes in sub-seafloor geologic formations. Equilibrium distribution coefficients are generally being evaluated at 4°C as functions of pH and nuclide concentration in solution. Data has been obtained for solutions containing a single sorbing species of either Cs, Rb, Sr, Ba, Ag, Cd, Eu, Gd, Ce, or Pm. Distribution coefficients varied from 10 to 10^4 or 10^5 ml/gm as the nuclide concentration in solution

varied from 10^{-2} to 10^{-7} M or less, respectively. These results appear consistent with data for other oceanic sediments and for similar clay minerals found within the continental United States. The distribution coefficients depended little on pH within the range of 6 to 8; however, below pH 2.7 the barium, silver and europium distribution coefficients were greatly diminished. It appears that the magnitude and behavior of the distribution coefficients result from multiple sorption mechanisms.

References

1. Crank, J., "The Mathematics of Diffusion," pp. 28-103, Clarendon Press, London, 1975.
2. Heath, G. Ross, "Seabed Disposal Program Annual Report January-December 1975," Appendix H, edited by D. M. Talbert, Sandia Laboratories, Albuquerque, NM, Report No. SAND76-0256, May 1976.
3. Dean, John A. (editor), "Lange's Handbook of Chemistry," 11th Ed., p. 10-21, McGraw-Hill, New York, 1973.
4. Dean, John A. (editor), "Lange's Handbook of Chemistry," 11th Ed., pp. 5-7, 5-11, McGraw-Hill, New York, 1973.
5. Mehra, O. P., and Jackson, M. L., in "Clay and Clay Minerals Proc.," V. 7, pp. 317-327.
6. Heath, G. R., Epstein, G., and Prince, R.A., in "Seabed Disposal Program Annual Report-Part II," Appendix E, edited by D.M. Talbert, Sandia Laboratories, Albuquerque, NM, Report No. SAND77-1270, October 1977.
7. Hamaguchi, Hiroshi (chief investigator), "Studies on the Sorption of Radioisotopes on Marine Sediments," final report IAEA Research Contract No. 881R2/RB, Japan Analytical Chemistry Research Institute, Tokyo, Japan, December 28, 1963.
8. Elliason, J. R., Amer. Mineral., (1966), 51, pp. 324-335.
9. Faucher, Joseph A., Southworth, Raymond W., and Thomas, Henry C., J. Chem. Phys., (1952), 20, pp. 157-160.
10. Faucher, Joseph A., and Thomas, Henry C., J. Chem. Phys., (1954), 22, pp. 258-261.
11. Frysinger, Galen R., and Thomas, Henry C., J. Phys. Chem., (1960), 64, pp. 224-228.
12. Gaines, George L., Jr., and Thomas, Henry C., J. Chem. Phys., (1955), 23, pp. 2322-2326.
13. Lewis, Russell J., and Thomas, Henry C., J. Phys. Chem., (1963), 67, pp. 1781-1783.
14. Grim, Ralph E., "Clay Mineralogy," p. 189, McGraw-Hill, New York, 1968.
15. Kurbatov, M. H., Wood, Gwendolyn B., and Kurbatov, J. D., J. Phys. Chem., (1951), 55, pp. 1170-1182.
16. Duval, J. E., and Kurbatov, M. H., J. Phys. Chem., (1952), 56, pp. 982-984.
17. Murray, D. J., Healy, T. W., and Fuerstenau, D. W., in "Adsorption from Aqueous Solution," *Advances in Chemistry*

- Series 79, pp. 74-81, American Chemical Society, Washington, D.C., 1968.
18. Jenne, E. A., in "Trace Inorganics in Water," Advances in Chemistry Series 73, pp. 337-387, American Chemical Society, Washington, D.C., 1968.
 19. Parks, G. A., and DeBruyn, P. L., J. Phys. Chem., (1962), 66, pp. 967-973.
 20. Grim, Ralph E., "Clay Mineralogy," p. 83, McGraw-Hill, New York, 1968.
 21. Parks, G. A., Chem. Rev., (1965), 65, pp. 177-198.
 22. Dean, John A. (editor), "Lange's Handbook of Chemistry," 11th Ed., pp. 5-46, 5-47, McGraw-Hill, New York, 1973.
 23. Baes, Charles F., Jr., and Mesmer, Robert, "The Hydrolysis of Cations," pp. 129-168, John Wiley & Sons, New York, 1976.

RECEIVED January 16, 1979.

Consequences of Radiation from Sorbed Transplutonium Elements on Clays Selected for Waste Isolation¹

R. G. HAIRE and G. W. BEALL

Oak Ridge National Laboratory, Oak Ridge, TN 37830

Recently there has been interest in the sorptive behavior of natural clays toward metal ions potentially present in radioactive wastes. Initial studies of the transplutonium elements have been carried out to define their sorption behavior with such materials (1). However, it is also important to understand the stability of the clay-actinide product with regard to radiation damage and to be able to predict what changes in behavior may occur after exposure to radiation, so that accurate transport models may be constructed.

In order to obtain some information on the effect of alpha radiation on the clay materials, two natural clays were selected for experiments with ^{253}Es . This isotope was chosen to provide an intense source of alpha radiation ($6 \times 10^{10} \alpha \text{ min}^{-1} \mu\text{g}^{-1}$, 6.6-MeV α) in hopes that the time base of the experiments could be reduced. However, this isotope is available only twice a year and its short half-life limited the experiments to a short period of time.

Reported here are the initial results of the experiments with ^{253}Es -clay mixtures and the tentative implications these results have for the other transplutonium elements.

Experimental

The methods used to purify the ^{253}Es have been reported (2). Portions of the purified Es chloride solution were evaporated to dryness in fused silica vessels and the residues taken up in 10^{-3} M HCl. These solutions were then used directly for the electron microscopy studies or mixed with sodium chloride-acetate buffer (pH=5) for the distribution coefficient experiments.

For electron microscopy, small amounts of clay were metered by using aliquots of a colloidal solution of the clay. These solutions were then mixed with the ^{253}Es . Portions of the resulting

¹ Research sponsored by the Division of Nuclear Sciences, Office of Basic Energy Sciences, U.S. Department of Energy under contract W-7405-eng-26 with the Union Carbide Corporation.

mixtures were periodically taken, evaporated on electron microscope grids and the material examined in a Philips EM 300 electron microscope. Similar clay suspensions without Es were used as controls.

For the distribution coefficients, an acetate buffer adjusted to pH 5 was used and the sodium chloride concentration of it varied from 0.25 to 4 M by dissolving sodium chloride in the buffer. Aliquots of the ^{253}Es solution were mixed with the buffer and a weighed quantity of the solid clay was mixed with this solution.

Periodically, these mixtures were centrifuged and an aliquot of the clay-free supernate taken for counting analysis. Two naturally-occurring clays were selected for the experiments; one was labeled kaolin (for the mineral kaolinite) while the second was referred to as attapulgite (or polygorshite). Both were obtained from the Source Clay Mineral Repository (3) as standard clays representative of each class of clay and were used as received. Stable, colloidal suspensions of each were prepared by ultrasonically dispersing weighed quantities of each clay in triple-distilled water.

Results and Discussion

Two naturally occurring clays, kaolin and attapulgite, were selected for the radiation damage study with ^{253}Es on the basis of their morphology. These clays together with a third clay, montmorillinite, were also used for sorption studies with the transplutonium elements (1). From electron micrographs of the kaolin, and attapulgite materials, it is apparent that the regular geometric forms of kaolin (platelets) and attapulgite (rods or fibers) are best suited for following any changes that may occur in their morphology as a result of radiation.

From sorption experiments with the rare earths and trivalent actinides, it was found that the distribution coefficients for kaolin and attapulgite were quite different, the latter having much higher values (1). Therefore, the radiation damage study with ^{253}Es was made with clays having different morphologies and different sorptive capacities.

In initiating these experiments it was recognized that only dilute colloidal suspensions of the clay could be employed to obtain reasonable Es/clay ratios, as only small amounts of ^{253}Es were available. During the course of the experiments, it also became evident that X-ray or electron diffraction were of limited value in following the effect of radiation on the clay, in contrast to radiation damage studies of radioactive compounds such as PuO_2 . With the ^{253}Es -clay mixtures, the sensitivity of these diffraction measurements was lower since only the undestroyed clay material was being monitored by diffraction analysis. There were also experimental problems with the radiation from the Es for X-ray diffraction analysis such as film blackening. Thus,

this radiation damage study was confined to following morphological changes in the clay structures.

With small Es/clay loadings, (1/1000-1/100 of the clay's capacity, with the capacity being 10^{-5} - 10^{-4} meq./mg clay) it was difficult to detect changes in the clay after 1-2 weeks by electron microscopy. However, when the clays were loaded to their capacity with Es, extensive destruction of the clay structures were noted in 2-4 days. In Figure 1 are micrographs of kaolin and attapulgite clays with and without exposure to ^{253}Es . Figures 1b and 1d show the early stages of the damage process in the clays. With attapulgite, the process proceeded as follows: first small voids and rough edges appeared, followed by clumping of fragments from the destruction process around the remaining fibers, and finally complete fragmentation of the rods or fibers occurred. For kaolin, the destruction process began by forming voids or holes in the platelets, followed by fragmentation of the platelets into smaller pieces. It should be noted that the platelets of kaolin were more sensitive to the electron beam in the electron microscope and it was necessary to use lower beam currents with the kaolin samples. The rate of destruction of both clays was a function of Es loading, and in accord with its higher sorptive capacity, the destruction appeared sooner with attapulgite samples. The fragmentation of both clays from radiation was similar to the self-irradiation damage that has been seen in the rod-like structures of $\text{Am}(\text{OH})_3$ and $^{244}\text{Cm}(\text{OH})_3$ (4). Quantitative decomposition rates were not measured in this work, but it was concluded that the destruction was more extensive than that expected if it was assumed that only one site on the clay was destroyed per alpha event. Thus, many other sites are destroyed along the path of the alpha particle.

Even though the clay structures were destroyed by the ^{253}Es radiation, the distribution ratios (Es in clay/Es in solution) for ^{253}Es -clay mixtures did not drop drastically with time but in fact increased slightly. This behavior has been interpreted in the following ways: (1) that the Es remains associated with the fragmented clay, which can still be centrifuged out of the solution; and/or (2) that the remaining Es itself has become insoluble (and non-colloidal) with time and also centrifuges out in the solid phase. The radiation field is sufficient that in time non-soluble Es species may be formed in the pH range of the solutions employed here. Intense alpha radiation can locally deplete the hydrogen ion concentration, generate radicals, etc. that may promote the formation of an insoluble hydroxide, oxyhalide, etc. species. It is apparent from the work that initially the Es is indeed sorbed on the clay materials. Whether the Es is released by the damaged clay to the solution where it again associates with undamaged clay sites, or whether it forms an insoluble product with the fragmented clay, cannot be determined from this work. The important aspect is that the Es did not form a soluble species in the solution after destruction of the clay site.

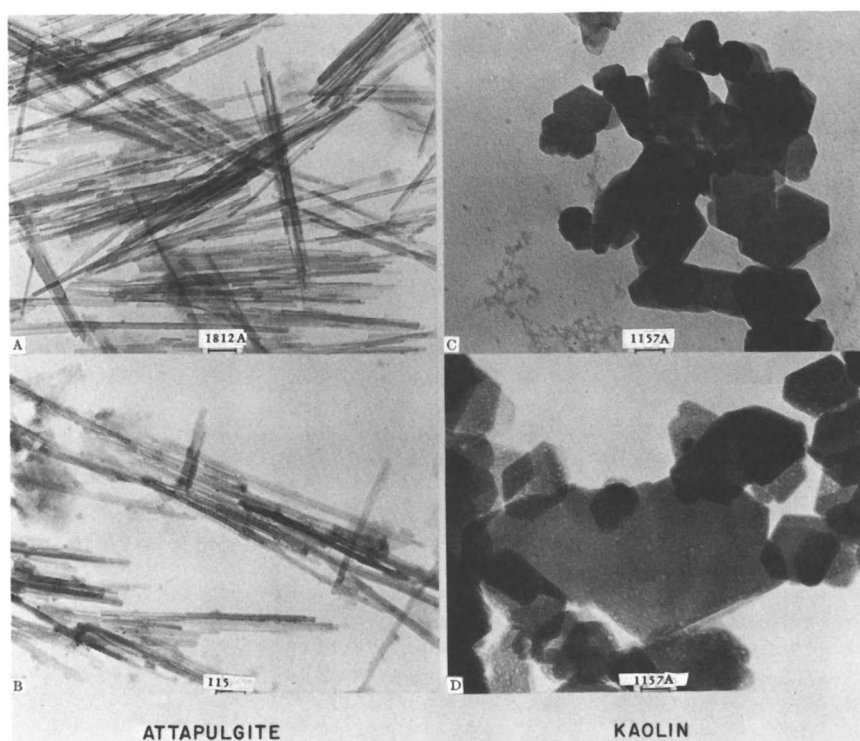


Figure 1. Electron micrographs of attapulgite and kaolin before (1a, 1c) and after (1b, 1d) contact with ^{253}Es

The conclusions reached from this preliminary study is that these clays can serve as sorbative material for the trivalent actinides and that even after damage to the clay structures, the actinide will not be released as a soluble species.

References

1. Beall, G. W., Ketelle, B. H., Haire, R. G., and O'Kelley, G. D., "Sorption Behavior of Trivalent Actinides and Rare Earths on Clay Minerals," ACS Symposium Series on Radioactive Waste in Geologic Storage, R. F. Gould, Ed., Miami Beach, Florida, Sept. 11-15, 1978.
2. Baybarz, R. D., Knauer, J. B., and Orr, P. B., USAEC Rept. ORNL-4672 (1973).
3. Source Clay Mineral Repository, University of Missouri, Rolla, Mo.
4. Haire, R. G., Lloyd, M. H., Milligan, W. O., and Beasley, M.L., *J. Inorg. Nucl. Chem.*, 39, 843 (1977).

RECEIVED January 16, 1979.

Ion-Exchange Equilibria between Montmorillonite and Solutions of Moderate-to-High Ionic Strength

S.-Y. SHIAO, P. RAFFERTY, and R. E. MEYER

Chemistry Division, Oak Ridge National Laboratory, Oak Ridge, TN 37830

W. J. ROGERS

Department of Chemistry, The University of Tennessee, Knoxville, TN 37916

Prediction of the migration rates of ions in geologic formations is of extreme importance in the fields of nuclear waste disposal and enhanced oil recovery. Demonstration of the safety of nuclear waste repositories requires that the repository be so designed and situated that migration rates from the repository be acceptably low in the event of water flow through the repository. On the other hand, the principal criterion for selection of tracers to monitor fluid flow in the flooding techniques of enhanced oil recovery is that the tracers be not retained on the formation, i.e., migration rates must be high. Migration rates are dependent on the distribution coefficient of the species between fluid and the geologic media such that the greater the distribution coefficient the slower the rate of migration. Therefore, for reliable prediction of migration rates, accurate knowledge of the adsorption behavior of the nuclides and tracers must be known as a function of all of the pertinent variables.

Obtaining the necessary data for this complex situation is complicated by both the large number of different minerals which may be present and the wide range of solution compositions. In order to accumulate a systematic body of information pertinent to this complex situation, we are measuring adsorption of ions of interest on minerals typical of classes, from a wide range of aqueous solution compositions. Initially, montmorillonite was selected for attention because its high adsorptive capacity for ions may cause it to dominate the adsorptive proportion of the formation in which it is present. Reported here are distribution coefficients of alkali metal and alkaline earth ions, and of one rare earth, between montmorillonite predominantly in the sodium and calcium forms and aqueous solutions of controlled pH, at moderate to high salinities ($>0.01\text{MNaCl}$). The ions were selected for initial study, not only because of their intrinsic interest for these applications but also because they allow evaluation of the extent to which equilibria can be described by conventional ion-exchange equations with minimum difficulties from hydrolysis, precipitation, and complexing. Correlation of results as a

0-8412-0498-5/79/47-100-297\$07.00/0

© 1979 American Chemical Society

function of ionic strength at controlled pH, temperature, and loading, so far as it is feasible, reduces greatly the number of measurements necessary to predict behavior.

The exchange of sodium and calcium on clay minerals is of special importance, because it largely determines the ionic form of the clay, which in turn affects the performance of surfactant and polymer floods and the distribution of other ions of interest. In concentrated NaCl environments, clay exists mainly in the sodium form; however, at low ionic strength and moderate hardness, clay may be essentially in the calcium form. Measurements with the sodium, calcium, and mixed forms are therefore of interest.

Previous studies of the adsorption of ions on montmorillonite have emphasized low salt concentration regions (see, e.g. ref. 1-11). Our main interest is in higher salt concentrations, because many of the brines in oil reservoirs are in this range, and because some favored locations for nuclear waste disposal, bedded salt deposits and salt domes, may result in high ionic strength environments.

Experimental

Clays. Two clays, SWy-a Na-montmorillonite (Crook County, Wyoming) and STx-1 Ca-montmorillonite (Gonzales County, Texas) were obtained from the Department of Geology, University of Missouri. Montmorillonite #27 (Bell Fourche, South Dakota) and montmorillonite #31 (Cameron, Arizona) were purchased from Ward's Natural Science Establishment.

Tracers. Radioactive tracers were employed in the experiments. Cs^{137} , Na^{22} , K^{42} , Ca^{47} , and Ba^{133} were made by neutron bombardment in the High Flux Isotope Reactor at Oak Ridge National Laboratory. Sr^{85} and Eu^{155} were purchased from New England Nuclear (Boston, Massachusetts).

Purification and Preparation of Clay Samples. The sand fraction of the clay samples was separated by slow-speed centrifugation of a suspension of the clay before the purification steps. The clay was purified following Jackson's purification procedure (12) (unless otherwise mentioned), that is, removing insoluble carbonates by using 1 M acetate buffer (pH 5), removing organic matter by using 30% hydrogen peroxide, and removing iron not incorporated in the clay structure by using sodium citrate and sodium dithionite. Finally, the clay was converted to a monoionic form (either sodium or calcium form) by contacting the clay with concentrated sodium or calcium chloride solutions several times. The excess calcium or sodium salts were washed out with 60% methanol-water mixtures. Removal of chloride by the washes was checked with a chloridometer (Buchler Instruments, Inc., Fort Lee, N. J.). The clay was then dried in a vacuum desiccator and ground in a jar mill. The fine fraction (<325 mesh size) was

collected for ion exchange experiments. The moisture content of the clay was determined from the loss in weight by heating a small portion at 110°C in an oven.

A frequently used method of preparing clay samples by soil scientists is to collect the fraction with particle diameters less than 2 μm by centrifugation and store it as a dilute suspension. We made no attempt to remove only the <2 μm fraction. Mingelgrin *et al.* (13) reported that even a mild grinding on bentonite could change its properties. However, in this study, no significant change in adsorbability was observed of Sr(II) upon grinding the Na-form Wyoming montmorillonite (14).

Distribution Coefficient. Distribution coefficients were determined using conventional batch equilibrations, in which a known amount of clay is contacted with a known volume of solution and shaken until equilibrium is essentially reached, at least overnight at room temperature. In tests with several ions and montmorillonite, equilibrium was reached in less than two hours.

Distribution coefficients are defined (for a cation A^{a+}) and computed by Equation 1.

$$D \equiv \frac{(A^{a+})_{\text{clay}}}{(A^{a+})} = \frac{(n_A)_{\text{clay}}/w}{(n_A)/V} = \frac{[(n_A)_i - (n_A)]}{(n_A)} \frac{V}{w} \quad (1)$$

where (A^{a+}) is the concentration of A^{a+} in solution, moles/liter.
 $(A^{a+})_{\text{clay}}$ is the concentration on the solid, in moles/kg dry solid,
 $(n_A)_{\text{clay}}$ and (n_A) are the counts of radioactive tracer on the solid and in the solution, respectively, at equilibrium (or the amounts of A, if analysis is done by other methods).
 $(n_A)_i$ is the initial total counts in the aqueous phase,
 w is the weight of dry solid in monoionic form in kg,
 V is the volume of solution, in liters.

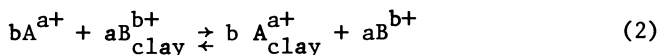
A NaI well-type scintillation was used to count the γ emission of the tracers in the solution before and after equilibration. Most of the clay samples were pre-equilibrated with the aqueous media to be used in the adsorption measurements to insure attaining the specified pH, usually 5, maintained with acetate buffer.

Montmorillonite, especially the sodium form, swells in low-ionic-strength solutions; consequently, centrifugation in moderately high fields is needed to separate the clay particles and the solutions. Clay suspensions were centrifuged with a Du Pont Sorvall RC-5 refrigerated super-speed centrifuge at 15,000 rpm (28,000 g) for 15 minutes, and the supernatant was then withdrawn for analysis. No correction was made for possible ion exclusion

in the water in the clay pack at the bottom of the centrifuge tube; it was assumed to have the same concentration as that of the supernatant. For solution-clay ratios used here, there would probably be no significant error if there were some ion exclusion in the clay pack. Polypropylene tubes were used for equilibration and centrifugation. Under the conditions of these experiments, the adsorption of radioactive tracers on the tubes was found not to have a significant effect on results.

Cation Exchange Capacity. Various techniques have been used to measure the cation exchange capacity of the clay samples. Unless otherwise noted, in computation of equilibrium quotients, we shall use a value of 0.78 equivalents/kg clay, determined by a column method (14) on the calcium form of Wyoming montmorillonite at pH 5.

Equations. The equilibrium between A^{a+} and B^{b+} (in a solution with a common monovalent anion, X^-) in aqueous (no subscript) and solid (subscript "clay") phases,



can be expressed by

$$K_{AB} = \frac{(A^{a+})_{\text{clay}}^b \cdot m_B^a}{m_A^b (B^{b+})_{\text{clay}}^a} \cdot \Gamma_{AB} = D_A^b \frac{m_B^a}{(B^{b+})_{\text{clay}}^a} \cdot \Gamma_{AB} \quad (3)$$

where the activity coefficient quotient is defined and can be evaluated by

$$\Gamma_{AB} = \frac{(\gamma_A)_{\text{clay}}^b (\gamma_B)_{\text{aq}}^a}{(\gamma_A)_{\text{aq}}^b (\gamma_B)_{\text{clay}}^a} = \frac{(\gamma_{\pm AX_a})_{\text{clay}}^{b(a+1)} (\gamma_{\pm BX_b})_{\text{aq}}^{a(b+1)}}{(\gamma_{\pm AX_a})_{\text{aq}}^{b(a+1)} (\gamma_{\pm BX_b})_{\text{clay}}^{a(b+1)}} = \Gamma_{\text{clay}} \Gamma_{\text{aq}} = \Gamma_{\text{clay}} \frac{(\gamma_{\pm BX_b})_{\text{aq}}^{a(b+1)}}{(\gamma_{\pm AX_a})_{\text{clay}}^{b(a+1)}} \quad (4)$$

The symbol, γ_{\pm} , denotes the mean ionic activity coefficient. Customarily, in the solution phase, the symbol γ is used in conjunction with concentrations in molality units, or moles per kg

of solvent. We have expressed solution-phase concentrations in Equation 3 in molality, m , for consistency; D is the distribution coefficient corresponding to this convention. For present purposes, there is little difference between molality and molarity scales up to one molar NaCl; differences in the range of 10% are incurred near saturated NaCl. The separation of Γ_{AB} into ratios for the solution and solid phases is useful when solution phase activity coefficients are available (see, e.g., 15) because it allows evaluation of variations from ideality of the clay phase over a range of experimental conditions. When measurements for the aqueous mixed electrolyte systems in question are not available, adequate estimates can frequently be made by Debye-Hückel equations or by various methods from measurements on two-component systems (see, e.g., 16).

Certain special cases are of interest here. When one ion is present at concentrations low enough for loading of the solid phase to be only a small fraction of ion exchange capacity, C , expressed in equivalents/kg of solid, Equation 3 may be written

$$K_{AB}/\Gamma_{AB} \sim D_A^b \frac{m_B^a}{(C/b)^a} \sim \frac{D_A^b (B^{b+})^a}{(C/b)^a} \quad (5)$$

If Γ_{AB} is constant over the range of conditions, and if the exclusion of coion X^- from the clay phase is essentially complete, Equation 5 can be differentiated to give

$$\frac{d \log D_A}{d \log (B^{b+})} = -a/b \quad (6)$$

i.e., a plot of $\log D_A$ vs $\log (B^{b+})$ will be linear, with slope $-(a/b)$, or, e.g., -2 if A^{a+} is Ca^{2+} and B^{b+} is Na^+ .

The restriction of coion exclusion, although implicitly included in "ideal" behavior here, is a somewhat different approximation than constancy of Γ_{AB} or Γ_{clay} . Equations which take invasion of coions into the clay phase into account can readily be developed, for example by assigning the same reference state to both phases and expressing concentration of ions in the clay phase in terms of moles/kg water, equivalent to $K = 1$ (17). The behavior of $\log D_A$ vs $\log (B^{b+})$ given by Equation 6 is approached as ionic strength is decreased, and coion concentration in the clay presumably becomes negligible in comparison with capacity. We have not measured coion invasion in this work and therefore will discuss results in terms of the equations given.

It is perhaps worthwhile to distinguish between the just-discussed coion exclusion in the layers of montmorillonite, where presumably most of the ion-exchange capacity is located, from the earlier reference to possible effects of exclusion in the water

of the clay pack on interpretation of experimental results. The latter, which we have assumed to be negligible, would arise from the influence on interstitial solution between particles of charges on the surface of the particles, the charge density of which, averaged over pack-water volume, would be far less than the fixed-charge density in the layers, if the layers are only 10 - 20 Å apart. Results reported here do not clarify the degree of coion exclusion in either environment.

Results

We shall first discuss effects of loading of the clay on distribution coefficients. With these results, we hope to identify conditions under which distribution coefficients are independent of loading ("linear isotherm" regions). Measurements made in these regions can then be used to evaluate effects of other variables, primarily of ionic strength. It is expected, of course, from Equation 3 that D will decrease substantially at high loading; what we are concerned with here are significant effects at lower loading than predicted for constant Γ_{clay} .

Because distribution coefficients are often dependent on pH, buffers were used. The pH of 5 was selected for most of the experiments because montmorillonite is stable at this acidity, interference of observations from hydrolysis and from precipitation of alkaline earth carbonates is precluded, and adsorption on possible hydrous oxide impurities is minimized. An acetate buffer was usually used to maintain pH because acetate does not have a strong tendency to complex many ions.

Loading

Sodium Form of Montmorillonite (Wyoming). Cs(I): Figure 1 summarizes the distribution coefficients of Cs^+ from 0.5 M NaCl, pH 5, solutions, as a function of loading of Cs^+ from trace level to well over 10% of capacity. There is an appreciable difference between trace and the lowest macro concentration, and a significant, though not precipitous, decline up to about 10% loading. Wahlberg and Fishman (3) reported loading curves for Cs^+ on two samples of montmorillonite at several concentrations of NaCl up to 0.2 M. They also found a gentle decrease of D_{Cs} with increasing loading.

Alkaline earths: The effect of Sr(II) loading on D_{Sr} for several different concentrations of Na^+ is shown in Figure 2. Up to 0.01 moles Sr(II)/kg clay, effects are very small, and values at tracer levels agree with those at macro concentrations. Wahlberg, et al. (7) report loading curves for a sample of montmorillonite at Na^+ concentrations up to 0.2 M. Their values of D_{Sr} appeared constant with loading up to about the same Sr(II) loading as in Figure 2, and their values of D in the linear isotherm region were about 50% higher than those in Figure 2 at overlapping

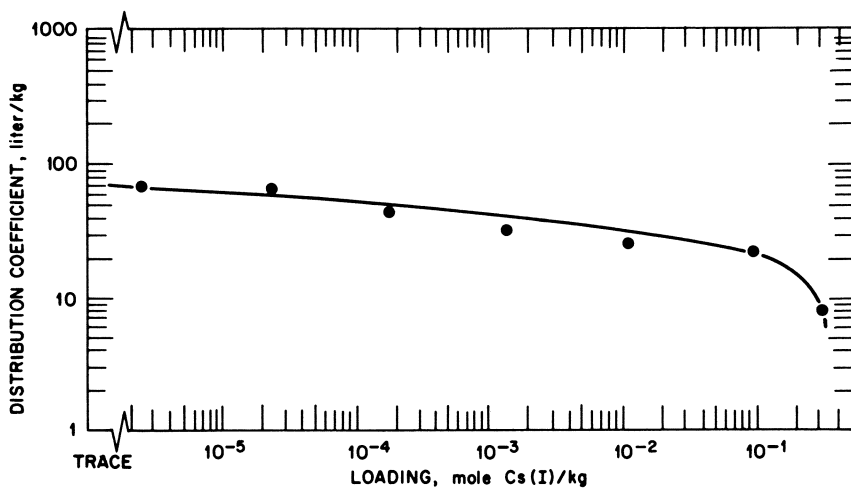


Figure 1. Effect of loading on distribution coefficients of Cs(I) on the sodium form of Wyoming montmorillonite (0.5M NaCl + 0.01M NaOAc, pH 5, equilibration for 74 hr)

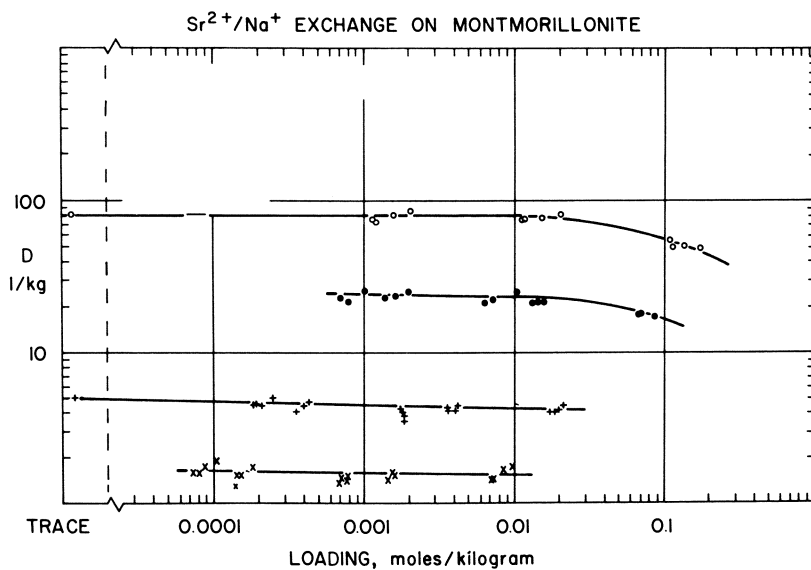


Figure 2. Effect of loading on distribution coefficients of Sr(II) on the sodium form of Wyoming montmorillonite. NaCl and pH 5 acetate buffer: (○), 0.1M Na⁺; (●), 0.2M Na⁺; (+), 0.6M Na⁺; (×), 1.1M Na⁺.

ionic strength. The agreement is considered good, in view of differences in clay samples and purifications (in ref. 7, clays were exposed to hot 1 M HCl-1 M NaCl solutions).

Figure 3 summarizes effects of loading on D for Ca(II), Sr(II), and Ba(II), for the sodium form of montmorillonite. The Sr(II) results are from a different set of measurements than those in Figure 2, but are in good agreement with them. Effects of loading are small up to the several percent of ion-exchange capacity covered. Values of distribution coefficients for these three ions fall in a narrow range.

Eu(III): The loading effect on the distribution coefficient of Eu(III) on the Na form of montmorillonite for both acetate-buffered and unbuffered solutions is shown in Figure 4. The D 's are fairly constant in the low loading range. We shall comment later on the differences in presence and absence of buffer.

Calcium Form of Montmorillonite (Wyoming). Alkali metal ions: We present these results in terms of plots of K/Γ_{clay} and K/Γ as a function of loading (Figures 5 and 6). The solution-phase activity coefficient ratio for sodium was obtained from a compilation of literature data on the NaCl-CaCl₂-H₂O systems (15), and the same values were used for cesium. Equilibrium quotients for the different Ca(II) concentrations agree well. In comparison with the results on the sodium form of montmorillonite, the most striking difference is the low fractional loading (about 0.1% of ion-exchange capacity) at which variations in D , reflected as changes in K/Γ_{clay} , become apparent, for both sodium and cesium.

Wahlberg and Fishman (3) also report strong decreases in D_{Cs} , starting at low loading from solutions up to 0.1 M CaCl₂. The values of their D 's at trace loadings imply much higher values of equilibrium quotients than those at lowest loading in Figure 6, two orders of magnitude for one clay sample they used and a factor of about 600 for the other. Their K/Γ values imply that at the same Ca(II) concentration, their D_{Cs} would be a factor of 10 to 25 lower than ours.

Van Bladel, et al., (9), report equilibrium quotients for Na(I)/Ca(II) exchange from aqueous NaCl-CaCl₂ solutions of total normality up to 0.025. It is not clear from their graphical presentation whether their measurements in the low-sodium-fraction region include points in the range of rapidly increasing D_{Na} (decreasing K/Γ_{clay}), although at least at their highest Ca(II) concentration, their values of the equilibrium quotient appear to level off, at values corresponding to those in Figure 6 at loadings of Na⁺ of about 1 to 10% of ion-exchange capacity.

In this regard, we wish to comment on some preliminary results reviewed at a recent meeting (18). At that time, we had not completed the loading studies of \bar{D} and of K/Γ . The values for the calcium form in Figures 15 and 16 of Ref. 18 are in the loading region in which they are rapidly changing. This accounts for differences with the results in Figure 6 of this paper, and probably

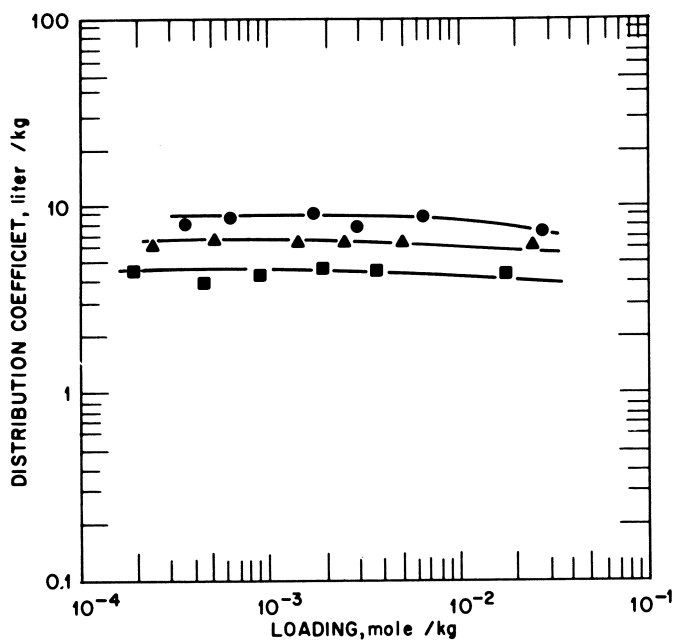


Figure 3. Effect of loading on distribution coefficients of Ca(II), Sr(II), and Ba(II) on the sodium form of Wyoming montmorillonite (0.5M NaCl + 0.1M NaOAc, pH 5, equilibration for more than 90 hr): (●), Ca(II); (▲), Ba(II); (■), Sr(II).

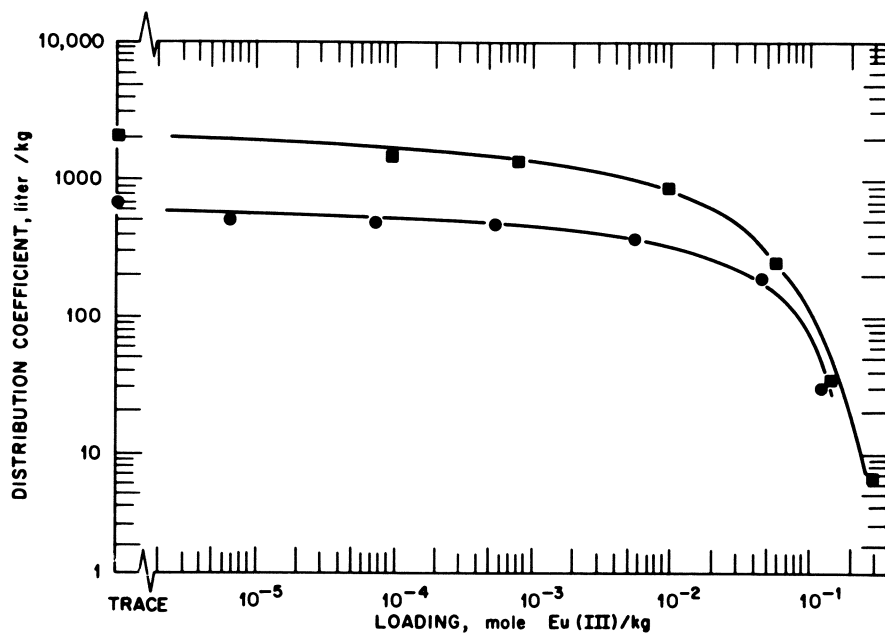


Figure 4. Effect of loading on distribution coefficients of Eu(III) on the sodium form of Wyoming montmorillonite (pH 5, equilibration for 44 hr): (■), 0.1M NaCl; (●), 0.1M NaCl + 0.01M NaOAc.

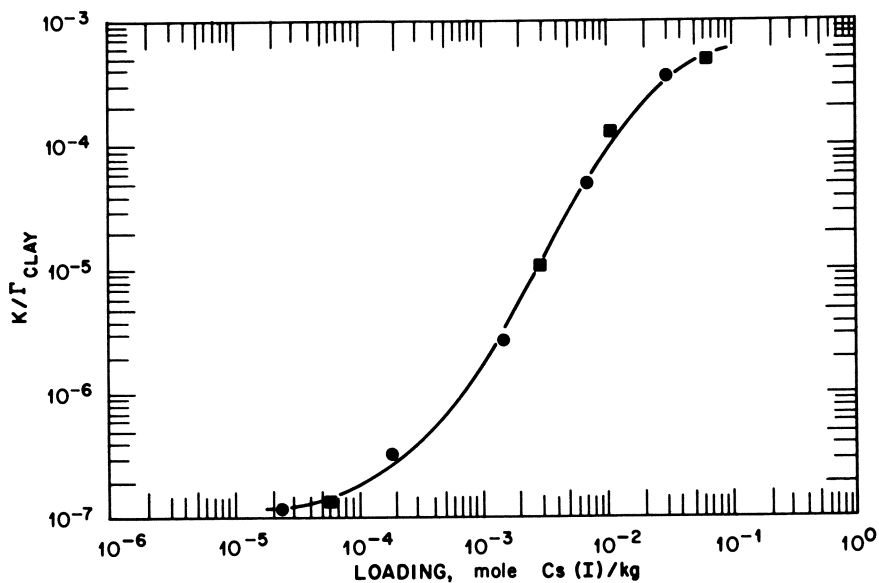


Figure 5. Effect of loading on equilibrium quotients $[m_{Ca} \Gamma_{aq} / (Ca^{2+})_{clay} D^2_{Cs}]$ of Wyoming montmorillonite predominately in the calcium form (pH 5, equilibration for 77 hr): (●), 0.5M $CaCl_2$ + 0.01M $Ca(OAc)_2$; (■), 0.05M $CaCl_2$ + 0.01M $Ca(OAc)_2$.

as well for the discrepancies noted in Ref. 18 from those in Ref. 9.

Sr(II): The effect of Sr(II) loading on D_{Sr} on the Ca(II) form of montmorillonite is shown in Figure 7. Up to 10^{-3} moles Sr(II)/kg clay, values of D_{Sr} are essentially constant, and do not vary greatly up to 10^{-2} moles Sr(II)/kg clay. As we have just discussed, effects were apparent at a factor of ten lower loading for Cs⁺ and Na⁺.

Wahlberg, et al., (7) report very similar loading effects on a calcium montmorillonite. The value of D_{Sr} they report for their clay at trace Sr(II), from 0.01 M Ca(II), is about 40% higher than the value in Figure 7.

D at Low Loading as a Function of Concentration of Equilibrating Ion

Sodium Form of Montmorillonite: Alkali metal ions: Distribution coefficients of Cs⁺ as a function of sodium concentration are summarized in Figure 8 for clays from four different sources. As we discussed in connection with Figure 1, there is a mild dependence on cesium loading for this exchange in the range of loading of these experiments, 0.02 to 5% of ion-exchange capacity. The slopes of $\log D_{\text{Cs}}$ vs $\log (\text{Na}^+)$ from 0.5 to 4 molar sodium are however close to the ideal value, -1 (Equation 6), for individual clay samples. As loading is higher at low (Na⁺) and D_{Cs} therefore relatively lower, the fact that the slopes appear slightly less than unity is in the right direction for a loading effect. These clays had been subjected to all steps in the Jackson purification procedure except removal of free iron oxide. With one sample, measurements were carried out at pH 5 (0.1 M sodium acetate plus acetic acid buffer) as well as 8 (0.1 M NaHCO₃ buffer), and there appeared to be little effect on D . Values of D at a fixed sodium concentration varied by about a factor of three between the montmorillonites of highest D_{Cs} (clay #31) and of the lowest (Wyoming and #27).

Extrapolation of the results in Figure 8 to 0.2 molar Na⁺, the highest concentration of measurements in Ref. 3, gives a range of D_{Cs} of about 60 to 180. Wahlberg and Fishman results for trace Cs at this sodium concentration were about 250 for one clay and 550 for the other. Some of the difference may arise from the higher loading in our experiments, but in any case this much variation between clay samples is probably not surprising. Their slopes of $\log D$ vs \log sodium concentration at trace Cs⁺ were somewhat less (absolute value) than minus one.

Tamura and Jacobs (19) report adsorption on a montmorillonite sample from 6 M NaNO₃, from which we compute $D_{\text{Cs}} \approx 5$, in the range of extrapolated values from Figure 8. Lewis and Thomas (4) report K/Γ of about 40 for low cesium loading and 0.04 M salt concentration, and Gast (10) about 35 for 0.001 M. These values are in the range implied by results in Figure 8 (K/Γ 15 to 50).

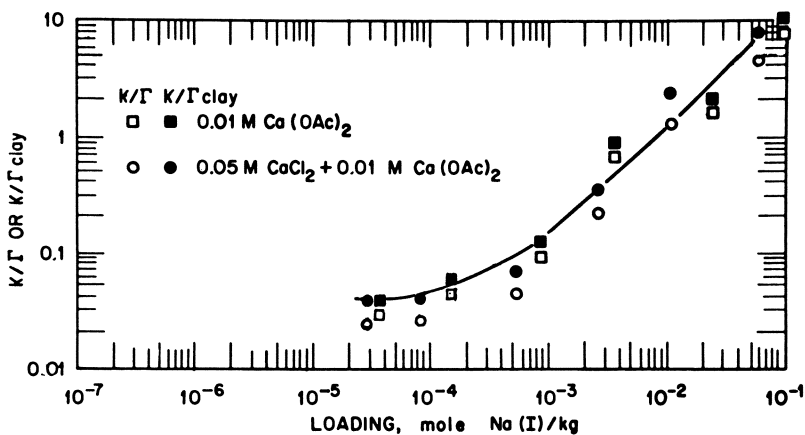


Figure 6. Effect of loading on equilibrium quotients $[m_{Ca} \Gamma_{aq} / (Ca^{2+})_{clay} D^2_{Na}]$ of Wyoming montmorillonite predominately in the calcium form (pH 5, equilibration for 14 hr)

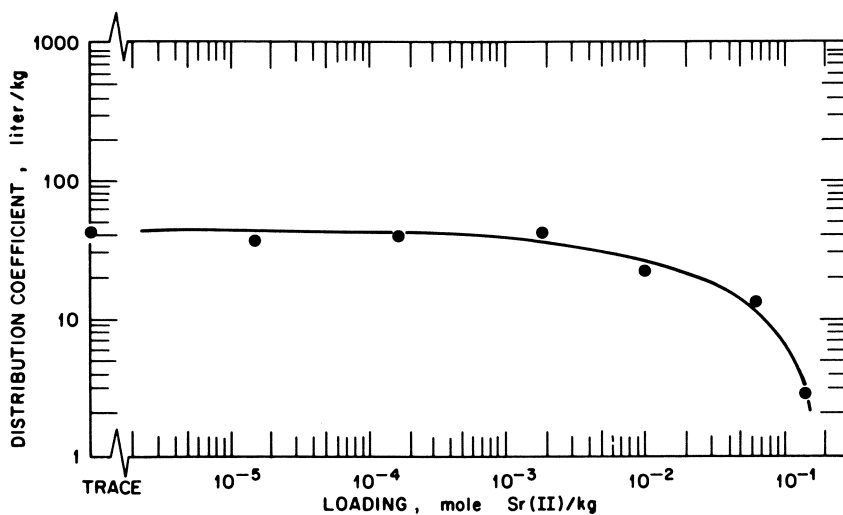
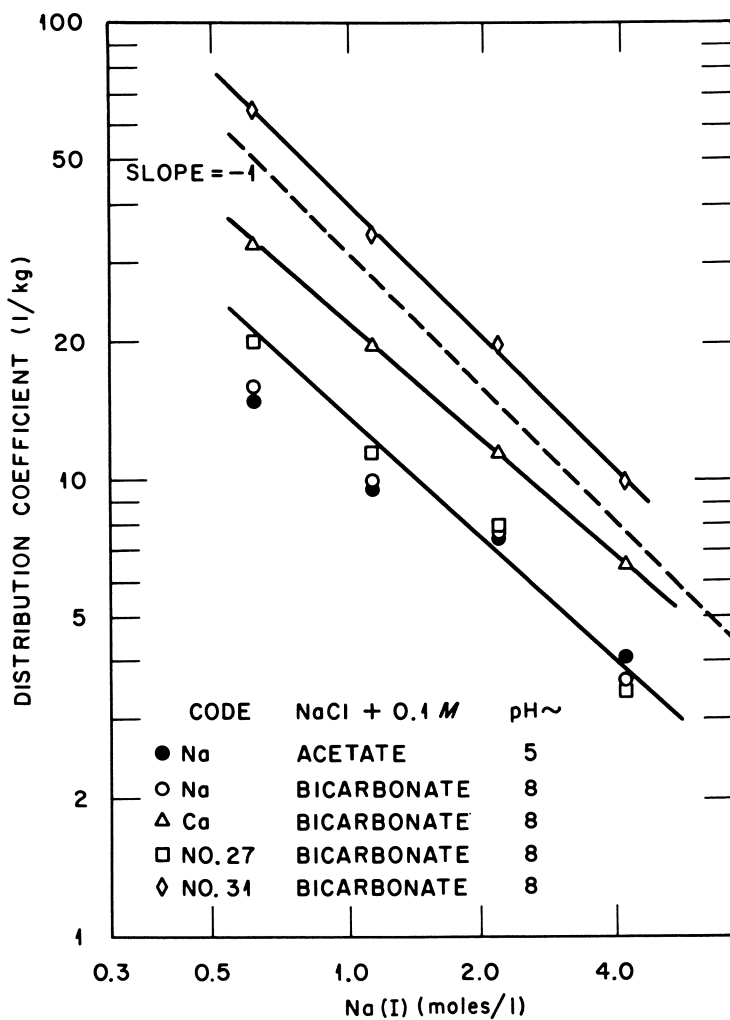


Figure 7. Effect of loading on distribution coefficients of Sr(II) on the calcium form of Wyoming montmorillonite (0.01M $Ca(OAc)_2$, pH 5, equilibration for 65 hr)



Distribution of Cs (I) Between Aqueous NaCl Solutions and Montmorillonite from Several Sources [$\sim 10^{-3} M$ Cs (I)]

Figure 8. Adsorption of Cs(I) on the sodium form of montmorillonites from several sources (Loading: $2 \times 10^{-4} - 4 \times 10^{-2}$ mol Cs(I)/kg, equilibration for 24 hr.).

Distribution coefficients for potassium on one clay are summarized in Figure 9. The ideal slope of -1 for $\log D_K$ vs \log sodium concentration was closely approximated. Values of D were about $1/3$ those for cesium on the same clay. A value of $K/\Gamma [(K^+)_{\text{clay}}(\text{Na}^+)/(\text{K}^+)(\text{Na}^+)_{\text{clay}}]$ of about 3.75 can be estimated from Figure 9. This agrees satisfactorily with values of about 2.5 reported both by Gast (10) for $0.001 M \text{ Na}^+$ and by Shainberg and Kemper (20) for $0.05 M \text{ Na}^+$.

Alkaline earth ions: The distribution coefficients of Ca(II) , Sr(II) , and Ba(II) on the Na form of Wyoming montmorillonite are shown in Figures 10a, b, and c. Values of D_{Ca} , D_{Sr} , and D_{Ba} are similar for equal sodium concentration. The slope of $\log D$ vs \log sodium concentration is close to -2 , the slope for ideal divalent-monovalent ion exchange. Measurements were carried out in the presence of sodium acetate buffer of $0.1 M$ and $0.01 M$, and the results were not significantly different at the same sodium concentration. This indicates that there is no interference from formation of complexes between the alkaline earths and acetate ions. One sample of Wyoming montmorillonite was purified only by passage through a Dowex 50 ion-exchange column in the sodium form. The D_{Ca} 's on this sample agreed within scatter with the same clay which had been subjected to the complete Jackson procedure.

From the results in Figures 10a, b, c, the computed values of $K/\Gamma [(A^{2+})_{\text{clay}}(\text{Na}^+)^2/(A^{2+})(\text{Na}^+)_{\text{clay}}^2]$ were approximately 3 . A value of 1.4 is reported for Ca(II) in $0.025 M \text{ NaCl}$ (9) and of about 1 for Ba(II) in $0.04 M \text{ NaCl}$ (4). Tamura (5) reported linear dependence of $\log D$ vs \log sodium concentration from 0.01 - 0.6 molar sodium with a slope of -2 ; his values of D_{Sr} were about half of those of Figure 10b at the same sodium concentrations. From results reported by Spitsyn and Gromov (1), we calculate a D_{Sr} of about 70 at $0.1 M \text{ NaCl}$, their highest concentration, in comparison with about 100 in Figure 10b.

Eu(III) : Figure 11 summarizes the adsorption of Eu(III) on the Na form of Wyoming montmorillonite at pH 5, controlled with $0.01 M$ acetate buffer, and adjusted to the same acidity without buffer by HCl . The values of D_{Eu} in the presence of acetate are about a third of those without, a difference similar to that seen in the loading curve, Figure 4. Formation of Eu(III) acetate complexes, presumably the source of the differences, has been reported elsewhere (21).

For the unbuffered system, the plot of $\log D_{\text{Eu}}$ vs \log sodium concentration approaches a slope of -3 as sodium concentration decreases. However, a minimum occurs just above one molar. We do not know the reason for this behavior.

Calcium Form of Montmorillonite. Cs^+ : Figure 12 summarizes measurements of D_{Cs} as a function of Ca(II) concentration. The strong loading effect evident in Figure 5 at low fractions of the clay in the cesium form are manifest in Figure 12 in the differences between results at trace loadings and at loadings over a few

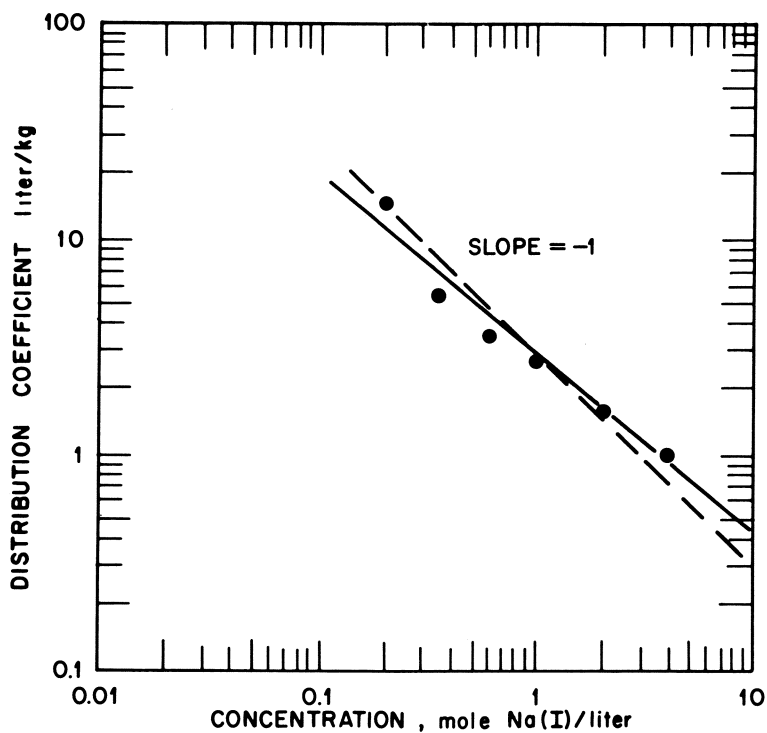


Figure 9. Adsorption of $K(I)$ on the sodium form of Wyoming montmorillonite (Loading: $2 \times 10^{-3} - 1 \times 10^{-2}$ mol $K(I)/kg$, $NaCl + 0.1M NaOAc$, pH 5, equilibration for 25 hr.).

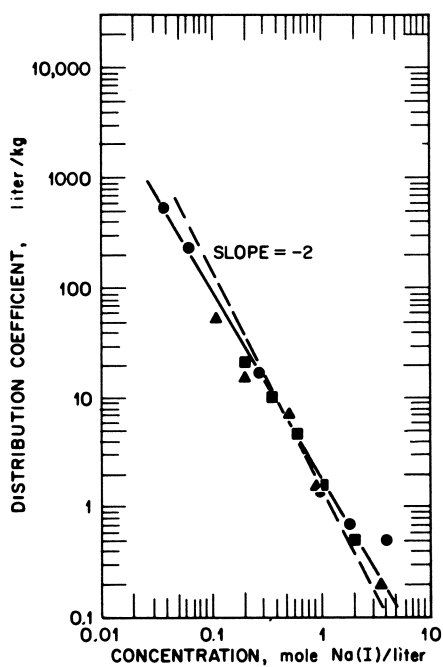


Figure 10a. Adsorption of Ca(II) on the sodium form of Wyoming montmorillonite (Loading: trace -1.4×10^{-2} mol Ca(II)/kg, pH 5, equilibration for 18 hr.) Clay samples from Jackson's purification procedure: (●), NaCl + 0.01M NaOAc; (■), NaCl + 0.1M NaOAc. Clay samples from Dowex column: (▲), NaCl + 0.1M NaOAc.

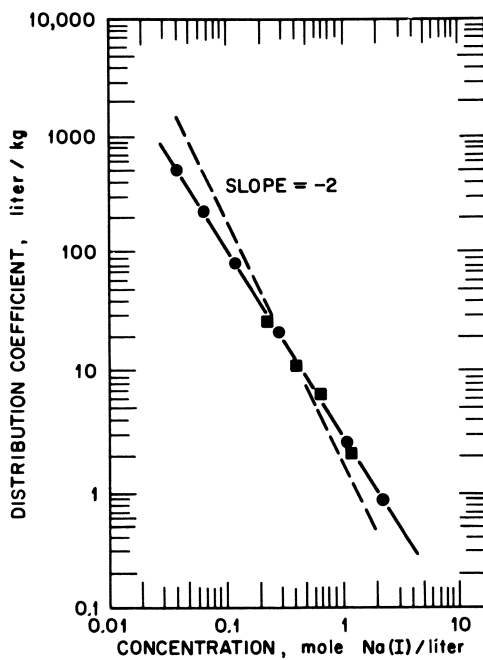


Figure 10b. Adsorption of Sr(II) on the sodium form of Wyoming montmorillonite (Loading: $6 \times 10^{-5} - 2 \times 10^{-2}$ mol Sr(II)/kg, pH 5, equilibration for 45 hr.): (●), NaCl + 0.01M NaOAc; (■), NaCl + 0.1M NaOAc.

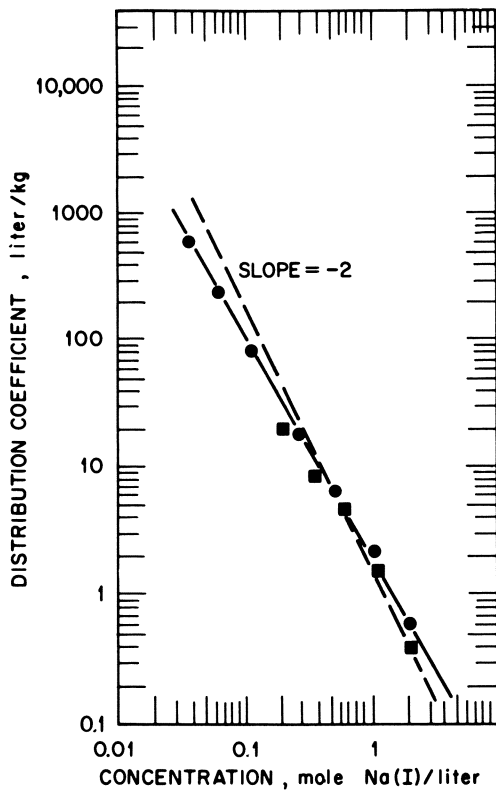


Figure 10c. Adsorption of Ba(II) on the sodium form of Wyoming montmorillonite (Loading: $8 \times 10^{-5} - 1.6 \times 10^{-2}$ mol Ba(II)/kg, pH 5, equilibration for 20 hr.): (●), NaCl + 0.01M NaOAc; (■), NaCl + 0.1M NaOAc.

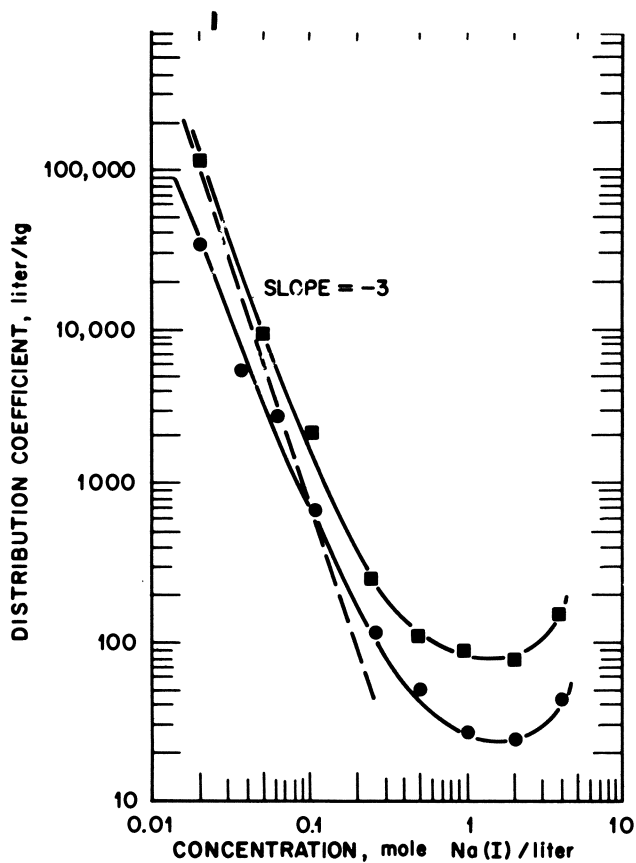


Figure 11. Adsorption of Eu(III) on the sodium form of Wyoming montmorillonite (trace loading, pH 5, equilibration for 16 hr): (■), NaCl + HCl; (●), NaCl + 0.01M NaOAc.

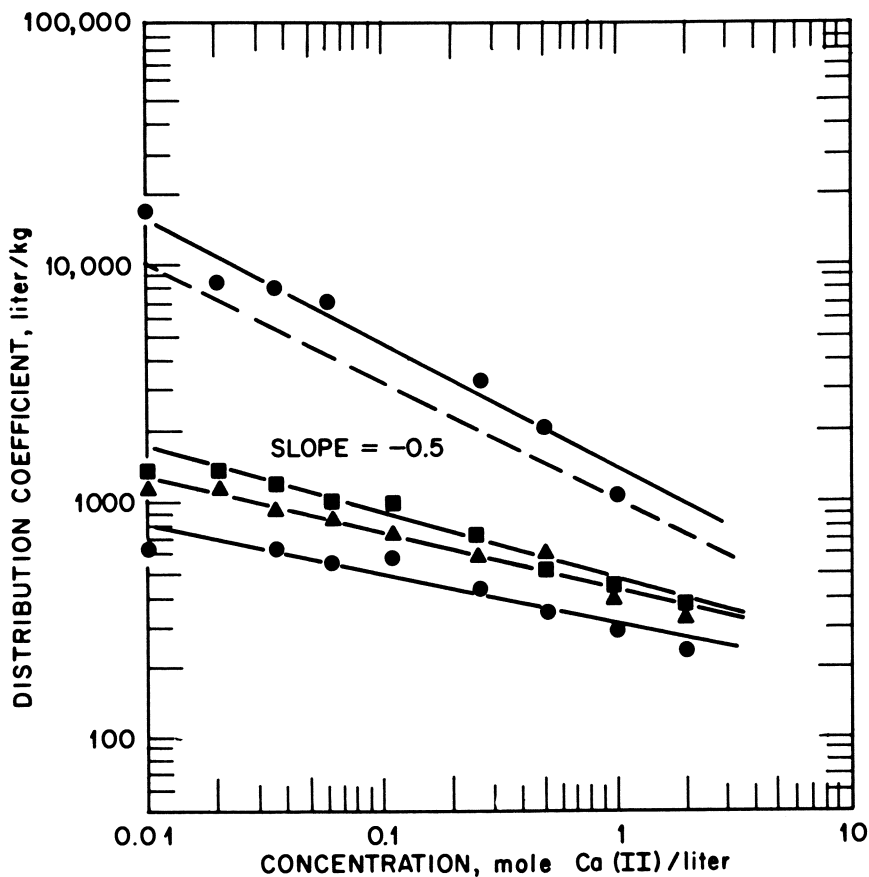


Figure 12. Adsorption of Cs(I) on the calcium form of Wyoming montmorillonite ($\text{CaCl}_2 + 0.01\text{M Ca(OAc)}_2$, pH 5, equilibration for more than 12 hr). Loading: (●), trace; (■), $2.3 \times 10^{-3} - 7.4 \times 10^{-3}$ mol Cs(I)/kg; (▲), $3.7 \times 10^{-3} - 1.1 \times 10^{-2}$ mol CsI/kg; (●), $5.3 \times 10^{-3} - 1.1 \times 10^{-2}$ mol Cs(I)/kg.

tenths of a percent of ion-exchange capacity. At trace loadings, the ideal slope, -0.5 , is realized within scatter, whereas at finite loadings, slopes are significantly less. We have already mentioned that the values of D_{Cs} reported in Ref. 3 are a factor of ten or more less than ours. Those reported by Sawhney (6) are about a hundredth of those obtained here at comparable loading.

Alkaline earths: Distribution coefficients for Sr(II) and Ba(II) as a function of concentration of Ca(II) are summarized in Figures 13a and 13b. The loadings in the case of Sr(II) (Figure 2) are in the linear isotherm range or only slightly out of it. Slopes of $\log D$ vs \log calcium concentration are close to the ideal value, -1 . Invariance of D_{Sr} between $0.01 M$ and $0.1 M$ acetate buffer indicates that there is no interference from acetate complexing. At the same Ca(II) concentration, D_{Ba} is a factor of about five higher than D_{Sr} .

The value of D_{Sr} reported by Wahlberg, et al., (7) at trace loading and at $0.1 M$ Ca(II), their highest concentration, is about 2.5, in comparison with about 7 in Figure 13a. Heald, (2), on the basis of equilibrations of montmorillonite with aqueous $SrCl_2$ -CaCl₂ solutions up to about $0.15 M$ total, reports an equilibrium quotient $[(Sr(II))_{clay}(Ca(II))/(Sr(II))(Ca(II))_{clay}]$ of 1.29. The value implied by Figure 13a is slightly less than one. We compute a D_{Sr} of about 30 from $0.025 M$ Ca(II) from data given by Spitsyn and Gromov (1), essentially the same as indicated in Figure 13a.

Eu(III): Figure 14 summarizes D_{Eu} as a function of Ca(II) concentration. A slope of -1.5 is approached at low salt concentration, but the values of D_{Eu} level out above $0.2 M$ Ca(II). Interpretation of behavior is somewhat clouded in view of the occurrence of complexing of Eu(III) by acetate, indicated elsewhere.

Discussion

Not surprisingly, although results appear self-consistent with clay from any one source, there are substantial differences between samples of different origins. Agreement of our results with earlier work, in comparisons by extrapolation where there was no overlap, is, with a few exceptions, reassuringly good, in that values of K/Γ or of D were about as close to one another as were our results on samples of clay from different sources.

Purification of the clay did not seem to have a marked effect on adsorptive properties. In this connection, it should be mentioned that in bringing the sample to a controlled ionic form before measurement, alkaline earth carbonates, if present, were probably removed, because the operation usually involved equilibration at pH 5. However, oxidation to remove organic matter and treatment with complexing agents to remove iron oxides apparently had little effect.

The adsorbability of monovalent and divalent ions on either the sodium or calcium form of montmorillonite decreases with supporting electrolyte concentration approximately as expected from

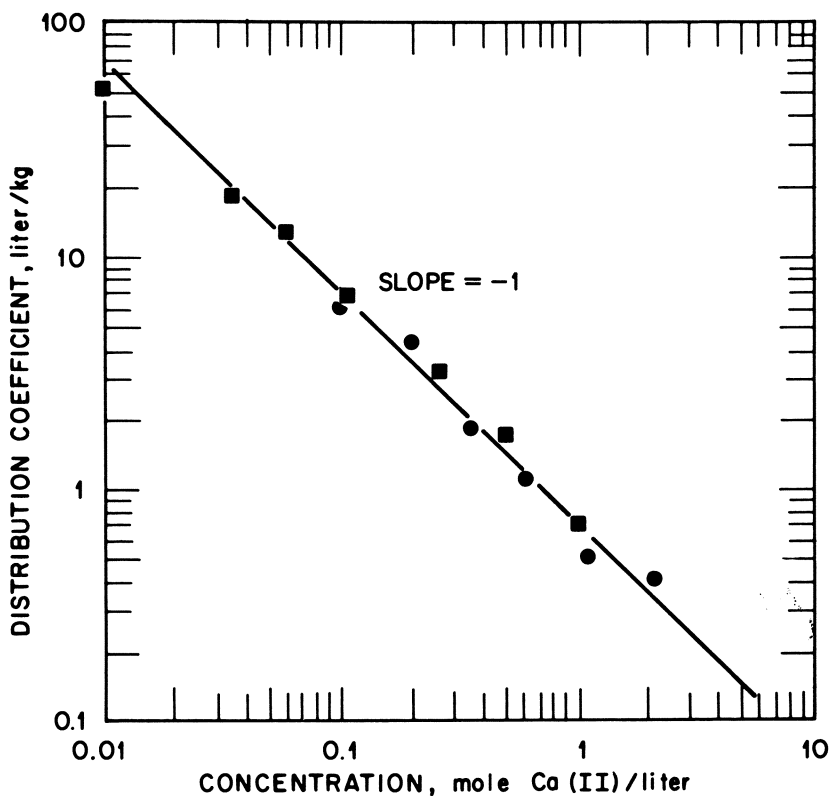


Figure 13a. Adsorption of Sr(II) on the calcium form of Wyoming montmorillonite (Loading: $7 \times 10^{-5} - 4.5 \times 10^{-3}$ mol Sr(II)/kg, pH 5, equilibration for 36 hr.): (●), $\text{CaCl}_2 + 0.1\text{M Ca(OAc)}_2$; (■), $\text{CaCl}_2 + 0.01\text{M Ca(OAc)}_2$.

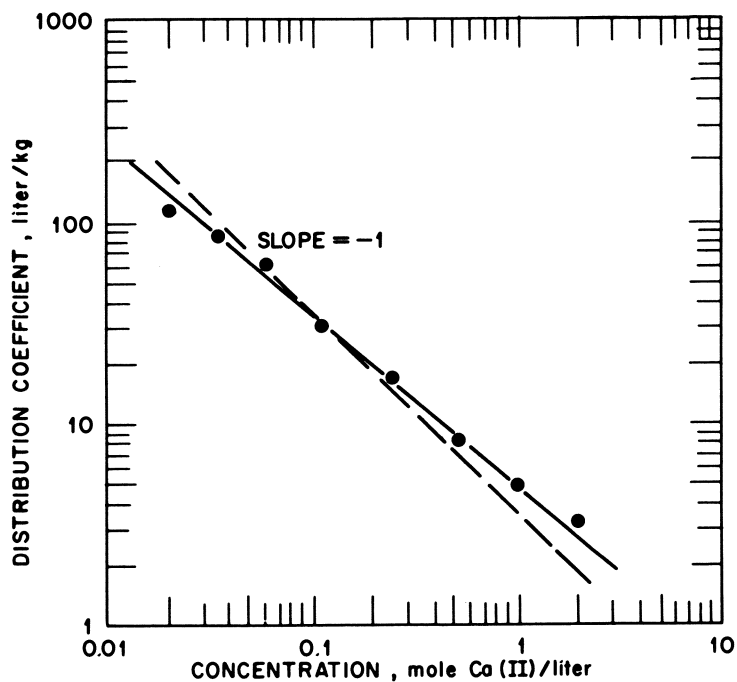


Figure 13b. Adsorption of Ba(II) on the calcium form of Wyoming montmorillonite ($\text{CaCl}_2 + 0.01\text{M Ca(OAc)}_2$, pH 5; loading: $5 \times 10^{-4} - 7.6 \times 10^{-3}$ mol Ba(II)/kg, equilibration for 30 hr.)

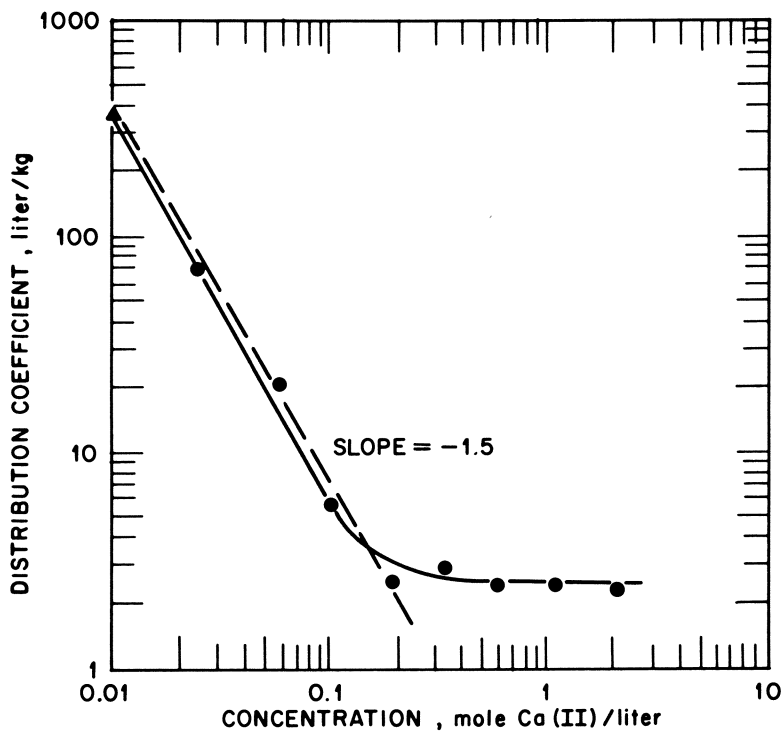


Figure 14. Adsorption of Eu(III) on the calcium form of Wyoming montmorillonite ($\text{CaCl}_2 + 0.01\text{M Ca(OAc)}_2$; loading: $1 \times 10^{-3} - 4 \times 10^{-2}$ mol Eu(III)/kg, pH 5, equilibration for 118 hr.)

conventional idealized ion exchange equations, at constant pH and loading. An adsorption minimum, however, seems to occur with the trivalent rare earth, Eu(III), with the clay in the sodium form. This minimum in adsorbability is reminiscent of the adsorption minima frequently observed with organic cation-exchange resins (Dowex 50 type) at high ionic strength (22).

Because of the occurrence of this adsorption minimum, adsorbability of Eu(III) remains high even at the high salinities of natural brines. In contrast, adsorbabilities of the alkali metals and alkaline earths become very low at high salinities. This implies that from the point of view of waste isolation the clay fraction of natural formations will not retard significantly the migration rates of the corresponding radioisotopes if the contacting aqueous phase is of high salinity. Conversely, the observation that the adsorbability of these ions is low is encouraging regarding the possible use of these elements for underground tracing of water (brine) flows.

Concern is frequently expressed regarding applicability of adsorption data obtained with clays at finite concentration of the ion of interest compared with true "trace" conditions. We have found, in agreement with a number of earlier investigators, that such worries are unfounded, particularly if the clay is primarily in the sodium form. In many of these systems, distribution coefficient under otherwise constant conditions are essentially the same under trace conditions and significant loadings. With the Ca form of the clay the linear isotherm region is much smaller than for the sodium form. However, even here there is no discontinuity between very low loading and "trace" levels even when Γ_{clay} varies substantially as loading of the monovalent ion becomes larger.

ACKNOWLEDGEMENTS

Research sponsored by the Office of Nuclear Waste Isolation and Oil, Gas, and Shale Technology, U. S. Department of Energy under contract W-7405-eng-26 with the Union Carbide Corporation.

Appreciation is expressed to Dr. B. H. Ketelle for his technical help in this research and to Dr. J. S. Johnson, Jr., and Dr. K. A. Kraus for their many helpful discussions and comments.

William J. Rogers, a Ph.D. candidate at the University of Tennessee, is supported in thesis work at Oak Ridge National Laboratory by an appointment to the Laboratory Graduate Participation Program, administered by Oak Ridge Associated Universities for the Department of Energy.

LITERATURE CITED

1. Spitsyn, V. I., and Gromov, V. V., "A Study of the Systematic Adsorption of Radioactive Strontium by Montmorillonite and Its Fixation by Roasting," *Sov. At. Energy (Engl. Transl.)*, (1958), 5, 1341.

2. Heald, W. R., "Characterization of Exchange Fractions of Strontium or Calcium on Four Clays," *Soil Sci. Soc. Proc.*, (1960), 24, 103.
3. Wahlberg, J. S., and Fishman, M. J., "Adsorption of Cesium on Clay Minerals," *U. S. Geol. Surv. Bull.*, (1962), 1140-A.
4. Lewis, R. J., and Thomas, H. C., "Adsorption Studies on Clay Minerals VIII. A Consistency Test of Exchange Sorption in the Systems Sodium-Cesium-Barium Montmorillonite," *J. Phys. Chem.*, (1963), 67, 1781.
5. Tamura, T., "Reactions of Cs¹³⁷ and Sr⁹⁰ with Soil Minerals and Sesquioxides," ORNL-P-438. Oak Ridge National Laboratory, Oak Ridge, Tenn., 1964.
6. Sawhney, B. L., "Sorption and Fixation of Microquantities of Cesium by Clay Minerals: Effect of Saturating Cations," *Soil Sci. Soc. Am. Proc.*, (1964), 28, 183.
7. Wahlberg, J. S., Baker, J. H., Vernon, R. W., and Dewar, R. S., "Exchange Adsorption of Strontium on Clay Minerals," *U. S. Geol. Surv. Bull.*, (1964), 1140C.
8. Wahlberg, J. S., and Dewar, R. S., "Ion Exchange on Minerals: Comparison of Distribution Coefficients for Strontium Exchange from Solutions Containing One and Two Competing Cations," *U. S. Geol. Surv. Bull.*, (1964), 1140-D.
9. Van Bladel, R., Gavine, G., and Laudelout, H., "A Comparison of the Thermodynamics Double Layer Theory, and Empirical Studies of the Na-Ca Exchange Equilibria in Clay Water Systems," *Proc. Inter. Clay. Conf.*, Madrid, Spain, (1972), 385.
10. Gast, R. G., "Alkali Metal Cation Exchange on Chambers Montmorillonite," *Soil Sci. Soc. Amer. Proc.*, (1972), 36, 14.
11. Gheyi, H. R., and Van Bladel, R., "Calcium-Sodium Exchange in Some Calcareous Soils and a Montmorillonite Clay as Compared with Predictions Based on a Double Layer Theory," *Geoderma*, (1976), 16, 159.
12. Jackson, M. L., *Soil Chemical Analysis - Advanced Course*, published by the author, Dept. of Soils, Univ. of Wis., Madison, Wis., (1956).
13. Mingelgrin, U., Kliger, L., Gal, M., and Saltsman, S., "The Effect of Grinding on the Structure and Behavior of Bentonite," *Clays & Clay Minerals*, (1978), 26, 299.
14. Papers in preparation.
15. Rush, R. M., "Parameters for the Calculation of Osmotic and Activity Coefficients and Tables of These Coefficients for Twenty-two Aqueous Mixtures of Two Electrolytes at 25°C," ORNL-4402. Oak Ridge National Laboratory, Oak Ridge, Tenn., (April 1969).
16. Scatchard, G., Rush, R. M., and Johnson, J. S., *J. Phys. Chemistry*, (1970), 74, 3786.
17. Nelson, F., and Kraus, K. A., *J. Am. Chem. Soc.*, (1958), 80, 4154.
18. Johnson, J. S., Paper A12, Preprints 4th Annual DOE-Symposium on Enhanced Oil and Gas Recovery, Tulsa, Okla., (August 1978).

19. Tamura, T., and Jacobs, D. G., *Health Physics*, (1960), 2, 391.
20. Shainberg, I., and Kemper, W. D., *Soil Science*, (1967), 103, 4.
21. Choppin, G. R., and Schneider, J. K., "The Acetate Complexing by Trivalent Actinide Ions," *J. Inorg. Nucl. Chem.*, (1970), 32, 328.
22. Nelson, F., Murase, T., and Kraus, K. A., *J. Chromatography*, (1964), 13, 503.

RECEIVED January 16, 1979.

INDEX

A	
Absorption	
coefficients of various radioisotopes	
with minerals	9
experiments with plutonium and	
americum, static	196t
rates of $^{241}\text{Am}^{3-}$ on basalt	195f
rates of $^{237}\text{Pu}^{4-}$ on basalt	195f
Abyssal red clays, radionuclide	
sorption studies on	267
Actinide(s)	
behavior, comparative	253
in aquatic food chains	250
biogeochemistry of	241
to bone from chronic exposure,	
estimating dose of	262
bone-soil ratios of	260
concentration	
in aquatic environments at	
nuclear fuel cycle facilities	253
in marine organisms	252
ratios in aquatic environments	256, 257
differential migration of	237
distribution coefficients for	202
element releases, man-made	241
in the environment, oxidation	
states of	247
field concentration ratios ([plant]/	
[soil]) for plants	246f
from the gastrointestinal tract,	
assimilation of	248
from the lung, adsorption of	247
to mammals, comparative terrestrial	
transport of	247
to mammals in contaminated	
environments, availability of	250
by mammals from contaminated	
soil, comparative accumulation	
of	251f
by man from soil, accumulation of	261t
naturally-occurring	256
in nitric acid solutions to animals,	
administration of	248
to people, assessing hazards of	
environmentally dispersed	260
plant uptake of	245
-Pu concentration ratios in the	
bullfrog	258t
radioecology studies, fresh-water	253
in soil	247
Actinide(s) (<i>continued</i>)	
by small mammals from soil,	
accumulation of	261t
sorption on geologic materials	215
surface phenomena and food chain	
behavior of	252
tracers	
characterization of	220
isotopic abundances of	217t
purification of	220
trivalent	121
on clay minerals, sorption	
behavior of	201
over Pu(IV) across biological	
membranes, enrichment of	249f
Activity median aerodynamic	
diameters (AMAD)	242
Adsorption	168
of actinides from the lung	247
americum	176
of Ba(II) on the calcium form of	
montmorillonite	320f
of Ba(II) on the sodium form of	
montmorillonite	315f
of Ca(II) on the sodium form of	
montmorillonite	313f
coefficients of geologic materials	233t
of Cs(I) on the calcium form of	
montmorillonite	317f
of Cs(I) on the sodium form of	
montmorillonites	310f
curve obtained for static fissure	
adsorption experiments	175f
of Eu(III) on the calcium form of	
montmorillonite	321f
of Eu(III) on the sodium form of	
montmorillonite	316f
experiments, fissure	171
adsorption curve obtained for	
static	175f
apparatus used in static	172f
by gray hornblende schist	174t
of K(I) on the sodium form of	
montmorillonite	312f
of the species (F), rate of	168
of Sr(II) on the calcium form of	
montmorillonite	319f
of Sr(II) on the sodium form of	
montmorillonite	314f
Adsorptive dispersion (T_a)	191

- Ba(II) 304
 on the calcium form of montmorillonite, adsorption of 320f
 effect of loading on distribution coefficients of 305f
 on the sodium form of montmorillonite, adsorption of 315f
- Barriers
 to radionuclide transport 9
 between waste and biosphere 6f
 to waste migration, natural 8
- Basalt 216
 absorption rates of $^{241}\text{Am}^{-3}$ and $^{237}\text{Pu}^{+4}$ on 195f
 flows below the Hanford reservation 4
 samples, results of contact experiments for 236
 samples, tracers and sorption experiments with 231f
- Batch equilibration 132
 activities of radionuclides remaining in high-level waste after 135t
 process, magnesium titanate 137
 of sodium titanate 134
- Batch (static) leaching procedure 94
- Batch-type technique 215
- Bed sediment 250
- Bedded salt 2
 repository for defense radioactive waste in southeastern New Mexico, WIPP— 13
- Bedrock, granitic
 chemical aspects of waste storage in disposal of radioactive waste in 47
 groundwater composition in 54t
- Bentonite-quartz
 mass related distribution coefficients for 64t
 measured distribution coefficients .. range of distribution coefficients for 58
 61f
- BET (Brunauer-Emmett-Teller) nitrogen adsorption technique 98, 119
- Biogeochemistry of actinides 241
- BIOPATH 70
- Biosphere
 barriers between waste and mechanism for the release of radionuclides to 6f
 8
 pathways by which wastes enter 37
- "Blank" samples, data from 287t
- Bone
 ash, contents of human 244t
 from chronic exposure, estimating dose of actinides to 262
 injection, thorium in 242
 injection, uranium in 242
 -soil ratios of actinides 260
- Borosilicate glasses, leach rates for 117
- Bouyancy effects of heated repository 32
- Breccia pipes 21
- Brine migration 31
 in a thermal gradient 32
 waste-rock interactions and 32
- Brunauer-Emmett-Teller nitrogen adsorption technique (BET) 119
- Bulk chemical analysis of rock samples 218
- Bulk glass leach rates 79
- Bullfrog, actinide-Pu concentration ratios in 258t
- Burial grounds of low-level radioactive waste, locations of 39f
- By-product material 38
- C**
- C_i , values of 280t
- Cadmium, distribution coefficients for 283f
- Calcine analysis 76
- Calcium on clay minerals, exchange of sodium and 298
- Calcium form of montmorillonite 304, 311
 adsorption of
 Ba(II) on 320f
 Cs(I) on 317f
 Eu(III) on 321f
 Sr(II) on 319f
- Calcium release during dissolution from rock types 225f
- Ca(II) 304
 effect of loading on distribution coefficients of 305f
 on the sodium form of montmorillonite, adsorption of 313f
- Californium exchange on kaolin, montmorillonite, and attapulgite plot of 205f
- Cambric
 re-entry hole (RNM-1) 151
 re-entry well RNM-1 151
 satellite well RNM-2S 151, 160
 site, geologic section at 150f
 source term at 10 years 151t
 test 149
- Zone II, analyses of water samples from 157f
- Canister
 material 51
 motions in salt, high-level waste 31
 -salt-repository system 31
 sectioning of high-level waste glass 77f
- Cation(s)
 compositions 228
 exchange and aqueous waste solutions 131

Cation(s) (<i>continued</i>)		Clay(s) (<i>continued</i>)	
-exchange capacity for cesium	272	distribution coefficients of	55
-exchange capacity of clay samples	300	on distribution coefficients, effects	
from rock sample breakdown,		of loading of	302
release of	222	by ²⁵³ Es radiation, destruction of	293
Ceramic(s)		kinetics of exchange between	202
form, titanium dioxide	130	minerals	201
forms for nuclear waste	129	exchange of sodium and calcium	
glass	130	on	298
titanate waste form	140f	sorption behavior of rare earths	
titanium dioxide matrix, atomically		on	201
dispersed waste oxides in	130	sorption behavior of trivalent	
waste form	138	actinides on	201
Cerium (Ce), distribution coefficients		morphological differences between	208
for	285f, 286f	-phase barium concentration	282
Cerium, tetravalent (¹⁴¹ Ce)	121	-phase strontium concentration	282
¹⁴⁴ Ce, leaching rate of	110f, 111	from radiation, fragmentation of	298
Cesium (Cs)		red	268
cation-exchange capacity for	272	radionuclide sorption studies on	
distribution coefficients for	276, 277f, 278	abyssal	267
exchange capacity	272	semi-quantitative analysis of	269t
in high-level waste	144	sorption capacity	274
sorption of	59, 66	rubidium salts in	270
Cs(I)		samples	
on the calcium form of montmoril-		cation-exchange capacity of	300
lonite, adsorption of	317f	distribution coefficients of	299
effect of loading on distribution		preparation of	298
coefficients of	303f	purification of	298
on the sodium form of montmoril-		Cobalt (Co) nuclides	111
lonites, adsorption of	310f	⁵⁷ Co, leaching rate of	105f
¹³⁴ Cs ⁺	121	⁵⁸ Co, leaching rate of	105f
absorbed on a column of Selma		⁶⁰ Co, leaching rate of	105f
chalk, activity curve for con-		¹³⁷ Co, leaching rate of	109f
centrations of	194f	Cold pressing/sintering	138
¹³⁷ Cs, leach rate as a function of time		Collapse chimneys	21
and glass section for	82f	Column infiltration experiments of	
¹³⁷ Cs in water from re-entry of		stronium	183
RNM-1, activity levels of	164t	Commercial nuclear fuel cycle, radio-	
Chelating agents	44	active wastes from	1
Chemical		Comparative accumulation of	
analysis of rock samples, bulk	218	actinides by mammals from	
aspects of waste storage in granitic		contaminated soil	251f
bedrock	47	Comparative actinide behavior	253
behavior of waste in unsaturated		in aquatic food chains	250
zone	44	Comparative terrestrial transport of	
interactions on migration of radio-		actinides to mammals	247
nuclides	68	Consolidated materials, evaluation of	139
retention of radionuclides in ground	52	Consolidated titanate waste	139
Chimney rubble, radionuclides		Consolidation of the ceramic waste	
leached from	94	form	138
Chimneys, collapse	21	Contact experiments	
Chronic exposure, estimating dose of		for basalt samples, results of	236
actinides to bone from	262	for quartz monzonite samples,	
Clay(s)		results of	236
-actinide product, stability of	291	rock-tracer	228
consequences of radiation from		for shale samples, results of	236
sorbed transplutonium		Contact-handled TRU waste	17t
elements on	291	disposal	15

Distribution coefficients (<i>continued</i>)	
of Ca(II), effect of loading on	305f
for cadmium	283f
for cerium	285f, 286f
for cesium	276, 277f, 278
of Cs(I), effect of loading on	303f
of clay	55
of clay samples	299
for divalent elements	62
effect of loading of clay on	302
effect of water composition on	62
for europium	285f, 286f, 287
of Eu(III), effect of loading on	306f
as functions of contact time for elements on granite	67f
as functions of surface-to-mass ratios for elements on granite	67f
for gadolinium	285f, 286f
for granite	
mass related	63t
measured	58
range of	60f
for lanthanides	284
low loading as a function of concentration of equilibrating ion	308
for M(III)-Na(I) exchange on kaolinite, montmorillonite, and attapulgite at pH 5	203t
nuclide concentrations and	65
for potassium	311
for promethium	285f, 286f
radionuclides used in laboratory measurements of	59t
for rare earths	202
of rock	55
for rubidium	276, 277f, 278
for silver	283f
and solution-phase concentration, correlation between	279
sorption equilibrium (K_{D1})	267
for strontium	278, 281f
of Sr(II), effect of loading on	303f, 305f, 309f
for technetium, mass related	66t
temperature effects on	65
for uranium, mass related	66t
Distribution studies, experimental conditions for	62t
Divalent elements	68
distribution coefficient for	62
DOE (<i>see</i> Department of Energy)	
Dynamic flow-through system	94
E	
E_d (<i>see</i> Effective retention factor)	
EDAX (energy dispersive analysis by x-rays)	218
Effective retention factor (E_d)	160
for nuclides	160
from water samples	161t
Effluent	137
form titanate solidification, comparison of radionuclide activity in	141t
Einsteinium-clay loadings	293
Einsteinium-clay ratios	292
Einsteinium-253 (^{253}Es)	291
attapulgite before and after	294f
-clay mixtures, diffraction measurements of	292
kaolin before and after	294f
radiation, destruction of clay by	293
EIS (Environmental Impact Statement)	3, 13
Electrolyte solution criteria	220
Elements	
on attapulgite, comparison of exchange of	209f
divalent	68
of DOE's waste isolation program	6t
on granite, distribution coefficients as functions of contact time and surface-to mass ratios for	67f
release fractions after 639 days	84t
tetravalent and trivalent	68
Elution	
dispersion of plutonium concentration during	192
experiments, fissure	173
peaks, predicted movement of	193f
of strontium from column of glauconite	184f, 186f
Emplacement	
on hydrologic properties of the site, effect of waste	42
operations	17f
of radioactive waste in rock salt	13
Energy dispersive analysis by x-rays (EDAX)	218
Energy Research and Development Administration (ERDA)	3
Office of Waste Isolation	3
Environment(s)	
availability of actinides to mammals in contaminated	250
interaction studies, leaching of waste-geologic	75
oxidation states of actinides in	247
release rate of radioactivity from solid waste form to	115
thorium in fresh-water	253
Environmental	
Impact Statement (EIS)	3, 13
Protection Agency (EPA)	3
Quality, Council of	3

- Environmentally-dispersed actinides
to people, assessing hazards of 260
- EPA (Environmental Protection
Agency) 3
- Equilibrating ion, distribution coeffi-
cients at low loading as a func-
tion of concentration of 308
- Equilibrium partitioning
of americium-III 171
experiments 171
of nuclides 170
- Equilibrium quotients of montmoril-
lonite, effect of loading on 307f, 309f
- Equilibrium quotients for Na(I)-
Ca(II) exchange 304
- ERDA (Energy Research and
Development Administration) 3
- ²⁵³Es (*see* Einsteinium-253)
- Europium, distribution coefficients
for 285f, 286f, 287
- Eu(III) 304, 311
on the calcium form of montmoril-
lonite, adsorption of 321f
effect of loading on distribution
coefficients of 306f
on the sodium form of montmoril-
lonite, adsorption of 316f
- ¹⁵⁴Eu, leach rate as a function of time
and glass section for 83f
- Exchange between clays, kinetics of .. 202
- Exchange capacity, Cs 272
- Exposure pathways to people 257
- F**
- (F), rate of adsorption of the species 168
- Fault-induced fracturing 8
- Faults at the WIPP site, techniques
used to search for 22
- Fennoscandian shield 50
- Fick's Law, fractional release using .. 86
- Field leach tests 120
- "Field verification" of strontium 282
- Fission products 149
- Fission waste nuclides on a sodium
titanate column, elemental
distribution of 136f
- Fissure(s) 170, 176, 192
adsorption experiments 171
adsorption curve obtained for
static 175f
apparatus used in static 172f
desorption experiments 173
elution experiments 173
apparatus for 175f
surfaces, distributions of americium
on 176, 177f-182f
surfaces into solution, rate for
desorption of americium from .. 183
- Fixed-bed ion-exchange column 134
- Flow, laminar 69
- Flow-through system, dynamic 94
- Food chain behavior of actinides,
surface phenomena and 252
- Food chains, comparative actinide
behavior in aquatic 250
- Fraction release, cumulative 86
- Fractional release using Fick's Law .. 86
- Fracture porosity 22
- Fractured rock, nuclide migration in 167
- Fractured rock, water velocity in 68
- Fracturing, fault-induced 8
- Fragmentation of clays from radiation 293
- Frenchman Flat 149
- Fresh-water actinide radioecology
studies 253
- Fresh-water environments, thorium in 253
- Frit composition 76
- Frit, zinc borosilicate 142
- Fuel
cycle, nuclear 241
radioactive wastes from
commercial 1
cycles, proliferation-resistant 2
disposal of spent 2
- G**
- Gadolinium, distribution coefficients
for 285f, 286f
- Gadolinium titanate 139
- Gamma counting 236
- Gamma ray(s)
analysis 123
counting of solutions 215
low-abundance 124
- Gas generation in the respiratory 34
- Gastrointestinal tract, assimilation of
actinides from 248
- Geochemistry of the repository 52
- Geologic
cross section WIPP site 20f
disposal and leaching, deep 143
environments, prediction of radio-
nuclide sorption in 215
features in site selection 22
formations, migration rates of
ions in 297
isolation of radioactive waste 37, 40
materials
actinide sorption on 215
adsorption coefficients of 233f
desorption coefficients of 234f
interactions of nuclear wastes
with 167
leaching of 167
structural breakdown of 222

Geologic (<i>continued</i>)		Glass (<i>continued</i>)	
medium, radioactive waste isolation in	40	waste(s) (<i>continued</i>)	
repository(ies)		isotopic leach rates from	79
deep	167	radioactive, composition of	78t
design	5	studies, leaching of radioactive	
risk assessment in siting	9	high-level	75
section at Cambrian site	150f	zinc borosilicate	142
storage scenarios	129	Glass #1, SEM photograph of	99f
Geological stability	50	Glass #2, SEM photograph of	99f
Geological strata, migratory behavior of ions in	191	Glass #3, SEM photograph of	99f
GETOUT	70	Glauconite	183
"Getter," radionuclide	34	elution of strontium from column	
G.I. tract assimilation coefficient for natural uranium	242	of	184f, 186f
Glass		strontium migration experiments in	183
ceramics	130	Globules, metallic	139
leach rate		Granite	58
for borosilicate	117	distribution coefficients for	
bulk	79	mass related	63t
for phosphate	117	measured	58
leach testing of radioactive zinc borosilicate	75	range of	60f
melt		distribution coefficients as functions of contact time and surface-to-mass ratios for elements on facility at the Nevada Test Site,	67f
#3	95, 104	deep	7, 8
experiment, single-pass leaching for	95, 98	proposed retention factors in	71t
by groundwater, single-pass leaching of nuclear	93	Granitic bedrock	
leaching experiment	100f	chemical aspects of waste storage in disposal of radioactive waste in	47
radionuclides leached from samples	94	groundwater composition in	54t
leaching experiment for	98	Granitic groundwater, proposed radionuclide species in nonoxidizing	69t
radionuclides observed in	101t	Granules, leaching of sintered	123
x-ray diffraction analysis of NTS	101t	Graphite encapsulated waste oxides	130
surface area	103t	Gray hornblende schist	
nuclear waste	76	adsorption by	174t
preparation of radioactive zinc borosilicate	75	Am ²⁴³ desorption from	174t
section		x-ray diffraction analysis of	170
for ¹³⁷ Cs, leach rate as a function of time and	82f	Ground	
cumulative fraction leached as a function of time—top	85f	chemical retention of radionuclides in	52
for ¹⁵⁴ Eu, leach rate as a function of time and	83f	KBS storage of HLW in	48f
leach rate as a function of time—upper-middle	80f, 81f	KSB storage of SUF in	49f
for ⁵⁴ Mn, leach rate as a function of time and	82f	material, physico-chemical conditions between radionuclides and	55
for ²³⁹⁺²⁴⁰ Pu, leach rate as a function of time and	83f	migration in	68
waste forms	129	Groundwater	
waste(s)	142	aqueous transport of nuclides via	129
canister, sectioning of high-level experimental procedure for making	77f	composition	53
making	76	in granitic bedrock	54t
		inflow, rate of	8
		flow	43
		flow paths	45
		from igneous rocks	53
		leach rates of radionuclides by	51
		leaching of radioactive isotopes with	115

- Groundwater (*continued*)
 proposed radionuclide species in
 nonoxidizing granitic 69*t*
 radionuclide species in 66
 redox potential of 53
 single-pass leaching of nuclear melt
 glass by 93
 from the sites of underground
 nuclear explosions, under-
 ground migration of radio-
 nuclides in 93
 -rock system around a waste
 depository 57*f*
- H**
- Hanford reservation, basalt flows
 below 4
 Hanford reservation near-surface test
 facility 7
 Heated repository, bouyancy effects of 32
 High Flux Research Reactor at Oak
 Ridge National Laboratory 202
 High-level liquid waste, compositions
 of AGNS Barnwell 133*t*
 High-level radioactive waste,
 composition of simulated 118*t*
 High-level waste (HLW) 13, 40, 47, 121
 after batch equilibration, activities
 of radionuclides remaining in .. 135*t*
 canister motions in salt 31
 Cs in 144
 glass canister, sectioning of 77*f*
 glass studies, leaching of radioactive 75
 I129 concentration profile at 1 mi .. 26*f*
 immobilization program 75
 KBS storage of 50*t*
 in the ground 48*f*
 radioactive isotopes in stored 116*t*
 repositories in salt, NRC licensing
 of 31
 repository for 43
 solidification 132, 144
 HLW (*see* High-level waste)
 Hornblende schist, adsorption by gray 174*t*
 Hornblende schist, Am³ desorption
 from gray 174*t*
 Host rock
 and backfill material 52
 ion-exchange properties of 9
 properties of 8
 retention in 70
 Human bone ash, Th-232 and U-238
 contents of 244*t*
 Human organs, distributions of
 Th-232, Th-230, and Th-228 in 259*t*
 Hydrodynamic dispersion (T_h) 191
 Hydrogen ion, titanate and 132
 Hydrogeologic transport 8
 Hydrologic
 considerations related to manage-
 ment of radioactive waste 37
 evaluation associated with the
 transport of radionuclides 37
 properties of the site, effect of
 waste emplacement on 42
 uncertainty in geologic isolation
 of radioactive waste 40
- I**
- I129 concentration profile at 1 mi—
 HLW 26*f*
 IAEA (*see* International Atomic
 Energy Association)
 Igneous rocks, groundwaters from 53
 Immobilization program, high-level
 waste 75
 Inflow, rate of groundwater 8
 Inhalation of thorium 241, 242
 Inhalation of uranium 241, 242
 Initial release mechanisms, slopes of .. 87*t*
 Initial solid-phase concentrations of
 desorbed species 276*t*
 Inorganic exchange materials 138
 INREM II code, radioactivity move-
 ment as modeled by 243*f*
 International Atomic Energy
 Association (IAEA) 79
 leaching apparatus, long-term 77*f*
 Ion-exchange
 column, fixed-bed 134
 equilibria between montmoril-
 lonite and solutions 297
 material chemistry 130, 131
 material preparation 130, 131
 materials with waste solutions,
 methods for contacting 132
 properties of the host rock 9
 resins 138
 leaching onto 119
 Ions in geologic formations, migration
 rates of 297
 Ions in geological strata, migratory
 behavior of 191
 Irradiation of solid waste forms,
 neutron 121
 Isolation
 in geologic medium, radioactive
 waste 40
 program, elements of DOE's waste .. 6*t*
 program, reviews concerning the
 DOE waste 5

- Leaching (*continued*)
 results, reporting of long-term 120
 of sintered granules 123
 with soxhlet apparatus 119
 studies 33
 system, one-pass 96f, 97f
 waste 33
 titanate 142
 of waste-geologic environment
 interaction studies 75
 Lead matrix materials, leaching of 124
 LEND 168
 Liquid waste, compositions of AGNS
 Barnwell high-level 133t
 LLW, Ra226 concentration profile at
 0.83 mi 27f
 LLW, U236 concentration profile at
 0.83 mi 28f
 Loading 302
 of clay on distribution coefficients,
 effects of 302
 on distribution coefficients of
 Ba(II), effect of 305f
 Ca(II), effect of 305f
 Cs(I), effect of 303f
 Eu(III), effect of 306f
 Sr(II), effect of 303f, 305f, 309f
 on equilibrium quotients of mont-
 morillonite, effect of 307f, 309f
 Loadings, Es-clay 293
 Long-lived radionuclides, sorption
 behavior of 55
 Long-term
 IAEA leaching apparatus 77f
 isolation of radioactive waste,
 Department of Energy program
 for 1
 leaching results, reporting of 120
 release mechanisms, slopes of 87t
 repository integrity 22
 "Los Medanos" 13
 Low-abundance gamma rays 124
 Low-level radioactive waste, locations
 of burial grounds of 39f
 Low-level waste buried within the
 conterminous United States,
 yearly volume of commercial 41f
 Low loading as a function of concen-
 tration of equilibrating ion, distri-
 bution coefficients at 308
 Lung, adsorption of actinides from 247
- M**
- M(III)-Na(I) exchange on kaolinite,
 montmorillonite, and attapulgite
 at pH 5, distribution coefficients
 for 203t
- Magnesium release during dissolution
 from rock types 226f
 Magnesium titanate batch equilibra-
 tion process 137
 Mammals
 comparative terrestrial transport of
 actinides to 247
 in contaminated environments,
 availability of actinides to 250
 from contaminated soil, compara-
 tive accumulation of actinides
 by 251f
 Man-made actinide element releases .. 241
 Man from soil, accumulation of
 actinides by 261t
 Marine organisms, actinide concen-
 trations in 252
 Mass related distribution coefficients
 for
 bentonite-quartz 64t
 granite 63t
 technetium 66t
 uranium 66t
 Measured distribution coefficients for
 bentonite-quartz 59
 Measured distribution coefficients for
 granite 58
 Mechanism for the release of radio-
 nuclides to the biosphere 8
 Melt glass
 #3 95
 calculation of leaching data for ... 104
 experiment, single-pass leaching ... 95, 98
 leaching experiment 98, 100f
 radionuclides leached from 94
 samples, radionuclides observed in .. 101t
 samples, x-ray diffraction analysis
 of NTS 101t
 size analysis 103t
 surface area 103t
 Metal
 alkoxides 131
 encapsulated waste oxides 130
 ions, sorptive behavior of natural
 clays toward 291
 Metallic globules 139
 Mice 250
 Migration
 of actinides, differential 237
 brine 31
 in a thermal gradient 32
 waste-rock interactions and 32
 characteristics of americium by
 water transport 173
 experiments, applicability of
 ARDISC model to 170
 experiments in glauconite, strontium
 in the ground 68

Migration (<i>continued</i>)		NAA (<i>see</i> Neutron activation analysis)	
kinetic effects in	191	Natural	
nuclide	268	barrier to waste migration	8
in fractured rock	167	clays toward metal ions, sorptive behavior of	291
through medium, rate of	170	thorium intakes by people	241
in porous rock	167	uranium, G.I. tract assimilation coefficient for	242
of the plutonium in WIPP aquifers	34	uranium intakes by people	241
radionuclide		Naturally-occurring actinides	256
a field study of	149	Near-surface facilities	7
program at the Nevada Test Site (NTS)	93	Near-surface test facility, Hanford reservation	7
chemical interactions on	68	Neptunium	247
in groundwater from the sites of underground nuclear explosions, underground	93	Neutron activation analysis (NAA)	117, 218
rate of peak concentration of strontium	185	method	121
rates of ions in geologic formations	297	technique, leach rate measurements on waste forms using	122
Migratory behavior of ions in geological strata	191	Neutron irradiation of solid waste forms	121
Minerals, absorption coefficients of various radioisotopes with	9	Nevada Test Site (NTS)	93
⁵⁴ Mn, leaching rate of	105f	composition of well-5B water	103f
as a function of time and glass section for	82f	deep granite facility at melt glass samples, x-ray diffraction analysis of	101f
Molecular diffusion	268	radionuclide migration program	93
Molybdenum	139	New Mexico, WIPP—bedded salt repository for defense radioactive waste in southeastern	13
Montmorillonite	202, 208, 292, 297, 298	Niobate	131
calcium form of	304, 311	sodium	132
adsorption of		Nitric acid solutions to animals, administration of actinides in	248
Ba(II) on	320f	Nitrogen adsorption technique, Brunauer-Emmett-Teller (BET)	98, 119
Cs(I) on	317f	Nonoxidizing granitic groundwater, proposed radionuclide species in	69t
Eu(III) on	321f	NRC licensing of HLW repositories in salt	31
Sr(II) on	319f	NTS (<i>see</i> Nevada Test Site)	
effect of loading on equilibrium quotients of	307f, 309f	Nuclear	
at pH 5, distribution coefficients for M(III)–Na(I) exchange on	203t	explosions, underground migration of radionuclides in groundwater from sites of underground	93
plot of Am and Cf exchange on	205f	fuel cycle	241
plot of Sm and Yb exchange on	204f	facilities, actinide concentration in aquatic environments at	253
sodium form of	302, 308	radioactive wastes from commercial	1
adsorption of		Fuel Safety Project	47
Ba(II) on	315f	material, special	38
Ca(II) on	313f	melt glass by groundwater, single-pass leaching of	93
Cs(I) on	310f	power program in Sweden	47
Eu(III) on	316f		
K(I) on	312f		
Sr(II) on	314f		
and solutions, ion-exchange equilibria between	297		
structural representation of	211f		
Multi-barrier principle	47		
N			
²² Na, leaching rate of	105f		
Na(I)–Ca(II) exchange, equilibrium quotients for	304		

Nuclear (<i>continued</i>)	
waste(s)	
ceramic forms for	129
with geologic materials, interactions of	167
glasses	76
repositories	297
Waste Isolation, Office of (ONWI)	4
Waste Management, Office of	3
Nuclide(s)	
concentrations and distribution	
coefficients	65
effective retention factor, E_{eff} , for	160
equilibrium partitioning of	170
through medium, rate of migration of	170
migration	268
in fractured rock	167
in porous rock	167
on a sodium titanate column, elemental distribution of fission waste	136f
via groundwater, aqueous transport of	129
waste	137
O	
Oak Ridge National Laboratory (ORNL)	13, 132, 242
High Flux Research Reactor at	202
Office of Nuclear Waste Isolation (ONWI)	4
Office of Nuclear Waste Management	3, 4
OKLO natural reactor in Gabon	93
One-pass leaching system	96f, 97f
ONWI (Office of Nuclear Waste Isolation)	4
Organics in TRU waste, decomposition of	34
Organism transfer, soil-sediment to	245
Organization of DOE's Waste Management Program	3
ORIGEN	76
ORNL (<i>see</i> Oak Ridge National Laboratory)	
Oversize rooms	32
Oxidation state selection of radionuclides, tracer	229t
Oxidation states of actinides in the environment	247
P	
Pacific Northwest Laboratory (PNL)	75
Task #2 of the Waste Isolation Safety Program at	87
Palladium	139
Particles, plutonium-contaminated soil	248
Permanent isolation of radioactive wastes	5
Petrographic studies of rock samples	216
pH changes during dissolution experiments	230f
Phosphate glasses, leach rates for	117
Physical properties of rock samples, characterization of	218, 220
Physical property data of rock samples	221t
Physico-chemical conditions between radionuclides and ground material	55
Pipes, breccia	21
Plant uptake of actinides	245
Plants, actinide field concentration ratios ([plant]/[soil]) for	246f
Plutonium	76, 149
and americium, static absorption experiments with	196t
concentration during elution, dispersion of	192
-contaminated soil particles	248
disposal of	2
isotopes	23
release rate of	86
sorption	34, 167
in WIPP aquifers, migration of	34
Pu(IV) across biological membranes, enrichment of trivalent actinides over	249f
Pu(IV), sorption of	172f
²³⁷ Pu infiltration of Bandelier tuff	192
²³⁷ Pu ⁴⁺	
on basalt, absorption rates of	195f
found in Bandelier tuff, relative activities of	194f
as a function of rate of deposition on Bandelier tuff, radial distribution of	198f
as a function of rate of deposition on Bandelier tuff, vertical distribution of	197f
²³⁸ Pu, concentrations of activity observed for	193f
Plutonium-239	252
²³⁹ + ²⁴⁰ Pu, leach rate as a function of time and glass section for	83f
PNL (<i>see</i> Pacific Northwest Laboratory)	
Porosity, fracture	22
Porous rock, nuclide migration in	167
Potash	22
Potassium, distribution coefficients for	311
Potassium release during dissolution from rock types	224f

Prepared waters with waters from natural systems, comparison of	235t	Radioactivity movement as modeled by the INREM II code	243f
Pressure sintering	138	Radioactivity from solid waste form to environment, release rate of	115
Pressurized water samples from RNM-2S, analyses of	164t	Radiochemical analyses of samples removed from RNM-1	155
Principle, multi-barrier	47	Radioecology studies, fresh-water actinide	253
Project Salt Vault	2	Radioisotopes, leach rate of	33
Proliferation-resistant fuel cycles	2	Radioisotopes with the minerals, absorption coefficients of various	9
Promethium, distribution coefficients for	285f, 286f	Radionuclide(s)	215
Q		activity in effluent from titanate solidification, comparison of	141t
Quartz monzonite	216	to the biosphere, mechanism for release of	8
samples	218, 232f, 236	chemical interactions on migra- tion of	68
water	228	"getter"	34
x-ray diffraction data for	219t	in the ground, chemical retention of and ground material, physico- chemical conditions between ..	55
x-ray diffraction studies of	218	by groundwater, leach rates of	51
R		in groundwater from sites of under- ground nuclear explosions, underground migration of	93
RA226 Concentration profile at 0.83 mi—LLW	27f	hydrologic evaluation associated with the transport of	37
Radiation, fragmentation of clays from Radiation from sorbed transplutonium elements on clays, consequences of	293	leached from chimney rubble	94
Radioactive	291	leached from melt glass	94
high-level waste glass studies, leaching of	75	leaching rates for Sb	111
isotopes with groundwater, leaching of	115	migration, a field study of	149
isotopes in stored high-level wastes waste(s)	116t	migration program at the Nevada Test Site	93
from commercial nuclear fuel cycle	1	nature of solid-phase concentra- tions of	269
composition of simulated high-level	118t	observed in leachate samples	101t
Department of Energy program for long-term isolation of	1	observed in melt glass samples	101t
forms, determining leach rates of simulated	115	remaining in high-level waste after batch equilibration, activities of sorption behavior of long-lived	135t
glass composition	78t	sorption in geologic environments, prediction of	55
in granitic bedrock, disposal of ..	47	sorption studies on abyssal red clays	215
hydrologic considerations related to management of	37	species in groundwater	267
hydrologic uncertainty in geologic isolation of	40	species in nonoxidizing granitic groundwater	66
isolation in geologic medium	40	tracer oxidation state selection of	69t
locations of burial grounds of low-level	39f	tracer purification of	229t
objective of geologic isolation of permanent isolation of	37	transport, barriers to	9
in rock salt, emplacement of	5	used in laboratory measurements of distribution coefficients	59t
on southeastern New Mexico, WIPP—bedded salt reposi- tory for defense	13	Radium vs. transuranics, uranium and	256, 257
zinc borosilicate glass, preparation and leach testing of	13	Rare earths (RE)	123
	75	on clay minerals, sorption behavior of	201

Rare earth(s) (<i>continued</i>)	
distribution coefficients for	202
leach rates	123
trivalent ¹⁵² Eu	121
Rate of ground water inflow	8
Rats, cotton	250
RE (<i>see</i> Rare earths)	123
Reaction rates of rock samples	222
Reactor, Argonne CP-5 Research	123
Red clay	268
radionuclide sorption studies on	
abyssal	267
semi-quantitative analysis of	269t
sorption capacity	274
Redox potential of groundwaters	53
Redox reactions and valence states	65
Re-entry hole, Cambric (RNM-1)	151
Release	
cumulative fraction	86
diffusion-controlled	86
experiment outline, waste form	89f
using Fick's Law, fractional	86
fractions after 639 days, element	84t
mechanisms, slopes of initial and	
long-term	87t
rate of plutonium	86
rate of radioactivity from solid	
waste form to environment	115
Repository(ies)	
buoyancy effects of heated	32
deep geologic	167
for defense radioactive waste in	
southeastern New Mexico,	
WIPP—bedded salt	13
gas generation in	34
geochemistry of	52
geologic design	5
for high-level waste	43
integrity, long-term	22
location	45
nuclear waste	297
risk assessment in siting geologic	9
in salt, NRC licensing of HLW	31
system, canister—salt—	31
under thermal load, stability of salt	31
Resins, ion exchange	119, 138
Retention	
in backfill material	70
factor (E_d)	68
in granite	71t
KBS report	70
for nuclides	160
in hostrock	70
Retrievable surface storage	3
Retrievable Surface Storage Facility	
(RSSF)	3
Reviews concerning the DOE waste	
isolation program	5
Risk assessment in designing and	
siting geologic repositories	9
RNM-1	152f
activity levels of ⁹⁰ Sr in water from	
re-entry of	164t
activity levels of ¹³⁷ Cs in water	
from re-entry of	164t
analyses of water samples pumped	
from	158t
cambric re-entry hole	151
construction details of	156f
radiochemical analyses of samples	
removed from	155
sampling points at	153f
source, ratios for	154t
γ-spectral analyses of samples	
removed from	155
water samples, activity levels in	162t
RNM-2S	152f
analyses of pressurized water	
samples from	164t
cambric satellite well	151, 160
future pumping at	165
Rock(s)	
dissolution experiment for sorption	
study of	220, 222
distribution coefficient of	55
-equipibrated water	171, 173
groundwaters from igneous	53
ion-exchange properties of the host	9
mechanics, properties of the host	8
nuclide migration in fractured	167
nuclide migration in porous	167
salt, emplacement of radioactive	
waste in	13
sample(s)	
breakdown, release of cations	
from	222
bulk chemical analysis of	218
characterization	216
physical properties of	218, 220
depth-of-leaching calculations	
for	229t
petrographic studies of	216
physical property data of	221t
reaction rates of	222
selection of	215
sorption differences among	237
specific surface area of	220
-tracer contact experiments	228
-tracer desorption experiments	239
types, dissolution from	
aqueous silica release during	227f
calcium release during	225f
magnesium release during	226f
potassium release during	224f
sodium release during	223f
wafers, autoradiography of	239

- Sodium titanate (*continued*)
 material, characterization of 131
 preparation 131
- Soil
 accumulation of actinides by small mammals and man from 261*t*
 actinides in 247
 -bone ratios of actinides 260
 comparative accumulation of actinides by mammals from contaminated 251*f*
 -sediment to organism transfer 245
 Th-U ratio 242
- Solid-phase concentrations of desorbed species 276*t*
- Solid-phase concentrations of radionuclides, nature of 269
- Solid waste form to environment, release rate of radioactivity from 115
- Solid waste forms, neutron irradiation of 121
- Solidification, comparison of radionuclide activity in effluent from titanate 141*t*
- Solidification, high-level waste 132, 144
- Solution-phase concentrations and distribution coefficients, correlation between 279
- Solutions
 determination of concentrations of tracers in 235
 gamma-ray counting of 215
 ion-exchange equilibria between montmorillonite and 297
- Sorbed transplutonium elements on clays, consequences of radiation from 291
- Sorption
 of americium 66, 167
 of americium III 172*f*
 of anionic technetium 59
 behavior of
 long-lived radionuclides 55
 rare earths on clay minerals 201
 trivalent actinides on clay minerals 201
 capacity, red clay 274
 of cesium (Cs) 59, 66
 coefficient, surface area (K_s) 171
 -desorption processes 215
 differences among rock samples 237
 equilibrium distribution coefficients (K_D) 267
 experiments with
 basalt samples 231*f*
 blank containers 230*f*
 quartz monzonite samples 232*f*
 shale samples 231*f*
- Sorption (*continued*)
 in geologic environments, prediction of radionuclide 215
 on geologic materials, actinide isotope 215
 kinetics 65, 167
 measurements 55
 mechanisms 65
 of plutonium 34, 167
 of plutonium IV 172*f*
 of strontium 66
 studies on abyssal red clays, radionuclide 267
 study of rocks, dissolution experiment for 220, 222
- Sorptive behavior of natural clays toward metal ions 291
- Source Clay Minerals Repository 202
- Source material 38
- Soxhlet apparatus, leaching with 119
- Special nuclear material 38
- Species (F), rate of adsorption of 168
- Specific surface area of rock samples .. 220
- γ -Spectral analyses of samples removed from RNM-1 155
- Spent fuel, disposal of 2
- Spent uranium fuel (SUF) 47
 in the ground, KBS storage of 49*f*, 50*t*
- Static
 adsorption experiments with plutonium and americium 196*t*
 (batch) leaching procedure 94
 fissure adsorption experiments, adsorption curves obtained for 175*f*
 fissure adsorption experiments, apparatus used in 172*f*
- Storage
 of HLW in the ground, KBS 48*f*, 50*t*
 retrievable surface 3
 scenarios, geologic 129
 of SUF in the ground, KBS 49*f*, 50*t*
- Structural breakdown of geologic materials 222
- Strontium
 from column of glauconite, elution of 184*f*, 186*f*
 column infiltration experiments of .. 183
 compounds 270
 concentration, clay-phase 282
 concentration in seawater 282
 distribution coefficients for 278, 281*f*
 "field verification" of 282
 migration experiments in glauconite 183
 migration rate of peak concentration of 185
 in seawater, concentration of 269*t*
 sorption of 66
 (^{88}Sr) 121

- Trench covers 44
- Tritium 149
 concentration as a function of
 volume of water pumped 163f
- Trivalent actinides 121
 on clay minerals, sorption behavior
 of 201
 over Pu(IV) across biological
 membranes, enrichment of 249f
- Trivalent elements 68
- Trivalent rare earths (^{152}Eu) 121
- TRU (*see* Transuranium contami-
 nated wastes)
- U**
- Underground migration of radio-
 nuclides in groundwater 93
- Underground nuclear explosions 93
- United States Geological Survey
 (USGS) 13
- Unsaturated zone, chemical behavior
 of waste in 44
- Upper-middle glass section, leach
 rate as a function of time 80f, 81f
- Uranium 76, 149
 in bone injection 242
 fuel, spent (SUF) 47
 ingestion 241
 inhalation 241, 242
 intake and diet 242
 intakes by people, natural 241
 isotopes 23
 mass related distribution
 coefficients for 66t
 and radium vs. transuranics 256, 257
 site-specific application of 245
- U-236 concentration profile at
 0.83 mi—LLW 28f
- U-238 contents of human bone ash 244t
- USGS (United States Geological
 Survey) 13
- U.S. Seabed Disposal Program 267
- V**
- Valence states, redox reactions and 65
- Vitrified wastes 129
- W**
- Waste(s)
 and biosphere, barriers between 6f
 categories of 38
 consolidated titanate 139
 depository, groundwater—rock
 system around a 57f
 defense (1985) 18t
 disposal problem 40
- Waste(s) (*continued*)
 emplacement on the hydrologic
 properties of the site, effect of .. 42
 enter the biosphere, pathways by
 which 37
 form(s) 7, 51
 ceramic 138
 determining leach rates of
 simulated radioactive 115
 to environment, release rate of
 radioactivity from solid 115
 PW-4 in distilled water, leach
 rates of 124t
 release experiment outline 89f
 temperature and 138
 transmission electron photo-
 micrograph of a ceramic
 titanate 140f
 glass 129
 leachability of 142
 neutron irradiation of solid 121
 using NAA technique, leach rate
 measurements on 122
- geologic environment interaction
 studies, leaching of 75
- glass
 canister, sectioning of high-level 77f
 isotopic leach rates from 79
 making 76
 nuclear 76
 studies, leaching of radioactive
 high-level 75
 high-level (HLW) 13, 40, 47
 after batch equilibration,
 activities of radionuclides
 remaining in 135t
 canister motions in salt 31
 cesium in 144
 compositions of AGNS Barnwell 133t
 glass canister, sectioning of 77f
 immobilization program 75
 radioactive isotopes in stored 116t
 repository for 43
 solidification 132, 144
- interactions 7
- isolation 291
 ERDA Office of 3
 Pilot Plant (WIPP) 4, 13, 143
 artist's concept of 14f
 concept, underground layout
 proposed for 16f
 conceptual design 15
 Experimental Program 25
 site
 evaluation for 18t
 geologic cross section 20f
 location map for proposed .. 19f
 selection factors considered .. 21t

